Deciphering the complexity of element incorporation into bivalve shells

Dissertation
zur Erlangung des akademischen Grades
"Doktor der Naturwissenschaften"
im Promotionsfach Geologie/Paläontologie

am Fachbereich 09 für Chemie, Pharmazie und Geowissenschaften
der Johannes Gutenberg-Universität Mainz

von
Liqiang Zhao
geb. In Hebei, China

Mainz 2016

Dekan: Not displayed for reasons of data protection

1. Berichterstatter: Not displayed for reasons of data protection

2. Berichterstatter: Not displayed for reasons of data protection

Hiermit erkläre ich, dass ich die vorliegende Arbeit selbstständig verfasst und keine anderen als die angegebenen Quellen und Hilfsmittel benutzt habe.

_____

(Liqiang Zhao)
Mainz, 06. Dezember 2016

Abstract

Bivalve shells can function as extraordinary archives of environmental change. Physical and chemical changes of the ambient environment that prevailed during growth can be recorded by the shells in the form of variable growth increment widths and geochemical properties such as oxygen and carbon isotope values and trace and minor elements. Unlike stable light isotopes, however, unravelling environmental signals from element impurities of bivalve shells remains an extremely challenging task. Perhaps the fundamental challenge lies in the fact that extrinsic and intrinsic factors governing the element incorporation are poorly constrained. With the aim of disentangling the controls on the incorporation of trace and minor elements into bivalve shells, the present study conducted a series of laboratory experiments and field studies. Results present herein are included in four papers which have been published in international peer-review journals as well as one manuscript which is currently under review in a peer-review journal.

Possible pathways by which trace and minor elements (Mg, Cu, Mn, Zn, Sr, Ba and Pb) are transported from the ambient water to the calcifying front are delineated. Chapter 2 demonstrated that increasing aqueous Ca^{2+} levels from 3 to 6 mM did not facilitate shell growth of the freshwater bivalve, *Corbicula fluminea*. However, the amounts of Mn, Cu and Pb incorporated into the shells significantly decreased, indicating the potential competition with Ca^{2+} in the same transport pathways. Moreover, blocking the Ca^{2+}-channels by lanthanum and Verapamil significantly reduced Mn, Cu, Zn and Pb incorporation into the shells, and Mn/Ca_{shell} and Cu/Ca_{shell} decreased simultaneously when inhibiting the Ca^{2+}-ATPase by ruthenium red. However, the amounts of Mg, Sr and Ba incorporated into the shells were virtually unaffected, implying that intracellular Ca^{2+} transport mechanisms are not responsible for their incorporation into the shells. These findings help decipher underlying mechanisms responsible for the element partitioning between the ambient water and the shells.

Building on the findings of chapter 2, specimens of *C. fluminea* were grown under different combinations of water chemistry, temperature and food availability to gain a better understanding of how environmental factors affect the incorporation of Sr and Ba into the shells. As shown in Chapter 3, the Sr/Ca_{shell} ratio of *C. fluminea* exhibited a statistically significant negative correlation with temperature and a positive correlation to Sr/Ca_{water}, but was not affected by changing food level or shell growth rate. On the contrary, Ba/Ca_{shell} was influenced by a complexly intertwined set of variables including temperature, food level, Ba/Ca_{water} and shell growth rate. Partition coefficients of $K_D^{Sr/Ca}$ (0.19 to 0.29) and $K_D^{Ba/Ca}$ (0.03 to 0.19)

confirmed the control of vital effects over strontium and barium incorporation into the shells. As indicated by the findings, Sr/Ca_{shell} of *C. fluminea* from freshwater environments can serve as a reliable proxy for past water temperature if the spatiotemporal variability of strontium-to-calcium in the water is small, well-known or can be estimated from other proxies. Interpreting Ba/Ca_{shell} values, however, is much more challenging because they are controlled by a large number of environmental and physiological variables. Sr/Ca_{shell} and Ba/Ca_{shell} of *C. fluminea* specimens from estuarine settings in which element-to-calcium ratios are more conservative can potentially serve as paleoenvironmental proxies. Findings of this study may also help to better understand the element incorporation into shells of other bivalves including marine species.

The following two chapters provide a more comprehensive and detailed understanding of how physiological influences affect the element incorporation into bivalve shells. Chapter 4 investigated the combined effects of seawater pH (8.1, 7.7 and 7.4) and temperature (16 and 22 °C) on the growth and sodium composition of the shells of the blue mussel, *Mytilus edulis*, and the Yesso scallop, *Patinopecten yessoensis*. Exposure of *M. edulis* to low pH (7.7 and 7.4) caused a significant decrease of shell formation, whereas a 6 °C warming significantly depressed the rate of shell growth in *P. yessoensis*. On the other hand, while the amount of Na incorporated into the shells of *P. yessoensis* did not increase in acidified seawater, an increase of Na/Ca_{shell} with decreasing pH was observed in *M. edulis*, the latter agreeing well with the aforementioned hypothesis. Moreover, a combined analysis of the shell growth and sodium content provides a more detailed understanding of shell formation processes. Under acidified conditions, mussels may maintain more alkaline conditions favorable for calcification, but a significant decrease of shell formation indicates that the mineralization processes are impaired. The opposite occurs in scallops; virtually unaffected shell growth implies that shell mineralization functions well. Finding of the present study may pave the way for deciphering the mechanisms underlying the impacts of ocean acidification and warming on bivalve shell formation.

Chapter 5 investigated the transgenerational epigenetic effect on the element composition of bivalve shells. Findings showed that reduced seawater pH projected for the end of this century (i.e., pH 7.7) led to a significant decrease of shell production of newly settled juvenile Manila clams, *Ruditapes philippinarum*. However, juveniles from parents exposed to low pH grew significantly faster than those from parents grown at ambient pH, exhibiting a rapid transgenerational acclimation to an acidic environment. The sodium composition of the shells may shed new light on the mechanisms responsible for beneficial transgenerational

acclimation. Irrespective of parental exposure, the amount of Na incorporated into shells increased with decreasing pH, implying active removal of excessive protons through the Na^+/H^+ exchanger which is known to depend on the Na^+ gradient actively built up by the Na^+/K^+-ATPase as a driving force. However, the shells with a prior history of transgenerational exposure to low pH recorded significantly lower amounts of Na than those with no history of acidic exposure. It therefore seems very likely that the clams may implement less costly and more ATP-efficient ion regulatory mechanisms to maintain pH homeostasis in the calcifying fluid following transgenerational acclimation. Our results suggest that marine bivalves may have a greater capacity to acclimate or adapt to ocean acidification by the end of this century than currently assumed.

Chapter 6 presented the first multi-year, high-resolution Mn/Cashell time series of the freshwater mussel, *Hyriopsis cumingii* (Lea, 1852) from a shallow eutrophic lake (Lake Taihu, China). Mn/Ca_{shell} time-series of the two studied shells exhibited a remarkable degree of synchrony after being placed in a precise temporal context by means of growth pattern analysis. There is a large inter-annual variability of Mn/Ca_{shell} records during 2011–2015, with higher values occurring during the first three years. Mn/Ca_{shell} also displayed a pronounced intra-annual variability with maxima consistently occurring during the summer. The high reproducibility of Mn/Ca_{shell} time-series among contemporaneous specimens highlighted the existence of strong environmental rather than biological control on the incorporation of Mn into the shells. In particular, the striking feature of summertime Mn/Ca_{shell} maxima occurred synchronously when reducing conditions prevailed beneath the sediment-water interface (SWI). The latter resulted in substantial increases of biologically available Mn^{2+} in the sediment pore water and organic particles which were rapidly taken up by the mussels and subsequently incorporated into their shells. Therefore, Mn/Ca_{shell} can potentially serve as a high-resolution proxy of the mobility of Mn at the SWI. As demonstrated by the present study, unravelling geochemical properties of bivalve shells can help to retrospectively monitor eutrophication-induced environmental change in aquatic ecosystems.

Zusammenfassung

Muschelschalen stellen ein außergewöhnliches Archiv für Umweltänderungen dar. Die physikalischen und chemischen Veränderungen der Umgebungsbedingungen, die während des Wachstums vorherrschten, können in Form variabler Inkrementbreiten und geochemischen Proportionen, wie Sauerstoff- und Kohlenstoffisotopen, Spuren- und Nebenelementen, aufgezeichnet werden. Im Gegensatz zu leichten stabilen Isotopen bleibt jedoch die Entschlüsselung von Umweltsignalen von Elementverunreinigungen von Muschelschalen eine äußerst anspruchsvolle Aufgabe. Die wahrscheinlich größte Herausforderung liegt darin begründet, dass äußere und innere Faktoren, die die Elementaufnahme steuern, wenig verstanden sind. In der vorliegenden Studie wurden eine Reihe von Laborexperimenten und Feldstudien durchgeführt, mit dem Ziel mögliche Steuerungen der Aufnahme von Spuren- und Nebenelementen zu entschlüsseln. Die hier vorgelegten Ergebnisse sind in vier Beiträgen in wissenschaftlichen Fachzeitschriften mit Begutachtungsverfahren veröffentlicht wurden, ein weiteres Manuskript befindet sich derzeit in Begutachtung bei einem Peer-Review-Journal.

Zuerst wurden mögliche Transportwege beschrieben, mit denen die Spuren- und Nebenelemente (Mg, Cu, Mn, Zn, Sr, Ba und Pb) vom Umgebungswasser zur Schalenwachstumsfront gelangten. Kapitel 2 zeigt, dass ein Anstieg gelösten Ca^{2+} von 3 auf 6 mM das Schalenwachstum der Süßwassermuschel *Corbicula fluminea* nicht begünstigt. Die Menge von Mn, Cu und Pb in die Schale sank jedoch signifikant, was auf einen potentiellen Wettbewerb von Ca^{2+} und o.g. Elementen auf denselben Transportwegen hindeutet. Darüber hinaus wurde über die Blockierung der Ca^{2+} -Kanäle durch Lanthan und Verapamil der Mn-, Cu-, Zn- und Pb-Einbau in die Schalen reduziert. Mn/Ca_{shell} und Cu/Ca_{shell} verringerten sich gleichzeitig, wenn die Ca^{2+} -ATPase durch Rutheniumrot gehemmt wurde. Jedoch blieben die eingebauten Mengen von Mg, Sr und Ba davon fast unbeeinflusst, was darauf hindeutet, dass interzelluläre Transportmechanismen von Ca^{2+} nicht für deren Einbau in die Schalen verantwortlich sind. Diese Ergebnisse liefern wichtige Information zu zugrundeliegenden Mechanismen, die für die Element-Verteilung zwischen Umgebungswasser und Schale verantwortlich sind.

Auf Grundlage der Ergebnisse von Kapitel 2 wurden Proben von *C. fluminea* unter verschiedenen Kombinationen von Wasserchemie, Temperatur und Nahrungsmittelverfügbarkeit gehalten, um ein besseres Verständnis davon zu erhalten, wie Umweltfaktoren den Einbau von Sr und Ba in die Schalen beeinflussen. Wie in Kapitel 3 dargestellt, zeigte das Sr/Ca_{shel}-Verhältnis von C. *fluminea* eine statistisch signifikante negative

Korrelation mit der Temperatur. Eine positive Korrelation mit Sr/Ca_{water}, wurde jedoch nicht durch die Veränderung des Nahrungsangebots oder der Schalenwachstumsrate beeinflußt. Im Gegenteil, Ba/Ca_{shell} war beeinflusst von komplexen Variablen wie Temperatur, Nahrungsmittelniveau, Ba/Ca_{water} und Schalenwachstumsrate. Verteilungskoeffizienten von $K_D^{Sr/Ca}$ (0,19 bis 0,29) und $K_D^{Ba/Ca}$ (0,03 bis 0,19) bestätigten, dass der Einbau von Strontium und Barium in die Schalen von physiologischen Aspekten gesteuert ist. Wie aus den Ergebnissen hervorgeht, kann Sr/Ca_{shell} von C. *fluminea* aus Süßwasser-Gewässern als zuverlässiger Proxy für die Wassertemperatur der Vergangenheit dienen, wenn die räumlich-zeitliche Variabilität von Strontium zu Kalzium im Wasser klein oder bekannt ist, oder sich durch andere Proxies abschätzen lässt. Das Interpretieren von Ba/Ca_{shell}-Werten ist jedoch viel schwieriger, da sie durch eine Vielzahl von physiologischen und Umweltvariablen gesteuert werden. Sr/Ca_{shell} und Ba/Ca_{shell} von *C. fluminea*-Exemplaren aus Küstenregionen, in denen Element-zu-Kalzium-Verhältnisse konservativer und stabiler sind, können potentiell als Paläoumweltproxies funktionieren. Die Ergebnisse dieser Studie können nützlich sein, um den Einbau von Elementen in die Schalen anderer Muscheln, einschließlich mariner Arten, besser zu verstehen.

Die folgenden beiden Kapitel bieten einen umfassenden Überblick darüber, wie die Physiologie der Muscheln den Elementeinbau in die Schalen beeinflusst. In Kapitel 4 wurde die kombinierte Auswirkung von Meerwasser-pH (8,1; 7,7 und 7,4) und Temperatur (16 und 22 °C) auf das Wachstum und die Natriumzusammensetzung der Muscheln *Mytilus edulis* und der Jesso-Jakobsmuschel, *Patinopecten yessoensis*, untersucht. War *M. edulis* einem niedrigem pH-Wert (7,7 und 7,4) ausgesetzt, so führte dies zu einer signifikanten Abnahme der Schalenbildungsrate, wohingegen eine Erwärmung um 6 ºC das Gegenteil erzeugt. Währende die Menge des in die Schalen von *P. yessoensis* eingebautem Na in Seewasser mit niedrigerem pH nicht anstieg, wurde andererseits in *M. edulis* eine Zunahme der Na/Ca_{shell}-Werte mit abnehmendem pH beobachtet, wobei letztere mit der oben erwähnten Hypothese übereinstimmte. Darüber hinaus liefert eine kombinierte Analyse des Schalenwachstums und des Natriumgehaltes ein detaillierteres Verständnis der Schalenbildungsprozesse. In versauerten Gewässern bewahren Muscheln eher alkalische Bedingungen, die günstiger für die Schalenbildung sind. Eine signifikante Abnahme der Schalenbildung zeigt jedoch, dass die Mineralisierungsprozesse beeinträchtigt sind. Das Gegenteil in ist bei Jakobsmuscheln zu beobachten; nahezu unbeeinflusstes Schalenwachstum impliziert, dass die Schalenmineralisierung gut funktioniert. Die Ergebnisse der Studie können den Weg ebnen, um

anhand von Muschelschalenwachstum die Mechanismen zu entschlüsseln, die die Auswirkungen der Ozeanversauerung und Erwärmung bestimmen.

In Kapitel 5 wurde erstmals der generationsübergreifende epigenetische Effekt auf die Elementzusammensetzung von Muscheln untersucht. Die Ergebnisse dieses Kapitels zeigten, dass ein verringerter Meerwasser-pH, der für das Ende dieses Jahrhunderts erwartet wird (d.h. pH 7,7), zu einer signifikanten Abnahme der Schalenproduktion bei juvenilen Manila-Muscheln (*Ruditapes philippinarum)* führte. Jedoch wuchs der Nachwuchs von Eltern, die einem niedrigen pH-Wert ausgesetzt waren, signifikant schneller als diejenigen, deren Eltern bei normalem pH gezüchtet wurden. Dies bedeutet, dass sich eine rasche generationsübergreifende Akklimatisierung an die saure Umgebung einstellte. Die Natriumzusammensetzung der Schalen kann ein neues Licht auf die Mechanismen werfen, die für eine günstige transgenerative Akklimatisierung verantwortlich sind. Unabhängig von der Belastung der Eltern nahm die Menge des in die Schalen eingebauten Na bei niedrigem pH-Wert zu, was auf eine aktive Entfernung überschüssiger Protonen durch den Na^+/H^+-Tauscher hinweist, von dem bekannt ist, dass er von dem Na^+-Gradienten abhängt. Jedoch zeigten die Schalen der Muscheln, welche in früheren Generationen niedrigem pH ausgesetzt waren, signifikant niedrigere Mengen von Na als diejenigen, welche diese Vorgeschichte nicht haben. Es scheint daher sehr wahrscheinlich, dass die Muscheln weniger aufwendige und mehr ATP-effiziente Ionenregelungsmechanismen anwenden können, um die pH-Homöostase in der kalzifizierenden Flüssigkeit nach der transgenerativen Akklimatisierung aufrechtzuerhalten. Unsere Ergebnisse deuten darauf hin, dass marine Muscheln mehr Möglichkeiten haben, sich zu akklimatisieren oder an die Ozeanversauerung bis zum Ende dieses Jahrhunderts anzupassen, als bisher angenommen.

Kapitel 6 zeigt die erste mehrjährige, hochauflösende Mn/Ca_{shell}-Zeitreihe der Süßwasser-Muschel, *Hyriopsis cumingii* (Lea, 1852) aus einem flachen eutrophischen See (Taihu-See, China). Die Mn/Ca_{shell} -Zeitreihen der beiden untersuchten Schalen zeigten eine bemerkenswerte Synchronität, nachdem sie mittels Wachstumsmusteranalyse in einen präzisen zeitlichen Zusammenhang gebracht worden waren. Es gibt eine große jährliche Variabilität der Mn/Ca_{shell}-Daten in den Jahren 2011-2015, wobei höhere Werte in den ersten drei Jahren auftreten. Mn/Ca_{shell} zeigte auch eine ausgeprägte Variabilität innerhalb eines Jahres mit Höchstwerten, die immer während des Sommers auftreten. Die hohe Synchroneitiät der Mn/Ca_{shell}-Zeitreihen bei zeitgleich lebenden Tieren zeigte, dass der Einbau von Mn in die Muschelschalen einer starken, nicht biologischen Steuerung unterliegt. Insbesondere fällt auf, dass die Mn/Ca_{shell}-Höchstwerte im Sommer synchron verlaufen, wenn reduzierende

Bedingungen unter der Sediment-Wasser-Grenzfläche (SWI) herrschten. Letztere führten zu höheren Gehalten an biologisch verfügbarem Mn^{2+} im Sedimentporenwasser und mehr organischen Partikeln (mit Mangan). Beides wurde von den Miesmuscheln rasch aufgenommen und Mn anschließend in ihre Schalen eingebaut. Daher kann Mn/Ca_{shell} gegebenenfalls als hochauflösender Proxy der Mobilität von Mn an der SWI dienen. Wie die vorliegende Studie zeigt, kann die Entschlüsselung geochemischer Eigenschaften von Muschelschalen dazu beitragen, Umweltveränderungen, die durch Eutrophierung hervorgerufen wurden, in aquatischen Ökosystemen retrospektiv zu überwachen.

Acknowledgements

Not displayed for reasons of data protection

Table of contents

List of figures

List of tables

Chapter 1

General introduction

1.1 Bivalve shells as environmental archives

Bivalve shells are becoming increasingly recognized as powerful tools in paleoenvironmental studies. Physicochemical properties of the ambient environment that prevailed during growth can be recorded by the shells for example in the form of variable growth increment widths (distances between consecutive growth lines) and various geochemical properties (e.g., Markich et al., 2002; Thébault et al., 2009; Holland et al., 2014). Three key characteristics make them extraordinary archives of environmental change.

First, periodic growth patterns can function as a unique time gauge, placing each shell portion into a precise temporal context and thereby permitting a precise temporal alignment of environmental proxy data. In particular, such growth patterns hold the potential to measure time at annual, seasonal, daily and even sub-daily scales (Fig. 1.1). Therefore, bivalve shells can provide time-constrained records of environmental change with unprecedented temporal resolution.

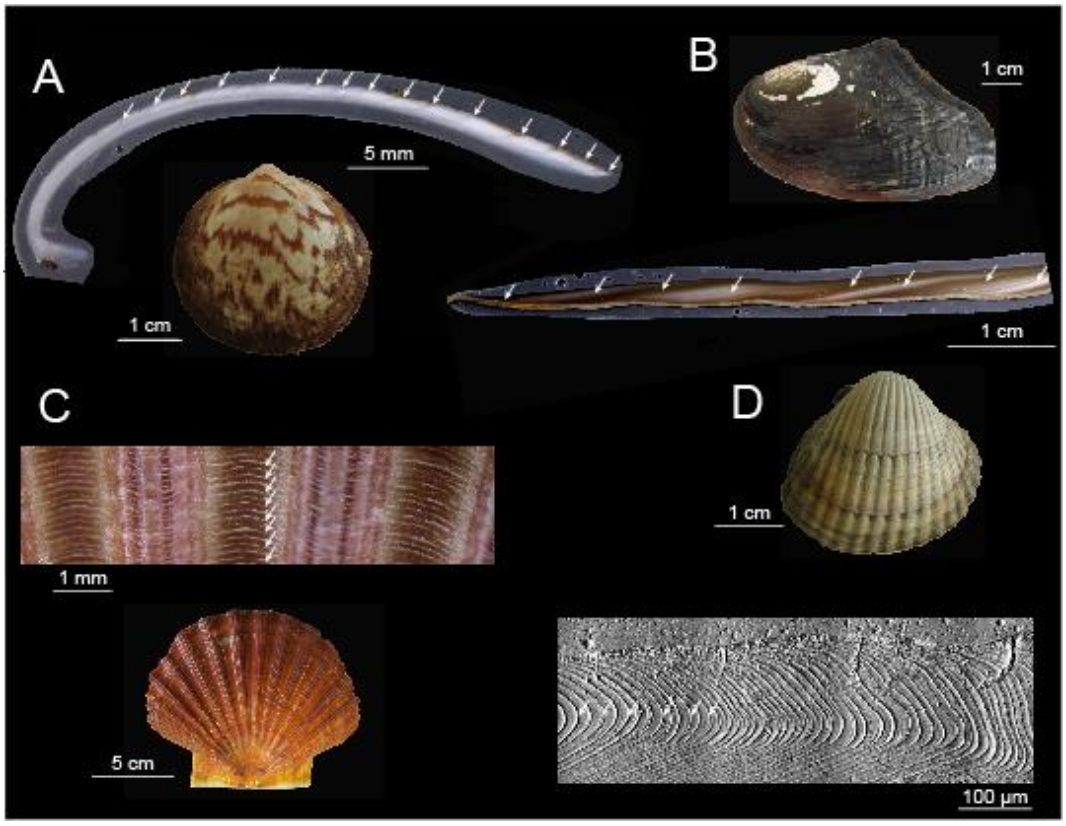

Fig. 1.1. Periodic growth patterns in bivalve shells. (A) Annual growth lines (indicated by white arrows) in the cross section of the dog cockle, *Glycymeris glycymeris*. (B) Seasonal growth bands (indicated by white arrows) in the cross-section of the triangle sail mussel, *Hyriopsis cumingii*. (C) Daily growth lines (indicated by white arrows in the surface of the great scallop, *Pecten maximus*. (D) Ultradian (sub-daily) growth lines (indicated by white arrows) in the cross-section of the common cockle, *Cerastoderma edule*.. Shells (A–C) were viewed under a stereomicroscope and D under a scanning electron microscopy.

Second, growth patterns in contemporaneous shells from the same locality are highly synchronous. It is therefore possible to string together annual growth increment width chronologies to construct a stacked chronology, permitting the reconstruction of environmental conditions over long time intervals. In this regard, shells of extremely long-lived bivalve species, for example *Arctica islandica* whose lifespan can exceed 500 years (Butler et al., 2013), are particularly valuable.

Third, bivalve mollusks have a very broad biogeographic distribution, extending from the deep sea to the intertidal zone, from the poles to the equator and from marine to freshwater habitats (Gosling, 2003). Such characteristic makes shells excellent archives for many aquatic settings. Moreover, bivalve shells occur abundantly in the fossil record and can be well preserved in sedimentary deposits (Steuber, 1996), providing a nearly inexhaustible resource for paleoenvironmental studies.

1.2 Bivalve shell formation

As demonstrated above, the prerequisite for the use of bivalve shells as environmental archives is the precise calendar dating by which proxy data can be temporally contextualized. It is therefore essential to gain a better understanding of the formation of periodic growth pattern in bivalves. Previous studies on *C. edule* (Richardson et al., 1980), *Ruditapes philippinarum* (Kim et al., 1999) and *Saxidomus purpuratus* (Kim et al., 2003) have shown that the periodicity of growth patterns is controlled by endogenous timekeeping mechanisms, so-called biological clocks (Rensing et al., 2001), which, in turn, are entrained by environmental and astronomical pacemakers (i.e., temperature, food availability, photoperiod and tides; Brockington and Clarke, 2001). Hence, biological clocks in conjunction with seasonal environmental stimuli may play a key role in determining the timing and length of the growing season (Schöne, 2008).

The underlying mechanisms by which bivalves build their shells, however, are far from being completely understood. In particular, it has never been resolved whether shell formation is an entirely extracellular process or partially intracellular process. As yet, two models have been developed. The matrix model suggests that shell mineralization takes place in the extrapallial fluid (EPF), a thin film of liquid between the calcifying shell and the outer mantle epithelium (Fig. 1.2), where the inorganic precipitation of calcium carbonate ($CaCO_3$) is facilitated by supersaturation of calcium and bicarbonate ions, and the crystallization of $CaCO_3$ is mediated by the organic matrix secreted from the outer epithelium (Bevelander and Nakahara, 1969; Wheeler, 1992). Thus, shell formation occurs extracellularly in the EPF according to the

matrix model. In contrast, the cellular model postulates that biomineralization is a partially intracellular process, i.e., shell crystals are formed in hemocytes in the hemolymph and then transported to the mineral front (Fig. 1.2; Mount et al., 2004; Zhang et al., 2012). Despite different mechanisms both models suggest that shell mineralization takes place in a microenvironment isolated from the ambient environment. This may be one reason why the shells are chemically different from abiogenic precipitates formed in the same water (Marin et al., 2012). More detailed information on the mechanisms involved in the formation of bivalve shells are reported in the following chapters where we consider that shell formation occurs in an extracellular EPF complying with the matrix model.

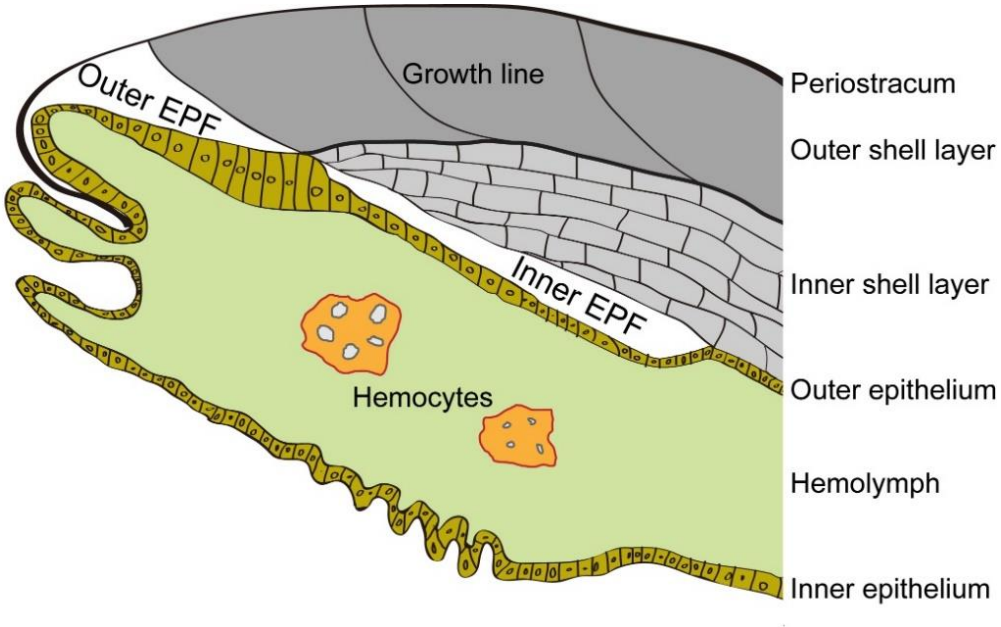

Fig. 1.2. Schematic longitudinal section through a bivalve which illustrates the shell edge and the mantle. EPF = Extrapallial fluid. For details refer to text. Modified from Wilbur and Saleuddin (1983).

1.3 Element impurities of bivalve shells as environmental proxies

Element impurities of bivalve shells potentially record physiochemical changes of the ambient environment during shell formation. Numerous characteristics of the environment – including but not limited to temperature, salinity, pH, hypoxia and redox potential, photoperiod, primary productivity and anthropogenic activities – have been derived from element impurities of the shells (Table 1.1), and a growing body of literature has been published since 1990s (Fig. 1.3). More recently, paleoenvironmental research concerning temporally resolved element records in bivalve shells has benefited greatly from technological advances in the field of *in situ* chemical analysis, in particular accurate and rapid element microanalysis via laser ablation

inductively coupled plasma mass spectrometry (LA-ICP-MS) which can extract uninterrupted element time-series at micro-meter resolution (reviewed in Müller and Fietzke, 2016).

Table 1.1 Overview (by no means exhaustive) of literature on quantitative reconstructions of past environmental conditions from the element signatures of bivalve shells. In most studies, such data are expressed as molar ratios relative to calcium.

Environmental conditions	Elements	References
Temperature	Sr/Ca, Mg/Ca, Li/Sr	Surge and Lohmann (2008); Mouchi et al. (2013); Yan et al. (2013); Füllenbach et al. (2015); Tynan et al. (2016)
Salinity	Na/Ca, B/Ca, Ba/Ca	Ishikawa and Ichikuni (1984); Roopnarine et al. (1998); Takesue et al. (2008); Poulain et al. (2015); Izzo et al. (2016)
pH	Na/Ca, U/Ca, Rare earth elements	Frieder et al. (2015); Zhao et al. (2017); Ponnurangam et al. (2016)
Photoperiod	Sr/Ca	Sano et al. (2012); Hori et al. (2015)
Hypoxia and redox potential	Mn/Ca	Ravera et al. (2007); Barats et al. (2008); Bolotov et al. (2015)
Primary productivity	Ba/Ca, Li/Ca, Mo/Ca; Mn/Ca	Stecher et al. (1996); Vander Putten et al. (2000); Lazareth et al. (2013); Thébault et al. (2009); Elliot et al. (2009); Barats et al. (2010); Thébault and Chauvaud (2013)
Seasonal upwelling	Mn/Ca; Ba/Ca	Langlet et al. (2007); Hatch et al. (2013)
Metal pollution	Pb/Ca, Cu/Ca, Fe/Ca, Cd/Ca, U/Ca, Zn/Ca	Schettler and Pearce (1996); Markich et al. (2002); Liehr et al. (2005); Pearce and Mann (2006); Dunca et al. (2009); Holland et al. (2014);
Anthropogenic activities	Na/Ca, Fe/Ca, U/Ca Rare earth elements	Markich et al. (2002); Holland et al. (2014); O'Neil and Gillikin (2014); Merschel and Bau (2015); Ponnurangam et al. (2016)

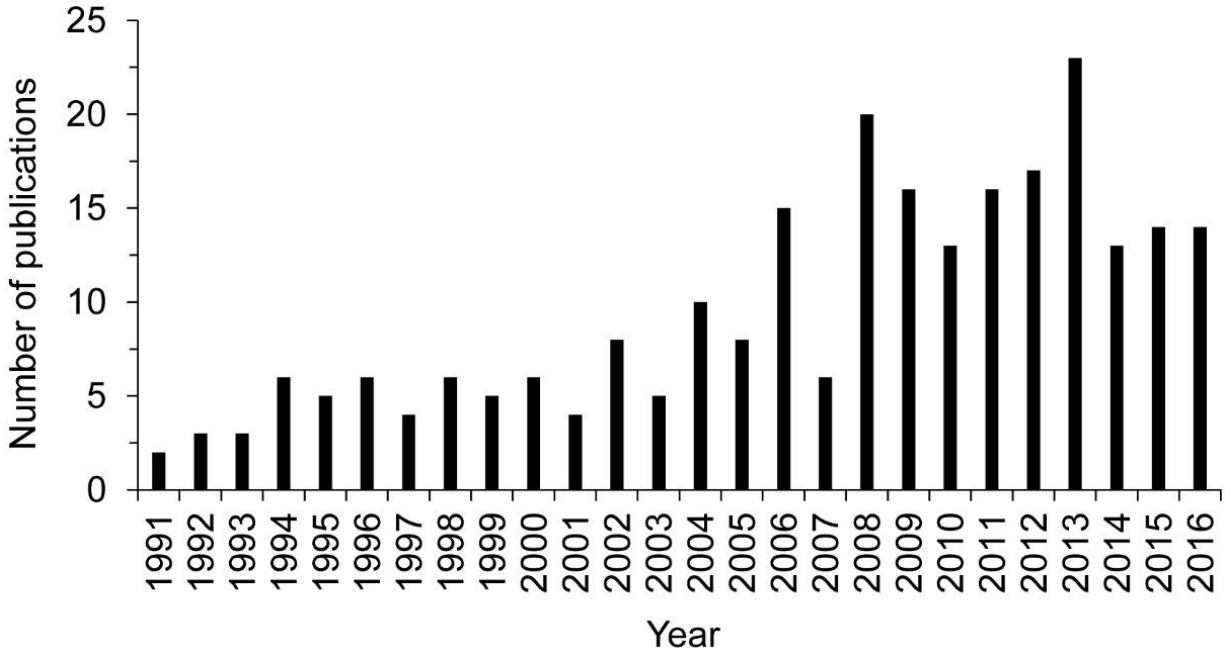

Fig. 1.3. Numbers of sclerochronological publications featuring the element composition of bivalve shells between 1991 and 2016. Data retrieved from Web of Science on 30 October 2016. Sharp rises in 2008 and 2013 can be attributed, at least in part, to two special issues from the 1st and 2nd International Sclerochronology Conferences published in journals of Geo-Marine Letters and Palaeogeography, Palaeoclimatology, Palaeoecology, respectively.

1.4 Challenges in the interpretation of element signatures of bivalve shells

Despite significant advances over the past two decades, unravelling environmental information from element signatures of bivalve shells remains an extremely challenging task. This is largely due to our limited knowledge of the processes involved in the incorporation of trace and minor elements into shells. A fundamental challenge confronting environmentalist and climatologist is to determine whether and to what extent physiological influences, in particular metabolic activity, growth rate and ontogenetic age, control the incorporation of trace and minor elements into the shells. More specifically, physiological influences can take place (1) during the uptake and transport of elements from the ambient environment (mainly water and food) to the calcifying front (i.e., EPF), where metabolic activity may discriminate elements (e.g., Cu, Zn, Mn) that play an essential role in metabolic functions and remove non-essential heavy metals (e.g., Pb, Cd) by various detoxification processes (Fig. 1.4), and (2) during the incorporation into shell carbonate. Growth rate which is closely linked to the rate of crystal growth and as such kinetics can exert a major control on element incorporation as well. Furthermore, species-specific differences should also be taken into account. In particular, marine bivalves are

considered osmoconformers while freshwater species are osmoregulators (Fig. 1.4). The latter needs to maintain a higher ionic concentration in the body fluids than prevailing in the ambient environment. Therefore, there is an urgent need to obtain a more comprehensive and better understanding of the mechanisms by which trace and minor elements are taken up by the bivalves and incorporated into the shells. Clearly, such work needs to be highly interdisciplinary, occurring at the interface between biology, ecology and geochemistry.

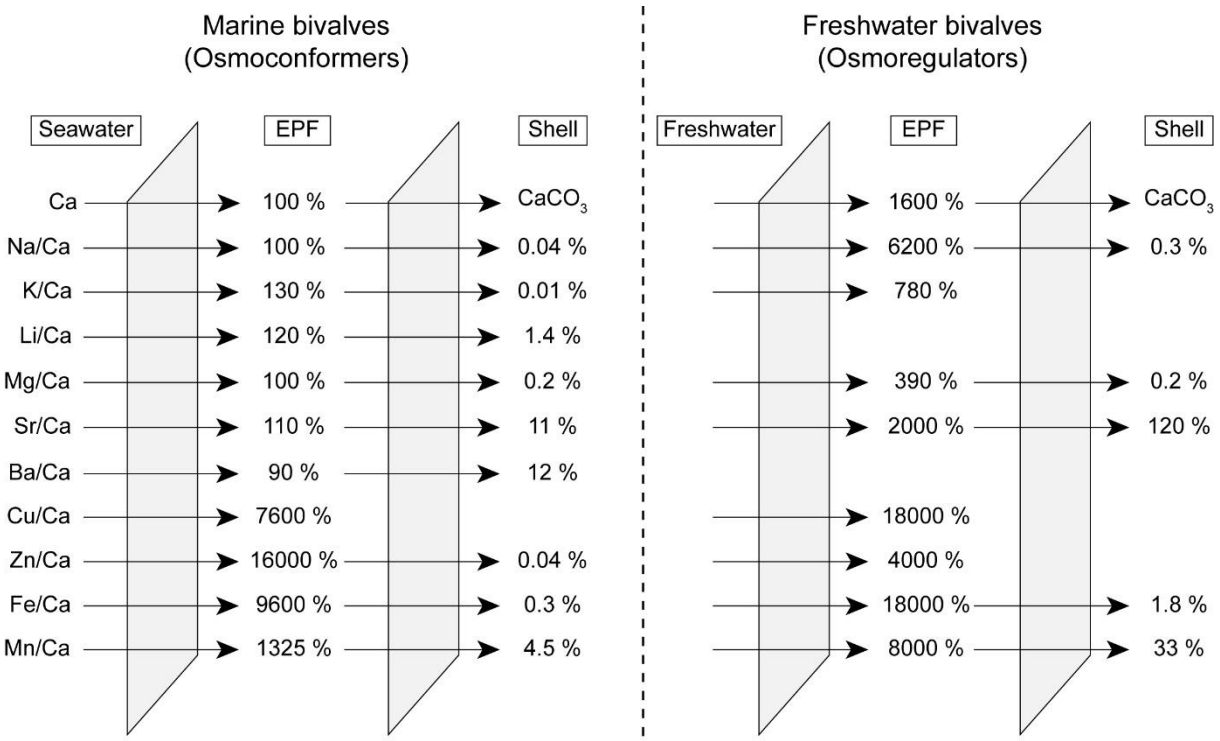

Fig. 1.4. Schematic illustrating the uptake and incorporation of trace and minor elements from the environment into bivalve shells. Species-specific differences between marine and freshwater bivalves are illustrated. Since shell formation takes place in the EPF and thus isolated from the ambient environment, the uptake and incorporation of any element into the shells can be regarded as a multi-stage process. For more details see text. Aside from Ba data adapted from Gillikin et al. (2006), values of other elements in seawater and EPF came from Wada and Fujinuki (1976). Data from shells from are by author of this thesis.

1.5 Aim of the research

Previous studies have suggested that physiological influences may blur environmental signals encoded in element signatures of bivalve shells (e.g., Gillikin et al., 2005; Schöne, 2008). As yet, however, little effort has been devoted to determine the degree to which the element content is physiologically influenced and to decipher the complexity of the incorporation of trace and minor elements into the shells. The present study aims to close these gaps of knowledge by conducting a series of laboratory and field experiments. The following aspects were addressed.

(1) Pathways of trace and minor elements taken up into the shells. It is commonly assumed that calcium and other divalent ions may share the same transport mechanisms because of similar electrochemical properties and ionic radii. If this is the case, then it would pave the way for deciphering how divalent ions are transported from the ambient environment to the calcifying front. Chapter 2 aims to test and verify this hypothesis by measuring the changes of the amounts of divalent ions (e.g., Mg^{2+}, Cu^{2+}, Mn^{2+}, Zn^{2+}, Sr^{2+}, Ba^{2+} and Pb^{2+}) incorporated into the shells of the freshwater bivalve, *Corbicula flumina* exposed to (1) different water Ca^{2+} levels, (2) two levels of lanthanum (a non-specific inhibitor of Ca^{2+} channels), (3) two levels of Verapamil (a voltage-dependent Ca^{2+} channel blocker), and (4) two levels of ruthenium red (a specific inhibitor of Ca^{2+}-ATPase). The results would help us to examine whether relevant ions are taken up by the bivalves from the environment as analogues of Ca^{2+} ion and quantify the influences of physiology on element impurities of the shells.

(2) Rigorous calibration of empirical relationships between environmental variables and the element composition of bivalve shells. Despite the curse of physiology, strontium- and barium-to-calcium ratios of bivalve shells have still received considerable attention as potential proxies for temperature and primary productivity (Table 1.1). However, most calibrations which have been conducted solely in the field are unable to rigorously exclude the potential interference of other environmental variables (e.g., Stecher et al., 1996; Bailey and Lear, 2006; Thébault et al., 2009). Hence, laboratory experiments are particularly important because they allow to determine the effect of a single environmental factor on the element incorporation. Chapter 3 presents the results of controlled experiments with the aim of rigorously determining the relationship between environmental variables and the element composition of the shells. Specimens of *C. fluminea* were grown under different combinations of water chemistry, temperature and food regimes for five weeks and the Sr/Ca and Ba/Ca ratios of the shells were measured. The results can help us to evaluate environmental influences on the incorporation of Sr and Ba into the shells and explore their potential as environmental proxies.

(3) The use of element signatures for estimating bivalve exposure to ocean acidification. Growing concerns about the impact of forthcoming ocean acidification on the calcifying organisms have intensified the search for geochemical proxies for ocean pH. The boron isotope signature ($\delta^{11}B$) and uranium-to-calcium ratio of coral aragonite and foraminiferal calcite have been explored as possible pH proxies (Levin et al., 2015). Frieder et al. (2014) demonstrated that U/Ca ratios in larval shells of *Mytilus*

californianus and *M. galloprovincialis* can serve as pH proxies, while Heinemann et al. (2012) suggested that the boron isotopic composition of *M. edulis* shells can record acid-base changes of the calcifying fluid rather than the ambient seawater. Such discrepancies can be attributed to the existence of different mechanisms responsible for shell formation at different life stages. Unlike larvae whose calcifying front may be directly exposed to the ambient environment (Waldbusser et al., 2014), the formation of juvenile and adult bivalve shells, following larval settlement and metamorphosis and the formation of the mantle tissue, occurs in the EPF. When subjected to lowered seawater pH, bivalves may implement compensatory mechanisms to maintain homeostasis at the calcifying front, making the development of a direct pH proxy from bivalve shells nearly impossible. On the other hand, the incorporation of sodium into the shells would increase if bivalves rely on the exchange of Na^+/H^+ to maintain pH homeostasis at the calcifying front. Chapter 4 investigates the influence of elevated pCO_2 and temperature on the sodium composition of the blue mussel, *M. edulis*, and the Yesso scallop, *Patinopecten yessoensis* with the aim of evaluating whether Na/Ca_{shell} holds the potential as a proxy of the acid-base and ionic regulation in the EPF. In particular, the chapter demonstrates that an integrated approach of combining Na/Ca_{shell} with the examination of the rate of shell formation may decipher the mechanisms by which bivalves respond to current and ongoing ocean acidification and warming.

(4) Can element signatures of bivalve shells provide information on epigenetic inheritance and evolution? It is well known that environmental stress experienced by the bivalves at one stage of life can generate carry-over effects at their subsequent life stages and also alter the response of their offspring in the next generation, the latter so-called transgenerational epigenetic effect (Youngson and Whitelaw, 2008). Such acclimation is of paramount importance for bivalves to cope with and survive harsh environmental conditions since it can take place over much short time frames. For example, Fitzer et al. (2014) reported that *M. edulis* following transgenerational to acidic seawater was no longer capable of precipitating aragonitic shells but only calcitic shells, probably because aragonite is more susceptible to dissolution than calcite (Mucci, 1983). If so, one would expect that the environmental information encoded in the shells in the form of various geochemical properties changes as the microstructure changes. Hence, special attention should be paid while exploring geochemical proxies in shells of short-lived bivalve species. Building on the findings of chapter 4, chapter 5 studies the transgenerational effects of ocean acidification on the sodium composition in the shell

of the Manila clam, *Ruditapes philippinarum*. Findings of this chapter can advance our understanding of the potential interference of epigenetic changes on the geochemical properties of bivalve shells.

(5) The deconvolution of environmental information from element profiles of bivalve shells. LA-ICP-MS can extract ultra-high resolution element time-series from the shells, and a growing body of *in situ* and satellite data in the field provides an exciting opportunity to recalibrate empirical proxies based on laboratory experiments. However, significant discrepancies between field studies and laboratory experiments are often evident. Aside from the interference of other environmental variables in the field, chapter 6 places more emphasis on the consideration of realistic field scenarios that bivalves inhabit. As a case study, multi-year, high-resolution manganese-to-calcium profiles in the shells of the freshwater bivalve, *Hyriopsis cumingii*, were measured by means of LA-ICP-MS. Environmental data were analyzed including temperature, dissolved oxygen, chlorophyll *a*, and Mn^{2+} concentrations in the water and phytoplankton in the overlying water column and redox potential levels and Mn^{2+} concentrations in the sediment pore water and organic matter. Findings of this chapter can lead to an improved understanding of environmental factors driving the incorporation of trace and minor elements into bivalve shells.

1.6 References

Bailey, T.R., Lear, C.H., 2006. Testing the effect of carbonate saturation on the Sr/Ca of biogenic aragonite: a case study from the River Ehen, Cumbria, UK. Geochem. Geophys. Geosyst. 7, Q03019.

Barats, A., Amouroux, D., Pécheyran, C., Chauvaud, L., Donard, O.F.X., 2008. High-frequency archives of manganese inputs to coastal waters (Bay of Seine, France) resolved by the LA-ICP-MS analysis of calcitic growth layers along scallop shells (*Pecten maximus*). Environ. Sci. Technol. 42, 86–92.

Barats, A., Amouroux, D., Pécheyran, C., Chauvaud, L., Donard, O.F.X., 2010. Spring molybdenum enrichment in scallop shells: a potential tracer of diatom productivity in temperate coastal environments (Brittany, NW France). Biogeosciences 7, 233–245.

Bevelander, G., Nakahara, H., 1969. An electron microscope study of the formation of the nacreous layer in the shell of certain bivalve molluscs. Calcif. Tissue Res. 3, 84–92.

Bolotov, J.N., Pokrovsky, O.S., Auda, Y., Bespalaya, J.V., Vikhrev, I.V., Gofarov, M.Y., Lyubas, A.A., Viers, J., Zouiten, C., 2015. Trace element composition of freshwater pearl mussels *Margaritifera* spp. across Eurasia: testing the effect of species and geographic location. Chem. Geol. 402, 125–139.

Brockington, S., Clarke, A., 2001. The relative influence of temperature and food on the metabolism of a marine invertebrates. J. Exp. Mar. Biol. Ecol. 258, 87–99.

Butler, P.G., Wanamaker, A.D., Scourse, J.D., Richardson, C.A., Reynolds, D.J., 2013. Variability of marine climate on the North Icelandic Shelf in a 1357 – year proxy archive based on growth increments in the bivalve *Arctica islandica*. Palaeogeogr. Palaeoclimatol. Palaeoecol. 373, 141–151.

Dunca, E., Mutvei, H., Göransson, P., Mörth, C.-M., Schöne, B.R., Whitehouse, M.J., Elfman, M., Baden, S.P., 2009. Using ocean quahog (*Arctica islandica*) shells to reconstruct palaeoenvironment in Öresund, Kattegat and Skaggerak, Sweden. Int. J. Earth Sci. 98, 3–17.

Elliot, M., Welsh, K., Chilcott, C., McCulloch, M., Chappell, J., Ayling, B., 2009. Profiles of trace elements and stable isotopes derived from giant long-lived *Tridacna gigas* bivalves: potential applications in paleoclimate studies. Palaeogeogr. Palaeoclimatol. Palaeoecol. 280, 132–142.

Frieder, C.A., Gonzalez, J.P., Levin, L.A., 2014. Uranium in larval shells as a barometer of molluscan ocean acidification exposure. Environ. Sci. Technol. 48, 6401–6408.

Füllenbach, C.S., Schöne, B.R., Mertz-Kraus, R., 2015. Strontium/lithium ratio in aragonitic shells of *Cerastoderma edule* (Bivalvia) – A new potential temperature proxy for brackish environments. Chem. Geol. 417, 341–355.

Gillikin, D.P., Dehairs, F., Lorrain, A., Steenmans, D., Baeyens, W., André, L., 2006. Barium uptake into the shells of the common mussel (*Mytilus edulis*) and the potential for estuarine paleo-chemistry reconstruction. Geochim. Cosmochim. Acta. 70, 395–407.

Gillikin, D.P., Lorrain, A., Navez, J., Taylor, J.W., André, L., Keppens, E., Baeyens, W., Dehairs, F., 2005. Strong biological controls on Sr/Ca ratios in aragonitic marine bivalve shells. Geochem. Geophys. Geosyst. 6, Q05009.

Gosling, E., 2003. An Introduction to Bivalves. Bivalve Molluscs: Biology, Ecology and Culture. Fishing News Books, Blackwell, Oxford.

Hatch, M.B., Schellenberg, S.A., Carter, M.L., 2013. Ba/Ca variations in the modern intertidal bean clam *Donax gouldii*: An upwelling proxy? Palaeogeogr. Palaeoclimatol. Palaeoecol. 373, 98–107.

Heinemann, A., Fietzke, J., Melzner, F., Böhm, F., Thomsen, J., Garbe-Schönberg, D., Eisenhauer, A., 2012. Conditions of *Mytilus edulis* extracellular body fluids and shell composition in a pH-treatment experiment: acid-base status, trace elements and $\delta^{11}B$. Geochem. Geophys. Geosyst. 13.

Holland, H.A., Schöne, B.R., Marali, S., Jochum, K.P., 2014. History of bioavailable lead and iron in the Greater North Sea and Iceland during the last millennium – A bivalve sclerochronological reconstruction. Mar. Poll. Bull. 87, 104–116.

Ishikawa, M., Ichikuni, M., 1984. Uptake of sodium and potassium by calcite. Chem. Geol. 42, 137–146.

Izzo, C., Manetti, D., Doubleday, Z.A., Gillanders, B.M., 2016. Calibrating the element composition of *Donax deltoids* shells as a palaeo-salinity proxy. Palaeogeogr. Palaeoclimatol. Palaeoecol. doi: 10.1016/j.palaeo.2016.11.038

Kim, W.S., Huh, H.T., Lee, J.H., Rumohr, H., Koh, C.H., 1999. Endogenous circatidal rhythm in the Manila clam *Ruditapes phillippinarum* (Bivalvia: Veneridae). Mar. Biol. 134, 107–112.

Kim, W.S., Huh, H.T., Je, J.G., Ham, K.N., 2003. Evidence of two- clock control of endogenous rhythm in the Washington clam, *Saxidomus purpuratus*. Mar. Biol. 142, 305–309.

Langlet, D., Alleman, L.Y., Plisnier, P.D., Hughes, H., André, L., 2007. Manganese content records seasonal upwelling in Lake Tanganyika mussels. Biogeosciences 4, 195–203.

Lazareth, C.E., Vander Putten, E., André, L., Dehairs, F., 2003. High-resolution trace element profiles in shells of the mangrove bivalve *Isognomon ephippium*: a record of environmental spatiotemporal variations? Estuar. Coast. Shelf Sci. 57, 1103–1114.

Levin, L.A., Hönisch, B., Frieder, C.A., 2015. Geochemical proxies for estimating faunal exposure to ocean acidification. Oceanography 28, 62–73.

Liehr, G.A., Zettler, M.L., Leipe, T., Witt, G., 2005. The ocean quahog *Arctica islandica* L.: a bioindicator for contaminated sediments. Mar. Biol. 147, 671–679.

Marin, F., Le Roy, N., Marie, B., 2012. The formation and mineralization of mollusk shell. Front. Biosci. S4, 1099–1125.

Markich, S.J., Jeffree, R.A., Burke, P.T., 2002. Freshwater bivalve shells as archival indicators of metal pollution from a copper-uranium mine in tropical northern Australia. Environ. Sci. Technol. 36, 821–832.

Masako, H., Sano, Y., Ishida, A., Takahata, N., Shirai, K., Watanabe, T., 2015. Middle Holocene daily light cycle reconstructed from the strontium/calcium ratios of a fossil giant clam shell. Sci. Rep. 5, 8734.

Merschel, G., Bau, M., 2015. Rare earth elements in the aragonitic shell of freshwater mussel Corbicula fluminea and the bioavailability of anthropogenic lanthanum, samarium and gadolinium in river water. Sci. Total. Environ. 533, 91–101.

Mouchi, V., De Rafélis, M., Lartaud, F., Fialin, M., Verrecchia, E., 2013. Chemical labelling of oyster shells used for time-calibrated high-resolution Mg/Ca ratios: a tool for estimation of past seasonal temperature variations. Palaeogeogr. Palaeoclimatol. Palaeoecol. 373, 66–74.

Mount, A.S., Wheeler, A.P., Paradkar, R.P., Snider, D., 2004. Hemocyte-mediated shell mineralization in the Eastern Oyster. Science 304, 297–300.

Mucci, A., 1983. The solubility of calcite and aragonite in seawater at various salinities, temperatures, and one atmosphere total pressure. Am. J. Sci. 283, 780–799.

Müller, W., Fietzke, J., 2016. The role of LA-ICP-MS in palaeoclimate research. Elements 12, 329–334.

O'Neil, D.D., Gillikin, D.P., 2014. Do freshwater mussel shells record road-salt pollution? Sci. Rep. 4, 6.

Pearce, N.J.G., Mann, V.L., 2006. Trace metal variations in the shells of *Ensis siliqua* record pollution and environmental conditions in the sea to the west of mainland Britain. Mar. Pollut. Bull. 52, 739–755.

Ponnurangam, A., Bau, M., Brenner, M., Koschinsky, A., 2016. Mussel shells of *Mytilus edulis* as bioarchives of the distribution of rare earth elements and yttrium in seawater and potential impact of pH and temperature on their partitioning behavior. Biogeosciences 13, 751–760.

Poulain, C., Gillikin, D.P., Thébault, J., Munaron, J.M., Bohn, M., Robert, R., Paulet, Y.-M., Lorrain, A., 2015. An evaluation of Mg/Ca, Sr/Ca and Ba/Ca ratios as environmental proxies in aragonite bivalve shells. Chem. Geol. 396, 42–50.

Ravera, O., Beone, G.M., Trincherini, P.R., Riccardi, N., 2007. Seasonal variations in metal content of two *Unio pictorum mancus* (Mollusca, Unionidae) populations from two lakes of different trophic state. J. Limnol. 66, 28–39.

Rensing, L., Meyer-Grahle, U., Ruoff, P., 2001. Biological timing and the clock metaphor: oscillatory and hourglass mechanisms. Chronobiol. Int. 18, 329–369.

Richardson, C.A., Crisp, D.J., Runham, N.W., 1980. An endogenous rhythm in shell deposition in *Cerastoderma edule*. J. Mar. Biol. Assoc. UK. 60, 991–1004.

Roopnarine, P.D., Fitzgerald, P., Byars, G., Kilb, K., 1988. Coincident boron profiles of bivalves from the Gulf of California: implications for the calculation of paleosalinities. Palaios 13, 395–400.

Sano, Y., Kobayashi, S., Shirai, K., Takahata, N., Matsumoto, K., Watanabe, T., Sowa, K., Iwai. K., 2012. Past daily light cycle recorded in the strontium/calcium ratios of giant clam shells. Nat. Comm. 3, 761.

Schettler, G., Pearce, N.J.G., 1996. Metal pollution recorded in extinct *Dreissena polymorpha* communities, Lake Breitling, Havel Lakes system, Germany: a laser ablation inductively coupled plasma mass spectrometry study. Hydrobiology 317, 1–11.

Schöne, B.R., 2008. The curse of physiology – Challenges and opportunities in the interpretation of geochemical data from mollusk shells. Geo-Mar. Lett. 28, 269–285.

Surge, D., Lohmann, K.C., 2008. Evaluating Mg/Ca ratios as a temperature proxy in the estuarine oyster, *Crassostrea virginica*. J. Geophys. Res. 113.

Stecher, H.A., Krantz, D.E., Lord, C.J., Luther, G.W., Bock, K.W., 1996. Profiles of strontium and barium in *Mercenaria mercenaria* and *Spisula solidissima* shells. Geochim. Cosmochim. Acta. 60, 3445-3456.

Steuber, T., 1996. Stable isotope sclerochronology of rudist bivalves: growth rates and Late Cretaceous seasonality. Geology 24, 315–318.

Takesue, R.K., Bacon, C.R., Thompson, J.K., 2008. Influences of organic matter and calcification rate on trace elements in aragonite estuarine bivalve shells. Geochimica. Cosmochimica. Acta. 72, 5431–5445.

Thébault, J., Chauvaud, L., 2013. Li/Ca enrichments in great scallop shells (*Pecten maximus*) and their relationship with phytoplankton blooms. Palaeogeogr. Palaeoclimatol. Palaeoecol. 373, 108–122.

Thébault, J., Chauvaud, L., L'Helguen, S., Clavier, J., Barats, A., Jacquet, S., Pécheyran, C., Amouroux, D., 2009. Barium and molybdenum records in bivalve shells: Geochemical proxies for phytoplankton dynamics in coastal environments? Limnol. Oceanogr. 54, 1002-1014.

Tynan, S., Opdyke, B.N., Walczak, M., Eggins, S., Dutton, A., 2016. Assessment of Mg/Ca in *Saccostrea glomerata* (the Sydney rock oyster) shell as a potential temperature record. Palaeogeogr. Palaeoclimatol. Palaeoecol. doi: org/10.1016/j.palaeo.2016.08.009

Vander Putten, E., Dehairs, F., Keppens, E., Baeyens, W., 2000. High resolution distribution of trace elements in the calcite shell layer of modern *Mytilus edulis*: Environmental and biological controls. Geochim. Cosmochim. Acta. 64, 997-1011.

Wada, K., Fujinuki, T., 1976. Biomineralization in bivalve molluscs with emphasis on the chemical composition of the extrapallial fluid. In Bryan, N.M., Wilbur, K.M. (eds), Mechanisms of Mineralization in the Invertebrates and Plants. University of South Carolina Press, Georgetown, 175–190.

Waldbusser, G.G., Hales, B., Langdon, C.J., Haley, B.A., Schrader, P., Brunner, E.L., Gray, M.W., Miller, C.A., Gimenez, I., 2014. Saturation-state sensitivity of marine bivalve larvae to ocean acidification. Nat. Clim. Change. 5, 273–280.

Wheeler, A.P., 1992. Mechanisms of molluscan shell formation. In: Bonucci, E. (Ed.), Calcification in biological systems. CRC press, Boca Raton, FL, p179-216.

Wilbur, K.M., Saleuddin, A.S.M., 1983. Shell formation. In Saleuddin, A. S. M. & K. M. Wilbur (eds) The Mollusca 4. Physiology. Academic Press, New York.

Yan, H., Shao, D., Wang, Y., Sun, L., 2013. Sr/Ca profile of long-lived *Tridacna gigas* bivalves from South China Sea: A new high-resolution SST proxy. Geochim. Gosmochim. Acta. 112, 52–65.

Youngson, N.A., Whitelaw, E., 2008. Transgenerational epigenetic effects. Annu. Rev. Genomics. Hum. Genet. 9, 233–257.

Zhang, G., Fang, X., Guo, X., Li, L., Luo, R., Xu, F., Yang, P., Zhang, L.,Wang, X., Qi, H., Xiong, Z., Que, H., Xie, Y., Holland, P.W.H., Paps, J., Zhu, Y.,Wu, F., Chen, Y.,Wang, J., Peng, C., Meng, J., Yang, L., Liu, J., Wen, B., Zhang, N., Huang, Z., Zhu, Q., Feng, Y., Mount, A., Hedgecock, D., Xu, Z., Liu, Y., Domazet-Lošo, T., Du, Y., Sun, X., Zhang, S., Liu, B., Cheng, P., Jiang, X., Li, J., Fan, D., Wang, W., Fu, W., Wang, T., Wang, B., Zhang, J., Peng, Z., Li, Y., Li, N., Wang, J., Chen, M., He, Y., Tan, F., Song,

X., Zheng, Q., Huang, R., Yang, H., Du, X., Chen, L., Yang, M., Gaffney, P.M., Wang, S., Luo, L., She, Z., Ming, Y., Huang,W., Zhang, S., Huang, B., Zhang, Y., Qu, T., Ni, P., Miao, G.,Wang, J.,Wang, Q., Steinberg, C.E.W., Wang, H., Li, N., Qian, L., Zhang, G., Li, Y., Yang, H., Liu, X., Wang, J., Yin, Y.,Wang, J., 2012. The oyster genome reveals stress adaptation and complexity of shell formation. Nature 490, 49–54.

Zhao, L., Schöne, B.R., Mertz-Kraus, R., Yang, F., 2017. Insights from sodium into the impacts of elevated pCO_2 and temperature on bivalve shell formation. J. Exp. Mar. Biol. Ecol. 486, 148–154.

Chapter 2

Delineating the role of calcium in shell formation and elemental composition of Corbicula fluminea *(Bivalvia)*

Published in Hydrobiologia

Liqiang Zhao[1], Bernd R. Schöne[1], Regina Mertz-Kraus[1]

[1] Institute of Geosciences, University of Mainz, Joh.-J.-Becher-Weg 21, 55128 Mainz, Germany

Author contribution

Concept: LZ, BRS

Execution: LZ

Data collection and analysis: LZ, RMK

Writing: LZ, BRS, RMK

Liqiang Zhao, Bernd R. Schöne, Regina Mertz-Kraus, 2016. Delineating the role of calcium in shell formation and elemental composition of *Corbicula fluminea* (Bivalvia). Hydrobiologia. doi: 10.1007/s10750-016-3037-7

Abstract

Calcium is one of the major constituent of bivalve shells. Other element impurities potentially record physicochemical changes of the ambient environment during growth. It is commonly assumed that Ca^{2+} and other divalent ions may share the same transport mechanisms because of similar ionic radii and electrochemical properties. However, little effort has been devoted to bolstering this hypothesis. Here, we investigated the effects of Ca^{2+} on shell formation and element composition of the freshwater bivalve, *Corbicula fluminea*. Our results showed that increasing aqueous Ca^{2+} levels from 3 to 6 mM did not facilitate shell production. However, the amounts of Mn, Cu and Pb incorporated into the shells significantly decreased, indicating the potential competition with Ca^{2+} in the same transport pathways. Furthermore, blocking the Ca^{2+}-channels by lanthanum and Verapamil significantly reduced Mn, Cu, Zn and Pb incorporation into the shells, and Mn/Ca_{shell} and Cu/Ca_{shell} decreased simultaneously when inhibiting the Ca^{2+}-ATPase by ruthenium red. However, the amounts of Mg, Sr and Ba incorporated into the shells were virtually unaffected, implying that intracellular Ca^{2+} transport mechanisms are not responsible for their incorporation into the shells. These findings help to decipher underlying mechanisms responsible for the element partitioning between the ambient water and the shells.

2.1. Introduction

Bivalve shells contain ultra-high resolution records of environmental change. During growth, physical and chemical changes of the ambient environment are preserved in the shells in the form of variable growth increment widths as well as geochemical and microstructural properties (Schöne, 2013). By using periodic shell growth patterns as a time gauge, environmental proxy data can be placed in a precise temporal context. Furthermore, bivalve mollusks have a broad biogeographic distribution and inhabit a variety of freshwater, brackish and marine habitats (Gosling, 2003), and fossil shells are abundant and often well-preserved in sedimentary settings. Therefore, shells of bivalves can serve as an excellent archive of paleoenvironmental change. Since shell growth is highly synchronous among contemporaneous specimens, it is possible to construct a stacked chronology by combining annual growth increment time-series. In particular, a combination of chronological and geochemical data from the shells can permit the reconstruction of environmental conditions over long time intervals (e.g., Black et al., 2008; Wanamaker et al., 2009; Krause-Nehring et al., 2012).

Despite significant advances in bivalve sclerochronology during the last decade, unraveling environmental histories from the shells is still more challenging than in the case of corals and other calcifiers. A fundamental challenge lies in the complexity of shell production. Biomineralization processes of the shells are far from being completely understood. However, it is commonly accepted that shell mineralization takes place in the extrapallial space (EPS), where crystallization is mediated by the organic matrix secreted from the outer mantle epithelium and facilitated by the supersaturation of calcium carbonate ($CaCO_3$) in the EPS (Wheeler, 1992). While our current understanding of the mechanisms underlying dissolved inorganic carbon (DIC) assimilation for shell mineralization and its responses to changes in aqueous carbonate chemistry is increasing (reviewed in McConnaughey & Gillikin, 2008), little effort has been devoted to teasing out the underlying processes involved in the uptake and incorporation of calcium into the shells aside from the general pathways of Ca^{2+} taken up into the EPS. Presumably, its basic pathway is from the external medium into the hemolymph via the gills and the inner mantle epithelium and possibly the gut, then into the EPS, and ultimately into the crystal lattice (Marin et al., 2012). As schematically illustrated in Fig. 2.1, Ca^{2+} transport across the interfaces of water-hemolymph and hemolymph-EPS can take place through three major pathways, namely an intercellular pathway driven by passive diffusion or an intracellular pathway driven by either Ca^{2+}-ATPase or Ca^{2+}-channel. In the outer mantle epithelium, the transport of Ca^{2+} into the EPS and the excretion of H^+ from the EPS are

intricately linked (McConnaughey & Gillikin, 2008). In particular, Ca^{2+}-ATPase likely plays a dual role in this regard, i.e., the enzyme transports Ca^{2+} into the EPS in exchange for H^+, thereby simultaneously increasing the mineral saturation state and alkalinizing the calcifying fluid which ultimately facilitates the precipitation of $CaCO_3$. Yet, although such enzyme has been localized on molluscan calcifying epithelia (Fan et al., 2007), it is still not clear how much of Ca^{2+} taken up into the EPS is transported through the Ca^{2+}-ATPase. A more detailed understanding of the transport mechanisms and pathways of Ca^{2+} to the site of calcification is therefore essential.

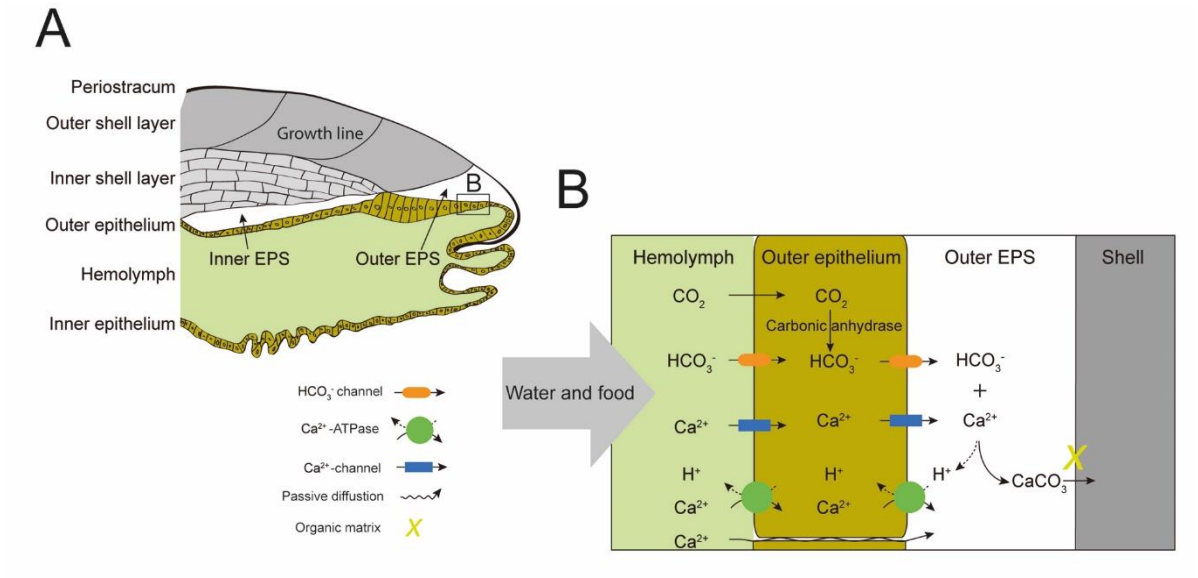

Fig. 2.1. (A) Schematic longitudinal section through a bivalve revealing the mantle and the shell edge. (B) Simplified shell formation. Three pathways by which Ca^{2+} is transported through the outer mantle epithelium into the EPS are schematically illustrated: an intracellular diffusive pathway (passive diffusion), an intracellular Ca^{2+}-ATPase pathway, and an intracellular Ca^{2+}-channel pathway. Gray arrow indicates the source of Ca^{2+} in the hemolymph is from water and food. Aside from the ambient environment, respiratory CO_2 can also be catalyzed into HCO_3^- by carbonic anhydrase. In the EPS, the (inorganic) precipitation of $CaCO_3$ ($Ca^{2+} + HCO_3^- \rightarrow CaCO_3 + H^+$) takes place and subsequently, the crystallization of $CaCO_3$ is mediated by the organic matrix. Protons (H^+ ions) generated during $CaCO_3$ precipitation are, at least in part, pumped out of the EPS by the Ca^{2+}-ATPase. EPS = extrapallial space. Modified from Wilbur and Saleuddin (1983) and Marin et al. (2012).

Trace and minor elements of bivalve shells can potentially serve as proxies of past environmental change. Of particular interest are divalent cations which can substitute calcium in the crystal lattice because their ionic radii and electrochemical properties are similar to that of Ca^{2+}. In particular Sr^{2+} and Ba^{2+} are best accommodated in the crystal structure of aragonite and Mg^{2+} of calcite (Kastner, 1999). Nevertheless, interpreting trace and minor element signatures of the shells remains a very challenging task because elemental incorporation

processes are strongly influenced by vital and kinetic effects (e.g., Gillikin et al., 2005; Schöne et al., 2010, 2011). Despite widespread awareness of these factors, only a few studies have attempted to disentangle how they work (e.g., Carré et al., 2006; Shirai et al., 2014), and to the best of our knowledge, little attention has so far been paid to the potential impacts of Ca^{2+} on the incorporation of trace and minor elements, specifically divalent cations with similar ionic radii. The latter are potentially taken up by the bivalves from the ambient water as analogues of Ca^{2+} (Simkiss & Taylor, 1989; Markich & Jeffree, 1994; Qiu et al., 2005), i.e., they may share the same transport systems and, accordingly, compete for all available binding sites. It is therefore conceivable that Ca^{2+} could influence the incorporation of other divalent cations into the shells, but the extent to which it occurs remains unknown. Yet, such knowledge may pave the way for delineating the transport mechanisms of trace and minor elements incorporated into the shells and disentangling the driving mechanisms of the element variability in the shells.

Here, we present the results from controlled laboratory experiments which evaluate the effects of calcium and its metabolic inhibitors on shell production and elemental composition. To our knowledge, this study is the first to simultaneously address the possible role of calcium in shell mineralization and the incorporation of trace elements into the shells. We deliberately selected the bivalve, *Corbicula fluminea* (Müller, 1774) (Bivalvia, Corbiculidae) as a model organism because of its broad biogeographic distribution and environmental tolerance (McMahon, 1983). Its aragonitic shell is subdivided into an inner shell layer (ISL: complex crossed-lamellar microstructure) and outer shell layer (OSL: crossed-lamellar microstructure) (Fig. 2.1; Prezant & Tan-Tiu, 1985). Findings of the present study contribute to a better understanding of the processes involved in elemental incorporation into aragonitic shells of freshwater bivalves.

2.2. Materials and methods

2.2.1. Bivalve collection and maintenance

Specimens of the Asian clam *C. fluminea* (22–24 mm shell length) were collected from a small creek near Kandel (49°4’33.61” N, 8°12’39.78” E), Rhineland-Palatinate, Germany. Upon arrival at the Institute of Geosciences, University of Mainz, they were initially maintained in 120-L tank with circulating water at 22-23 °C for one week. The temperature during acclimation is comparable to that of the water in the creek at the sampling day (21.4 °C; 18 July 2015). The photoperiod was set at a 14:10 light-dark cycle. Bivalves were fed every two days with the microalgae *Chlorella vulgaris* Beijerinck, 1890 (10,000 cells/ml). No mortality was observed prior to the experiment.

2.2.2. Experimental setup

After one week of acclimation, bivalves were randomly assigned to 10 L experimental aquaria at a density of fifteen specimens per aquarium. To accurately identify the newly formed shell portion during the experiment, they were immersed in a 150 mg/L calcein solution for three hours (Thébault et al., 2006) and returned to the respective aquarium. Calcein is a fluorescent dye which can be incorporated into the biomineral and fluoresce bright green when viewed under a UV-light microscope (Kaehler & McQuaid, 1999). During the following four weeks, bivalves were reared in three sets of experiments. In the first set of experiments, four nominal Ca^{2+} concentrations in the ambient water (3, 4, 5 and 6 mM) were simulated by adding a stock solution of $CaCl_2$. The minimum and maximum nominal Ca^{2+} concentrations (i.e., 3 and 6 mM) are comparable to those observed in the creek (i.e., 2.7 mM and 6.5 mM; measured in this study). In the second set of experiments, bivalves were exposed to lanthanum (1 and 10 µM), a nonspecific inhibitor of Ca^{2+}-channels (Verbost et al., 1989), or Verapamil (0.1 and 1 µM), a voltage-dependent Ca^{2+}-channel blocker (Guerrero & Martin, 1984). Ruthenium red (0.1 and 1 µM) was used in the third set of experiments as a specific inhibitor of Ca^{2+}-ATPase (Watson et al., 1971). The 3 mM Ca^{2+} treatment in the first set of experiments was used as the control for the latter two sets given that its Ca^{2+} concentration is close to that of the natural habitat (i.e., 2.7 mM). Exposure to high levels of lanthanum (10 µM), Verapamil (1µM) and ruthenium red (1 µM) did not cause shell closure and other adverse reactions, specifically termination of water pumping activity.

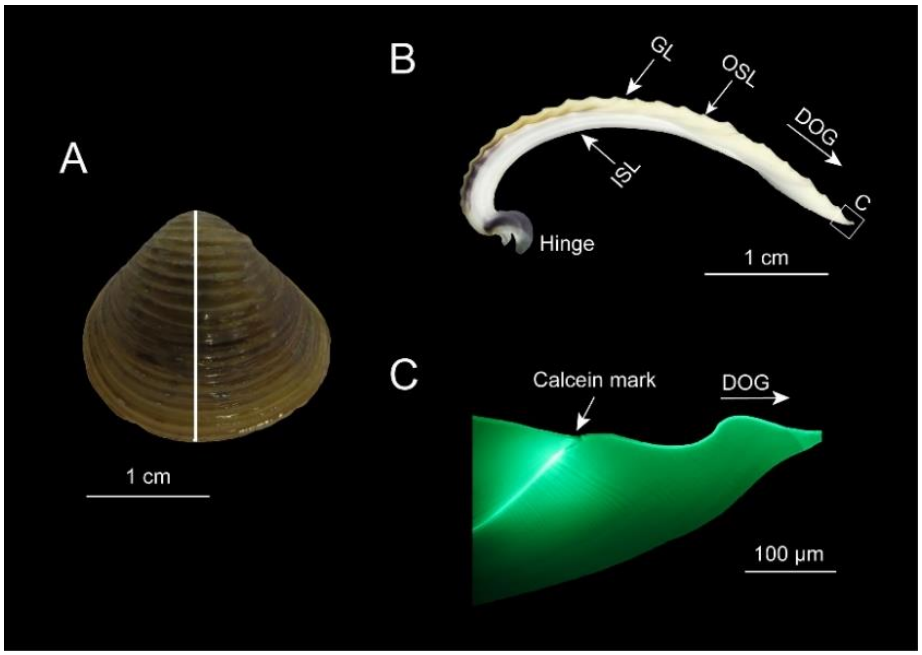

Fig. 2.2. Shell of *Corbicula fluminea*. (A) Outer shell surface of the left valve. A 3 mm-thick section was cut from the shell along the axis of maximum growth (white line). (B) Cross-section of the shell showing major shell structures. GL = growth line; ISL = inner shell layer, OSL = outer shell layer; DOG = direction of growth. (C) Magnification of the outer shell margin revealing a light calcein mark and newly formed shell portion.

2.2.3. Chemical analysis of the water

Calcium concentration of the water samples was determined by a Spectro CIROS Version^{SOP} inductively coupled plasma – optical emission spectrometer (ICP-OES) at the Institute of Geosciences, University of Mainz. Calcium standard solutions were prepared from Roti® Star certified single element reference solution. Based on five measurements of each external standard solution, relative standard deviation (RSD) was better than 1 RSD%. Accuracy determined by Roth Solution X multi element standard solution Lot W54710 was better than 3 %.

2.2.4. Shell preparation and analysis

Ten specimens from each aquarium were randomly selected for analysis. After thawing at room temperature, the whole soft tissues were removed from the shell and dried to constant mass at 50 °C for 48 h. The condition index (CI) of each specimen was calculated following the ratio method of Lucas & Beninger (1985): CI = dry soft tissue mass (g)/air-dried shell mass (g) × 100. Afterwards, the left valve of each specimen was mounted on a plexiglass cube with a quick-drying plastic welder and covered with a protective layer of JB KWIK fast-drying metal epoxy resin. Along the axis of maximum growth (Fig. 2.2A), a three-millimeter-thick section was cut from each specimen using a low-speed saw (Buehler IsoMet 1000; 250 rpm). Shell sections were mounted on glass slides, ground on glass plates with 800 and 1200 grit SiC powder and polished with 1 µm Al_2O_3 powder.

For shell growth analysis, polished shell sections were subsequently examined using a fluorescent light microscope (Zeiss Axio Imager A1.m stereomicroscope equipped with a Zeiss HBO 100 mercury lamp). When a Zeiss filter set 38 (excitation wavelength, ~450-500 nm; emission wavelength, ~500-550 nm) was added to the optical path, calcein marks appeared as distinct green lines (Fig. 2.2C). Images of shell portions were taken using a Canon EOS 600D digital camera connected to the microscope. The newly formed shell portion of each specimen, i.e. shell increment between calcein mark and ventral margin, was measured using the free image processing software ImageJ (http: //rsbweb.nih.gov/ij). Afterwards, the average daily

shell growth rate of each specimen was calculated by dividing the experimental duration (28 days).

2.2.5. Chemical analysis of the shells

The polished shell section of each specimen was used for chemical analysis. Magnesium (Mg) manganese (Mn), copper (Cu), zinc (Zn), strontium (Sr), barium (Ba) and lead (Pb) were determined by means of laser ablation – inductively coupled plasma – mass spectrometry (LA-ICP-MS) in "spot" mode at the Institute of Geosciences, University of Mainz. In each shell, three discrete spot measurements were conducted in the newly formed shell portion, i.e., between the calcein mark and the ventral margin (Fig. 2.2C). Since the element signature is strongly linked to the shell ultrastructure, sampling was completed in the same shell layer, here the inner portion of the outer shell layer, and within structurally similar shell portions. Analyses were performed on an Agilent 7500ce quadrupole ICP-MS coupled to an ESI NWR193 ArF excimer laser ablation system equipped with the TwoVol^2 ablation cell. Ablation was achieved using a pulse repetition rate of 10 Hz, an energy density of ~2.5 J/cm^2 and a beam diameter of 55 µm. Backgrounds were measured for 15 s, followed by 20 s ablation time and 20 s wash out. Monitored isotopes were ^{26}Mg, ^{43}Ca, ^{55}Mn, ^{65}Cu, ^{66}Zn, ^{88}Sr, ^{137}Ba and ^{208}Pb. NIST SRM 610 (synthetic glass) was used as calibration material, applying the preferred values reported in the GeoReM database (http://georem.mpch-mainz.gwdg.de/, Application Version 18) (Jochum et al., 2005, 2011) as the "true" concentrations to calculate the element concentrations in the samples. NIST SRM 612 (synthetic glass), USGS BCR-2G (basalt glass) and MACS-3 (synthetic calcium carbonate) were analyzed as quality control materials (QCM) to monitor accuracy and reproducibility of the analyses. All reference materials were analyzed at the beginning and at the end of a sequence and after ca. 60 spots on the samples. For all materials, ^{43}Ca was used as internal standard. For the reference materials, we applied the Ca concentrations reported in the GeoReM database, and for the samples 56.03 wt. %., the stoichiometric CaO content of aragonite. The time-resolved signal was processed using the program GLITTER 4.4.1 (www.glitter-gemoc.com, Macquarie University, Sydney, Australia). Reproducibility expressed as the relative standard deviation based on repeated measurements of the QCM was always better than 3 % for NIST SRM 612 (N = 18), 4 % for USGS BCR-2G (N = 9) and 7 % for MACS-3 (N = 9). The measured Mg, Mn, Cu, Zn, Sr, Ba and Pb concentrations of NIST SRM 612 agree within 17 %, 1.5 %, 0.6 %, 4.1 %, 1.3 %, 2.8 % and 2.2 % with the preferred values of the GeoReM database and within 12.1 %, 1.4 %, 12 %, 32 %,

0.7 %, 1.5 % 3.0 % for USGS BCR-2G, and within 3.2 %, 2.7 %, 2.5 %, 9.5 %, 4.1 %, 10.1 % and 14.0 % with the preliminary reference values for USGS MACS-3 (personal communication S. Wilson, USGS, in Jochum et al. 2012), respectively. The larger deviation in Cu and Zn of BCR-2G can be explained by polyatomic interferences on masses 65 and 66 by TiO^+ and $MgAr^+$. Minimum detection limits were 0.70 µg/g, 0.15 µg/g, 0.26 µg/g, 0.19 µg/g, 0.012 µg/g, 0.063 µg/g, and 0.016 µg/g for Mg, Mn, Cu, Zn, Sr, Ba and Pb.

2.2.6. Statistical analysis

Given that the incorporation of many trace elements into the shell can occur with a short time lag, typically spanning hours to several days (Jeffree et al., 1995; Thébault et al., 2009), so that the sample spot closest to the calcein mark may still reflect the control element signature. Therefore, only the data collected from the two laser spots closest to the ventral margin were chosen for statistical analyses. Prior to the analysis, normality of the data was tested using the Shapiro–Wilk's test and homogeneity of variance by means of the Levene's *F*–test using the software IBM SPSS Statistics 19.0. One-way analysis of variance (ANOVA) was carried out to evaluate whether the manipulations from each set of experiments significantly affect the rate of shell production and the elemental contents. Statistically significant difference was set at $p \leq 0.05$.

2.3. Results

2.3.1. Effect of water Ca level and Ca inhibitors on growth performance

To evaluate the growth performance of *C. fluminea* during the experiment, the average daily rate of shell growth between the calcein mark and the ventral margin and the condition index were calculated. As shown in Fig. 2.3A, the rate of shell growth and the condition index were not significantly different among treatments in the first set of experiments ($p > 0.05$). For example, shell growth rate slightly increased from 7.11 ± 0.61 µm/d at a Ca^{2+} level of 3 mM to 7.39 ± 0.66 µm/d at 4 mM Ca^{2+}. A further increase of Ca^{2+} level, however, resulted in slower growth rates, i.e., only 5.86 ± 1.52 µm of shell material was added every day at the highest Ca^{2+} level of 6 mM. Likewise, the maximum condition index occurred at 4 mM Ca^{2+} and then decreased at higher Ca^{2+} levels (Fig. 2.3B).

As demonstrated in Fig. 2.3A, lanthanum (1 and 10 µM) and Verapamil (0.1 and 1 µM) did not significantly affect the rate of shell growth ($p > 0.05$). On average, shells grew 7.09 µm/d, which is nearly identical to the 7.11 µm/d observed in the control group. Likewise, the condition index showed no significant difference among treatments ($p > 0.05$; Fig. 2.3B). In contrast to lanthanum and Verapamil, ruthenium red severely affected shell production and the condition index. Whereas shells forming in the presence of 0.1 µM ruthenium red had a growth performance similar to that of the control population, shell growth rate decreased by ca. 32 % to 4.84 ± 0.41 µm/d at 1 µM ruthenium red ($p < 0.05$; Fig. 2.3A). At the same time, a ca. 13 % reduction of the condition index was recorded (Fig. 2.3B).

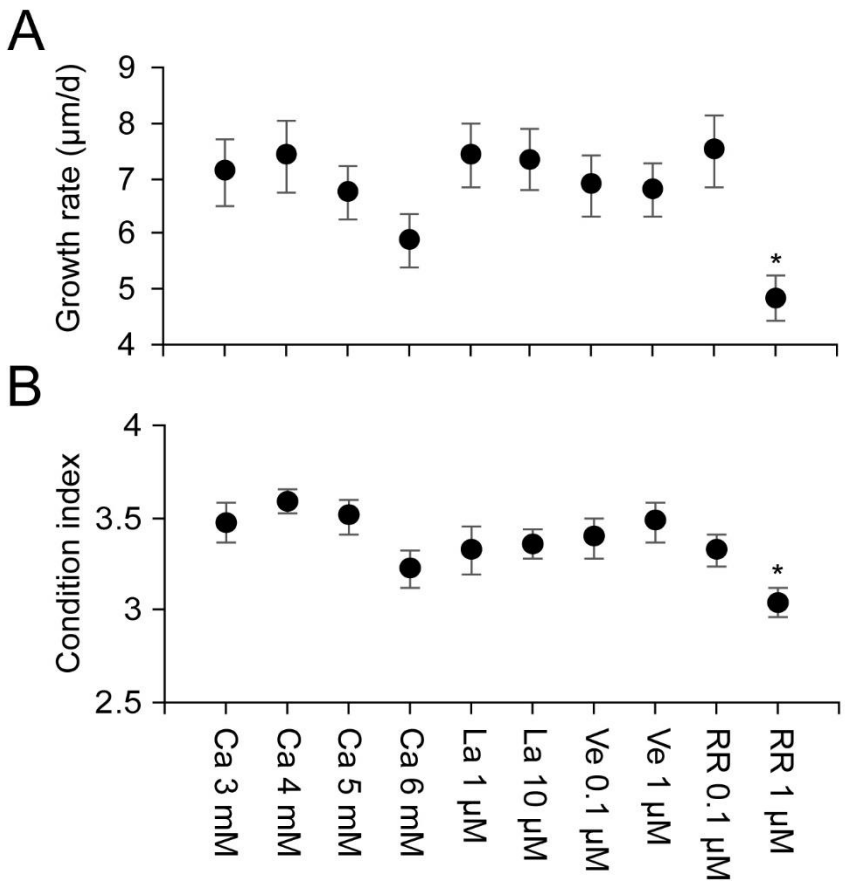

Fig. 2.3. Growth performance of *Corbicula fluminea* which grew in each treatment. (A) Shell growth rate. (B) Condition index. Values are expressed as average ± standard error (n = 10). La = lanthanum; Ve = Verapamil, RR = ruthenium red. *: $p < 0.05$.

2.3.2. Effect of water Ca level on element-to-calcium ratios of the shells

To more accurately evaluate the effect of water Ca^{2+} level on the elemental composition of the shells, specimens were reared at four different Ca^{2+} concentrations, i.e., 2.93 ± 0.13, 3.67 ± 0.13, 4.88 ± 0.14 and 6.27 ± 0.21 mM corresponding to nominal concentrations of 3, 4, 5 and 6 mM,

respectively. The amounts of Mg, Zn, Sr and Ba incorporated into the shells remained constant and virtually unaffected by varying water Ca^{2+} level ($p > 0.05$; Fig. 2.4A and Fig. 2.4D-F). However, shells forming at the lowest Ca^{2+} level of 3 mM contained significantly larger amount of Cu than those that grew at Ca^{2+} levels between 4 and 6 mM ($p < 0.05$; Fig. 2.4B). Mn/Ca_{shell} and Pb/Ca_{shell} ratios were significantly lower at Ca^{2+} levels of 5 and 6 mM than lower levels of 3 and 4 mM ($p < 0.05$; Fig. 2.4C and Fig. 2.4G).

2.3.3. Effect of Ca inhibitors on element-to-calcium ratios of the shells

In the following sets of experiments water Ca^{2+} level was maintained constant at 2.88 ± 0.04 mM (close to the value of the natural habitat). Irrespective of the reagent concentration, lanthanum did not significantly affect the amounts of Mg, Zn, Sr and Ba incorporated into the shells ($p > 0.05$; Fig. 2.5A and Fig. 2.5D-F), whereas significant decreased incorporation was observed in Cu, Mn and Pb ($p < 0.05$; Fig. 2.5B-C and Fig. 2.5G).

As in the case of lanthanum, Mg/Ca_{shell}, Sr/Ca_{shell} and Ba/Ca_{shell} were not significantly affected by Verapamil at both levels ($p > 0.05$; Fig. 2.6A and Fig. 2.6E-F), whereas Zn incorporation was significantly decreased ($p < 0.05$; Fig. 2.6D). Likewise, Verapamil significantly suppressed the incorporation of Cu and Mn into the shells ($p < 0.05$; Fig. 2.6B-C). Ruthenium red significantly reduced the amount of Cu incorporated into the shells ($p < 0.05$; Fig. 2.7B) and Mn at higher level of 1 µM ($p < 0.05$; Fig. 2.7C). Nevertheless, ruthenium red had little effect on the incorporation of other studied elements into the shells ($p > 0.05$; Fig. 2.7A and Fig. 2.7D-G).

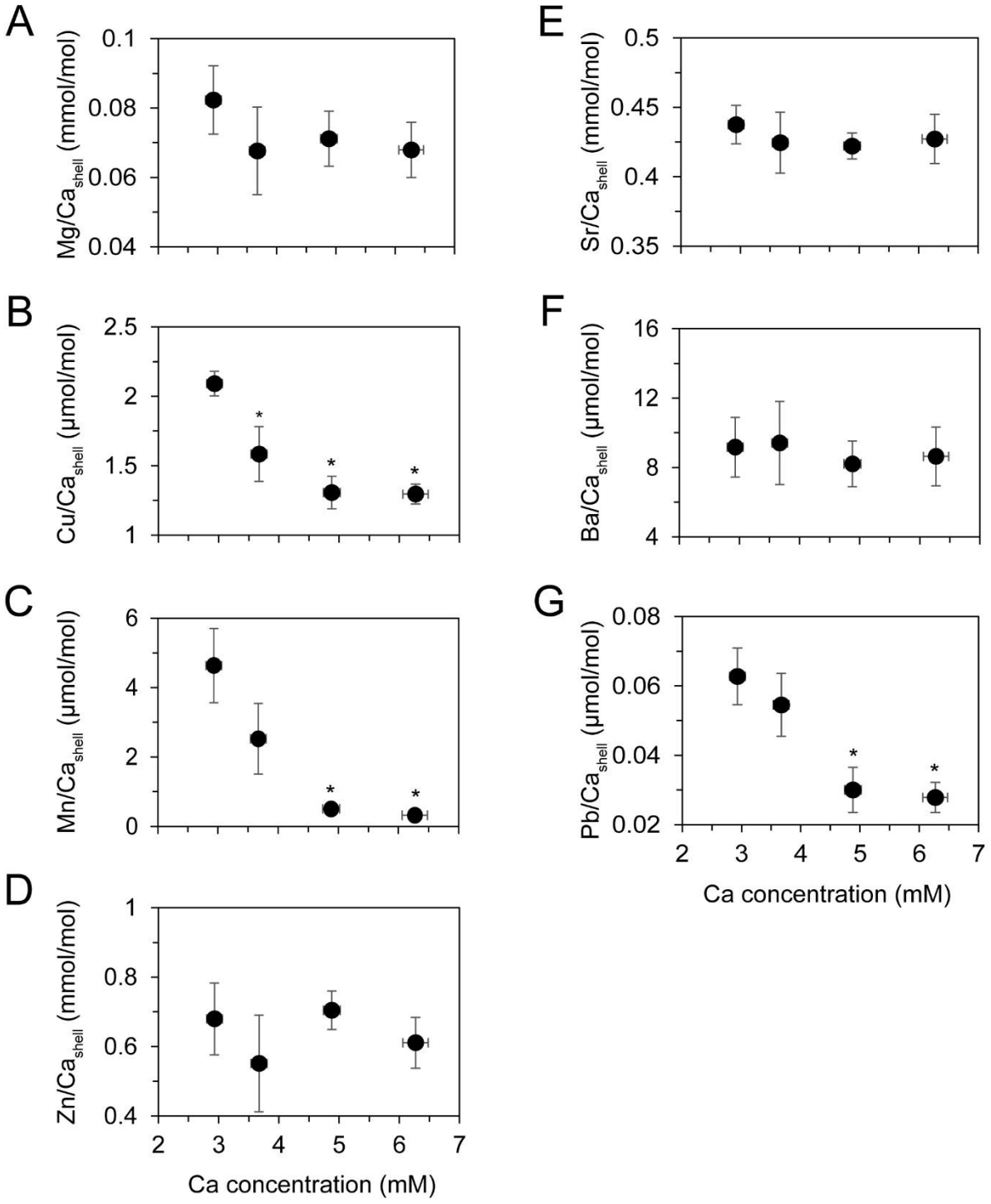

Fig. 2.4. Element-to-calcium ratios in the shells of *Corbicula fluminea* which grew at different water Ca^{2+} levels. Values are expressed as average ± standard error (n = 10). *: $p < 0.05$.

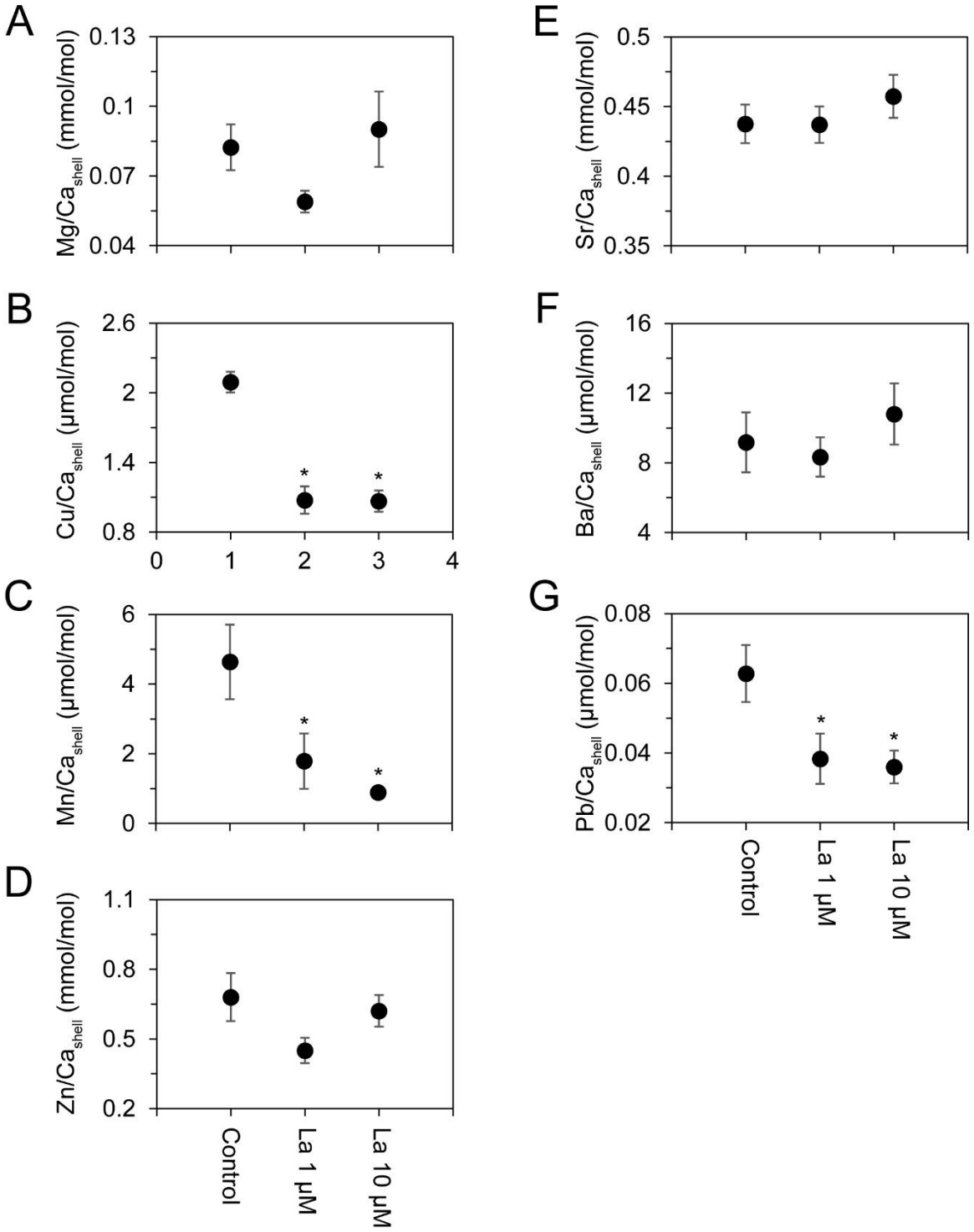

Fig. 2.5. Element-to-calcium ratios in the shells of *Corbicula fluminea* which grew in the presence of Ca^{2+}-channel blockers (lanthanum: 1 and 10 µM). Values are expressed as average ± standard error (n = 10). La = lanthanum. *: $p < 0.05$.

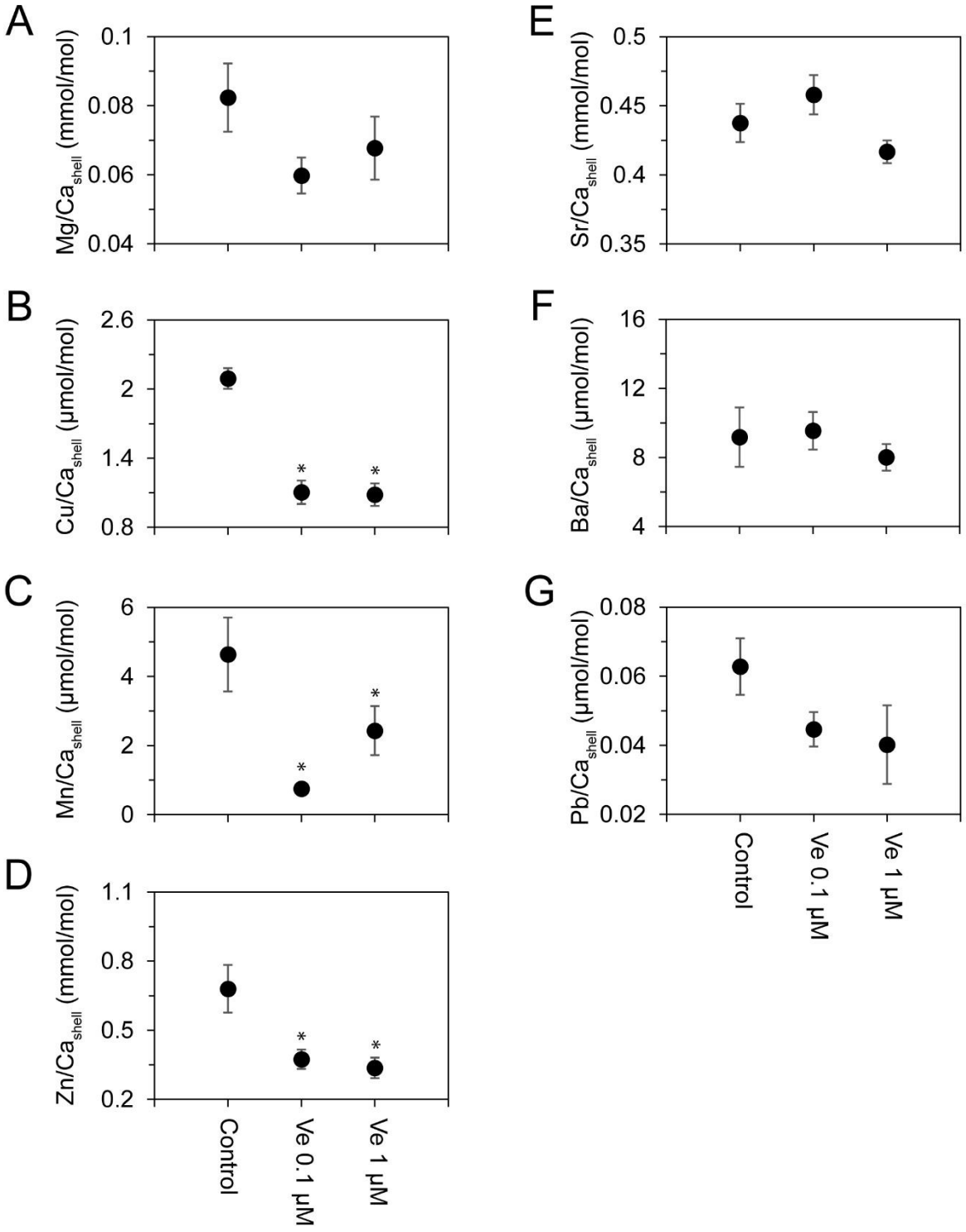

Fig. 2.6. Element-to-calcium ratios in the shells of *Corbicula fluminea* which grew in the presence of Ca^{2+}-channel blockers (Verapamil: 0.1 and 1 µM). Values are expressed as average ± standard error (n = 10). Ve = Verapamil. *: $p < 0.05$.

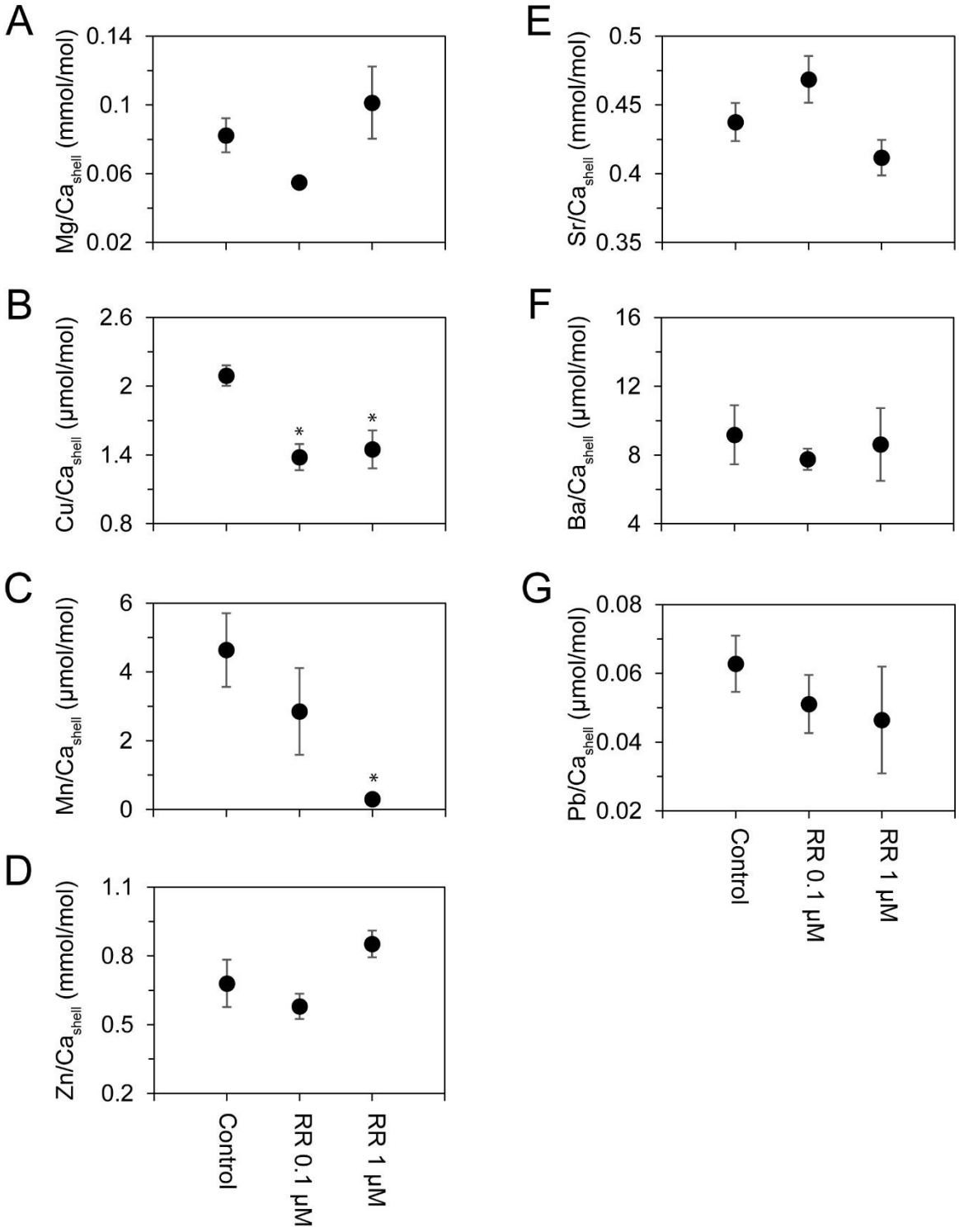

Fig. 2.7. Element-to-calcium ratios in the shells of *Corbicula fluminea* which grew in the presence of Ca^{2+}-ATPase inhibitors (ruthenium red: 0.1 and 1 µM). Values are expressed as average ± standard error (n = 10). RR = ruthenium red. *: $p < 0.05$.

2.4. Discussion

2.4.1. Calcium: in most cases, a non-limiting substrate for biomineralization

The matrix model advanced for biomineral formation postulates that bivalve mollusks increase the secretion of the organic matrix and the calcium carbonate saturation state of the EPS during active calcification (Wheeler, 1992). If this is the case, then one would expect shell formation to increase as Ca^{2+} levels and hence $CaCO_3$ saturation state rise. Evidently, this was not the case here in the present study. Our results demonstrated that higher concentrations of Ca^{2+} in the ambient water did not result in faster shell growth. This finding agrees well with the general hypothesis that CO_3^{2-} , not Ca^{2+} is the limiting factor for biogenic calcification (Kleypas & Langdon, 2000), because the Ca^{2+} concentration in seawater (10 mM; Bruland, 1983) is much higher than that of CO_3^{2-} (0.24 mM; Millero et al., 2008). While calcium demands for shell calcification are easily satisfied in marine environments, Ca^{2+} limitation may take place in natural freshwaters which are characterized by extremely low Ca^{2+} concentrations. It has been elucidated that water contributes up to 80% of calcium deposited in the shells of the freshwater mussel *Dreissena polymorpha* (Pallas, 1771) (Vinogradov et al., 1993) and the critical water Ca^{2+} concentrations for its growth and survival are 0.21 mM (Hincks & Mackie, 1997) and 0.30 mM (Sprung, 1987), respectively. In North America, *D. polymorpha* only inhabits waters with Ca^{2+} concentrations of above 0.37 mM, with dense populations developing above 0.52 mM (Mellina & Rasmussen, 1994). *C. fluminea* appears to be less tolerant of low Ca^{2+} concentrations than *D. polymorpha* (McMahon, 2002). Despite this, it is still able to grow and reproduce in calcium-poor waters. In the rivers of Southern China where *C. fluminea* is widespread, for example, Ca^{2+} varies from 0.57 to 8.51 mM (Qiu et al., 2005). Presumably, calcium limitation for shell production of *C. fluminea* should be lower than 0.57 mM, a critical threshold far below ca. 3–6 mM in the present study.

The mechanisms underlying the calcium limitation for shell calcification are not yet fully understood. Freshwater bivalves are typical osmoregulators, i.e., they need to maintain a higher ionic concentration in the body fluids than that of the ambient environment (Deaton, 1981). The minimum concentration required for normal calcium metabolism (hemolymph Ca^{2+} regulation) is 0.35 mM for *D. polymorpha* (Vinogradov et al., 1993). Such value corresponds well with the threshold for its shell growth (0.21–0.37 mM; Mellina & Rasmussen, 1994; Hincks & Mackie, 1997). Therefore, if the uptake of Ca^{2+} by the bivalves from the ambient environment cannot fully satisfy normal calcium metabolism, shell dissolution may occur to maintain a high hemolymph Ca^{2+} concentration (Murphy & Dietz, 1976).

Furthermore, results of our study showed that the rate of shell growth was not linearly correlated to the aqueous Ca^{2+} level. Despite that the differences were not statistically significant, maximum growth occurred at a Ca^{2+} level of 4 mM beyond which it decreased. A similar curvilinear pattern has also been observed in *D. polymorpha* (Hincks & Mackie, 1997). These phenomena can be attributed to the potential disturbance of the cationic balance in the body fluids (Nduku & Harrison, 1976). This interpretation agrees well with the variability of the condition index, a useful barometer reflecting environmental stress on molluscan health (Gosling, 2003). In the present study, the condition index was simultaneously decreased when Ca^{2+} level was above the optimum of 4 mM.

2.4.2. Multiple roles of calcium in elemental incorporation into the shells

Divalent metals with ionic radii similar to that of Ca^{2+} are generally considered to compete with Ca^{2+} in the same uptake pathways (Simkiss & Taylor, 1989). In the present study, this holds particularly true for Cu^{2+}, Mn^{2+} and Pb^{2+}. With increasing Ca^{2+} level in the ambient water, the amounts of Cu, Mn and Pb incorporated into the shells decreased, implying lowered amounts of these elements moving into the EPS. This interpretation agrees well with Phillips (1976) who examined the effect of salinity (and hence Ca^{2+}) on Cu^{2+} uptake in *Mytilus edulis* (Linnaeus, 1758), and Markich & Jeffree (1994) who examined the effect of Ca^{2+} on Mn^{2+} and Pb^{2+} uptake in *Hyridella depressa* (Lamarck, 1819) and *Velesunio ambiguous* (Philippi, 1847).

According to Campbell (1995), the uptake of dissolved metals by aquatic organisms should be proportional to the activity of free metal ions rather than to the total dissolved metal concentration. With increasing aqueous Ca^{2+} and hence ionic strength, the free ion activities of other coexisting metals decrease accordingly (Allison et al., 1991). Therefore, decreases of free Cu^{2+}, Mn^{2+} and Pb^{2+} activities occurring concomitantly with increases of Ca^{2+} concentration may also account for the reduced incorporation of these metals into the shells of *C. fluminea*.

Increasing Ca^{2+} did not significantly affect the total amounts of Mg, Zn, Sr and Ba incorporated into the shells. Given that Mg^{2+} has a much smaller ionic radius than Ca^{2+} (Kastner, 1999), it is unlikely to be taken up through the Ca^{2+} transport systems, i.e., Mg^{2+} may not compete for the uptake with Ca^{2+}. However, the insignificant effect of Ca^{2+} on Zn^{2+} uptake is at odds with the observations by Qiu et al. (2005) according to which the inhibitory effect of Ca^{2+} on Zn^{2+} uptake in *C. fluminea* was evident. These authors, however, primarily considered the uptake of Zn^{2+} from the ambient water, but not a dietary contribution. The latter may represent the dominant source of Zn^{2+} in bivalves (Shi & Wang, 2004), due to its high affinity

to organic particles (i.e., high particle reactivity; Bruland, 1983). Likewise, some sclerochronological studies postulated that Ba/Ca_{shell} peaks can most likely be attributed to the ingestion of Ba-rich phytoplankton (e.g., Thébault et al., 2009; Hatch et al., 2013). Presumably, this also holds the truth for the incorporation of Sr^{2+} into the shells. Therefore, it is likely that calcium may affect the uptake of elements which are primarily taken up from the water by the bivalves. Apparently, a detailed understanding of the pathways of elemental uptake into the shells has significant implications to better interpret shell element signatures.

2.4.3. Pathways of elemental incorporation into the shells

Since it has been clearly shown that divalent cations may share the same uptake pathways with Ca^{2+} (Simkiss & Taylor, 1989), it is essential to gain a more detailed understanding of the processes involved in the incorporation of Ca^{2+} into the shells. In marine bivalve mollusks, the similarity of elemental composition between water, hemolymph and EPS highlights a large proportion of diffusible Ca^{2+} in the EPS (Crenshaw, 1972; Wada & Fujinuki, 1976). On the other hand, calcium concentrations in the EPS of freshwater bivalves (e.g., *Hyriopsis schlegeli* (Martens, 1861), *Cristaria plicata* (Leach, 1815); Wada & Fujinuki, 1976) are 11 to 15 times higher than in the ambient water implying that Ca^{2+} uptake (at least across the water-hemolymph interface) occurs actively via the Ca^{2+}-ATPase process. Findings of the present study line up with this interpretation. Whereas shell growth was virtually unaffected by Ca^{2+}-channel blockers (lanthanum and Verapamil), the inhibitory effect of ruthenium red (a specific inhibitor of Ca^{2+}-ATPase) at 1 µM was implying that Ca^{2+}-ATPase plays a major role in Ca^{2+} transport from the ambient water to the EPS. However, since Ca^{2+} used for calcification is supplied directly by the hemolymph which reportedly is chemically similar to that of the EPS (Crenshaw, 1972), the diffusion of Ca^{2+} through the hemolymph-EPS interface (i.e., the outer mantle epithelium) cannot be ruled out in freshwater bivalves.

In the present study, substantial suppression of intracellular Ca^{2+} transport mechanisms by chemical reagents significantly reduced the incorporation of Cu, Mn, Zn and Pb into the shells. These observations suggest that they may be taken up through the same pathway as Ca^{2+}, consistent with the general notion that divalent metals are absorbed as analogues of Ca^{2+} (Markich & Jeffree, 1994). Nevertheless, divalent metals like Cu^{2+}, Mn^{2+}, and Zn^{2+} are biologically essential and therefore, they are generally accumulated in the soft tissues of bivalves (Bellotto & Miekeley, 2007), so that only a small fraction or even none of these metals would be transferred into the shells. Likewise, bivalves actively remove non-essential metals

like Pb^{2+} by various detoxification processes (Viarengo & Nott, 1993) resulting in lower levels of lead in the shells. For example, lead is ten-fold higher concentrated in the soft tissues of *M. edulis* than in the shells (Bourgoin, 1990). Nevertheless, if the capacity of bivalves to regulate their metal uptake is limited when facing increasing metal pollution pressures, one would expect an increase of metal storage in the shells. Richardson et al. (2001) for example observed that Cu, Zn and Pb levels in the shells of *Modiolus modiolus* (Linnaeus, 1758) inhabiting a polluted estuary were significantly higher than those from a pristine environment. The eastern oyster, *Crassostrea virginica* (Gmelin, 1791), can concentrate Mn, Cu and Zn in the shells as their concentrations increase in the surrounding seawater (Carriker et al., 1980). Taking into account that Cu, Mn and Zn, aside from substituting Ca^{2+} in the crystal lattice, may also be associated with the organic matrix (Carriker et al., 1980; Takesue et al., 2008), it is conceivable that shells may act as a reservoir for these physiologically regulated metals, i.e., they can substantially accumulate certain excessive (or unwanted) metals. This interpretation compares well with the observations by Bolotov et al. (2015) according to which Mn/Ca_{shell} of freshwater mussels (*Margaritifera* spp.) was up to five-fold higher than that of the ambient water.

It appears that intracellular Ca^{2+} transport is not involved in the incorporation of Sr and Ba into the shells. This finding is at odds with the concept that divalent metals are treated as metabolic analogues of Ca^{2+} (Markich & Jeffree, 1994) and the models that the discrimination of Sr and Ba occurs during their transport to the EPS (Klein et al., 1996; Carré et al., 2006). For example, according to the Ca^{2+}-channel model (Carré et al., 2006), Sr/Ca variability in the EPS relies on Ca^{2+}-channel selectivity against Sr^{2+}, and a reduction of Sr^{2+} discrimination is expected at high calcification rate. In the Ca^{2+}-ATPase model (Klein et al., 1996), however, selective uptake of Ca^{2+} occurs during active calcification, causing a decrease of Sr/Ca in the EPS. Evidently, both models fail to explain why neither blocking Ca^{2+}-channel nor inhibiting Ca^{2+}-ATPase affected the incorporation of Sr into the shells, i.e., Sr/Ca ratios in the EPS were virtually unaffected. Strontium partitioning between the ambient water and the shells may occur at any or all of the following interfaces: water-hemolymph, hemolymph-EPS and EPS-shell. Bivalves inhabiting freshwater are considered osmoregulators which have a higher ionic strength in their body fluids than in the ambient water (Dietz, 1979), i.e., they need to actively uptake exogenous ions. It is likely that Sr^{2+} may reach the hemolymph through the Ca^{2+}-ATPase process. Clearly, this interpretation is at odds with the findings of the present study. Moreover, if most of the discrimination against Sr^{2+} occurs during its transport to the EPS and given that Sr^{2+} deposited in the shells is derived from hemolymph rather than the surrounding medium, it is likely that a higher level of ionic discrimination takes place at the hemolymph-EPS interface.

However, this was also not the case in the present study as discussed above. The chemical composition of the EPS appears to be closer to that of hemolymph (Crenshaw, 1972; Coimbra et al., 1993) implying that passive diffusion plays a major role in ionic transport through the hemolymph-EPS interface, i.e., the outer mantle epithelium behaves as a passive barrier which is highly permeable to Ca^{2+} (Coimbra et al., 1988) and probably Sr^{2+} whose ionic radius is nearly identical to that of Ca^{2+} (Shannon, 1976). On the other hand, strontium-to-calcium in the shells of *C. fluminea* is linearly proportional to Sr/Ca_{water} which is obtained by manipulating either Ca^{2+} in the present study or Sr^{2+} (Zhao et al., 2015). Such linear correlation cannot consistently hold true if Sr^{2+} discrimination occurs during its transport to the EPS, the process which is mediated by various saturated ionic carriers and channels. Therefore, it is most likely that the majority of Sr^{2+} discrimination occurs at the EPS-shell interface, i.e., during shell crystallization (Gillikin et al., 2005). Presumably, this is also the case for Ba^{2+}, although controls on its incorporation process are much more complex than that of Sr^{2+} (Zhao et al., 2015).

2.5. Conclusions

As demonstrated by the findings of this study, higher water Ca^{2+} levels did not lead to faster shell production implying that other factors limit shell growth. Accordingly, our observations suggest that shell formation is not dependent on the $CaCO_3$ saturation state changed by altering aqueous Ca^{2+} levels. However, calcium ions exhibit substantial effects on the incorporation of trace elements into the shells. For example, the amounts of Mn, Cu and Pb incorporated into the shells decreased with increasing water Ca^{2+} levels, presumably due to the competition with Ca^{2+} in the same transport pathways. This interpretation is partially verified by the findings of our experiments. The incorporation of Mn, Cu, Zn and Pb into the shells decreased when blocking Ca^{2+}-channel and/or depressing Ca^{2+}-ATPase, suggesting that they can potentially be taken up though intracellular Ca^{2+} transport routes. Although neither Sr/Ca_{shell} nor Ba/Ca_{shell} were affected, competitive effects occurring during passive diffusion cannot be excluded. In addition, Mg/Ca_{shell} was virtually unaffected in all sets of experiments, which may be attributed to its much smaller radius than that of calcium ion. Thus, further studies are required to evaluate how much of Ca^{2+} deposited into the shells is transported through the intracellular Ca^{2+} pathways, i.e., the relative contribution of each transport pathway to the Ca^{2+} pool at the site of

calcification (EPS). Such knowledge is crucial to determine the extent to which elemental discrimination occurs during the transport to the EPS.

2.6. Acknowledgments

Not displayed for reasons of data protection

2.7. References

Allison, J. D., D. S. Brown & J. Kevin, 1991. MINTEQA2/PRODEFA2, a geochemical assessment model for environmental systems: version 3.0 user's manual. Athens, GA: Environmental Research Laboratory, Office of Research and Development, U.S. Environmental Protection Agency.

Bellotto, V. R. & N. Miekeley, 2007. Trace metals in mussel shells and corresponding soft tissue samples: a validation experiment for the use of *Perna perna* shells in pollution monitoring. Analytical and Bioanalytical Chemistry 389: 769–776.

Black, B. A., D. C. Gillespie, S. E. MacLellan & C.M. Hand, 2008. Establishing highly accurate production-age data using the tree-ring technique of crossdating: a case study for Pacific geoduck (*Panopea abrupta*). Canadian Journal of Fisheries and Aquatic Sciences 65: 2572–2578.

Bolotov, I. N., O. S. Pokrovsky, Y. Auda, J. V. Bespalaya, I. V. Vikhrev, M. Y. Gofarov, A. A. Lyubas, J. Viers & C. Zouiten, 2015. Trace element composition of freshwater pearl mussels *Margaritifera* spp. across Eurasia: testing the effect of species and geographic location. Chemical Geology 402: 125–139.

Bourgoin, B. P., 1990. *Mytilus edulis* shell as a bioindicator of lead pollution: considerations on bioavailability and variability. Marine Ecology Progress Series 61: 253–262.

Bruland, K. W., 1983. Trace elements in seawater. In Wong, C.S., Bruland, K.W., Burton, D. & E. D. Goldberg (eds), Chemical Oceanography. Academic Press, London, 157–220.

Campbell, P. G., 1995. Interactions between trace metals and aquatic organisms: a critique of the free-ion activity model. In Tessier, A. & D. R. Turner (eds), Metal speciation and bioavailability in aquatic systems. Wiley, New York, 45–102.

Carré, M., I. Bentaleb, O. Bruguier, E. Ordinola, N. T. Barrett & M. Fontugne, 2006. Calcification rate influence on trace element concentrations in aragonitic bivalve shells: evidences and mechanisms. Geochimica et Cosmochimica Acta 70: 4906–4920.

Carriker, M. R., R. E. Palmer, L. V. Sick & C. C. Jonhson, 1980. Interaction of mineral elements in sea water and shell of oysters (*Crassostrea virginica* (Gmelin)) cultured in controlled and natural systems. Journal of Experimental Marine Biology and Ecology 46: 279–96.

Coimbra, A. M., K. G. Ferreira, P. L. Fernandes & H. G. Ferreira, 1993. Calcium exchanges in *Anodonta cygnea*: barriers and driving gradients. Journal of Comparative Physiology 163: 196–202.

Coimbra, J., J. Machado, P. L. Fernandes, H. G. Ferreira & K. G. Ferreira, 1988. Electrophysiology of the mantle of *Anodonta cygnea*. Journal of Experimental Biology 140: 65–88.

Crenshaw, M. A., 1972. Inorganic composition of molluscan extrapallial fluid. Biological Bulletin 143: 506–512.

Deaton, L. E., 1981. Ion regulation in freshwater and brackish water bivalve mollusks. Physiological Zoology 54: 109–121.

Dietz, T. H., 1979. Uptake of sodium and chloride by freshwater mussels. Canadian Journal of Zoology 57: 156–160.

Fan, W., C. Li, S. Li, Q. Feng, L. Xie & R. Zhang, 2007. Cloning, characterization, and expression patterns of three sarco/endoplasmic reticulum Ca^{2+}-ATPase isoforms from pearl oyster (*Pinctada fucata*). Acta Biochimica et Biophysica Sinica 39: 722–730.

Gillikin, D. P., A. Lorrain, J. Navez, J. W. Taylor, L. André, E. Keppens, W. Baeyens & F. Dehairs, 2005. Strong biological controls on Sr/Ca ratios in aragonitic marine bivalve shells. Geochemistry Geophysics Geosystems 6: Q05009.

Gosling, E., 2003. An Introduction to Bivalves. Bivalve Molluscs: Biology, Ecology and Culture. Fishing News Books, Blackwell, Oxford. doi: 10.1002/9780470995532.ch1

Guerrero, J. & S. S. Martin, 1984. Verapamil, full spectrum Ca channel blocking agent: an overview. Medicinal Research Reviews 4: 87–109.

Hatch, M. B., S. A. Schellenberg & M. L. Carter, 2013. Ba/Ca variations in the modern intertidal bean clam *Donax gouldii*: An upwelling proxy? Palaeogeography Palaeoclimatology Palaeoecology 373: 98–107.

Hincks, S. S. & G. L. Mackie, 1997. Effects of pH, calcium, alkalinity, hardness, and chlorophyll on the survival, growth, and reproductive success of zebra mussel (*Dreissena polymorpha*) in Ontario lakes. Canadian Journal of Fisheries and Aquatic Sciences 54, 2049–2057.

Jeffree, R.A., S. J. Markich, F. Lefebvre, M. Thellier & C. Ripoll, 1995. Shell microlaminations of the freshwater bivalve *Hyridella depressa* as an archival monitor of manganese water concentration: experimental investigation by depth profiling using secondary ion mass spectrometry (SIMS). Experientia 51, 838–848.

Jochum, K. P., U. Nohl, K. Herwig, E. Lammel, B. Stoll & A. W. Hofmann, 2005. GeoReM: a new geochemical database for reference materials and isotopic standards. Geostandards and Geoanalytical Research 29: 87–133.

Jochum, K. P., U. Weis, B. Stoll, D. Kurmin, Q. Yang, I. Raczek, D. E. Jacob, A. Stracke, K. Birbaum, D. A. Frick, D. Günther & J. Enzweiler, 2011. Determination of reference values for NIST SRM 610-617 glasses following ISO guidelines. Geostandards and Geoanalytical Research 35: 397–429.

Jochum, K. P., D. Scholz, B. Stoll, U. Weis, S. A. Wilson, Q. Yang, A. Schwalb, N. Börner, D. E. Jacob & M. O. Andreae, 2012. Accurate trace element analysis of speleothems and biogenic calcium carbonates by LA-ICP-MS. Chemical Geology 318-319: 31–44.

Kaehler, S. & C. D. McQuaid, 1999. Use of the fluorochrome calcein as an in situ growth marker in the brown mussel *Perna perna*. Marine Biology 133: 455–460.

Kastner, M., 1999. Oceanic minerals: their origin, nature of their environment and significance. Proceedings of the National Academy of Sciences 96: 3380–3387.

Klein, R. T., K. C. Lohman & C. W. Thayer, 1996. Sr/Ca and $^{13}C/^{12}C$ ratios in skeletal calcite of *Mytilus trossulus*: covariation with metabolic rate, salinity and carbon isotopic composition of sea water. Geochimica et Cosmochimica Acta 60: 4207–4221.

Kleypas, J. & C. Langdon, 2000. Overview of CO_2-induced changes in seawater chemistry. Proceedings of the 9th International Coral Reef Symposium, Bali, Indonesia, 23–27 October 2000, 2: 1085–1089.

Krause-Nehring, J., T. Brey & S. R. Thorrold, 2012. Centennial records of lead contamination in northern Atlantic bivalves (*Arctica islandica*). Marine Pollution Bulletin 64: 233–240.

Lucas, A. P. & G. Beninger, 1985. The use of physiological condition index in marine bivalve aquaculture. Aquaculture 44: 187–200.

Marin, F., N. L. Le Roy & B. Marie, 2012. The formation and mineralization of mollusk shells. Frontiers in Bioscience 4: 1099–1125.

Markich, S. J. & R. A. Jeffree, 1994. Absorption of divalent trace metals as analogues of calcium by Australian freshwater bivalves: an explanation of how water hardness reduces metal toxicity. Aquatic Toxicology 29: 257–290.

McConnaughey, T. A. & D. P. Gillikin, 2008. Carbon isotopes in mollusk shell carbonates. Geo-Marine Letters 28: 287–299.

McMahon, R. F., 1983. Ecology of an invasive pest bivalve, *Corbicula*. Mollusca 6, 505–561.

McMahon, R. F., 2002. Evolutionary and physiological adaptations of aquatic invasive animals: r selection versus resistance. Canadian Journal of Fisheries and Aquatic Sciences 59: 1235–1244.

Mellina, E. & J. B. Rasmussen, 1994. Patterns in the distribution and abundance of zebra mussel (*Dreissena polymorpha*) in rivers and lakes in relation to substrate and other physicochemical factors. Canadian Journal of Fisheries and Aquatic Sciences 51: 1024–1036.

Millero, F. J., R. Feistel, D. G. Wright & T. J. McDougall, 2008. The composition of standard seawater and the definition of the reference-composition salinity scale. Deep-Sea Research 55: 50–72.

Murphy, W. A. & T. H. Dietz, 1976. The effects of salt depletion on blood and tissue ion concentrations in the freshwater mussel, *Ligumia subrostrata* (Say). Journal of Comparative Physiology 108: 233–242.

Nduku, W. K. & A. D. Harrison, 1976. Calcium as a limiting factor in the biology of *Biomphalaria pfeifferi* (Krauss) (Grastropoda: Planorbidae). Hydrobiologia 49: 143–170.

Phillips, D. J. H., 1976. The common mussel *Mytilus edulis* as an indicator of pollution by zinc, lead, and copper, I: effects on environmental variables on uptake of metals. Marine Biology 38: 59–69.

Prezant, R. S. & A. Tan-Tiu, 1985. Comparative shell microstructure of North American *Corbicula* (Bivalvia: Sphaeriacea). Veliger 27: 312–319.

Qiu, J. W. & W. X. Wang, 2005. Effects of calcium on the uptake and elimination of cadmium and zinc in Asiatic clams. Archives of Environmental Contamination and Toxicology 48: 278–287.

Richardson, C. A., S. R. N. Chenery & J. M. Cook, 2001. Assessing the history of trace metal (Cu, Zn, Pb) contamination in the North Sea through laser ablation ICP-MS of horse mussel *Modiolus modiolus* shells. Marine Ecology Progress Series 211: 157–167.

Schöne, B. R., 2013. *Arctica islandica* (Bivalvia): a unique paleoenvironmental archive of the northern North Atlantic Ocean. Global and Planetary Change 111: 199–225.

Schöne, B. R., Z. Zhang, D. Jacob, D. P. Gillikin, T. Tütken, D. Garbe-Schönberg & A. Soldati, 2010. Effect of organic matrices on the determination of the trace element chemistry (Mg, Sr, Mg/Ca, Sr/Ca) of aragonitic bivalve shells (*Arctica islandica*) – Comparison of ICP-OES and LA-ICP-MS data. Geochemical Journal 44: 23–37.

Schöne, B. R., Z. Zhang, P. Radermacher, J. Thébault, D. E. Jacob, E. V. Nunn & A. F. Maurer, 2011. Sr/Ca and Mg/Ca ratios of ontogenetically old, long-lived bivalve shells (*Arctica islandica*) and their function as paleotemperature proxies. Palaeogeography Palaeoclimatology Palaeoecology 302: 52–64.

Shannon, R. D., 1976. Revised effective ionic radii and systematic studies of interatomic distances in halides and chalcogenides. Acta Crystallographica B 32: 751–767.

Shirai, K., B. R. Schöne, T. Miyaji, P. Radermacher, R. A. Krause Jr & K. Tanabe, 2014. Assessment of the mechanism of elemental incorporation into bivalve shells (*Arctica islandica*) based on elemental distribution at the microstructural scale. Geochimica et Cosmochimica Acta 126: 307–320.

Shi, D. L. & W. X. Wang, 2004. Understanding the differences in Cd and Zn bioaccumulation and subcellular storage among different populations of marine clams. Environmental Science & Technology 38: 449–456.

Simkiss, K. & M. G. Taylor, 1989. Metal fluxes across the membranes of aquatic organisms. Aquatic Sciences 1: 173–188.

Sprung, M., 1987. Ecological requirements of developing *Dreissena polymorpha* eggs. Archiv für Hydrobiologie, Supplementband 79: 69–86.

Takesue, R. K., C. R. Bacon & J. K. Thompson, 2008. Influences of organic matter and calcification rate on trace elements in aragonitic estuarine bivalve shells. Geochimica et Cosmochimica Acta 72: 5431–5445.

Thébault, J., L. Chauvaud, J. Clavier, R. Fichez & E. Morize, 2006. Evidence of a 2-day periodicity of striae formation in the tropical scallop *Comptopallium radula* using calcein marking. Marine Biology 149: 257–267.

Thébault, J., L. Chauvaud, S. L. Helguen, J. Clavier, A. Barats, S. Jacquet, C. Pécheyran & D. Amouroux, 2009. Barium and molybdenum records in bivalve shells: Geochemical proxies for phytoplankton dynamics in coastal environments? Limnology and Oceanography 54: 1002–1014.

Viarengo, A. & J. A. Nott, 1993. Mechanisms of heavy metal cation homeostasis in marine invertebrates. Comparative Biochemistry and Physiology C 104: 355–372.

Verbost, P. M., J. Van Rooij, G. Flik, R. A. C. Lock & S. E. Wendelaar Bonga, 1989. The movement of cadmium through freshwater trout branchial epithelium and its interference with Ca transport. Journal of Experimental Biology 145: 185–197.

Vinogradov, G. A., N .F. Smirnova, V. A. Sokalov & A. A. Bruznitsky, 1993. Influence of chemical composition of the water on the mollusk *Dreisennia polymorpha*. In Nalepa, T. F. & D. W. Schloesser (eds), Zebra mussels: biology, impacts, and control. Lewis Publishers/CRC Press, Boca Raton, 283–293.

Wada, K. & T. Fujinuki, 1976. Biomineralization in bivalve molluscs with emphasis on the chemical composition of the extrapallial fluid. In Bryan, N. M. & K. M. Wilbur (eds), Mechanisms of Mineralization in the Invertebrates and Plants. University of South Carolina Press, Georgetown, 175–190.

Wanamaker Jr., A. D., K. J. Kreutz, B. R. Schöne, K. A. Maasch, A. Pershing, H. W. Borns, D. S. Introne & S. Feindel, 2009. A late Holocene paleo-productivity record in the Western Gulf of Maine, USA, inferred from growth histories of the long-lived ocean quahog (*Arctica islandica*). International Journal of Earth Sciences 98: 19–29.

Watson, E. L., F. F. Vincenzi & P. W. Davis, 1971. Ca^{2+}-activated membrane ATPase: selective inhibition by ruthenium red. Biochimica et Biophysica Acta 249: 606–610.

Wheeler, A. P., 1992. Mechanisms of molluscan shell formation. In Bonucci, E. (ed), Calcification in biological systems. CRC press, Boca Raton, FL, 179–216.

Wilbur, K. M. & A. S. M. Saleuddin, 1983. Shell formation. In Saleuddin, A. S. M. & K. M. Wilbur (eds) The Mollusca 4. Physiology. Academic Press, New York.

Zhao, L. Q., B. R. Schöne & R. Mertz-Kraus, 2015. Controls on strontium and barium incorporation into freshwater bivalve shells (*Corbicula fluminea*). Palaeogeography Palaeoclimatology Palaeoecology. http://dx.doi.org/10.1016/j.palaeo.2015.11.040.

Chapter 3

*Controls on strontium and barium incorporation into freshwater bivalve shells (*Corbicula fluminea*)*

Published in Palaeogeography, Palaeoclimatology, Palaeoecology

Liqiang Zhao[1], Bernd R. Schöne[1], Regina Mertz-Kraus[1]

[1] Institute of Geosciences, University of Mainz, Joh.-J.-Becher-Weg 21, 55128 Mainz, Germany

Author contribution

Concept: LZ, BRS

Execution: LZ

Data collection and analysis: LZ, RMK

Writing: LZ, BRS, RMK

Liqiang Zhao, Bernd R. Schöne, Regina Mertz-Kraus, 2017. Controls on strontium and barium incorporation into freshwater bivalve shells (*Corbicula fluminea*). Palaeogeography Palaeoclimatology Palaeoecology 465, 386–394.

Abstract

Trace elements of bivalve shells can potentially serve as proxies of environmental change. However, to reconstruct past environments using the geochemical properties of the shells and determine the degree to which the element levels are biologically influenced, it is essential to experimentally determine the relationship between environmental variables and the element composition of the shells. To disentangle possible controls on the incorporation of strontium and barium into freshwater bivalve shells, we conducted controlled laboratory experiments using the extremely salinity and temperature tolerant Asian clam, *Corbicula fluminea* as a model species. Bivalves were reared for five weeks in two sets of experiments: (1) combinations of different water temperature (10, 16 and 22 °C) and food levels (0.2, 2, 4 and 8 × 10^4 cells/ml) with constant Sr/Ca_{water} (2.45 mmol/mol) and Ba/Ca_{water} (367 µmol/mol) levels; (2) combinations of different water temperature (10, 16 and 22 °C) and different Sr/Ca_{water} (ca. 4, 8 and 12 mmol/mol) and Ba/Ca_{water} levels (ca. 600, 1150 and 1500 µmol/mol) with constant food level (4 × 10^4 cells/ml). The Sr/Ca_{shell} ratio of *C. fluminea* exhibited a statistically significant negative correlation with temperature and a positive correlation to Sr/Ca_{water}, but was not affected by changing food level or shell growth rate. On the contrary, Ba/Ca_{shell} was influenced by a complexly intertwined set of variables including temperature, food level, Ba/Ca_{water} and shell growth rate. Partition coefficients of $K_D^{Sr/Ca}$ (0.19 to 0.29) and $K_D^{Ba/Ca}$ (0.03 to 0.19) confirmed the control of vital effects over strontium and barium incorporation into the shells. As indicated by the findings, Sr/Ca_{shell} of *C. fluminea* from freshwater environments can serve as a reliable proxy for past water temperature if the spatiotemporal variability of strontium-to-calcium in the water is small, well-known or can be estimated from other proxies. Interpreting Ba/Ca_{shell} values, however, is much more challenging because they are controlled by a large number of environmental and physiological variables. Sr/Ca_{shell} and Ba/Ca_{shell} of *C. fluminea* specimens from estuarine settings in which element-to-calcium ratios are more conservative and stable can potentially function as paleoenvironmental proxies. Findings of this study can be useful to better understand the element incorporation into shells of other bivalves including marine species.

3.1. Introduction

Trace and minor element signatures of many biogenic carbonates serve as reliable proxies of past environmental variables. Of particular interest are cations that can substitute Ca^{2+} in the crystal lattice because of similar ionic radii and electrochemical properties, specifically Sr^{2+} and Ba^{2+} in aragonite (orthorhombic crystal structure: Bragg, 1924) and Mg^{2+} in calcite (trigonal-rhombohedral crystal structure: Bragg, 1913) (Kastner, 1999). Under ideal circumstances, the incorporation of these ions into the biomineral occurs proportionately to the concentration of the respective dissolved element in the ambient medium and is thermodynamically controlled, but not affected by vital effects. For example, coral Ba/Ca values can document changes in riverine influx (McCulloch et al., 2003; Sinclair and McCulloch, 2004), because freshwater contains much larger amounts of barium than seawater (50 µg/L vs. 6 µg/L Ba^{2+}; Schroeder et al., 1972) and the Ba/Ca ratio of the corals is linearly correlated to that of the water (Sinclair and McCulloch, 2004). The Sr/Ca value of coral aragonite can provide details on ambient temperature during growth (Beck et al., 1992). With increasing water temperature, the Sr/Ca in aragonite decreases because the substitution of calcium by strontium in this polymorph of $CaCO_3$ is an exothermic reaction (Rosenthal and Linsley, 2006). Since the Sr/Ca_{water} ratio is nearly invariant (~8.6-8.8 mmol/mol) in modern seawater above 8 to 10 PSU (Dodd and Crisp, 1982) and corals form their skeletons near equilibrium with the ambient medium with respect to Sr/Ca_{water} (Hanna and Muir, 1990), coral Sr/Ca values can provide reliable temperature estimates over a wide range of different salinities.

Interpreting the trace and minor element content of bivalve shells is a very challenging task, possibly more challenging than in the case of corals and many other organisms. Vital and kinetic effects (Urey et al., 1951, Epstein et al., 1951) dominate the partition of these elements between the shell and water so that the distribution coefficients often deviate significantly from expected thermodynamic equilibrium (see Schöne et al., 2010, for a brief review). For example, the relationship between the Sr/Ca ratio of shell carbonate and temperature varies massively between different species (Dodd, 1965; Gillikin et al., 2005; Stecher et al., 1996; Surge and Walker, 2006; Yan et al., 2013; Izumida et al., 2011) and among specimens of the same species (e.g., Toland et al., 2000; Hart and Blusztajn, 1998; Schöne et al., 2011). Aside from Sr/Ca and Mg/Ca, the Ba/Ca ratio of bivalve shells has received considerable attention as a potential proxy for salinity and primary productivity (e.g., Stecher et al., 1996; Vander Putten et al., 2000; Gillikin et al., 2006, 2008; Thébault et al., 2009; Elliot et al., 2009; Hatch et al., 2013). Ba/Ca_{shell} chronologies of marine bivalves are typically characterized by a relatively stable background

interrupted by sharp peaks (e.g., Stecher et al., 1996; Gillikin et al., 2006, 2008; Poulain et al., 2015). Background Ba/Ca_{shell} seems to be proportional to Ba/Ca_{water} which, in turn, is inversely correlated to salinity (Gillikin et al., 2006). The Ba/Ca_{shell} peaks are highly synchronous among specimens (e.g., Stecher et al., 1996; Gillikin et al., 2008; Elliot et al., 2009) suggesting a common environmental control. However, it remains a matter of debate if phytoplankton blooms account for these peaks (e.g., Stecher et al., 1996; Vander Putten et al., 2000; Thébault et al., 2009) or another, unknown environmental forcing (Gillikin et al., 2008).

Here, we present the results of laboratory experiments that study the combined effects of temperature, amount of food and element chemistry of the water as well as growth rate on the Sr/Ca and Ba/Ca ratios of aragonitic shells of the freshwater bivalve mollusk *Corbicula fluminea* (Fig. 3.1). *C. fluminea* belongs to the family Corbiculidae (Bivalvia, Mollusca). Its aragonitic shell is subdivided into an outer shell layer (OSL: crossed-lamellar microstructure) and an inner shell layer (ISL: complex crossed-lamellar microstructure) (Taylor et al., 1973; Prezant and Tan-Tiu, 1985; Fig. 3.1). To our knowledge, this is the first study that addresses the simultaneous influence of the above listed variables on the incorporation of trace elements into (freshwater) bivalve shells. We deliberately selected this species as a model organism because it is relatively easy to keep alive in laboratory tanks. It grows fast and precipitates new shell in an artificial environment. In addition, *C. fluminea* is particularly tolerant against a broad range of temperature (0-43 °C) and salinity regimes (< 24 PSU; McMahon, 1983). Close relatives (*C. japonica*) can even survive in fully marine environments (Komendantov, 1984). In near-freshwater conditions (< 3 PSU), *Corbicula* is a typical osmoregulator, i.e., it needs to maintain a higher ionic and osmotic concentration in the body fluids than that of the ambient environment. However, at higher salinities, this species becomes an osmoconformer (Gainey Jr and Greenberg, 1977) like most marine invertebrates. Its remarkable salinity tolerance and hyperosmotic body fluid are likely associated with its evolutionary roots. Ancestors of *Corbicula* inhabited estuarine settings (McMahon, 1983). Furthermore, this species exhibits a broad biogeographic distribution and belongs to a group of very successful invasive species (McMahon, 1983). Results of this study can contribute to a more detailed understanding of which factors control the partition of trace elements, specifically strontium and barium, between bivalve shells and the environment and identify potential synergetic factors controlling this element fractionation. Such information is prerequisite to evaluate the potential use of element signatures of fossil bivalve shells as paleoenvironmental proxies.

3.2. Materials and methods

3.2.1 Experimental setup

Individuals of *Corbicula fluminea* (16–24 mm shell length) were collected from Otterbach (49°4'33.61" N, 8°12'39.78" E), a small creek near Kandel, Rhineland-Palatinate, Germany. Bivalves were transported to the aquarium facility at the Institute of Geosciences, University of Mainz, where they were kept at 16 °C in recirculating water (120 L tank) under a 14:10 light-dark cycle for two weeks. Bivalves were fed daily with a mixture of two microalgae, *Scenedesmus quadricanda* and *Chlorella vulgaris* that were grown in sterilized water enriched with Bold's basal medium (Bischoff and Bold, 1963). Cell concentration was measured using a haemocytometer.

Afterward, specimens were randomly assigned to 1 L tanks at a density of five bivalves per aquarium. During the following week, they were acclimated to the experimental conditions. Each aquarium contained a 5 cm thick layer of sand and was gently aerated to minimize evaporation. Temperatures were maintained by immersing these aquariums in temperature controlled water baths held at 10, 16 and 22 °C, respectively. Each bath was equipped with a UA-001-08 HOBO® data logger which recorded temperature on an hourly basis. To increase the strontium and barium levels, a stock solution of $SrCl_2 \times 6H_2O$ and $BaCl_2 \times 2H_2O$ was added to the tanks until the desired element-to-calcium ratios were attained. By simultaneously increasing both elements, potential interactions between these elements were reduced (de Vries et al., 2005).

To accurately identify the shell portion that grew during the subsequent experiment, bivalves were immersed in a calcein solution (150 mg/L) for three hours (Thébault et al., 2006) and returned to the respective tank. Calcein is incorporated into the biomineral and fluoresces bright green when viewed under a UV-light microscope (Kaehler and McQuaid, 1999). Bivalves were reared in two sets of experiments in which combinations of environmental conditions were simulated that *C. fluminea* can experience under natural conditions in the river Rhine (Petter et al., 2014). In the first set of experiments, element chemistry was kept constant (Sr/Ca: ca. 2.4 mmol/mol and Ba/Ca: ca. 370 µmol/mol), whereas combinations of different water temperature (10, 16 and 22 °C) and different food level (an equal mixture of *S. quadricanda* and *C. vulgaris*; total concentrations of 0.2, 2, 4 and 8×10^4 cells/ml) were offered (Table 3.1). In the second set of experiments; food level was kept constant (4×10^4 cells/ml), whereas combinations of different water temperature (10, 16 and 22 °C) and water chemistry (pairs of Sr/Ca_{water} and Ba/Ca_{water}: ca. 4 mmol/mol and 600 µmol/mol, 8 mmol/mol and 1150

µmol/mol, 12 mmol/mol and 1500 µmol/mol, respectively) were simulated (Table 3.1). Each experiment was replicated three times.

During the experiment, 50% of the water in each tank was exchanged every third day to maintain the water quality. Several batches of new water with identical Sr/Ca and Ba/Ca ratios were prepared before each water exchange to ensure identical spiking levels were maintained in each tank (Table 3.1). The photoperiod was set at a 14:10 light-dark cycle. Bivalves were reared under controlled conditions for five weeks. At the end of the experiment, all specimens were stored at –20 °C until dissection and further analysis.

Table 3.1. Mean and standard error of Sr/Ca_{water} and Ba/Ca_{water} during the experiment. N = 5 water samples per analysis.

Temperature (°C)	Food supply (10^4 cells/ml)	Sr/Ca_{water} (mmol/mol)	Ba/Ca_{water} (µmol/mol)
First set of experiments			
10	0.2	2.34 ± 0.13	353 ± 11
	2	2.40 ± 0.12	329 ± 7
	4	2.45 ± 0.07	348 ± 9
	8	2.51 ± 0.15	381 ± 12
16	0.2	2.33 ± 0.11	357 ± 17
	2	2.37 ± 0.14	372 ± 7
	4	2.43 ± 0.08	387 ± 9
	8	2.56 ± 0.10	376 ± 24
22	0.2	2.44 ± 0.11	373 ± 16
	2	2.53 ± 0.06	365 ± 13
	4	2.42 ± 0.04	380 ± 14
	8	2.59 ± 0.12	387 ± 19
Second set of experiments			
10	2	4.32 ± 0.14	575 ± 36
	2	8.03 ± 0.24	1114 ± 53
	2	11.87 ± 0.29	1554 ± 94
16	2	4.53 ± 0.14	709 ± 19
	2	8.26 ± 0.20	1156 ± 75
	2	11.43 ± 0.29	1529 ± 143
22	2	4.47 ± 0.03	649 ± 46
	2	7.97 ± 0.13	1179 ± 87
	2	11.94 ± 0.25	1439 ± 102

3.2.2 Collection and chemical analysis of the water samples

Water samples (30 ml) for elemental analysis were taken from each tank on a weekly basis. Samples were filtered through 0.25 µm membrane filters, acidified with 100 µl of concentrated ultrapure HNO_3 and then stored in acid-washed teflon vials at 4 °C until analysis. The concentrations of calcium, strontium and barium were determined by means of a Spectro CIROS Vision^{SOP} inductively coupled plasma – optical emission spectrometer (ICP-OES) at the Institute of Geosciences, University of Mainz (Table 3.1). Mixed standard solutions were prepared from Roti® Star certified single element reference solutions. Relative standard deviations (RSD; based on five measurements of each external standard solution) were better than 1 RSD% for calcium, stronitum and barium. Accuracy was better than 3 % for all elements (determined by Roth Solution X multi element standard solution Lot W54710).

3.2.3 Shell preparation and analysis

Three clams from each aquarium were randomly selected for analysis. Bivalves were eviscerated with a scalpel and shells then rinsed in de-ionized water and air-dried. Subsequently, the left valve of each specimen was labelled and mounted on a Plexiglas cube with a quick-drying plastic welder. To avoid fracture during sawing, a thin layer of JB KWIK epoxy resin was applied to the shell surface along the axis of maximum growth (Fig. 3.1A). On that axis, a 3 mm-thick section was cut from each specimen using a Buehler Isomet 1000 low-speed saw (Fig. 3.1B). The shell sections were mounted on glass slides using epoxy resin, ground on glass plates with 800 and 1200 grit SiC powder and then polished on a Buehler G-cloth using 1 µm Al_2O_3 powder. All samples were finally ultrasonically cleaned with ultrapure water (18.2 MΩ cm).

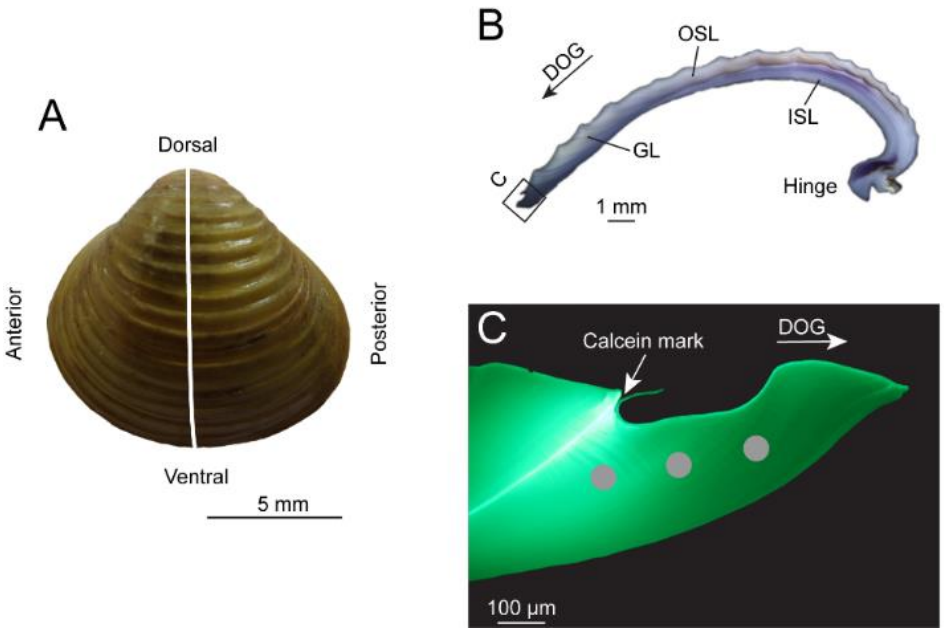

Fig. 3.1. Shell of *Corbicula fluminea*. (A) Outer shell surface of the left valve. A 3 mm-thick section was cut from the shell along the axis of maximum growth (white line). (B) Cross-section of the shell showing major shell structures. GL = growth line; ISL = inner shell layer, OSL = outer shell layer. (C) Magnification of the outer shell margin revealing a light calcein mark and newly formed shell portion. Grey dots indicate the positions for LA-ICP-MS. DOG = direction of growth.

To locate the calcein marks, polished shell sections were examined under a fluorescent light microscope (Zeiss Axio Imager A1.m stereomicroscope equipped with a Zeiss HBO 100 mercury lamp and filter set 38: excitation wavelength, ~450-500 nm; emission wavelength, ~500-550 nm). Photographs were taken with a Canon EOS 600D digital camera attached to the microscope. In each specimen, the amount of new shell material deposited after the calcein marks was measured using the image processing software ImageJ. To compute average daily growth rates, these values were then divided by 35, i.e. the number of days during which these shell portions were formed.

3.2.4 Chemical analysis of the shells

Strontium (measured as ^{88}Sr) and barium (measured as ^{137}Ba) of *C. fluminea* shells were determined by means of laser ablation – inductively coupled plasma – mass spectrometry (LA-ICP-MS) in "spot" mode at the Institute of Geosciences, University of Mainz. In each shell, three discrete spot measurements were completed in shell portions that formed during the experiment (i.e. between the ventral margin and the calcein mark) in the outer shell layer (Fig.

3.1C). Analyses were performed during three sequences on an Agilent 7500ce quadrupole ICP-MS coupled to a New Wave UP213 Nd: YAG laser ablation system. The laser was operated at a pulse rate of 10 Hz with laser energy at the sample site of ~4-6 J/cm^2. The measurements were completed with a beam diameter of 55 µm. Backgrounds were measured for 20 s prior to each ablation. Ablation time was 40 s followed by 20 s wash out. NIST SRM 610 was used for calibration, applying the preferred values reported in the GeoReM database (http://georem.mpch-mainz.gwdg.de/; Application Version 17; Jochum et al., 2005, 2011) as the "true" concentrations to calculate the element concentrations in the samples. During each sequence, basaltic USGS BCR-2G and synthetic carbonate USGS MACS-3 were analyzed as quality control materials (QCM) to monitor accuracy and reproducibility of the analyses. All references materials were analyzed at the beginning and at the end of a sequence and after ca. 39 spots on the samples (n = 9 to 18). For all materials, ^{43}Ca was used as internal standard. For the reference materials, we applied the calcium concentrations reported in the GeoReM database, and for the samples, the stoichiometric CaO content of 56.03 wt% for aragonite was used. The time-resolved signal was processed using the program GLITTER 4.4.1 (www.glitter-gemoc.com, Macquarie University, Sydney, Australia). Reproducibility based on repeated measurements of the external standards was always better than 7% (1 RSD). The measured strontium and barium concentrations of the QCM agree within 5 % with the preferred values of the GeoReM database for USGS BCR-2G, and within 8 % with the preliminary reference values for USGS MACS-3 (personal communication S. Wilson, USGS, in Jochum et al. 2012), respectively.

3.2.4 Statistical analysis

Data collected from the experiments were analyzed by means of the statistical software SPSS 19.0. Normality was tested by means of the Shapiro-Wilk's test and homogeneity of variance by means of the Levene's F-test. All data passed these two tests and were thus analyzed by means of parametric techniques. Two-way analysis of variance (ANOVA) was used to test for significant effects among treatments. Relationships between the Sr/Ca_{shell} and Ba/Ca_{shell} ratios of *C. fluminea* and environmental variables were studied by means of Pearson correlation analysis. Then, the root mean square error (RMSE) of the respective relationship was computed. The relationship between Sr/Ca_{shell} and growth rate was determined in a similar manner. Statistically significant difference was set at p values < 0.01.

3.3. Results

3.3.1 Effect of temperature, food level and water element-to-calcium ratio on Sr/Cashell and Ba/Cashell

To evaluate the combined effects of temperature and food supply on strontium incorporation into shells of *Corbicula fluminea*, the Sr/Ca_{water} level was maintained, on average, at 2.45 ± 0.02 mmol/mol (Table 3.1). As shown in Figure 3.2A, Sr/Ca_{shell} decreased by ca. 0.02 mmol/mol with every increase of temperature by 1 °C. Whereas 0.71 mmol/mol was recorded in the shells at 10 °C, only 0.48 mmol/mol was measured at 22 °C. As demonstrated by two-way ANOVA, this trend was virtually unaffected by food supply (Table 3.1S). The corresponding $K_D^{Sr/Ca}$ (= Sr/Ca_{shell} / Sr/Ca_{water}) values changed from 0.29 ± 0.02 at 10 °C to 0.19 ± 0.01 at 22 °C, i.e. -0.008 per 1 °C increase (Fig. 3.2B). Details on the regression analysis are given in Table 2.

The strontium content of the shells was directly proportional to the strontium concentration of the water in which the bivalves lived (Fig. 3.2C; Table 3.1S). At Sr/Ca_{water} levels of 4.44 ± 0.06, 8.09 ± 0.09 and 11.74 ± 0.16 mmol/mol, corresponding shell values equaled, on average, 1.07 ± 0.12, 2.00 ± 0.15 and 2.88 ± 0.16 mmol/mol, respectively (Fig. 3.2C). Accordingly, an increase of Sr/Ca_{water} by 1 mmol/mol resulted in an increase of Sr/Ca_{shell} by 0.25 ± 0.01 mmol/mol. Details on the regression analysis are given in Table 3.2.

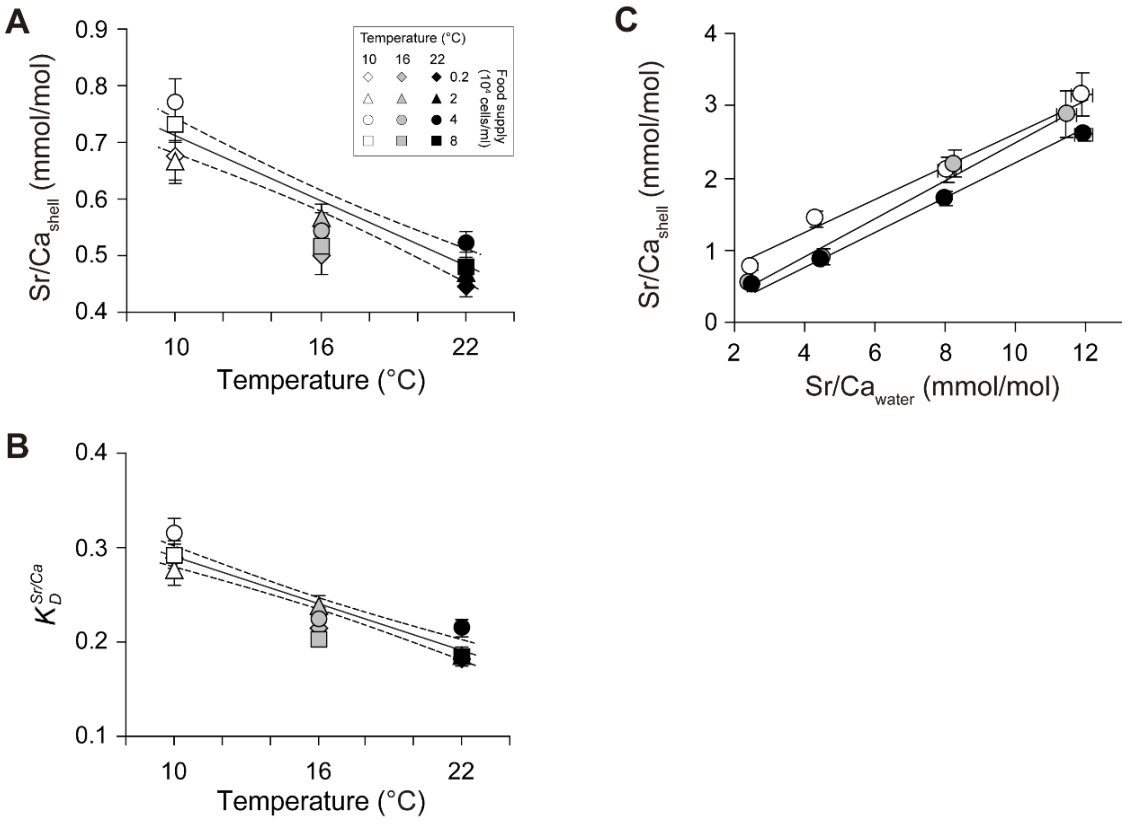

Fig. 3.2. Effect of temperature, food level, and Sr/Ca_{water} on the strontium incorporation into the shells of *Corbicula fluminea*. (A) Mean and standard error of Sr/Ca_{shell} for clams reared at different combinations of water temperature and food level. Sr/Ca_{shell} exhibited a statistically significant negative correlation with temperature ($R^2 = 0.490$; $p < 0.001$). Dashed lines represent 95% confidence intervals. (B) Mean and standard error of $K_D^{Sr/Ca}$ for clams reared at different combinations of water temperature and food level. A statistically significant negative relationship between $K_D^{Sr/Ca}$ and temperature was observed ($R^2 = 0.521$; $p < 0.001$). Dashed lines represent 95% confidence intervals. (C) Mean and standard error of Sr/Ca_{shell} for clams reared at different combinations of water temperature and Sr/Ca_{water} level. Sr/Ca_{shell} increased linearly proportional to Sr/Ca_{water} at 10 °C ($R^2 = 0.742$; $p < 0.001$); 16 °C ($R^2 = 0.740$; $p < 0.001$) and 22 °C ($R^2 = 0.922$; $p < 0.001$).

The incorporation of barium into shells of *C. fluminea* was more complex (Fig. 3.3). In the first set of experiments, Ba/Ca_{water} level was kept at 367 ± 5 µmol/mol (Table 3.1). At all four food levels, Ba/Ca_{shell} was negatively correlated to temperature (Fig. 3.3A). However, the slope of the regression lines increased with food supply. At low and moderate food levels (0.2 to 2×10^4 cells/ml), Ba/Ca_{shell} values decreased, on average, from ca. 31.00 µmol/mol at 10 °C to ca. 12.62 µmol/mol at 22 °C, i.e., Ba/Ca_{shell} changed by -1.53 µmol/mol per 1 °C temperature increase. Corresponding $K_D^{Ba/Ca}$ values decreased from ca. 0.09 ± 0.02 at 10 °C to 0.03 ± 0.01 at 22 °C (Fig. 3.3B). However, at higher food levels ($\geq 4 \times 10^4$ cells/ml), on average, Ba/Ca_{shell} reached values of 63.01 ± 13.13 µmol/mol at 10 °C ($K_D^{Ba/Ca} \approx 0.17 \pm 0.04$) and 20.17 ± 4.42 µmol/mol at 22 °C ($K_D^{Ba/Ca} \approx 0.05 \pm 0.01$). This corresponds to a slope of -3.57 µmol/mol per 1 °C change (Figs. 3.3A+B). The findings were confirmed by statistical tests. Two-way ANOVA confirmed a significant negative relationship between temperature and $K_D^{Ba/Ca}$ and a significant positive relationship between food level and $K_D^{Ba/Ca}$ (Table 3.2S). Details on the regression analysis are given in Table 3.2.

As in the case of strontium, Ba/Ca_{shell} increased proportionally with elevated Ba/Ca_{water} (Fig. 3.3C; Table 3.2S). However, a steeper slope was found at lower temperatures. At 10 °C, Ba/Ca_{shell} increased from 65.88 ± 15.23 µmol/mol at Ba/Ca_{water} of 348.36 ± 9.29 µmol/mol to 239.74 ± 63.39 µmol/mol at Ba/Ca_{water} of 1553.84 ± 93.88 µmol/mol. Hence, every increase in Ba/Ca_{water} by 100 µmol/mol was accompanied by a Ba/Ca_{shell} shift of 13.7 µmol/mol. In warmer water (16 ° and 22 °C), however, a change of Ba/Ca_{water} by 100 µmol/mol resulted only in a Ba/Ca_{shell} change of ca. 6.1 µmol/mol (Fig. 3.3C). Details on the regression analysis are given in Table 3.2.

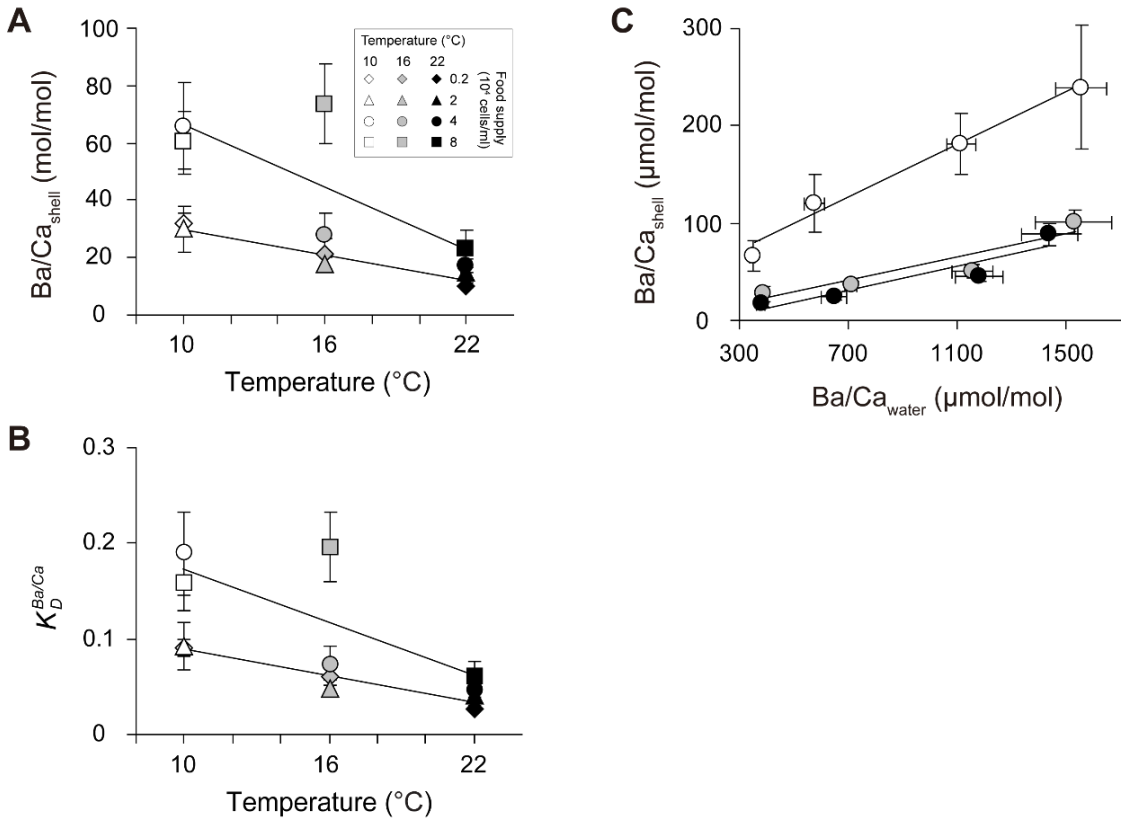

Fig. 3.3. Effect of temperature, food level, and Ba/Ca_{water} on barium incorporation into shells of *Corbicula fluminea*. (A) Mean and standard error of Ba/Ca_{shell} for clams reared at different combinations of water temperature and food level. Regression lines were computed for lower (0.2 and 2 × 10^4 cells/ml) and higher food supply (4 and 8 × 10^4 cells/ml). (B) Mean and standard error of $K_D^{Ba/Ca}$ for clams reared at different combinations of water temperature and food level. As in A, regression lines were calculated for lower and higher food levels. (C) Mean and standard error of Ba/Ca_{shell} for clams reared at different combinations of water temperature and Ba/Ca_{water} level. Ba/Ca_{shell} increased linearly proportional to Ba/Ca_{water} at 10 °C (R^2 = 0.252; p < 0.001); 16 °C (R^2 = 0.510; p < 0.001) and 22 °C (R^2 = 0.588; p < 0.001).

Table 3.2. Linear regression analyses of the geochemical properties of the shells of *Corbicula fluminea* and environmental variables (temperature [T]; food level [10^4 cells/ml]: 0.2 [F_1]; 2 [F_2]; 4 [F_3]; 8[F_4]; water chemistry: Sr/Ca_{water}; Ba/Ca_{water}). RMSE: root mean square error of the regression.

Variable	Regression	*n*	R^2	*p*	RMSE
Temperature					
at F_1 – F_4	Sr/Ca_{shell} = –0.019 (±0.002) × T + 0.883 (±0.032)	108	0.490	<0.001	0.098
	$K_D^{Sr/Ca}$ = –0.008 (±0.001) × T + 0.369 (±0.013)	108	0.521	<0.001	0.039
at F_1 & F_2	Ba/Ca_{shell} = – 1.532 (±0.356) × T + 45.586 (±5.950)	54	0.263	<0.001	12.801
	$K_D^{Ba/Ca}$= – 0.005 (±0.001) × T + 0.136 (±0.018)	54	0.281	<0.001	0.038
at F_3 & F_4	Ba/Ca_{shell} = – 3.570 (±0.926) × T + 101.76 (±15.494)	54	0.222	<0.001	33.334
	$K_D^{Ba/Ca}$= – 0.010 (±0.003) × T + 0.282 (±0.042)	54	0.236	<0.001	0.091
Water chemistry					
at 10 °C	Sr/Ca_{shell} = 0.242 (±0.025) × Sr/Ca_{water} + 0.246 (±0.186)	36	0.742	<0.001	0.532
	Ba/Ca_{shell} = 0.137 (±0.040) × Ba/Ca_{water} + 28.661 (±41.03)	36	0.252	<0.001	114.13
at 16 °C	Sr/Ca_{shell} = 0.273 (±0.028) × Sr/Ca_{water} – 0.189 (±0.208)	36	0.740	<0.001	0.576
	Ba/Ca_{shell} = 0.061 (±0.010) × Ba/Ca_{water} – 2.935 (±10.579)	36	0.510	<0.001	26.459
at 22 °C	Sr/Ca_{shell} = 0.222 (±0.011) × Sr/Ca_{water} – 0.055 (±0.084)	36	0.922	<0.001	0.238
	Ba/Ca_{shell} = 0.061 (±0.000) × Ba/Ca_{water} – 12.08 (±8.85)	36	0.588	<0.001	22.169

3.3.2 Effect of temperature and food level on shell growth rate

During the experiments (= manipulation phase: calcein mark to ventral margin), the bivalves added between 134 and 374 µm of shell material along the axis of maximum growth. The rate of shell production was clearly linked to the combined effects of temperature and food supply (Fig. 3.4). Shells grew faster at higher temperatures and if more food was offered. The fastest increase occurred, if both food level and temperature were elevated (Fig. 3.4). For example, at low food levels (0.2×10^4 cells/ml), ca. 3.84 ± 0.08 µm of shell material was added every day when temperatures were around 10 °C. However, at 22 °C, the rate of shell growth increased by ca. 130% to reach levels of 4.97 ± 0.18 µm per day. Greater amounts of algae favored faster shell growth and a more rapid growth rate increase at rising temperatures. For example, a tenfold increase in algal concentration (to 2×10^4 cells/ml)

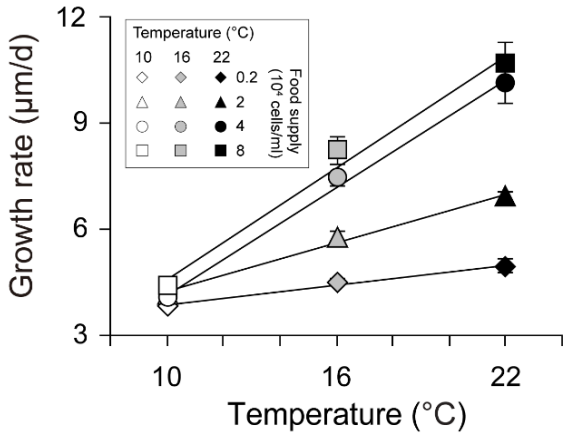

Fig. 3.4. Mean and standard error of shell growth rate for *Corbicula fluminea* reared at different combinations of water temperature and food level.

at 22 °C nearly caused a doubling of daily shell growth (6.92 ± 0.17 µm/day). At a further twofold increase of food supply (4×10^4 cells/ml), shells grew 10.10 ± 0.55 µm/day (Fig. 3.4). However, higher food levels did not result in a significant further increase in growth rate (Fig. 3.4). Between food levels of 0.2 and 8×10^4 cells/ml, every change in temperature by 1 °C resulted in a change of daily shell growth between 0.09 and 0.52 µm. Further details on the regression analysis are given in Table 3.3.

Table 3.3. Linear regression analyses of shell growth rate (GR) of *Corbicula fluminea* and temperature (T) at different food levels. RMSE: root mean square error of the regression.

Food level (10^4 cells/ml)	Regression	*n*	R	R^2	RMSE
0.2	GR = 0.094 (±0.015) × T + 2.934 (±0.247)	27	0.621	<0.001	0.375
2	GR = 0.229 (±0.021) × T + 1.970 (±0.350)	27	0.827	<0.001	0.533
4	GR = 0.502 (±0.041) × T – 0.845 (±0.686)	27	0.857	<0.001	1.044
8	GR = 0.524 (±0.049) × T – 0.609 (±0.822)	27	0.819	<0.001	1.250

3.3.3 Effect of growth rate on Sr/Cashell and Ba/Cashell

As demonstrated in Figure 3.5, the rate of shell growth had only a negligible effect on Sr/Ca_{shell}, particularly at lower temperatures. For example, Sr/Ca_{shell} values of shell portions that grew at different rates at 16 °C were statistically indistinguishable (average Sr/Ca_{shell} at 16 °C = 0.53 mmol/mol) (Table 3.4). At 22 °C, slightly higher Sr/Ca_{shell} were observed in faster growing shell portions (Table 3.4), but again this relationship is statistically not significant at $p < 0.01$.

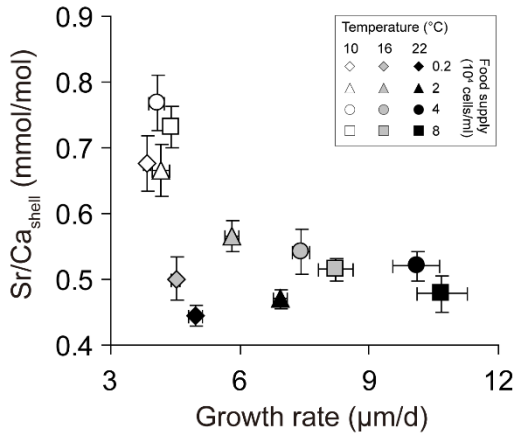

Fig. 3.5. Effect of growth rate on strontium incorporation into shells of *Corbicula fluminea*. Mean and standard error is shown for Sr/Ca_{shell} and growth rate at different combinations of water temperature and food level.

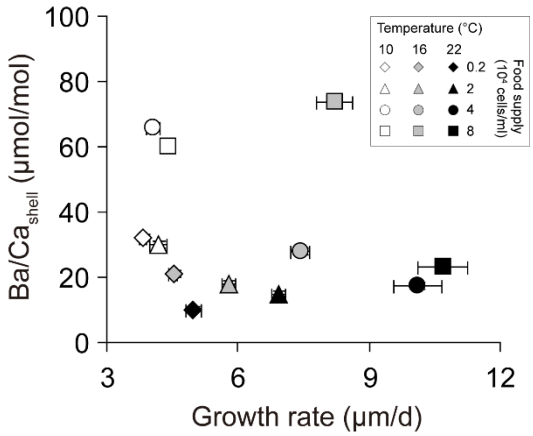

Fig. 3.6. Effect of growth rate on barium incorporation into shells of *Corbicula fluminea*. Mean and standard error is shown for Ba/Ca_{shell} and growth rate at different combinations of water temperature and food level.

Figure 3.6 shows the statistical relationship between shell growth rate and Ba/Ca_{shell}. At a given temperature, Ba/Ca_{shell} appeared to be higher in faster growing shell portions. However, with increasing water temperature, the effect of growth rate on Ba/Ca_{shell} values decreased. For example, at 16 °C Ba/Ca_{shell} increased by 6.58 µmol/mol per 1 µm/day increase in shell height, whereas at 22 °C the slope decreased sharply to 1.19 µmol/mol per 1 µm/day shell growth (Fig. 3.6). Note that none of these relationships reached the significance level (Table 3.4). In general, highest Ba/Ca_{shell} values were observed in food-enriched cold water and when shell formation was slowest.

Table 3.4. Linear regression analyses of the geochemical properties of the shells of *Corbicula fluminea* and its shell growth rate at different temperature regimes. RMSE: root mean square error of the regression.

Temperature (°C)	Regression	*n*	R^2	*p*	RMSE
10 °C	Sr/Ca_{shell} = –0.031 (±0.043) × GR + 0.840 (±0.178)	36	0.015	0.470	0.122
	Ba/Ca_{shell} = 1.059 (±0.522) × GR + 27.42 (±11.078)	36	0.108	0.050	34.432
16 °C	Sr/Ca_{shell} = –0.003 (±0.009) × GR + 0.551 (±0.059)	36	0.004	0.726	0.086
	Ba/Ca_{shell} = 6.582 (±3.348) × GR – 7.543 (±22.377)	36	0.102	0.057	32.058
22 °C	Sr/Ca_{shell} = 0.005 (±0.004) × GR + 0.438 (±0.036)	36	0.040	0.024	0.066
	Ba/Ca_{shell} = 1.186 (±0.697) × GR + 6.711 (±5.979)	36	0.078	0.098	10.933

3.4. Discussion

3.4.1. Controls on strontium incorporation into the shells

Like many other bivalves, *C. fluminea* seems to actively control how much strontium substitutes calcium in the shell carbonate. Between 10 and 22 °C, the distribution coefficient ($K_D^{Sr/Ca} \approx$ 0.23; Fig. 3.2B) was four to five times smaller than that of abiogenic aragonite (Gaetani & Cohen 2006) and compared well to $K_D^{Sr/Ca}$ values reported for a range of other marine (*Saxidomus giganteus*: ~0.25, Gillikin et al., 2005; *Mya arenaria*: ~0.23, Strasser et al., 2008a; *Arctica islandica*: ~0.13-0.28, Schöne et al., 2011) and freshwater bivalves (e.g., *Lampsilis* sp.: ~0.25, Faure et al., 1967; *Margaritifera margaritifera*: ~0.28, Bailey & Lear, 2006; *Hyriopsis* sp.: ~0.2, Izumida et al., 2011).

Irrespective of the amount of food offered, Sr/Ca_{shell} increased linearly proportional to Sr/Ca_{water} (Fig. 3.2C) suggesting that shell strontium content came exclusively from dissolved strontium of the ambient water. This interpretation agrees well with observations by Lorens and Bender (1980) according to which Sr/Ca_{shell} of both layers (aragonite and calcite) of *Mytilus edulis* was linearly correlated to Sr/Ca_{water}. Likewise, Sr/Ca_{shell} of some freshwater bivalves (Faure et al., 1967: *Lampsilis* sp.; Bailey and Lear, 2006: *M. margaritifera*; Carroll and Romanek, 2008: *Elliptio complanata*) and gastropods (Buchardt and Fritz, 1978; Anadón et al., 2010) is directly proportional to Sr/Ca_{water}. The linear correlation between Sr/Ca in the water and the shell is somewhat surprising. Freshwater invertebrates including bivalves are osmoregulators, i.e., a higher ionic and osmotic concentration is maintained in the body fluids and the cytoplasma than in the ambient environment. This is accomplished by pumping salts, specifically Na^+, into the body fluids (Dietz, 1977). Unlike many other freshwater bivalves, *C. fluminea* shows a very high osmotic concentration in the body fluids (= hyperosmotic species) which requires high metabolic rates (Dietz, 1979). If specific Sr^{2+} pumps were present and Sr^{2+} was actively transported to the EPF, one would expect a significant positive relationship between metabolic rate (growth rate) and Sr/Ca_{shell}. Evidently, this was not the case (Fig. 3.5; Table 3.4). Presumably, the great majority of Sr^{2+} comes from the ambient water and can freely pass through ion channels of the mantle epithelia (Stewart, 1984) to reach the EPF or is absorbed by the gills (Simkiss, 1981), enters the hemolymph and finally reaches the EPF through ion channels of the inner mantle epithelium (Anderson, 1979; Simkiss and Taylor, 1995). A negligible amount of Sr^{2+} may also reach the body fluids through Ca^{2+}-ATPase enzymes (Fujimori and Jencks, 1992; Champeil, 1996).

We were unable to verify that kinetic effects occurred. When temperature was maintained constant, neither changes in shell growth rate (which is closely linked to the rate of crystal growth and hence, kinetics) nor changes in food supply had a statistically significant effect on Sr/Ca_{shell} values of *C. fluminea* (Figs. 3.2+3.5; Table 3.4). This finding is at odds with the results of abiogenic precipitation experiments by Gaetani and Cohen (2006) according to which fast growing synthetic aragonite contains larger amounts of strontium than aragonite that was precipitated slowly. However, equivalent studies by Kinsman and Holland (1969), Zhong and Mucci (1989) and Mucci et al. (1989) suggested that kinetic effects do not affect Sr/Ca ratios of abiogenic aragonite.

In agreement with Gaetani and Cohen (2006), some sclerochronological studies postulated a link between Sr/Ca_{shell} and growth rate of several bivalve species such as *Modiolus modiolus*, *Mytilus edulis* and *Mya arenaria* (Swan, 1956), *Protothaca staminea* (Takesue and van Geen 2006), *Pecten maximus* (Lorrain et al, 2005) and the freshwater bivalve *Hyriopsis* sp. (Izumida et al., 2011). Other authors were unable to find such a correlation. For example, it was absent in the specimens of *Cerastoderma edule* studied by Füllenbach et al. (2015). Thus, growth rate and Sr/Ca_{shell} were not directly linked. In the long-lived *Arctica islandica*, Sr/Ca_{shell} was apparently negatively correlated to shell growth rate (Schöne et al., 2011). However this relationship demonstrably did not reflect a causal link, but merely an increase in the number of Sr-enriched annual growth lines per shell unit in older shell portions (Schöne et al., 2010, 2011). When sampled with the same spatial resolution, an ontogenetically young shell portion returned low strontium levels, because a greater proportion of strontium-poor growth increments were present, whereas a slow-growing, ontogenetically old shell portion returned higher strontium levels, because the proportion of growth lines to increments was larger. Thus, the apparent increase in strontium through ontogeny in *A. islandica* is merely a sampling bias. However, we can still not preclude the possibility that a causal link exists between growth rate and Sr/Ca_{shell} in some bivalve species.

The only other environmental variable aside from Sr/Ca_{water} that statistically significantly affected Sr/Ca_{shell} (and $K_D^{Sr/Ca}$) in our experiment was temperature. Shells of *C. fluminea* formed in warmer water contained lower amounts of strontium than those grown in cold water (Fig. 3.2A). This negative relationship has not only been observed in some other bivalve species (Dodd, 1965; Schöne et al., 2011; Yan et al., 2013), but also in abiogenic precipitation experiments (Kinsman and Holland, 1969; Dietzel et al., 2004; Gaetani and Cohen, 2006). Furthermore, the slope between temperature and Sr/Ca_{shell} (-0.02; Table 3.2) is close to

that of synthetic aragonite (-0.04; Dietzel et al., 2004) and corals (-0.04; Corrège, 2006) implying that Sr/Ca_{shell} of *C. fluminea* is at least partially under thermodynamic control.

3.4.2. Controls on barium incorporation into the shells

Distribution coefficients for Ba/Ca_{shell} were generally lower than for Sr/Ca_{shell} indicating a stronger vital effect. Between 10 and 22 °C, the distribution coefficient ($K_D^{Ba/Ca} \approx 0.09$; Fig. 3.3B) was ca. 16 to 32 times smaller than that of abiogenic aragonite (Dietzel et al., 2004; Gaetani and Cohen 2006), but agreed well with $K_D^{Ba/Ca}$ values of many other bivalves including marine and estuarine species (e.g., Strasser et al., 2008a; Gillikin et al., 2008; Poulain et al., 2015; Barats et al., 2009; Tabouret et al., 2012). Interestingly, *Donax gouldii* has a much higher $K_D^{Ba/Ca}$ value of 0.95 (Hatch et al., 2009).

As in the case of strontium, shell barium levels and temperature were anticorrelated (Fig. 3.3A). Similar findings were reported for other bivalves (e.g. Strasser et al., 2008a) and abiogenic aragonite (Gaetani and Cohen, 2006). However, Ba/Ca_{shell} values were also strongly influenced by a number of other complexly intertwined factors, namely food supply, shell growth rate and Ba/Ca_{water}. Higher concentrations of barium (relative to calcium) in the water resulted in proportionately higher Ba/Ca_{shell} values suggesting the primary source for barium is the ambient water (see also Lorens and Bender, 1990; Gillikin et al., 2006; Tabouret et al., 2012). Presumably, barium can freely pass through transmembrane ion channels of the mantle epithelia (Anderson, 1979; Stewart, 1994; Simkiss and Taylor, 1995).

The relationship between Ba/Ca_{shell} and growth rate has barely been explored. Strasser et al. (2008b) observed a negative relationship between Ba/Ca_{shell} and growth rate of *Mya arenaria*. Conversely, Izumida et al. (2011) claimed that Ba/Ca_{shell} of *Hyriopsis* sp. and shell growth rate were positively correlated. Following the results of the present study, Ba/Ca_{shell} was simultaneously controlled by temperature and food availability. Highest barium levels occurred in shells that grew in cold, food enriched water (Fig. 3.3A). When food levels were doubled or quadrupled (increase from 2 to 4 and 8 × 10^4 cells/ml) at 10 °C, Ba/Ca_{shell} values increased twofold, whereas shell growth rates remained nearly unchanged (Fig. 3.6). This observation can be explained as follows. The additional barium that was incorporated into the shells most likely originated from the algae. Although the barium content of the phytoplankton was not determined in this study, existing studies noticed the presence of barium in phytoplankton (Stecher et al., 1998; Choudhury and Cary, 2001; Thébault et al., 2009; Hatch et al., 2013).

Gillikin et al. (2006) proposed a simple test to check if food-derived barium ended up in the shell. If the regression line between Ba/Ca_{shell} and Ba/Ca_{water} goes through the origin, shell barium comes exclusively from the ambient water, otherwise a contribution of barium from food is likely. In our study, the latter was the case (Fig. 3.6). However, such interpretation fails to explain the following observations. In warmer water, the surplus of food lead to significantly increased shell growth rates (Figs. 3.3A + 3.6) without increasing the Ba/Ca_{shell} beyond values observed in shells of specimens that had received less food (Fig. 3A; but excluding the anomalous high Ba/Ca_{shell} that occurs with high food supply at 16 °C).

During digestion, the barium is released from the phytoplankton, enters the hemolymph in dissolved form, then eventually reaches the extrapallial fluid (EPF) through Ca^{2+} ion channels (Markich and Jeffree, 1994) and can be incorporated into the crystal lattice (Takesue et al., 2008). Within the EPF, organic macromolecules control the amount of trace and minor elements that become part of the biomineral (Shirai et al., 2014). The selection efficiency likely increases with metabolic rate which, in turn, increases with temperature and food level. Hence, larger amounts of barium become incorporated into the shell when plenty of food is offered and temperatures are low, but lower amounts of barium when temperature and metabolic rate (and thus, growth rate) increase. Furthermore, during faster shell growth, the amount of barium in the EPF that can potentially be incorporated into the shell is distributed over a larger shell portion. The concentration in a given unit of shell will hence be smaller than during slow shell formation. An alternative hypothesis is that different types of organic macromolecules are produced during increased metabolic rates that exclude barium more efficiently from the biomineral. Support for this hypothesis comes from the different color of the fecal pellets expelled during slow (low food level) and fast shell growth (high food level).

To quantify how much food-derived barium becomes incorporated into the biomineral, future studies should isotopically label phytoplankton and measure the isotope ratios of barium in the shell by means of LA-Multi Collector-ICP-MS. This approach would also require to precisely determine the amount of food ingested (and digested) by individual specimens; evidently this is an extremely challenging task. Notably, Gillikin et al. (2006) noticed that the microalgae *Chlamidomonas reinhardii* grown in differently enriched Ba^{2+} media did not significantly affect the Ba/Ca_{shell} ratio of *Mytilus edulis*. Most likely, the Ba^{2+} concentration of the phytoplankton is species-specific (Fisher et al., 1991), and therefore, it needs to be assessed how much barium is contributed to the biomineral by different algal species.

3.4.3. Significance for environmental reconstructions based on Sr/Cashell and Ba/Cashell

As demonstrated by the regression analysis of Figure 3.2, Sr/Ca_{shell} of *C. fluminea* can potentially provide temperature estimates to the nearest 3.5 °C if the Sr/Ca_{water} signature is known (Fig. 3.2A; Table 3.2). Since Sr/Ca_{water} of freshwater ecosystems can vary throughout different seasons and between years, Sr/Ca_{shell}-based temperature reconstructions can be more imprecise if these variations are not considered. Factors that can potentially affect Sr/Ca_{water} include precipitation rate, river runoff, eolian dust and the geological setting etc. An unnoticed shift of Sr/Ca_{water} by 0.1 mmol/mol results in a temperature error of ca. 0.65 °C (Fig. 3.2C). Knowledge of the geological setting during shell formation is therefore essential. Modern rivers can provide an idea on possible Sr/Ca_{water} fluctuations. From the upper portion of the river Rhine, Müller (1969) reported seasonal extremes of 4.67 and 11.82 mmol/mol, equivalent to ± 23.3 °C. Sr/Ca_{water} values of 0.43 to 1.75 mmol/mol have been reported for different rivers of the Great Lakes region by Faure et al. (1967). This variation could cause a temperature uncertainty of ± 4.3 °C. Significantly less variability (1.90 and 1.36 mmol/mol; ± 1.8 °C) occurred at different localities of the river Ehen, U.K. (Bailey and Lear, 2006). During the monsoon season, the Sr/Ca_{water} values of the river Buha in the NE Tibetan Plateau varied between 1.4 and 1.7 mmol/mol, which would result in a temperature error of ca. ± 1 °C if it remained unnoticed. These examples illustrate that no generalized statement is possible on the potential use of Sr/Ca_{shell}-based temperature reconstructions using *C. fluminea*. In freshwater ecosystems with low Sr/Ca_{water} variance, Sr/Ca_{shell} values can serve as a useful temperature proxy, likely better than $\delta^{18}O$ values. However, at localities with large Sr/Ca_{water} changes, this thermometer is unsuitable. Shells of *C. fluminea* from estuarine settings at salinities above 8 to 10, i.e., where Sr/Ca_{water} signatures remain fairly invariant (Dodd and Crisp, 1982), may provide the most reliable Sr/Ca_{shell}-based temperature data.

Interpreting the Ba/Ca_{shell} data of *C. fluminea* is much more challenging, because the number of variables controlling the barium levels in the shell are much more complex and interwoven with each other. Furthermore, the Ba/Ca_{water} values of freshwater ecosystems exhibit similar spatiotemporal variations as Sr/Ca_{water} (e.g., Izumida et al., 2011).

Since the experiments of the present study have been conducted with a species that evolved – on a geological time scale – only quite recently from marine ancestors and that tolerate a broad range of different salinity regimes, the findings may be applicable to some marine bivalves as well. Therefore, future studies should conduct similar laboratory

experiments and consider that shell element chemistry is often controlled by multiple, complexly interwoven environmental and physiological factors.

3.5. Summary and conclusions

As demonstrated by the findings of this study, the amount of trace impurities in shells of *Corbicula fluminea* is controlled by a complex interaction of vital effects, temperature, food supply, element-to-calcium level in the water and, perhaps, kinetics (shell growth rate). Although the results of this study can likely not be directly transferred to other freshwater and marine species, they can serve as a guideline which environmental and physiological variables should be monitored in more detail in subsequent field and laboratory experiments.

Reliable paleotemperature reconstructions based on Sr/Ca_{shell} of *C. fluminea* from freshwater habitats will remain challenging unless the spatiotemporal variability of Sr/Ca_{water} is known. However, at salinities above 8 to 10, both element-to-calcium ratios are more conservative than in freshwater environments (Dodd and Crisp, 1982). Element signatures in shells of *C. fluminea* that survived in such habitats (and grew shell) can potentially serve as faithful recorders of past temperature.

Interpreting Ba/Ca_{shell} of *C. fluminea* in terms of (paleo) environmental change is much more challenging because food level (and shell growth rate) also exerts a noticeable influence on shell barium enrichment. If the same is true for marine species, the potential use of Ba/Ca_{shell} as indicators of salinity (e.g., Gillikin et al., 2006, 2008) or phytoplankton abundance (e.g., Stecher et al., 1996; Vander Putten et al., 2000; Thébault et al., 2009) should be critically re-assessed.

3.6. Acknowledgments

Not displayed for reasons of data protection

3.7. References

Anadón, P., Martín-Rubio, M., Robles, F., Rodriguez-Lázaro, J., Utrilla, R., Vázquez, A., 2010. Variation in Sr uptake in the shell of the freshwater gastropod *Bithynia tentaculata* from Lake Arreo (northern Spain) and culture experiments. Palaeogeogr. Palaeoclimatol. Palaeoecol. 288, 24-34.

Anderson, M., 1979. Mn^{2+} ions pass through Ca^{2+} channels in myoepithelia cells. J. Exp. Biol. 82, 227-238.

Bailey, T.R., Lear, C.H., 2006. Testing the effect of carbonate saturation on the Sr/Ca of biogenic aragonite: a case study from the River Ehen, Cumbria, UK. Geochem. Geophys. Geosyst. 7, Q03019. DOI: 10.1029/2005GC001084.

Barats, A., Amouroux, D., Chauvaud, L., Pécheyran, C., Lorrain, A., Thébault, J., Church, T.M., Donard, O.F.X., 2009. High frequency barium profiles in the shells of the great scallop *Pecten maximus*: a methodical long-term and multi-site survey in Western Europe. Biogeosci. 6, 157-170.

Beck, J.W., Edwards, R.L., Ito, E., Taylor, F.W., Recy, J., Rougerie, F., Joannot, P., Henin, C., 1992. Sea-surface temperature from coral skeletal strontium/calcium ratios. Science 257, 644-647.

Bischoff, H.W., Bold, H.C., 1963. Physiological studies. IV. Some algae from enchanted rock and related algal species. University of Texas. Publ. 6318, 95.

Bragg, W.L., 1913. The Structure of some crystals as indicated by their diffraction of X-rays. Proc. R. Soc. London A89, 248-277.

Bragg, W.L., 1924. The structure of aragonite. Proc. R. Soc. London A105, 16-39.

Buchardt, B., Fritz, P., 1978. Strontium uptake in shell aragonite from the freshwater gastropod *Limnaea stagnalis*. Science 199, 291-292.

Carroll, M., Romanek, C.S., 2008. Shell layer variation in trace element concentration for the freshwater bivalve *Elliptio complanata*. Geo-Mar. Lett. 28, 369-381.

Champeil, P., 1996. Kinetic characterization of sarcoplasmic reticulum Ca^{2+}-ATPase. Biomembranes: A Multi-Volume Treatise 5, 43-76.

Choudhury, H., Cary, R., 2001. Barium and barium compounds. Concise Int. Chem. Assess. Doc. 33, 1-52.

Corrège, T., 2006. Sea surface temperature and salinity reconstruction from coral geochemical tracers. Palaeogeogr. Palaeoclimatol. Palaeoecol. 232, 408-428.

de Vries, M.C., Gillanders, B.M., Elsdon, T.S., 2005. Facilitation of barium uptake into fish otoliths: influence of strontium concentration and salinity. Geochim. Cosmochim. Acta. 69, 4061-4072.

Dietz, T.H., 1979. Uptake of sodium and chloride by freshwater mussels. Can. J. Zool. 57, 156-160.

Dietz, T.H., 1977. Solute and water movement in freshwater bivalve mollusks (Pelecypoda; Unionidae; Corbiculidae; Margaritiferidae.). In: Jungreis, A.M., Hodges, T.K., Kleinzeller, A., Schultz, S.G. (Eds), Water relations in membrane transport in plants and animals. Academic Press, Inc., New York, pp. 111-119.

Dietzel, M., Gussone, N., Eisenhauer, A., 2004. Co-precipitation of Sr^{2+} and Ba^{2+} with aragonite by membrane diffusion of CO_2 between 10 and 50 °C. Chem. Geol. 203, 139-151.

Dodd, J.R., 1965. Environmental control of strontium and magnesium in *Mytilus*. Geochim. Cosmochim. Acta. 29, 385-398.

Dodd, J.R., Crisp, E.L., 1982. Non-linear variation with salinity of Sr/Ca and Mg/Ca ratios in water and aragonitic bivalve shells and implications for paleosalinity studies. Palaeogeogr. Palaeoclimatol. Palaeoecol. 38, 45-56.

Elliot, M., Welsh, K., Chilcott, C., McCulloch, M., Chappell, J., Ayling, B., 2009. Profiles of trace elements and stable isotopes derived from giant long-lived *Tridacna gigas* bivalves: potential applications in paleoclimate studies. Palaeogeogr. Palaeoclimatol. Palaeoecol. 280, 132-142.

Epstein, S., Buchsbaum, R., Lowenstam, H., Urey, H.C., 1951. Carbonate-water isotopic temperature scale. Bull. Geol. Soc. Am. 62, 417-426.

Faure, G., Crocket, J.H., Hueley, P.M., 1967. Some aspects of the geochemistry of strontium and calcium in the Hudson Bay and the Great Lakes. Geochim. Cosmochim. Acta. 31, 451-461.

Fisher, N.S., Guillard, R.R.L., Bankston, D.C., 1991. The accumulation of barium by marine phytoplankton grown in culture. J. Mar. Res. 49, 339-354.

Fujimori, T, Jencks, W.P., 1992. Binding of two Sr^{2+} ions changes the chemical specificities for phosphorylation of the sarcoplasmic reticulum Calcium ATPase through a stepwise mechanism. J. Biol. Chem. 267, 18475-18487.

Füllenbach, C.S., Schöne, B.R., Mertz-Kraus, R., 2015. Strontium/lithium ratio in aragonitic shells of *Cerastoderma edule* (Bivalvia) — A new potential temperature proxy for brackish environments. Chem. Geol. 417, 341-355.

Gaetani, G.A., Cohen, A.L., 2006. Element partitioning during precipitation of aragonite from seawater: a framework for understanding paleoproxies. Geochim. Cosmochim. Acta. 70, 4617-4634.

Gainey Jr, L.F., Greenberg, M.J., 1977. Physiological basis of the species abundance-salinity relationship in molluscs: a speculation. Mar. Biol. 40, 41-49.

Gillikin, D.P., Dehairs, F., Lorrain, A., Steenmans, D., Baeyens, W., André, L., 2006. Barium uptake into the shells of the common mussel (*Mytilus edulis*) and the potential for estuarine paleo-chemistry reconstruction. Geochim. Cosmochim. Acta. 70, 395-407.

Gillikin, D.P., Lorrain, A., Navez, J., Taylor, J.W., André, L., Keppens, E., Baeyens, W., Dehairs, F., 2005. Strong biological controls on Sr/Ca ratios in aragonitic marine bivalve shells. Geochem. Geophys. Geosyst. 6, Q05009. DOI: 10.1029/2004GC000874.

Gillikin, D.P., Lorrain, A., Paulet, Y.M., André, L., Dehairs, F., 2008. Synchronous barium peaks in high-resolution profiles of calcite and aragonite marine bivalve shells. Geo-Mar. Lett. 28, 351-358.

Hanna, R.G., Muir, G.L., 1990. Red sea corals as biomonitors of trace metal pollution. Environ. Monit. Assess. 14, 211-222.

Hart, S.R., Blusztajn, J., 1998. Clams as recorders of ocean ridge volcanism and hydrothermal vent field activity. Science 280, 883-886.

Hatch, M.B., Schellenberg, S.A., Carter, M.L., 2013. Ba/Ca variations in the modern intertidal bean clam *Donax gouldii*: An upwelling proxy?. Palaeogeogr. Palaeoclimatol. Palaeoecol. 373, 98-107.

Izumida, H., Yoshimura, T., Suzuki, A., Nakashima, R., Ishimura, T., Yasuhara, M., Inamura, A., Shikazono, N., Kawahata, H., 2011. Biological and water chemistry controls on Sr/Ca, Ba/Ca, Mg/Ca and $\delta^{18}O$ profiles in freshwater pearl mussel *Hyriopsis* sp. Palaeogeogr. Palaeoclimatol. Palaeoecol. 309, 298-308.

Jochum, K.P., Nohl, U., Herwig, K., Lammel, E., Stoll, B., Hofmann, A.W., 2005. GeoReM: a new geochemical database for reference materials and isotopic standards. Geostand. Geoanal. Res. 29, 87-133.

Jochum, K.P., Scholz, D., Weis, U., Wilson, S.A., Yang, Q., Schwalb, A., Börner, N., Jacob, D.E., Andreae, M.O., 2012. Accurate trace element analysis of speleothems and biogenic calcium carbonates by LA-ICP-MS. Chem. Geol. 318-319, 31-44.

Jochum, K.P., Weis, U., Stoll, B., Kurmin, D., Yang, Q., Raczek, I., Jacob, D.E., Stracke, A., Birbaum, K., Frick, D.A., Günther, D., Enzweiler, J., 2011. Determination of reference values for NIST SRM 610-617 glasses following ISO guidelines. Geostand. Geoanal. Res. 35, 397-429.

Kaehler, S., McQuaid, C.D., 1999. Use of the fluorochrome calcein as an in situ growth marker in the brown mussel *Perna perna*. Mar. Biol. 133, 455-460.

Kastner, M., 1999. Oceanic minerals: Their origin, nature of their environment and significance. Proc. Natl. Acad. Sci. 96, 3380-3387.

Kinsman, D.J., Holland, H.D., 1969. The co-precipitation of cations with $CaCO_3$—IV. The co-precipitation of Sr^{2+} with aragonite between 16° and 96 °C. Geochim. Cosmochim. Acta. 33, 1-17.

Komendantov A.Y. 1984. Osmoregulation capacities of *Corbicula japonica* (Bivalvia, Corbiculidae) in water of various salinity. Zool. J. 63, 769-771. (In Russian with English summary).

Lorens, R. B., Bender, M.L., 1980. The impact of solution chemistry on *Mytilus edulis* calcite and aragonite. Geochim. Cosmochim. Acta. 44, 1265-1278.

Lorrain, A., Gillikin, D., Paulet, Y.M., Chavaud, L., Lemercier, A., Navez, J., Andre, J., 2005. Strong kinetic effects on Sr/Ca ratios in the calcitic bivalve *Pecten maximus*. Geology 33, 965-968.

Markich, S.J., Jeffree, R.A., 1994. Adsorption of divalent trace metals as analogues of calcium by Australian freshwater bivalves: an explanation of how water hardness reduces metal toxicity. Aquat. Toxicol. 29, 257-290.

McCulloch, M, Fallon, S., Wyndham, T., Hendy, E., Lough, J., Barnes, D., 2003. Coral record of increased sediment flux to the inner Great Barrier Reef since European settlement. Nature 421, 727-730.

McMahon, R.F., 1983. Ecology of an invasive pest bivalve, *Corbicula*. Mollusca. 6, 505-561.

Mucci, A., Canuel, R., Zhong, S., 1989. The solubility of calcite and aragonite in sulphate-free seawater and the seeded growth kinetics and composition of the precipitates at 25 °C. Chem. Geol. 74, 309-320.

Müller, G., 1969. High strontium contents and Sr/Ca-ratios in Lake Constance waters and carbonates and their sources in the drainage area of the Rhine River (Alpenrhein). Mineral. Deposita. 4, 75-84.

Petter, G., Weitere, M., Richter, O., Moenickes, S., 2014. Consequences of altered temperature and food conditions for individuals and populations: a Dynamic Energy Budget analysis for *Corbicula fluminea* in the Rhine. Freshw. Biol. 59, 832-846.

Poulain, C., Gillikin, D.P., Thebault, J., Munaron, J.M., Bohn, M., Robert, R., Paulet, Y.-M., Lorrain, A., 2015. An evaluation of Mg/Ca, Sr/Ca, and Ba/Ca ratios as environmental proxies in aragonite bivalve shells. Chem. Geol. 396, 42-50.

Prezant, R.S., Tan-Tiu, A., 1985. Comparative shell microstructure of North American Corbicula (Bivalvia: Sphaeriacea). Veliger 27, 312-319.

Rosenthal Y., Linsley B., 2006. Mg/Ca and Sr/Ca paleothermometery from calcareous marine fossils. In: S. Elias and C. Mock (Eds.), Encyclopedia of Quaternary Sciences. Elsevier, pp. 871-883.

Schöne, B.R., Zhang, Z., Jacob, D., Gillikin, D.P., Tütken, T., Garbe-Schönberg, D., Soldati, A., 2010. Effect of organic matrices on the determination of the trace element chemistry (Mg, Sr, Mg/Ca, Sr/Ca) of aragonitic bivalve shells (*Arctica islandica*) – Comparison of ICP-OES and LA-ICP-MS data. Geochem. J. 44, 23-37.

Schöne, B.R., Zhang, Z., Radermacher, P., Thébault, J., Jacob, D.E., Nunn, E.V., Maurer, A.F., 2011. Sr/Ca and Mg/Ca ratios of ontogenetically old, long-lived bivalve shells (*Arctica islandica*) and their function as paleotemperature proxies. Palaeogeogr. Palaeoclimatol. Palaeoecol. 302, 52-64.

Schroeder, H.A., Tipton, I.H., Nason, A.P., 1972. Trace metals in man: strontium and barium. J. Chronic. Dis. 25, 491-517.

Shirai, K., Schöne, B.R., Miyaji, T., Radermacher, P., Krause, R.A. Jr., Tanabe, K,. 2014. Assessment of the mechanism of elemental incorporation into bivalve shells (*Arctica*

islandica) based on elemental distribution at the ultrastructural scale. Geochim. Cosmochim. Acta. 126, 307-320.

Simkiss, K., 1981. Cellular discrimination processes in metal accumulating cells. J. Exp. Biol. 94, 317-327.

Simkiss, K., Taylor, M.G., 1995. Transport of metals across memebranes, 3. In: Tessier, A., Turner, D.R. (Eds.), Metal speciation and bioavailability in aquatic systems. John Wiley & Sons, New York, pp. 1-44.

Sinclair, D.J, McCulloch, M.T., 2004. Corals record low mobile barium concentrations in the Burdekin River during the 1974 flood: evidence for limited Ba supply to rivers?. Palaeogeogr. Palaeoclimatol. Palaeoecol. 214, 155-174.

Stecher, H.A., Krantz, D.E., Lord, C.J., Luther, G.W., Bock, K.W., 1996. Profiles of strontium and barium in *Mercenaria mercenaria* and *Spisula solidissima* shells. Geochim. Cosmochim. Acta. 60, 3445-3456.

Strasser, C.A., Mullineaux, L.S., Thorrold, S.R., 2008a. Temperature and salinity effects on elemental uptake in the shells of larval and juvenile softshell clams *Mya arenaria*. Mar. Ecol. Prog. Ser. 370, 155-169.

Strasser, C.A., Mullineaux, L.S., Walther, B.D., 2008b. Growth rate and age effects on *Mya arenaria* shell chemistry: Implications for biogeochemical studies. J. Exp. Mar. Biol. Ecol. 355, 153-163.

Stewart, M.H., 1984. Permeability and epidermal transport. In: Bereiter-Hahn, J., Matoltsy, A.G., Richards, K.S. (Eds.), Biology of the integument. Invertebrates. Springer, Berlin, pp. 486-501.

Surge, D., Walker, K.J., 2006. Geochemical variation in microstructural shell layers of the southern quahog (*Mercenaria campechiensis)*: implications for reconstructing seasonality. Palaeogeogr. Palaeoclimatol. Palaeoecol. 237, 182-190.

Swan, E.F., 1956. The meaning of strontium-calcium ratios. Deep-Sea. Res. 4, 71.

Tabouret, H., Pomerleau, S., Jolivet, A., Pécheyran, C., Riso, R., Thébault, J., Chauvaud, L., Amourous, D., 2012. Specific pathways for the incorporation of dissolved barium and molybdenum into the bivalve shell: An isotopic tracer approach in the juvenile Great Scallop (*Pecten maximus*). Mar. Environ. Res. 78, 15-25.

Takesue, R.K., van Geen, A., 2004. Mg/Ca, Sr/Ca, and stable isotopes in modern and Holocene *Protothaca staminea* shells from a northern California coastal upwelling region. Geochim. Cosmochim. Acta. 68, 3845-3861.

Takesue, R.K., Bacon, C.R., Thompson, J.K., 2008. Influences of organic matter and calcification rate on trace elements in aragonitic estuarine bivalve shells. Geochim. Cosmochim. Acta. 72, 5431-5445.

Taylor, J.D., Kennedy, W.J., Hall, A., 1973. The shell structure and mineralogy of the Bivalvia II. Lucinacea-Clavagellacea Conclusions. Bull. Nat. Hist. Mus. Zool. 22, 255-294.

Thébault, J., Chauvaud, L., Clavier, J., Fichez, R., Morize, E., 2006. Evidence of a 2-day periodicity of striae formation in the tropical scallop *Comptopallium radula* using calcein marking. Mar. Biol. 149, 257-267.

Thébault, J., Chauvaud, L., L'Helguen, S., Clavier, J., Barats, A., Jacquet, S., Pécheyran, C., Amouroux, D., 2009. Barium and molybdenum records in bivalve shells: Geochemical proxies for phytoplankton dynamics in coastal environments? Limnol. Oceanogr. 54, 1002-1014.

Toland, H., Perkins, B., Pearce, N., Keenan, F., Leng, M.J., 2000. A study of sclerochronology by laser ablation ICP-MS. J. Anal. At. Spectrom. 15, 1143-1148.

Urey, H.C., Lowenstam, H.A., Epstein, S., McKinney, C.R., 1951. Measurement of paleotemperatures and temperatures of the Upper Cretaceous of England, Denmark, and the southeastern United States. Bull. Geol. Soc. Am. 62, 399-416.

Vander Putten, E., Dehairs, F., Keppens, E., Baeyens, W., 2000. High resolution distribution of trace elements in the calcite shell layer of modern *Mytilus edulis*: Environmental and biological controls. Geochim. Cosmochim. Acta. 64, 997-1011.

Yan, H., Shao, D., Wang, Y., Sun, L., 2013. Sr/Ca profile of long-lived *Tridacna gigas* bivalves from South China Sea: A new high-resolution SST proxy. Geochim. Gosmochim. Acta. 112, 52-65.

Zhong, S., Mucci, A., 1989. Calcite and aragonite precipitation from seawater solutions of various salinities: Precipitation rates and overgrowth compositions. Chem. Geol. 78, 283-299.

Supplementary data

Table 3.1S Results of two-way ANOVA examining the effects of environmental variables on Sr/Ca_{shell} and $K_D^{Sr/Ca}$ of *Corbicula fluminea*.

Source of variation	*df*	Sr/Ca_{shell}			$K_D^{Sr/Ca}$		
		MS	*F*	*p*	MS	*F*	*p*
Temperature	2	0.325	18.047	< 0.001	0.061	20.092	< 0.001
Food supply	3	0.037	2.059	0.112	0.003	0.920	0.435
Temperature × food	6	0.005	0.275	0.947	0.001	0.240	0.962
Residual	96						

		Sr/Ca_{shell}		
		MS	*F*	*p*
Temperature	2	1.703	7.259	0.001
Sr/Ca_{water}	3	27.782	118.418	< 0.001
Temp. × Sr/Ca_{water}	6	0.195	0.832	0.548
Residual	96			

Table 3.2S Results of two-way ANOVA examining the effects of environmental variables on Ba/Ca_{shell} and $K_D^{Ba/Ca}$ of *Corbicula fluminea*.

Source of variation	*df*	Ba/Ca_{shell}			$K_D^{Ba/Ca}$		
		MS	*F*	*p*	MS	*F*	*p*
Temperature	2	8494.033	12.454	< 0.001	0.069	13.300	< 0.001
Food supply	3	5455.050	7.999	< 0.001	0.029	5.894	0.001
Temperature × food	6	1404.648	2.060	0.041	0.011	2.128	0.036
Residual	96						

		Ba/Ca_{shell}		
		MS	*F*	*p*
Temperature	2	127476.756	25.887	< 0.001
Ba/Ca_{water}	3	56841.026	11.543	< 0.001
Temp. × Ba/Ca_{water}	6	6388.049	1.297	0.266
Residual	96			

Chapter 4

Insights from sodium into the impacts of elevated pCO_2 and temperature on bivalve shell formation

Published in Journal of Experimental Marine Biology and Ecology

Liqiang Zhao[1], Bernd R. Schöne[1], Regina Mertz-Kraus[1], Feng Yang[2]

[1] Institute of Geosciences, University of Mainz, Joh.-J.-Becher-Weg 21, 55128 Mainz, Germany

[2] Engineering Research Center of Shellfish Culture and Breeding in Liaoning Province, Dalian Ocean University, 116023 Dalian, China

Author contribution

Concept: LZ, BRS

Execution: LZ, FY

Data collection and analysis: LZ, RMK, FY

Writing: LZ, BRS, RMK, FY

Liqiang Zhao, Bernd R. Schöne, Regina Mertz-Kraus, Feng Yang, 2017. Insights from sodium into the impacts of elevated pCO_2 and temperature on bivalve shell formation. Journal of Experimental Marine Biology and Ecology 486, 148-154.

Abstract

Ocean acidification and warming are predicted to affect the ability of marine bivalves to build their shells, but little is known about the underlying mechanisms. Shell building is an extremely complex process requiring considerations from both aspects, calcification and mineralization. Sodium incorporation into the shells would increase if bivalves rely on the exchange of Na^+/H^+ to maintain homeostasis for calcification, thereby shedding new light on the acid-base and ionic regulation at the calcifying front. Here, we investigated the combined effects of seawater pH (8.1, 7.7 and 7.4) and temperature (16 and 22 °C) on the growth and sodium composition of the shells of the blue mussel, *Mytilus edulis*, and the Yesso scallop, *Patinopecten yessoensis*. Exposure of *M. edulis* to low pH (7.7 and 7.4) caused a significant decrease of shell formation, whereas a 6 °C warming significantly depressed the rate of shell growth in *P. yessoensis*. On the other hand, while the amount of Na incorporated into the shells of *P. yessoensis* did not increase in acidified seawater, an increase of Na/Ca_{shell} with decreasing pH was observed in *M. edulis*, the latter agreeing well with the aforementioned hypothesis. Moreover, a combination of the growth responses with the sodium behaviors provides a more detailed understanding of the processes of shell building. Under acidified conditions, mussels may maintain more alkaline conditions favorable for calcification, but a significant decrease of shell formation indicates that the mineralization processes are impaired. The opposite occurs in scallops; virtually unaffected shell growth implies that shell mineralization functions well. Finding of the present study may pave the way for deciphering the mechanisms underlying the impacts of ocean acidification and warming on bivalve shell formation.

4.1. Introduction

Rapidly increasing anthropogenic CO_2 emissions are not only resulting in ocean warming, but also ocean acidification (OA) and altered seawater carbonate chemistry (Doney et al., 2009). These changing environmental conditions may have widespread implications for marine biota, especially bivalve mollusks (Kroeker et al., 2010; Rodolfo-Metalpa et al., 2011; Hendriks et al., 2015). There is mounting evidence that OA can impair the capacity of marine bivalves to produce their shells, leading to reduced calcification and growth rates (Gazeau et al., 2013; Kroeker et al., 2013; Waldbusser et al., 2014; Milano et al., 2016) and, in extreme cases, decalcification and mortality (McClintock et al., 2009; Gazeau et al., 2013). Furthermore, the negative effects of OA on shell mineralization may have significant functional and ecological implications. Reduced shell mechanical properties may increase the susceptibility to predation and, ultimately, alter the predator-prey dynamics in marine ecosystems (Gaylord et al., 2011; Schalkhausser et al., 2013; Kroeker et al., 2014).

OA does not act in isolation but usually interacts with other environmental stressors, specifically temperature (Pörtner and Farrell, 2008; Kroeker et al., 2013). The interactive effects of OA and temperature, which can be antagonistic or synergistic, may shape highly variable responses of marine bivalves to near-future climate change scenarios. For example, elevated temperature, within the thermal tolerance window, may alleviate the detrimental effects of OA on bivalve shell formation (Parker et al., 2009; Ko et al., 2014; Li et al., 2016) and, conversely, may exacerbate these threats (Hiebenthal et al., 2013; Schalkhausser et al., 2013; Li et al., 2015). Evidently, predicting the impacts of elevated pCO_2 and temperature on marine bivalves is fraught with great difficulty given the complexity and diversity of the responses observed. Therefore, it becomes critical to gain a better understanding of the processes and mechanisms determining their sensitivity and resilience to ocean acidification and warming.

Biomineralization of bivalve shells takes place in the extrapallial fluid (EPF), a thin film of liquid between the outer mantle epithelium (OME) and the calcifying shell (Wheeler, 1992). Bivalve mollusks can elevate the pH of the EPF to facilitate inorganic $CaCO_3$ precipitation (Crenshaw and Neff, 1969). For example, the oyster *Crassostrea gigas* appears to alkalinize the EPF by ca. 0.23 pH unit during the growing season (Wada and Fujinuki, 1976). Over a tidal cycle, the formation of shell growth increment in the intertidal cockle *Cerastoderma edule* is favored by the raise of extrapallial pH during immersion (Richardson et al., 1981). *In situ* measurements of the EPF in *Arctica islandica* show that pH rises rapidly from the calcifying front toward to the OME (Stemmer, 2013), indicating active removal of protons generated

during $CaCO_3$ precipitation. It is therefore conceivable that the acid-base homeostasis at the calcifying front is a key determinant of the formation of bivalve shells. OA has been shown to acidize the EPF and shift the pH towards lower values (Thomsen et al., 2010; Heinemann et al., 2012; Zittier et al., 2015). Presumably, bivalves exposed to high pCO_2 need to actively remove more protons from the EPF to maintain an elevated pH level and a sufficient $CaCO_3$ saturation state that favor shell deposition (Cyronak et al., 2015). However, the processes involved in the proton removal in the EPF are poorly understood, probably because continuous monitoring of the pH at the calcifying front remains an extremely challenging task.

Under acidified conditions, bivalves rely on the active proton equivalent ion exchange to prevent ongoing extracellular pH drops and maintain steady-state values (Pörtner et al., 2004; Fabry et al., 2008; Melzner et al., 2009; Parker et al., 2013). Support for the existence of such active transport processes comes from the significantly increased expression of genes involved in ion and acid-base regulation, for example in the OME of the pearl oyster *Pinctada fucata* exposed to elevated pCO_2 of 862 µatm (Li et al., 2016). Two membrane transporters, vacuolar type H^+-ATPase and Na^+/H^+ exchanger, have been identified as being responsible for active removal of more H^+ ions (Liu et al., 2016). In the latter process, the Na^+/K^+-ATPase likely plays a key role through creating ionic and electrochemical gradients used by secondary active ion transporters specifically the Na^+/H^+ exchanger (Melzner et al., 2009). For example, the rate of Na^+/H^+ exchange relies on the Na^+ gradient between the extracellular fluid and the ambient water which is actively built up by the Na^+/K^+-ATPase (Fabry et al., 2008; Parker et al., 2013). Since the activity of Na^+/K^+-ATPase is highly sensitive to changes in extracellular pH caused by elevated pCO_2 (Pörtner et al., 2000; Lannig et al., 2010), the extracellular Na^+ concentration may be shifted toward higher or lower values. For example, an increase of extracellular Na^+ has previously been observed in *Mytilus edulis* exposed to higher CO_2 levels (Thomsen et al., 2010), whereas a reduction occurred in *C. gigas* (Lannig et al., 2010). Likewise, if bivalves actively alkalinize the EPF through the exchange of Na^+/H^+ when subjected to OA, an increase of Na^+ transported into the EPF could be anticipated. If this is the case, then one would expect that the sodium content of the shells to increase given that the amount of Na^+ incorporated into the shells is directly proportional to its corresponding level in the EPF (Lorens et al., 1980).

Here, we investigated the influence of elevated pCO_2 and temperature on the formation of bivalve shells. The blue mussel, *M. edulis*, and the Yesso scallop, *Patinopecten yessoensis* were selected as model species not only because of their ecological and economical significance but also because they inhabit distinctly different habitats which may shape differential growth responses. Furthermore, the sodium composition of the shells was analyzed with the aim of

evaluating whether Na/Ca_{shell} holds the potential as a proxy of the acid-base and ionic regulation in the EPF. Specifically, it is expected that the amount of Na incorporated into the shells would increase with decreasing seawater pH when bivalves rely on the Na^+/H^+ exchanger to achieve the acid-base and ionic regulation and homeostasis. Finally, we demonstrated that an integrated approach of combining Na/Ca_{shell} with the examination of the rate of shell deposition may help decipher the mechanisms by which bivalves respond to current and ongoing ocean acidification and warming.

4.2. Materials and methods

4.2.1. Experimental setup

Specimens of the blue mussel, *Mytilus edulis* (24–32 mm shell length) were collected by hand from the rocky intertidal shore of Xinghai Bay (38°52'34.51" N, 121°33'42.47" E), Yellow Sea, China, while Yesso scallops, *Patinopecten yessoensis* (41–45 mm shell length) were collected from the shallow subtidal zone near Zhangzi Island (39°01'58.46" N, 122°44'22.48" E). The monthly average seawater temperature and pH provided by marine stations (Dalian Oceanic and Fishery Administration) nearest to the sample localities vary between 3.4 °C and 24.6 °C and 7.91 and 8.09 at Xinghai Bay, and between 4.6 °C and 23.2 °C and 8.04 and 8.13 at Zhangzi Island, respectively. Upon arrival in the laboratory, the bivalves were kept in 500 L tanks supplied with circulating water for two weeks and were fed daily with an equal mixture of microalgae, *Platymonas subcordiformis* and *Nitzschia closterium*. Water temperature, salinity, pH_T (total scale) and dissolved oxygen were maintained constant at 16 °C, 31, 8.0–8.1 and 7–8 mg/L.

To evaluate the influence of seawater pH and temperature, six separate, but identical, recirculating systems were established, as schematically illustrated by Xu et al. (2016). Each system comprised two exposure chambers (i.e. each species per chamber), a filter chamber, a temperature controlling chamber, and a gas mixing chamber and each held a total volume of ca. 480 L seawater. After acclimation to laboratory conditions, specimens of each species were randomized into six groups and assigned into each system at a density of 20 individuals per chamber. Afterwards, the bivalves were exposed to six combined treatments with different seawater pH (7.4, 7.7 and 8.1) and different temperature (16 and 22 °C) regimes. No replicate systems were performed for each treatment in the present experiment. The acidified conditions

mimicked near-future climate change scenarios, i.e., pH 7.7 projected for the year 2100 and 7.4 projected for 2300 (Caldeira and Wickett, 2003). The temperature of 16 °C represents the annual mean sea surface temperature in the Yellow Sea (Lin et al., 2005), and 22 °C corresponds to an additional warming of ca. 5.1 °C projected for the end of the 21st century (Sokolov et al., 2009). During the subsequent two weeks, they were acclimated to the experimental conditions. No mortality was observed.

To identify newly formed shell portions during the experiment (Fig. 4.1), bivalves were exposed to a 150 mg/L calcein solution for three hours (Thébault et al., 2006). Calcein is a fluorescent dye which can be incorporated into biogenic calcium carbonate and fluoresce under blue light (Kaehler and McQuaid, 1999). Afterwards, bivalves were reared under controlled conditions for five weeks. Throughout the duration of the experiment, fifty percent of the tank water was renewed every two days to maintain water quality. To minimize potential influence of high phytoplankton biomass on seawater carbonate chemistry, bivalves were fed every two days with an equal mixture of *P. subcordiformis* and *N. closterium* at a concentration of ca. 40,000 cells/mL.

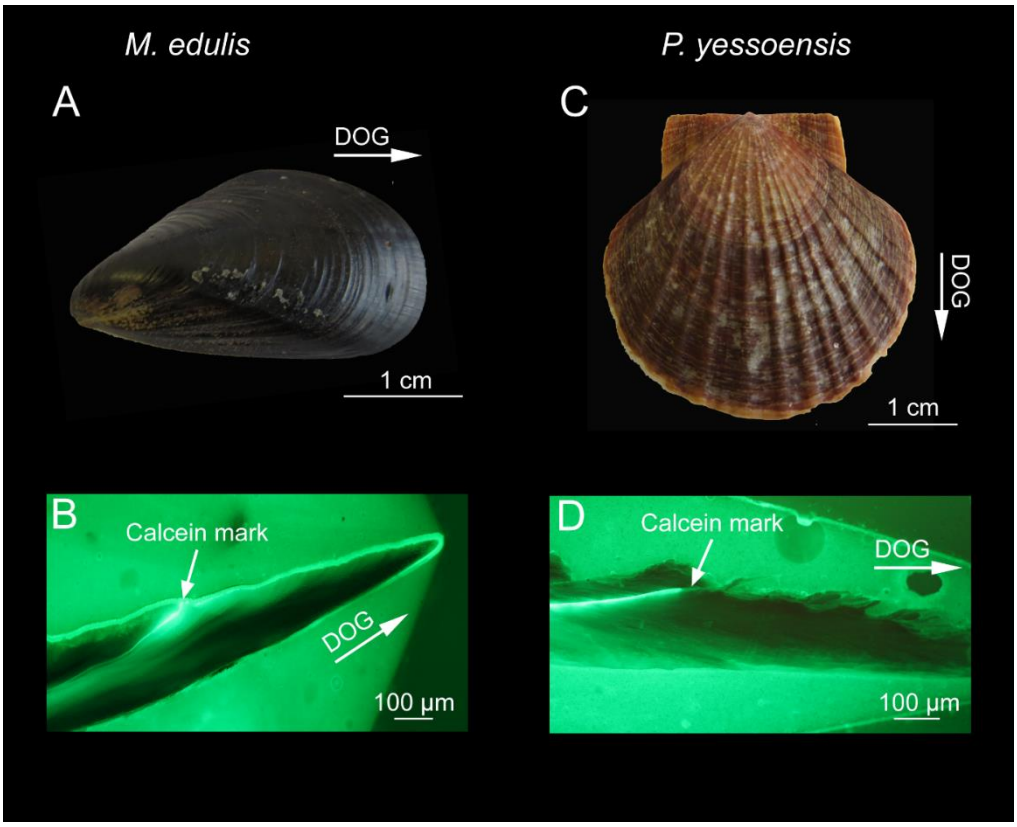

Fig. 4.1. Studied bivalve species. Outer shell surface of *Mytilus edulis* (A) and magnification of the outer shell margin revealing a light calcein mark and newly formed shell portion (B). Outer shell surface of *Patinopecten yessoensis* (C) and magnification of the outer shell margin revealing a light calcein mark and newly formed shell portion (D). DOG = direction of growth.

4.2.2. Chemical analysis of the water samples

Temperature and pH were monitored every day. Water samples for chemical analysis were taken on a weekly basis. Total alkalinity (TA) was determined by means of an alkalinity titrator. Water temperature, salinity, pH and TA were used to calculate the carbonate system parameters using the CO2SYS software program (Pierrot et al., 2006). A detailed overview on experimental conditions is provided in Table 4.1. The concentration of Ca^{2+} and Na^{+} of the water samples were determined by means of a Thermo Electron IRIS Intrepid II XSP inductively coupled plasma – atomic emission spectrometer (ICP-AES). Analytical precision was better than 1 % (1RSD) for Ca^{2+} and Na^{+}. Accuracy which was determined by a multi-element standard solution (National Research Center for Certified References Materials, China; GNM-M25748-2013) and was better than 5 % for all elements.

Table 4.1 Seawater carbonate chemistry (average ± standard error, n = 5). Partial pressure of CO_2 in seawater (pCO_2) and saturation state of calcite (Ωcal) were calculated from the measured temperature, salinity, pH and total alkalinity (TA).

Treatments (pH × T)	T (°C)	S	pH_T	TA (µmol/kg)	pCO_2 (µatm)	Ωcal
8.1 × 16	16.56 ± 0.04	31.62 ± 0.03	8.06 ± 0.01	2265 ± 25	346 ± 4	4.18 ± 0.04
7.7 × 16	16.38 ± 0.08	31.60 ± 0.07	7.71 ± 0.01	2285 ± 28	904 ± 11	2.02 ± 0.02
7.4 × 16	16.28 ± 0.07	31.36 ± 0.04	7.39 ± 0.01	2231 ± 31	1702 ± 24	1.10 ± 0.02
8.1 × 22	22.36 ± 0.10	31.50 ± 0.04	8.07 ± 0.02	2247 ± 28	380 ± 5	4.64 ± 0.06
7.7 × 22	22.58 ± 0.07	31.46 ± 0.06	7.72 ± 0.01	2274 ± 16	894 ± 6	2.55 ± 0.02
7.4 × 22	21.88 ± 0.08	31.29 ± 0.05	7.40 ± 0.01	2263 ± 26	1949 ± 23	1.26 ± 0.03

4.2.3. Shell preparation and analysis

Five specimens of each species from each treatment were randomly selected for analysis. Soft tissues were removed immediately after collection. All specimens were carefully cleaned with tap water and then air-dried. The left valve of each specimen was mounted on a Plexiglass cube. Subsequently, a fast-drying metal epoxy resin was applied along the axis of maximum growth to avoid fractures during the cutting process. Along this axis, a three-millimeter-thick section was cut from each specimen using a low-speed saw (Buehler IsoMet 1000; 250 rpm). Shell slabs were mounted on glass slides and subsequently ground (800, 1200 grit SiC powder) and polished using 1 µm Al_2O_3 powder.

Samples were examined under a fluorescent light microscope (Zeiss Axio Imager A1.m

stereomicroscope equipped with a Zeiss HBO 100 mercury lamp and filter set 38: excitation wavelength, ~450-500 nm; emission wavelength, ~500-550 nm) to locate the calcein marks. Photographs were taken with a Canon EOS 600D digital camera attached to the microscope. The free image processing software ImageJ (http: //rsbweb.nih.gov/ij) was used to measure the distance between calcein mark and ventral margin. The average daily shell growth rate was calculated from the newly formed shell portion of each specimen divided by the experimental duration (35 days).

4.2.4. Chemical analysis of the shells

Shells of *M. edulis* (Kobayashi, 1969) and *P. yessoensis* (Akiyama, 1966) comprise two major $CaCO_3$ polymorphs, an outer layer consisting of calcite (prismatic layer) and an inner layer consisting of aragonite (nacreous layer). In both species, newly formed shell portion was exclusively observed in the calcitic prismatic layer. The polished shell slab of each specimen was used for chemical analysis by means of laser ablation – inductively coupled plasma – mass spectrometry (LA-ICP-MS) in "spot" mode at the Institute of Geosciences, University of Mainz. Sodium (measured as ^{23}Na) concentrations were determined in the newly formed shell portions (Fig. 4.1). Three discrete spots per specimen were measured. Analyses were performed on an Agilent 7500ce quadrupole ICP-MS coupled to an ESI NWR193 ArF excimer laser ablation system. Ablation was achieved using a pulse rate of 10 Hz, an energy density of ~3 J/cm^2 and a beam diameter of 55 µm. Backgrounds were measured for 15 s, followed by 40 s ablation time and 20 s wash out. NIST SRM 610 was used as calibration material, applying the preferred values reported in the GeoReM database (http://georem.mpch-mainz.gwdg.de/, Application Version 18) (Jochum et al., 2005, 2011) as the "true" concentrations to calculate the element concentrations in the samples. USGS BCR-2G and MACS-3 were analyzed as quality control materials (QCM) to monitor accuracy and reproducibility of the analyses. All reference materials were analyzed at the beginning and at the end of a sequence and after ca. 39 spots on the samples. For all materials, ^{43}Ca was used as internal standard. For the reference materials, we applied the Ca concentrations reported in the GeoReM database, and for the samples 56.03 wt.%., the stoichiometric CaO content of aragonite. The time-resolved signal was processed using the program GLITTER 4.4.1 (www.glitter-gemoc.com, Macquarie University, Sydney, Australia). Reproducibility based on repeated measurements (N = 33) of the QCM was always better than 2 % (1RSD) for USGS BCR-2G and 4 % (1RSD) for MACS-3. The measured Na concentrations of the QCM agree within 2 % with the preferred values of the GeoReM database

for USGS BCR-2G, and within 3 % with the preliminary reference values for USGS MACS-3 (personal communication S. Wilson, USGS, in Jochum et al. 2012), respectively.

4.2.5. Statistical analysis

Although the experiments were pseudo-replicate, it remains reasonable to assume that the sampling method allows us to obtain an adequate estimate of variation within each treatment (Hurlbert, 2004). Therefore, in the present study, five specimens within each treatment were treated as replicates here. Prior to the analysis, normality of the data was tested by means of the Shapiro–Wilk's test and homogeneity of variance by means of the Levene's *F*–test using the software IBM SPSS Statistics 19.0. The combined effects of seawater pH and temperature and their interaction on shell growth and Na/Ca_{shell} of each species were evaluated by means of two-way analysis of variance (ANOVA) followed by the LSD post-hoc test to evaluate differences between experimental treatments. Pairwise comparisons were carried out by means of Student's *t* test. Pearson correlation analysis was performed to test whether Na/Ca_{shell} was significantly correlated to shell growth rate. Statistically significant difference was set at $p \leq 0.05$.

4.3. Results

4.3.1. Effect of pH and temperature on shell growth rate

To evaluate the growth performance of *M. edulis* and *P. yessoensis* in response to reduced pH and elevated temperature, the average daily rate of shell production between the calcein mark and the ventral margin was calculated. As shown in Figure 4.2A, irrespective of temperature which had no significant effect on shell growth ($p > 0.05$; Table 4.2), *M. edulis* grew significantly faster at pH 8.1 than at pH 7.7 or 7.4 (LSD post-hoc test, $p < 0.05$). A further reduction of pH from 7.7 to 7.4, however, did not result in slower growth rate (LSD post-hoc test, $p > 0.05$). In contrast, irrespective of pH ($p > 0.05$; Table 4.2), the rate of shell growth observed in *P. yessoensis* at 16 °C was significantly higher than that at 22 °C ($p < 0.05$; Fig. 4.2B). While maximum growth occurred at 8.1, no significant reductions were observed at pH 7.7 and 7.4 (LSD post-hoc test, $p > 0.05$).

4.3.2. Effect of pH and temperature on Na/Cashell

To examine the effect of pH and temperature on the incorporation of Na^+ into the shells, the Na^+ and Ca^{2+} levels in seawater storage tanks were kept constant at 10485.8 ± 318.54 mg/L and 396.8 ± 13.22 mg/L, corresponding to a $Na/Ca_{seawater}$ level of 45.97 ± 1.08 mol/mol. As shown in Figure 4.3A, the average amount of Na^+ incorporated into the shells of *M. edulis* increased non-linearly with decreasing pH, whereas only a slight decrease occurred in *P. yessoensis* (Fig. 4.3B). Irrespective of temperature, pH had a significant effect on Na/Ca_{shell} of *M. edulis* ($p < 0.05$; Table 4.2). At 16 °C, Na/Ca_{shell} of *M. edulis* was significantly lower at pH 8.1 than at pH 7.7 and 7.4 (LSD post-hoc test, $p < 0.05$), whereas at 22 °C shells incorporated significantly larger amount of Na^+ at pH 7.4 than at pH 8.1 and 7.7 (LSD post-hoc test, $p < 0.05$). The effect of temperature was most pronounced at pH 7.7 than at pH 8.1 and 7.4, i.e., Na/Ca_{shell} of *M. edulis* was significantly higher at 16 °C than at 22 °C (Student's *t* test, $p < 0.05$). In addition, Figure 4.4 illustrates that Na/Ca_{shell} ratios are not significantly linked to the growth performance of *M. edulis* and *P. yessoensis*.

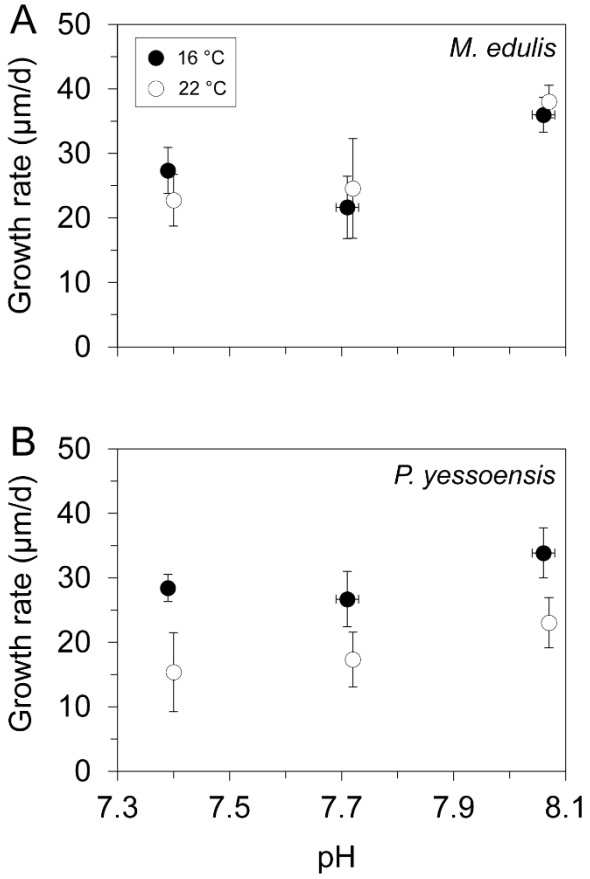

Fig. 4.2. Rates of shell growth of *Mytilus edulis* (A) and *Patinopecten yessoensis* (B) which grew at different combinations of seawater pH (7.4, 7.7 and 8.1) and temperature (16 and 22 °C). Values are expressed as average ± standard error (n = 5).

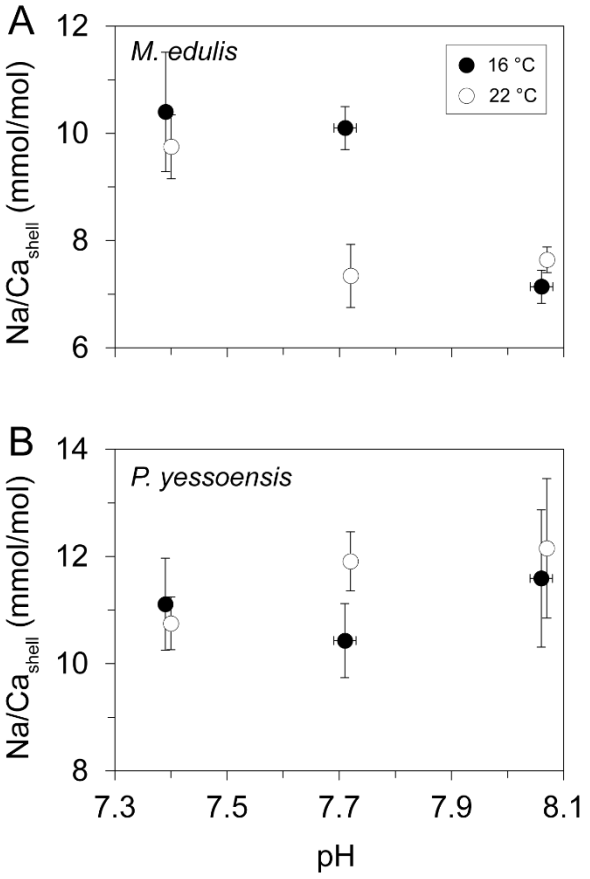

Fig. 4.3. Sodium-to-calcium ratios in the shells of *Mytilus edulis* (A) and *Patinopecten yessoensis* (B) which grew at different combinations of seawater pH (7.4, 7.7 and 8.1) and temperature (16 and 22 °C). Values are expressed as average ± standard error (n = 5).

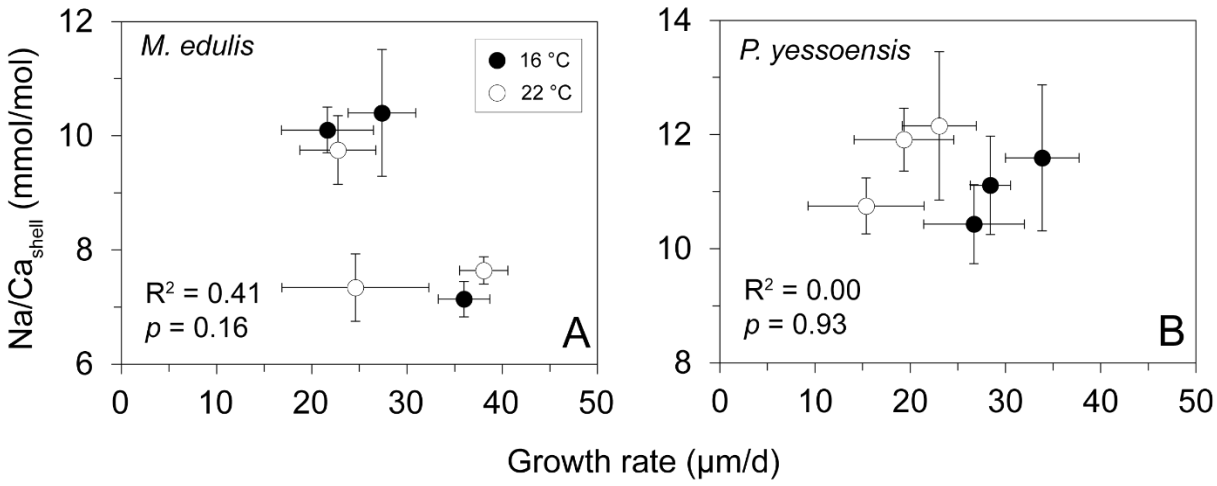

Fig. 4.4. Sodium-to-calcium ratios in the shells of *Mytilus edulis* and *Patinopecten yessoensis* plotted against shell growth rate.

Table 4.2 Summary of two-way ANOVA results on the combined effect of seawater pH and temperature on the rate of shell growth and the ratio of sodium-to-calcium in shells of *Mytilus edulis* and *Patinopecten yessoensis* which grew at different combinations of pH (7.4, 7.7 and 8.1) and temperature (16 and 22 °C).

Source of variations	*df*	Shell growth rate			Na/Ca_{shell}		
		MS	*F*	*p*	MS	*F*	*p*
M. edulis							
pH	2	567	5.43	<0.05	75.90	11.60	<0.05
Temperature	1	0.12	0.00	0.97	21.58	3.30	0.07
pH × Temperature	2	42.71	0.41	0.66	18.26	2.79	0.06
P. yessoensis							
pH	2	14.23	0.24	0.78	10.34	0.70	0.49
Temperature	1	1380	23.24	<0.05	21.70	1.48	0.22
pH × Temperature	2	116	1.95	0.16	28.09	1.91	0.15

4.4. Discussion

Our results demonstrate that the growth performance of marine bivalves under acidified and warmer conditions is species-specific. For example, *M. edulis* grew significantly slower when subjected to acidified seawater (pH 7.7 and 7.4), whereas *P. yessoensis* was highly susceptible to a 6 °C warming and, accordingly, reduced shell growth. Our findings lend further support to the increasing recognition that the impacts of ocean acidification and warming on bivalve shell formation vary greatly among different species and even within the same species (Gazeau et al.,

2013; Kroeker et al., 2013). Recently, attempts have been made to understand the mechanisms driving the complexity of the responses (Bach, 2015; Cyronak et al., 2015; Waldbusser et al., 2015). To cope with environmental stressors such as elevated pCO_2 and temperature, bivalves likely respond by either increasing the rate of proton removal from the EPF to facilitate the precipitation of $CaCO_3$, or stimulating the secretion of organic matrix from the OME to mediate the crystallization of $CaCO_3$ (Elhadj et al., 2006; Cyronak et al., 2015). However, it remains unclear whether, and to what extent, each mechanism could confer bivalve resilience to climate change, thereby limiting our ability to gain deeper insight into the specific mechanisms of shell formation. The search for a proxy that records the acid-base and ion-regulatory processes in the EPF therefore represents a critical step. As will be demonstrated below, sodium in the shells is potentially of great value in this regard. On this basis, an integrated approach of combining the acid-base and ionic regulation at the calcifying front with the rate of shell deposition can shed new light on the mechanisms underlying the biomineralization responses of bivalves to climate change.

Our results show that Na/Ca_{shell} of *M. edulis* was non-linearly correlated to seawater pH, but exhibited a general increasing trend under acidified conditions. The latter provides evidence in support of our hypothesis that, if bivalves increase the proton removal from the EPF through the Na^+/H^+ exchange, an increase of Na/Ca_{shell} would occur. Hence, Na/Ca_{shell} of *M. edulis* could potentially function as a proxy of the acid-base and ionic regulation in the EPF during exposure to OA. This is also in line with the observations by Thomsen et al. (2010) according to which exposure of *M. edulis* to elevated pCO_2 of 4000 µatm resulted in a significant increase of Na^+ in the hemolymph, and Saphörster (2008) who observed that the activity of Na^+/K^+-ATPase in the OME of CO_2-exposed *M. edulis* increased significantly. The latter lends support to the idea that the rate of Na^+/H^+ exchange depends on the Na^+ gradient actively built up by the Na^+/K^+-ATPase (Fabry et al., 2008; Parker et al., 2013). Therefore, it seems very likely that *M. edulis* may respond to OA through tight control of the acid-base and ion-regulatory processes. Such efficient ion-regulatory machinery equipped in the OME is likely derived from mussel-specific life-habits. In the present study, specimens of *M. edulis* were collected from an intertidal zone where they frequently experienced aerial exposure over a tidal cycle, so that they are used to cope with respiratory acidosis (i.e., the retention of metabolically produced CO_2) and metabolic acidosis (i.e., the accumulation of metabolic acids produced by anaerobic metabolism) at low tide (Booth et al., 1984; Burnett, 1988). As a consequence of that, intertidal *M. edulis* might evolve an efficient compensatory mechanism to maintain homeostasis for shell mineralization in an acidified environment. For example, despite high and variable seawater pCO_2 in Kiel

Fjord (Western Baltic Sea, Germany) where natural upwelling drives pCO_2 up to 2300 µatm for large parts of the year (Thomsen et al., 2010), *M. edulis* is still able to calcify and survive (Thomsen et al., 2010, 2013), potentially exhibiting local adaption to high pCO_2. It has been elucidated that the rate of local adaption of an organism to a changing environment depends on the degree of genetic variability in a population (Lande and Shannon, 1996). Extremely harsh environmental conditions may elicit strong stress responses in marine invertebrates (Kurihara, 2008), potentially stimulating the expression of genetic differences among individuals. In the present study, a large amount of Na/Ca_{shell} variation was observed in *M. edulis* under extremely acidified condition of pH 7.4, indicating a high genetic variability in this population and, thus, a considerable potential for local adaptation to OA.

With decreasing seawater pH, however, the amount of Na^+ incorporated into the shells of *P. yessoensis* insignificantly decreased, indicating that the Na^+/H^+ exchanger might play a relatively small role in the removal of more protons from the EPF. Therefore, Na/Ca_{shell} of *P. yessoensis* cannot be explored as a potential proxy of the acid-base and ionic regulation at the calcifying front. In the present study, scallops came from a shallow subtidal population where the physiochemical environment varies on a seasonal basis, so that they might be more sensitive to OA compared with intertidal mussels. Accumulating evidence indicates that scallops may trigger metabolic depression in response to OA (Ries et al., 2009; Schalkhausser et al., 2013). In many cases, metabolic depression can act as an intrinsic and adaptive strategy that allows the animal to tolerate short-term hypercapnia (Guppy and Withers, 1999). To save energy, *P. yessoensis* is therefore likely to utilize less costly ion transporters to remove protons from the EPF. If this is the case, then one would expect the Na^+ concentration in the EPF to decrease as the activity of Na^+/K^+-ATPase is depressed. A similar shift from less to more ATP-efficient ion transporters has been suggested in CO_2-exposed oysters (*Crassostrea gigas*) according to the observed decrease of extracellular Na^+ and increase of K^+ compared with oysters grown at ambient pCO_2 (Lannig et al., 2010). Likewise, Malley et al. (1988) found that acidified waters depressed the Na^+/K^+-ATPase activity in the OME of the mussel *Anodonta grandis grandis*.

As mentioned above, intertidal mussels and subtidal scallops may employ differential ion-regulatory mechanisms to maintain homeostasis for calcification in the face of OA. This may have profound implications for biomineralization processes, because shell formation is a complex process requiring considerations from both aspects, calcification and mineralization. The former is controlled by the acid-base status in the EPF and the latter mediated by the organic matrix. It seems very likely that mussels fail to enhance shell production by generating alkaline conditions at the calcifying front, in agreement with the insignificant relationship between

Na/Ca_{shell} and the rate of shell growth. The latter is closely linked to the rate of crystal growth. While scallop calcification may occur in less alkaline conditions, virtually unaffected shell growth rate indicates the increased synthesis of organic matrix which, in turn, may stimulate $CaCO_3$ crystallization. The most likely reason for such distinctly different responses could be an energy trade-off among mineralization processes. The active removal of more protons from the EPF is energetically expensive. Under acidified conditions, increased rates of ATP synthesis and ion transport require a higher energy supply, so that bivalves will inevitably reallocate energy away from the organic matrix synthesis and excretion which also entail a considerable amount of energetic consumption. For example, the energy committed to the latter process may account for up to 60 % of that for somatic growth (Palmer, 1992). Hence, if bivalves are used to alkalinize the EPF at the expense of endogenous energy reserves rather than exogenous energy sources, a potential limitation of organic substrate for shell mineralization may occur, thereby leading to a substantial decrease of shell production. Thus, a fundamental basis underlying these complex responses lies in whether energy supply could keep pace with energy cost under acidified conditions.

Taking into account the habitat traits may also help explain the differential responses of bivalves to OA. Periostracum, an outer organic shell layer, provides critical protection against external shell dissolution and predators. Tyrosinase is a critical enzyme catalyzing the synthesis of proteinaceous matrix in shell periostracum (Waite and Wilbur, 1976). When subjected to high pCO_2 of 1120 µatm, significantly increased tyrosinase expression has been observed in the OME of *M. edulis* (Hüning et al., 2013), helping to explain why intertidal mussels are highly resilient to high pCO_2. However, the expression of chitinase, a functional molecule for shell mineralization (Weiss et al., 2006), is strongly depressed, thereby causing a substantial decrease of shell production (Hüning et al., 2013). In contrast to intertidal mussels, *P. yessoensis* inhabits the subtidal environment where physiochemical properties are relatively stable and exhibits an excellent swimming capacity to escape from predators (Ventilla, 1982), so that the protective function of scallop periostracum might be limited. Therefore, subtidal scallops might spend less energy on periostracum formation, but invest more energy into the synthesis of organic matrix for shell mineralization. Evidence in support of this interpretation comes from the significant up-regulation of chitinase expression observed in the OME of scallop *Argopecten purpuratus* under acidified conditions (Ramajo et al., 2015).

OA usually interacts with temperature, but the degree of the interaction highly relies on the thermal window of marine bivalves. Since sufficient food (energy) was supplied during the experiment of the present study, temperature – which is thought to be the most important

modifier of energy flow in bivalves (Gosling, 2003) – likely plays a key role in allocating the energy for shell production. In a recent study of *P. fucata*, Li et al. (2016) demonstrated that elevated temperature within the thermal window did not induce increased expression of genes involved in ion and acid-base regulation but facilitated shell calcification, thereby alleviating the negative effects of OA. In the present study, although a 6 °C warming did not significantly favor mussel shell formation, the capacity of *M. edulis* to alkalinize the EPF under moderate OA stress (i.e., at pH 7.7) appeared substantially improved. This is perhaps best exemplified by the significant decrease of Na/Ca_{shell} in warmer water, implying that mussels reduced the dependence of the active proton equivalent ion exchange to actively remove protons from the EPF. However, if the thermal window is exceeded, elevated temperature may exacerbate OA impacts on shell mineralization. Elevated temperature can potentially alter the cell membrane permeability of the OME (Moura et al., 2004), causing an increase of energetic cost required to maintain alkaline conditions in the EPF, and suppress the activities of enzymes involved in the synthesis of organic matrix (Moura et al., 2004). Moreover, elevated temperature can lead to metabolic disturbance, consequently affecting the individual energy budget (Pörtner and Farrell, 2008). Consistent with these interpretations, scallop *P. yessoensis* grew significantly lower at higher temperature of 22 °C, which is much above the optimal temperature of 17 °C for its growth (Ventilla, 1982). Therefore, it is likely that ocean warming beyond the thermal tolerance window, more than acidification, affects molluscan growth.

4.5. Summary and conclusions

The present study demonstrates the differential molluscan growth responses under near-future climate scenarios. Under acidified conditions, the ability of intertidal mussels to cope with CO_2-induced extracellular acidosis is likely stronger than that of subtidal scallops. Our findings lend support to this hypothesis, where sodium in mussels shells probably probes the acid-base and ionic regulation at the calcifying front. However, shell building is a complex process requiring considerations from both aspects, calcification and mineralization. Therefore, it is unlikely that increasing the removal of protons to facilitate $CaCO_3$ precipitation (i.e., calcification) can fully compensate for the impact of ocean acidification. A significant decrease of mussel shell growth supports our understanding. Scallops appear less able to create favorable calcifying conditions, but they may enhance the synthesis and secretion of organic matrix which, in turn, facilitates mineralization and ultimately shell formation. Therefore, it becomes imperative to disentangle

to what extent each strategy works. Furthermore, since both strategies are energetically costly, a better understanding of how climatic stressors affect the energy budget at the individual level and the energy partitioning in differential shell building processes advances our understanding of the complexity of these biomineralization responses.

4.6. Acknowledgments

Not displayed for reasons of data protection

4.7. References

Akiyama, M., 1966. Conchiolin-constituent amino acids and shell structures of bivalved shells. Proc. Jpn. Acad. 42, 800-805.

Bach, L.T., 2015. Reconsidering the role of carbonate ion concentration in calcification by marine organisms. Biogeoscience 12, 4939-4951.

Booth, C.E., McDonald, D.G., Walsh, P.J., 1984. Acid-base balance in the sea mussel, *Mytilus edulis*. II: Effects of hypoxia and air-exposure on hemolymph acid-base status. Mar. Biol. Lett. 5, 359-369.

Burnett, L.E., 1988. Physiological responses to air exposure: acid-base balance and the role of branchial water stores. Am. Zool. 28, 125-135.

Caldeira, K., Wickett, M.E., 2003. Oceanography: anthropogenic carbon and ocean pH. Nature 425, 365-365.

Crenshaw, M.A., Neff, J.M., 1969. Decalcification at mantle-shell interface in molluscs. Am. Zool. 9, 881-885.

Cyronak, T., Schulz, K.G., Jokiel, P.L., 2015. The omega myth: what really drives lower calcification rates in an acidifying ocean. ICES J. Mar. Sci. fsv075.

Doney, S.C., Fabry, V.J., Feely, R.A., Kleypas, J.A., 2009. Ocean acidification: the other CO_2 problem. Ann. Rev. Mar. Sci. 1, 169-192.

Elhadj, S., De Yoreo, J.J., Hoyer, J.J., Dove, P.M., 2006. Role of molecular charge and hydrophilicity in regulating the kinetics of crystal growth. P. Nat. Acad. Sci. USA. 103, 19237-19242.

Fabry, V.J., Seibel, B.A., Feely, R.A., Orr, J.C., 2008. Impacts of ocean acidification on marine fauna and ecosystem processes. ICES J. Mar. Sci. 65, 414-432.

Gaylord, B., Hill, T.M., Sanford, E., Lenz, E.A., Jacobs, L.A., Sato, K.N., Russell, A.D., Hettinger, A., 2011. Functional impacts of ocean acidification in an ecologically critical foundation species. J. Exp. Biol. 241, 2586-2594.

Gazeau, F., Parker, L.M., Comeau, S., Gattuso, J.P., O'Connor, W.A., Martin, S., Pörtner, H.O., Ross, P.M., 2013. Impacts of ocean acidification on marine shelled mollusks. Mar. Biol. 160, 2201-2245.

Gosling, E., 2003. Bivalve growth. Bivalve molluscs: biology, ecology and culture. Fishing News Books, Blackwell, Oxford, p169-200.

Guppy, M., Withers, P., 1999. Metabolic depression in animals: physiological perspectives and biochemical generalizations. Biol. Rev. Cambr. Philos. Soc. 74, 1-40.

Hall-Spencer, J.M., Rodolfo-Metalpa, R., Martin, S., Ransome, E., Fine, M., Turner, S.M., Rowley, S.J., Tedesco, D., Buia, M.C., 2008. Volcanic carbon dioxide vents show ecosystems effects of ocean acidification. Nature 454, 96-99.

Heinemann, A., Fietzke, J., Melzner, F., Böhm, F., Thomsen, J., Garbe-Schönberg, D., Eisenhauer, A., 2012. Conditions of *Mytilus edulis* extracellular body fluids and shell composition in a pH-treatment experiment: acid-base status, trace elements and $\delta^{11}B$. Geochem. Geophys. Geosyst. 13.

Hendriks, I.E., Duarte, C.M., Olsen, Y.S., Steckbauer, A., Ramajo, L., Moore, T.S., Trotter, J.A., McCulloch, M., 2015. Biological mechanisms supporting adaptation to ocean acidification in coastal ecosystems. Estuar. Coast. Shelf. Sci. 86, 1-8.

Hettinger, A., Sanford, E., Hill, T.M., Hosfelt, J.D., Russell, A.D., Gaylord, B., 2013. The influence of food supply on the response of Olympia oyster larvae to ocean acidification. Biogeosciences 10, 6629-6638.

Hiebenthal, C., Philipp, E.E.R., Eisenhauer, A., Wahl, M., 2013. Effects of seawater pCO_2 and temperature on shell growth, shell stability, condition and cellular stress of Western Baltic Sea *Mytilus edulis* (L.) and *Arctica islandica* (L.). Mar. Biol. 160, 2073-2087.

Hurlbert, S.H., 2004. On misinterpretations of pseudoreplication and related matters: a reply to Oksanen. Oikos 104, 591-597.

Hüning, A.K., Melzner, F., Thomsen, J., Gutowska, M.A., Krämer, L., Frickenhaus, S., Rosenstiel, P., Pörtner, H.O., Philipp, E.E.R., Lucassen, M., 2013. Impacts of seawater acidification on mantle gene expression patterns of the Baltic Sea blue mussel: implications for shell formation and energy metabolism. Mar. Biol. 160, 1845-1861.

Jochum, K.P., Nohl, U., Herwig, K., Lammel, E., Stoll, B., Hofmann, A.W., 2005. GeoReM: a new geochemical database for reference materials and isotopic standards. Geostand. Geoanal. Res. 29, 87-133.

Jochum, K.P., Weis, U., Stoll, B., Kurmin, D., Yang, Q., Raczek, I., Jacob, D.E., Stracke, A., Birbaum, K., Frick, D.A., Günther, D., Enzweiler, J., 2011. Determination of reference values for NIST SRM 610-617 glasses following ISO guidelines. Geostand. Geoanal. Res. 35, 397-429.

Jochum, K.P., Scholz, D., Stoll, B., Weis, U., Wilson, S.A., Yang, Q., Schwalb, A., Börner, N., Jacob, D.E., Andreae, M.O., 2012. Accurate trace element analysis of speleothems and biogenic calcium carbonates by LA-ICP-MS. Chem. Geol. 318-319, 31-44.

Kaehler, S., McQuaid, C.D., 1999. Use of the fluorochrome calcein as an *in situ* growth marker in the brown mussel *Perna perna*. Mar. Biol. 133, 455-460.

Ko, G.W., Dineshram, R., Campanati, C., Chan, V.B., Havenhand, J., Thiyagarajan, V., 2014. Interactive effects of ocean acidification, elevated temperature, and reduced salinity on early-life stages of the pacific oyster. Environ. Sci. Technol. 48, 10079-10088.

Kobayashi, I., 1969. Internal microstructure of shell of bivalve molluscs. Am. Zool. 9, 663-672.

Kroeker, K.J., Kordas, R.L., Crim, R.N., Hendriks, I.E., Ramajo, L., Singh, G.S., Duarte, C.M., 2013. Impacts of ocean acidification on marine organisms: quantifying sensitivities and interactions with warming. Glob. Change. Biol. 19, 1884-1896.

Kroeker, K.J., Kordas, R.L., Crim, R.N., Singh, G.G., 2010. Meta-analysis reveals negative yet variable effects of ocean acidification on marine organisms. Ecol. Lett. 13, 1419-1434.

Kroeker, K.J., Sanford, E., Jellison, B.M., Gaylord, B., 2014. Predicting the effects of ocean acidification on predator-prey interactions: a conceptual framework based on coastal molluscs. Biol. Bull. 226, 211-222.

Kurihara, H., 2008. Effects of CO_2-driven ocean acidification on the early developmental stages of invertebrates. Mar. Ecol. Prog. Ser. 373, 275-284.

Lande, R., Shannon, S., 1996. The role of genetic variation in adaptation and population persistence in a changing environment. Evolution 50, 434-437.

Lannig, G., Eilers, S., Pörtner, H.O., Sokolova, I.M., Bock, C., 2010. Impact of ocean acidification on energy metabolism of oyster, *Crassostrea gigas*–changes in metabolic pathways and thermal response. Mar. Drugs. 8, 2318-2339.

Li, S., Liu, C., Huang, J., Liu, Y., Zhang, S., Zheng, G., Xie, L., Zhang, R., 2015. Interactive effects of seawater acidification and elevated temperature on biomineralization and amino acid metabolism in the mussel *Mytilus edulis*. J. Exp. Biol. 218, 3623-3631.

Li, S., Liu, C., Huang, J., Liu, Y., Zhang, S., Zheng, G., Xie, L., Zhang, R., 2016. Transcriptome and biomineralization responses of the pearl oyster *Pinctada fucata* to elevated $_{p}CO_2$ and temperature. Sci. Rep. 6, 18493.

Lin, C.L., Ning, X.R., Su, J.L., Lin, Y., Xu, B., 2005. Environmental changes and the responses of the ecosystems of the Yellow Sea during 1976–2000. J. Marine. Syst. 55, 223-235.

Malley, D.F., Huebner, J.D., Donkersloot, K., 1988. Effects on ionic composition of blood and tissues of *Anodonta grandis grandis* (Bivalvia) of an addition of aluminum and acid to a lake. Arch. Environ. Contam. Toxicol. 17, 479-491.

McDonald, M.R., McClintock, J.B., Amsler, C.D., Rittschof, D., Angus, R.A., Orihuela, B., Lutostanski, K., 2009. Effects of ocean acidification over the life history of the barnacle *Amphibalanus amphitrite*. Mar. Ecol. Prog. Ser. 385, 179-187.

Melzner, F., Gutowska, M.A., Langenbuch, M., Dupont, S., Lucassen, M., Thorndyke, M. C., Bleich, M., Pörtner, H.O., 2009. Physiological basis for high CO_2 tolerance in marine ectothermic animals: pre-adaptation through lifestyle and ontogeny?. Biogeosciences 6, 2313-2331.

Melzner, F., Stange, P., Trübenbach, K., Thomsen, J., Casties, I., Panknin, U., Gorb, S.N., Gutowska, M.A., 2011. Food supply and seawater pCO_2 impact calcification and internal shell dissolution in the blue mussel *Mytilus edulis*. PLoS. One. 6, e24223.

Milano, S., Schöne, B.R., Wang, S., Müller, W.E., 2016. Impact of high pCO_2 on shell structure of the bivalve *Cerastoderma edule*. Mar. Environ. Res. 119, 144-155.

Moura, G., Almeida, M.J., Machado, M.J.C., Vilarinho, L., Machado, J., 2004. The action of environmental acidosis on the calcification process of *Anodonta cygnea* (L.). In: Kobayashi, I., Ozawa, H. (Eds.), Biomineralization (BIOM2001)—formation, diversity, evolution, and application. Tokai University Press, Japan, p 178-182.

Palmer, A.R., 1983. Relative cost of producing skeletal organic matrix versus calcification: evidence from marine gastropods. Mar. Biol. 75, 287-292.

Palmer, A.R., 1992. Calcification in marine molluscs: how costly is it?. Proc. Natl. Acad. Sci. USA. 89, 1379-1382.

Parker, L.M., Ross, P.M., O'Connor, W.A., 2009. The effect of ocean acidification and temperature on the fertilization and embryonic development of the Sydney rock oyster *Saccostrea glomerata* (Gould 1850). Glob. Change. Biol. 15, 2123-2136.

Parker, L.M., Ross. P.M., O'Connor, W.A., Pörtner, H.O., 2013. Predicting the response of molluscs to the impact of ocean acidification. Biology 2, 651-692.

Pierrot, D.E., Lewis, E., Wallace, D.W.R., 2006. MS Excel program developed for CO_2 system calculations, ORNL/CDIAC-105a, carbon dioxide information analysis center. Oak Ridge National Laboratory, U.S. Department of Energy, Oak Ridge, Tennessee.

Pörtner, H.O., Bock, C., Reipschläger, A., 2000. Modulation of the cost of pHi regulation during metabolic depression: a 31P-NMR study in invertebrate (*Sipunculus nudus*) isolated muscle. J. Exp. Biol. 203, 2417-2428.

Pörtner, H.O., Farrell, A.P., 2008. Physiology and climate change. Science 322, 690-692.

Pörtner, H.O., Langenbuch, M., Reipschläger, A., 2004. Biological impact of elevated ocean CO_2 concentrations: lessons from animal physiology and earth history. J. Oceanogr. 60, 705-718.

Ramajo, L., Marbà, N., Prado, L., Peron, S., Lardies, M.A., Rodriguez-Navarro, A., Vargas, C.A., Lagos, N.A., Duarte, C.M., 2015. Biomineralization changes with food supply confer juvenile scallops (*Argopecten purpuratus*) resistance to ocean acidification. Glob. Change. Biol. doi: 10.1111/gcb.13179

Ramajo, L., Pérez-León, E., Hendriks, I.E., Marbà, N., Krause-Jensen, D., Sejr. M.K., Blicher, M.E., Lagos, N.A., Olsen, Y.S., Duarte, C.M., 2016. Food supply confers calcifers resistance to ocean acidification. Sc. Rep. 6, 19374.

Richardson, C.A., Crisp, D.J., Runham, N.W., 1981. Factors influencing shell deposition during a tidal cycle in the intertidal bivalve *Cerastoderma edule*. J. Mar. Biol. Assoc. UK. 61, 465-476.

Ries, J.B., Cohen, A.L., McCorkle, D.C., 2009. Marine calcifiers exhibit mixed responses to CO_2-induced ocean acidification. Geology 37, 1131-1134.

Rodolfo-Metalpa, R., Houlbreque, F., Tambutte, E., Boisson, F., Baggini, C., Patti, F.P., Jeffree, R., Fine, M., Foggo, A., Gattuso, J.P., Hall-Spencer, J.M., 2011. Coral and mollusc resistance to ocean acidification adversely affected by warming. Nat. Climate. Change. 1, 308-312.

Sanders, M.B., Bean, T.P., Hutchinson, T.H., Le Quesne, W.J., 2013. Juvenile king scallop, *Pecten maximus*, is potentially tolerant to low levels of ocean acidification when food is unrestricted. PLoS. One. 8, e74118.

Saphoerster, J., 2008. The physiology of the blue mussel (*Mytilus edulis*) in relation to ocean acidification. Doctoral dissertation, Christian-Albrechts-Universität.

Schalkhausser, B., Bock, C., Stemmer, K., Brey, T., Pörtner, H.O., Lannig, G., 2013. Impact of ocean acidification on escape performance of the king scallop, *Pecten maximus*, from Norway. Mar. Biol. 160, 1995-2006.

Sokolov, A.P., Stone, P.H., Forest, C.E., Prinn, R., Sarofim, M.C., Webster, M., Paltsev, S., Schlosser, C.A., Kicklighter, D., Dutkiewicz, S., Reilly, J., Wang, C., Felzer, B., Jacoby, H.D., 2009. Probabilistic forecast for twenty-first-century climate based on uncertainties in emissions (without policy) and climate parameters. J. Clim. 22, 5175-5204.

Stemmer, K., 2013. Shell formation and microstructure of the ocean quahog Arctica islandica: Does ocean acidification?. Doctoral dissertation, Staats-und Universitaetsbibliothek Bremen.

Thébault, J., Chauvaud, L., Clavier, J., Fichez, R., Morize, E., 2006. Evidence of a 2-day periodicity of striae formation in the tropical scallop *Comptopallium radula* using calcein marking. Mar. Biol. 149, 257-267.

Thomsen, J., Casties, I., Pansch, C., Körtzinger, A., Melzner, F., 2013. Food availability outweighs ocean acidification effects in juvenile *Mytilus edulis*: laboratory and field experiments. Glob. Change. Biol. 19, 1017-1027.

Thomsen, J., Gutowska, M. A., Saphörster, J., Heinemann, A., Trübenbach, K., Fietzke, J., Hiebenthal, C., Eisenhauer, A., Körtzinger, A., Wahl, M., Melzner, F., 2010. Calcifying invertebrates succeed in a naturally CO_2-rich coastal habitat but are threatened by high levels of future acidification. Biogeosciences 7, 3879-3891.

Ventilla, R.F., 1982. The scallop industry in Japan. Adv. Mar. Biol. 20, 309-382.

Wada, K., Fujinuki, T., 1976. Biomineralization in bivalve molluscs with emphasis on the chemical composition of the extrapallial fluid. In: Watabe, N., Wilbur, K.M. (Eds.), The Mechanisms of Mineralization in Invertebrates and Plants. University of South Carolina Press, Columbia, p175-190.

Waite, J.H., 1983. Quinone-tanned scleroproteins. In: Hochachka, P.W. (Ed) The Mollusca, metabolic biochemistry and molecular biomechanics, vol 1. Academic Press, New York, p 467-504.

Waldbusser, G.G., Brunner, E.L., Haley, B.A., Hales, B., Langdon, C.J., Prahl, F.G., 2013. A developmental and energetic basis linking larval oyster shell formation to acidification sensitivity. Geophys. Res. Lett. 40, 2171-2176.

Waldbusser, G.G., Hales, B., Langdon, C.J., Haley, B.A., Schrader, P., Brunner, E.L., Gray, M.W., Miller, C.A., Gimenez, I., 2014. Saturation-state sensitivity of marine bivalve larvae to ocean acidification. Nat. Clim. Change. 5, 273-280.

Weiss, I.M., Schönitzer, V., 2006. The distribution of chitin in larval shells of the bivalve mollusk *Mytilius galloprovincialis*. J. Struct. Biol. 153, 264-277.

Wheeler, A.P., 1992. Mechanisms of molluscan shell formation. In: Bonucci, E. (Ed.), Calcification in biological systems. CRC press, Boca Raton, FL, p179-216.

Xu, X., Yang, F., Zhao, L., Yan, X., 2016. Seawater acidification affects the physiological energetics and spawning capacity of the Manila clam *Ruditapes philippinarum* during gonadal maturation. Comp. Biochem. Phys. 196A, 20-29.

Zittier, Z.M.C., Bock, C., Lannig, G., Pörtner, H.O., 2015. Impact of ocean acidification on thermal tolerance and acid-base regulation of *Mytilus edulis* (L.) from the North Sea. J. Exp. Mar. Biol. Ecol. 473, 16-25.

Chapter 5

Sodium provides unique insights into transgenerational effects of ocean acidification on bivalve shell formation

Published in Science of the Total Environment

Liqiang Zhao[1], Bernd R. Schöne[1], Regina Mertz-Kraus[1], Feng Yang[2]

[1] Institute of Geosciences, University of Mainz, Joh.-J.-Becher-Weg 21, 55128 Mainz, Germany

[2] Engineering Research Center of Shellfish Culture and Breeding in Liaoning Province, Dalian Ocean University, 116023 Dalian, China

Author contribution

Concept: LZ, BRS

Execution: LZ, FY

Data collection and analysis: LZ, RMK, FY

Writing: LZ, BRS, RMK, FY

Liqiang Zhao, Bernd R. Schöne, Regina Mertz-Kraus, Feng Yang, 2017. Sodium provides unique insights into transgenerational effects of ocean acidification on bivalve shell formation. Science of the Total Environment 577, 360–366.

Abstract

Ocean acidification is likely to have profound impacts on marine bivalves, especially on their early life stages. Therefore, it is imperative to know whether and to what extent bivalves will be able to acclimate or adapt to an acidifying ocean over multiple generations. Here, we show that reduced seawater pH projected for the end of this century (i.e., pH 7.7) led to a significant decrease of shell production of newly settled juvenile Manila clams, *Ruditapes philippinarum*. However, juveniles from parents exposed to low pH grew significantly faster than those from parents grown at ambient pH, exhibiting a rapid transgenerational acclimation to an acidic environment. The sodium composition of the shells may shed new light on the mechanisms responsible for beneficial transgenerational acclimation. Irrespective of parental exposure, the amount of Na incorporated into shells increased with decreasing pH, implying active removal of excessive protons through the Na^+/H^+ exchanger which is known to depend on the Na^+ gradient actively built up by the Na^+/K^+-ATPase as a driving force. However, the shells with a prior history of transgenerational exposure to low pH recorded significantly lower amounts of Na than those with no history of acidic exposure. It therefore seems very likely that the clams may implement less costly and more ATP-efficient ion regulatory mechanisms to maintain pH homeostasis in the calcifying fluid following transgenerational acclimation. Our results suggest that marine bivalves may have a greater capacity to acclimate or adapt to ocean acidification by the end of this century than currently understood.

5.1. Introduction

During the past 250 years, atmospheric carbon dioxide (CO_2) concentrations have increased by nearly 40% due to human activities (Doney et al., 2009). Approximately one third of anthropogenic CO_2 emissions has entered the oceans, reducing ocean pH and driving unprecedented changes in seawater carbonate chemistry (IPCC, 2013). This phenomenon, termed ocean acidification (OA), is predicted to have widespread implications for calcifying organisms (Orr et al., 2005; Hendriks et al., 2010; Bach, 2015). Juvenile specimens are particularly vulnerable to lower pH levels (Kroeker et al., 2013). There is ample evidence that OA may impair the ability of pelagic larvae and early juveniles to produce their skeletal structures, leading to developmental delay and high mortality (e.g., Kurihara, 2008; Parker et al., 2009; Stumpp et al., 2013; Waldbusser et al., 2014).

Profound effects of OA occurring at one stage of life may generate negative or positive carry-over effects in subsequent life stages. For example, Hettinger et al. (2012, 2013) found that OA had detrimental effects on larval growth and survival of tank-grown specimens of the Olympia oyster, *Ostrea lurida*, and these effects persisted into the juvenile stage and continued for another four months even when they were transferred to the natural environment. In contrast, positive carry-over effects have been observed in the bay scallop, *Argopecten irradians*, and the hard clam, *Mercenaria mercenaria* (Gobler and Talmage, 2013). Juveniles of both species reared at elevated pCO_2 during larval development grew faster under natural conditions compared to those exposed to ambient pCO_2 (= current ocean pH of 8.1). Given that many calcifying species such as mollusks have complex life cycles, it is essential to investigate carry-over effects during all life stages. Furthermore, it is relevant to know if such carry-over effects can possibly persist into the next generation (Ross et al., 2016). Such information is critical for understanding whether marine biota will be able to acclimate and/or adapt to long-term OA exposure.

Environmental stress experienced by parents may alter the response of their offspring to harsh environmental conditions, a phenomenon known as transgenerational epigenetic effect (Youngson and Whitelaw, 2008). A growing body of evidence suggests that transgenerational effects, i.e., carry-over effects from parents to offspring, might confer environmental resilience to the offspring if they are subjected to the same environmental situation as their parents (Marshall, 2008; Marshall and Morgan, 2011; Ross et al., 2016). Such acclimation is of paramount importance for marine calcifiers to cope with OA as it can occur over much shorter time frames. Markedly increased growth rates, survival rates and fecundity in subsequent

generations through transgenerational epigenetic effects have been reported from calcifying species with short generation times such as coccolithophores (Lohbeck et al., 2012) and copepods (e.g., Fitzer et al., 2012; De Wit et al., 2015; Thor and Dupont, 2015) that were exposed to elevated CO_2-levels. However, relevant studies on calcifiers with relatively long generation times such as bivalve mollusks are very limited (Ross et al., 2016). Parker et al. (2012, 2015) demonstrated positive transgenerational effects on growth and physiological performances of the Sydney rock oyster, *Saccostrea glomerata*, whereas the underlying mechanisms are still not fully understood (Goncalves et al., 2016).

Amongst others, shells provide protection against predators. However, OA may seriously impair physical properties of the shells (Beniash et al., 2010; Fitzer et al., 2014; Milano et al., 2016). In particular, the maintenance of larval and juvenile shell integrity becomes much more difficult when subjected to lowered seawater pH and saturation state (Fitzer et al., 2014; Waldbusser et al., 2014), thereby increasing the susceptibility of bivalves to predation (Kroeker et al., 2014). Since rapid juvenile growth after larval settlement and metamorphosis is the most important factor affecting molluscan recruitment success (Gosling, 2003), elucidating the mechanisms driving decreased shell growth under OA conditions can provide a better understanding of how OA will affect the recruitment and population dynamics of bivalves.

Following larval settlement and metamorphosis and the formation of the mantle tissue, the mineralization of juvenile and adult bivalve shells takes place in the extrapallial space (EPS) which is located between the outer mantle epithelium (OME) and the calcifying shell (Wheeler, 1992). During the growing season, bivalves can actively elevate the pH of the EPS, which facilitates the (inorganic) precipitation of $CaCO_3$, and stimulate the synthesis and secretion of organic matrix by the OME which in turn, governs the precipitation of $CaCO_3$ (Marin et al., 2012). Hence, the acid-base status of the EPS is a critical determinant of shell production. OA has been shown to lower the pH of the EPS due to the passive proton leakage (Thomsen et al., 2010; Heinemann et al., 2012). However, it is not yet clear whether and to what extent bivalves are able to actively remove these excessive protons to maintain alkaline conditions at the calcifying front, partly due to the technical challenge of continuous monitoring of the pH in the EPS. The search for a proxy that can record temporal changes of calcifying pH has therefore received growing interest. For example, Frieder et al. (2014) found that uranium-to-calcium ratios in shells of *Mytilus californianus* and *M. galloprovincialis* may fulfill this task as uranium exists almost exclusively as a group of multiple uranyl carbonate complexes whose relative abundances are strongly dependent on pH (Djogić et al., 1986). Likewise, the boron isotopic composition of *Mytilus edulis* shells (Heinemann et al., 2012) has been suggested as an

alternative pH proxy (Klochko et al., 2006). Moreover, sodium-to-calcium ratio in shells will likely contribute to a better understanding of the specific mechanisms by which bivalves regulate the pH at the site of calcification (Zhao et al., in review).

The Manila clam, *Ruditapes philippinarum*, is a eurythermal and euryhaline mollusk species that is worldwide distributed in estuarine and coastal waters (Gosling, 2003). It is also amongst the commercially most important species in global fisheries (FAO, 2012). Due to such ecological and economical significance, quantifying the influence of OA on *R. philippinarum* becomes imperative. A recent study has shown that OA can severely impair adult physiological energetics and spawning ability during reproductive conditioning (Xu et al., 2016). Spawning failure can lead to a significant reduction of larval supply. However, a fundamental challenge ultimately affecting larval recruitment and population maintenance of *R. philippinarum* lies in whether parental exposure will generate positive carry-over effects to their offspring, especially at the early life stages, thereby helping them to acclimate to OA. In the present study, we exposed adult clams to reduced seawater pH (7.7) during gonadal maturation and then compared the rate of shell growth of newly settled juveniles to those from parents were exposed to seawater pH 8.1. More specifically, we analyzed the sodium composition of the shells in order to gain a more detailed understanding of the underlying mechanisms. The results represent a first look at whether transgenerational acclimation of this species to OA would be expected.

5.2. Materials and methods

5.2.1 Adult collection and maintenance

Specimens of 2-year-old *R. philippinarum* (32 ± 2 mm shell length) were collected from the intertidal zone of Liangshui Bay (39°04'14.41" N, 122°01'47.70" E), Yellow Sea during April 2014. Seawater temperature, salinity and pH at Liangshui Bay varied between 1.2 and 23.8 °C, 30.8 and 32.8, and 7.98 and 8.26 in the year 2014, respectively (monthly variations see Fig. 1 in supplementary material). Upon arrival in the laboratory, they were maintained in a 600-L tank with circulating seawater at temperature of 9 °C, salinity of 32 and pH 8.1 for a 2-week acclimation period. The acclimation conditions were comparable to those recorded at the sampling site and day of collection. During the acclimation and the following experimental period, seawater was taken from the storage tank (120 m^3; Engineering Research Center of Shellfish Culture and Breeding in Liaoning Province, Dalian Ocean University) where seawater

is pumped approximately 1 km offshore and passed through a sand-filter and salinity and pH are relatively stable. Clams were fed every two days with the microalgae *Chlorella vulgaris*. Histological analysis showed that up to 60 % of the specimens were at the early developmental stage of gametogenesis.

5.2.2 Parental exposure and spawning

At this stage of the experiment, two circulating systems were built. Each system consisted of three exposure chambers (in triplicate), a gas mixing chamber and a temperature controlling chamber, holding a final volume of 600-L seawater (for detailed information see Xu et al., 2016). Two levels of seawater pH were considered: 8.1 and 7.7 corresponding to the control and projected level for the year 2100 (IPCC, 2013), respectively. Since clams were collected from an intertidal zone where seawater pH fluctuates over a tidal cycle (up to 0.3-0.5 pH units; Duarte et al., 2013), it is very likely that they may frequently experience a reduction of ca. 0.4 pH units projected for the open oceans by the end of this century. Hence, a decrease of seawater pH from 8.1 to 7.7 in our experiments represents an environmentally realistic scenario that might be encountered by *R. philippinarum* in natural habitats. Reduced seawater pH was adjusted by bubbling pure CO_2 gas into the gas mixing chamber. Adult clams were randomly assigned to each system at a density of 150 specimens per chamber, and then acclimated to the target pH level during the subsequent two weeks. Following acclimation, temperature in each system was gradually increased from 10 to 20 °C (ca. 0.3 °C per day) over the following 30 days and then kept constant at 20 °C for 40 days. Half of the water in each system was renewed every 4-5 days. To fulfill the nutritional requirement for gonadal development the clams were fed twice daily with an equal mixture of four species of microalgae (*Chaetoceros muelleri*, *Nitzschia closterium*, *Isochrysis galbana* and *C. vulgaris*). After 70 days of artificial ripening, a total of 300 clams selected at random from each system were induced to spawn by temperature shock (+ 4 °C), and afterward more than 95 % of individuals spawned.

5.2.3 Larval and juvenile rearing

The following experiment was carried out in 100-L tanks. 26 hours after fertilization, six million D-veliger larvae were filtered out through a 50 μm mesh sieve from each system and equally divided into six tanks at a density of ca. 10 larvae/ml. As schematically illustrated in Figure 5.1, three tanks were set at pH 8.1, while the other three were set at pH 7.7. The water was bubbled

continuously with ambient air or pure CO_2 gas to reach the target pH level. Larval rearing conditions were maintained identically for all three replicates. Larvae were fed twice daily with *I. galbana* at a concentration of 20,000 cells/ml from day 1 to day 3 and an equal mixture of *I. galbana* and *C. vulgaris* at a concentration of 60,000 cells/ml from day 4 onward. Given that pH may significantly interact with other environmental parameters specifically temperature and salinity (Cole et al., 2016), those parameters were kept constant at 20 °C and 31 (Fig. 2s), respectively, to minimize the potential influence of temperature and salinity fluctuations on the rate of shell growth. According to Fig. 1s, temperature of 20 °C and salinity of 32 were also comparable to natural conditions experienced by larval and juvenile clams following adult spawning in August in the Yellow Sea (Zhao et al., 2012). Every two days the water in each tank was half renewed using freshly prepared water with identical pH, temperature and salinity to ensure rearing conditions remained consistent throughout the duration of the experiment. Once most larvae had developed to the pediveliger stage (eyespot and protruding foot appeared, 180-210 µm shell length, 12-15 days after fertilization), a complete water change was made twice daily to help larval settlement and metamorphosis. On day 20, newly settled juveniles in each tank were quantified and stocking density was reset to ca. 1000 individuals per aquarium. Over the following 30 days they were fed daily with *C. vulgaris* at a concentration of 80,000 cells/ml, and experimental conditions and daily care were handled in the same manner as during larval rearing.

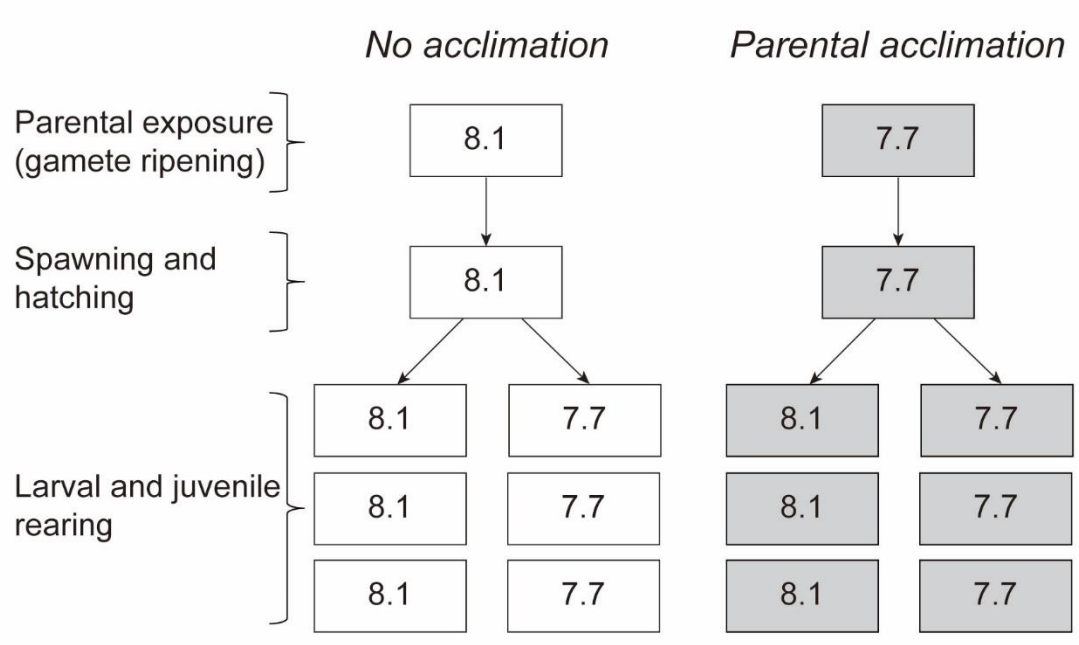

Fig. 5.1. Transgenerational experimental design. Each box represents one tank. For details refer to text.

During the experiment, temperature, salinity and pH were monitored daily. On a weekly basis, water samples were taken for the measurements of total alkalinity by means of an alkalinity titrator. The remaining carbonate system parameters in seawater such as the partial pressure of CO_2 and the saturation state of aragonite were calculated from temperature, salinity, pH and total alkalinity using the CO2SYS software program (Pierrot et al., 2006). Table 5.1 summarizes these parameters of seawater carbonate chemistry throughout the duration of juvenile rearing.

Table 5.1. Seawater carbonate chemistry throughout the duration of juvenile rearing. Seawater temperature, salinity and pH were monitored daily, and total alkalinity (TA) on a weekly basis. Partial pressure of CO_2 in seawater (pCO_2) and saturation state of aragonite (Ω_{ara}) were calculated from the measured temperature, salinity, pH and TA at the sampling day. Data are expressed as mean ± standard error (n = 30 for temperature, salinity and pH; n = 5 for TA, pCO_2 and Ω_{ara}). Daily variations of temperature, salinity and pH are provided in Fig. 2s. NA: no acclimation (i.e., parental exposure to pH 8.1); PA: parental acclimation (i.e., parental exposure to pH 7.7).

Treatments	T (°C)	S (PSU)	pH	TA (µmol/kg)	pCO_2 (µatm)	Ω_{ara}
NA × 8.1	20.21 ± 0.06	31.37 ± 0.05	8.05 ± 0.01	2250 ± 25	378 ± 22	2.82 ± 0.11
NA × 7.7	20.38 ± 0.05	31.49 ± 0.07	7.71 ± 0.01	2228 ± 19	982 ± 39	1.35 ± 0.03
PA × 8.1	20.29 ± 0.06	31.41 ± 0.06	8.07 ± 0.01	2235 ± 23	3390 ± 28	2.75 ± 0.13
PA × 7.7	20.44 ± 0.05	31.38 ± 0.05	7.69 ± 0.01	2292 ± 31	976 ± 28	1.43 ± 0.02

5.2.4 Shell measurements and chemical analysis

Twenty 30 days-old juveniles from each treatment were randomly taken out to evaluate the rate of shell growth after larval settlement and metamorphosis. Under a dissecting microscope two valves of each shell were carefully split open, rinsed thoroughly with deionized water and then air-dried. Each left valve was mounted on a glass slide using double-sided tape and an image was taken with a Canon EOS 550D digital camera attached to the microscope. Shell height (the perpendicular distance between umbo and ventral margin) was measured using the image analysis software ImageJ. The daily rate of juvenile shell growth was subsequently calculated by dividing the measured growth advance by the number of days of the experiment (i.e. 30 days).

The other valve of each shell was used for elemental analysis by means of laser ablation – inductively coupled plasma – mass spectrometry (LA-ICP-MS) in spot mode at the Institute of Geosciences, University of Mainz. Prior to the analyses, samples were immersed in Teflon beakers containing 15 ml 15 % H_2O_2 buffered with 0.05 M NaOH overnight (ca. 14 hours) to remove organic matrices from the shell. Afterward, each valve was ultrasonically rinsed with

deionized water and carefully mounted on a glass slide using double-sided tape. Sodium (measured as ^{23}Na) concentrations were determined in each shell (three discrete laser ablation spots per shell). Analyses were performed on an Agilent 7500ce quadrupole ICP-MS coupled to an ESI NWR193 ArF excimer laser ablation system equipped with the TwoVol2 ablation cell. Ablation was achieved using a pulse rate of 5 Hz, an energy density of ~2.8 J/cm^2 and a beam diameter of 100 µm. Backgrounds were measured for 15 s, followed by 25 s ablation time and 20 s wash out time. NIST SRM 610 was used as a calibration material, applying the preferred values reported in the GeoReM database (http://georem.mpch-mainz.gwdg.de/, Application Version 19) (Jochum et al., 2005, 2011) as the 'true' concentrations to calculate the element concentrations in the samples. USGS BCR-2G and MACS-3 were analyzed as quality control materials (QCM) to monitor accuracy and reproducibility of the analyses. All reference materials were analyzed at the beginning and at the end of a sequence and after ca. 60 laser spots. For all materials, ^{43}Ca was used as internal standard. For the reference materials, we applied the Ca concentrations reported in the GeoReM database, and for the samples 56.03 wt%, i.e., the stoichiometric CaO content of aragonite. The time-resolved signal was processed using the program GLITTER 4.4.1 (www.glitter-gemoc.com, Macquarie University, Sydney, Australia). Reproducibility based on repeated measurements (n = 39) of the QCM was always better than 3 % (1 RSD) for USGS BCR-2G and 7 % (1 RSD) for MACS-3. The measured Na concentrations of the QCM agrees within 5 % the preferred value of the GeoReM database for USGS BCR-2G, respectively, and within 7 % with the preliminary reference value for USGS MACS-3 (personal communication S. Wilson, USGS, in Jochum et al. 2012), respectively.

5.2.5 Statistical analysis

The normality and homogeneity of the data were tested by means of the Shapiro-Wilk's test and the Levene's F-test, respectively, using the statistical software SPSS 19.0. Combined effects of parental exposure and pH as well as the interaction between these two factors on shell growth and Na/Ca_{shell} were evaluated by means of two-way analysis of variance (ANOVA). Once two-way ANOVA showed significant interactive results, a Student-Newman-Keuls (SNK) *post hoc* test was performed to evaluate differences among groups. Statistically significant difference was set at $p \leq 0.05$.

5.3. Results

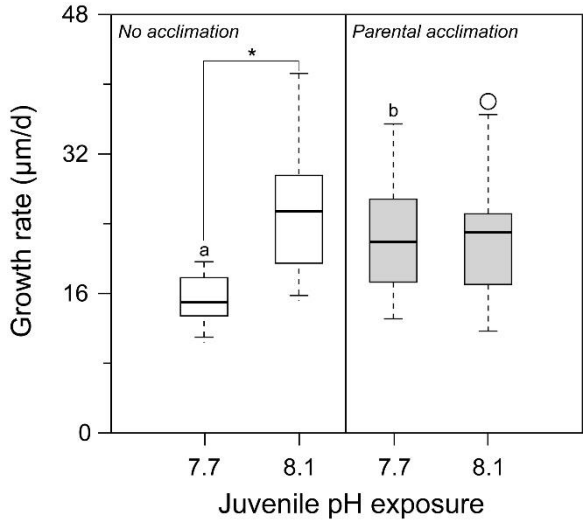

Fig. 5.2. Box plot comparing the rate of shell growth of newly settled *Ruditapes philippinarum* juveniles grown at pH 7.7 and 8.1 following parental exposure to pH 8.1 (no acclimation) and 7.7 (parental acclimation). Medians are highlighted in bold. Edges of each box represent the 25% and 75% quartiles, respectively. Whiskers represent the lowest and highest data points (n = 20). Open circle stands for the outlier (i.e., value deviating from the median by more than 1.5 times of the height of the box). The boxes sharing an asterisk are significantly different ($p < 0.05$). The boxes denoted "a" and "b" are significantly different at pH 7.7 ($p < 0.05$).

As shown in Figure 5.2, the rate of shell growth was significantly affected by parental exposure, pH and interaction between those two factors ($p < 0.05$; Table 5.2). Clams from parents that were exposed to pH 8.1 grew significantly slower at pH 7.7 than at pH 8.1 ($p < 0.05$; Fig. 5.2), whereas no significant reduction of shell formation was observed in those from parents grown at pH 7.7 ($p > 0.05$; Fig. 5.2). In particular, at pH 7.7, clams with a prior history of parental exposure to low pH grew significantly faster than those with no prior experience with low pH ($p < 0.05$; Fig. 5.2).

As shown in Figure 5.3, the amount of Na incorporated into the shells was significantly affected by pH and the interaction between parental exposure and pH ($p < 0.05$; Table 5.2). Irrespective of parental exposure, the shells forming at pH 7.7 contained significantly larger amounts of Na than those grown at pH 8.1 ($p < 0.05$; Fig. 5.3). At pH 7.7, the shells derived from parents exposed to low pH showed significantly lower Na/Ca_{shell} values than those from parents grown at pH 8.1 ($p < 0.05$; Fig. 5.3).

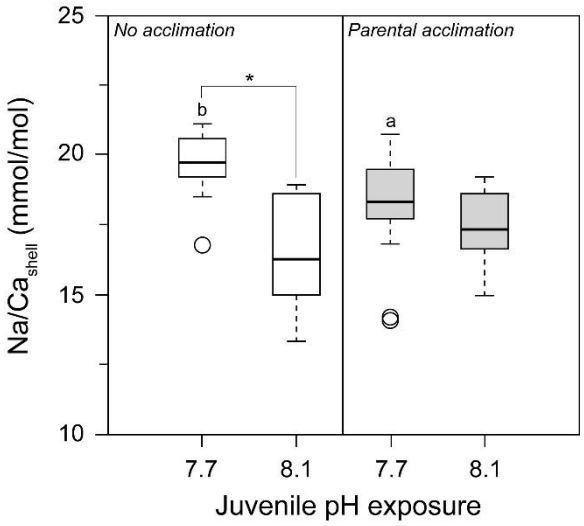

Fig. 5.3. Box plot comparing the ratio of sodium-to-calcium in shells of newly settled *Ruditapes philippinarum* juveniles grown at pH 7.7 and 8.1 following parental exposure to pH 8.1 (no acclimation) and 7.7 (parental acclimation). Medians are highlighted in bold. Edges of each box represent the 25% and 75% quartiles, respectively. Whiskers represent the lowest and highest data points (n = 20). Open circles stand for the outliers (i.e., values deviating from the median by more than 1.5 times of the height of the boxes). The boxes sharing an asterisk are significantly different ($p < 0.05$). The boxes denoted "a" and "b" are significantly different at pH 7.7 ($p < 0.05$).

Table 5.2. Summary of two-way ANOVA results on the effects of pH on the rate of shell growth and the ratio of sodium-to-calcium in shells of newly settled *Ruditapes philippinarum* juveniles following parental exposure to pH 8.1 and 7.7.

Source of variations	*df*	Growth rate			Na/Ca$_{shell}$		
		MS	*F*	*p*	MS	*F*	*p*
Parental exposure	1	132.767	4.092	0.047	0.491	0.208	0.650
pH	1	481.475	14.841	0.000	78.467	33.219	0.000
Parental exposure × pH	1	429.108	13.227	0.001	29.077	12.310	0.001
Residual	76	32.446			2.362		
Total	80						

5.4. Discussion

Our findings demonstrate that transgenerational effects may alleviate the adverse effects of OA on juvenile *R. philippinarum* shell formation. For example, clams derived from parents exposed

to increased CO_2-levels (pH 7.7) grew significantly faster at an environmentally relevant OA scenario (i.e., pH 7.7), compared to those from parents maintained under normal ocean pH (8.1). This finding is in line with previous studies on the oyster *Saccostrea glomerata* (Parker et al., 2012), where parental exposure to elevated pCO_2 of 856 µatm generated positive carry-over effects on larval growth and development when subjected to the same pCO_2 environment. In particular, these transgenerational effects not only benefit early stages of life, but also persist into adulthood and the subsequent generation (Parker et al., 2015). Furthermore, Fitzer et al. (2014) reported that the blue mussel, *Mytilus edulis* following transgenerational exposure to elevated pCO_2 of 1000 µatm was no longer capable of precipitating aragonitic shells but only calcitic shells, probably because aragonite is more susceptible to dissolution than calcite (Mucci, 1983). It is therefore conceivable that marine bivalves (at least species hitherto studied) may have the ability to acclimate or adapt to near-future OA conditions.

Without exception, all three of the aforementioned species inhabit shallow coastal zones, where the progress of OA may occur at a much faster rate than in the open oceans due to local oceanographic processes and intensive anthropogenic activities (Duarte et al., 2013). Thus, disentangling the mechanistic bases for beneficial transgenerational effects under open ocean OA scenarios will help to better understand how bivalves from coastal ecosystems respond and evolve to rapidly changing environmental conditions over multiple generations. In particular, such knowledge may pave the way for more accurately predicting the ecological consequences of OA since many bivalve species are not only commercially important but also ecologically critical.

It has been hypothesized that bivalves utilize two primary mechanisms to compensate for the adverse effects of OA on shell formation. One hypothesis proposes that they can remove excessive protons from the EPS in order to produce conditions that favor $CaCO_3$ precipitation (Cyronak et al., 2015). The other hypothesis suggests that bivalves may enhance the synthesis of organic matrix to facilitate $CaCO_3$ crystallization (Marin et al., 2012). However, very little is known about whether, and to what extent, each mechanism contributes to the resilient responses of the bivalves to OA, thereby hampering our understanding of the mechanisms responsible for their rapid transgenerational acclimation. In particular, it remains a matter of debate whether, and how, bivalves maintain pH homeostasis at the calcifying front. The search for a proxy that can indicate the acid-base status and ionic regulation in the EPS is therefore of great value. As will be demonstrated below, the sodium composition of the shells hold great potential in this regard and, more importantly, shed valuable insights into the underlying

processes involved in positive transgenerational effects on shell formation when combining analyses of growth patterns and chemical properties of the shells.

Sodium in bivalve shells may shed new light on the processes involved in extracellular acid-base and ion regulatory responses to OA. To maintain alkaline conditions which are favorable for $CaCO_3$ precipitation, bivalves can actively remove protons generated at the calcifying front through membrane transporters in the outer mantle epithelium. For example, *in situ* measurements of the EPS in *Arctica islandica* show that pH rises rapidly toward the OME (Stemmer, 2013), indicating that protons are actively removed from the EPS. Support for the existence of such active transport processes also comes from a growing body of transcriptome studies. In a recent study of the pearl oyster, *Pinctada fucata*, Li et al. (2016) surveyed the transcriptome response of the OME following exposure to elevated pCO_2 of 862 µatm and found significantly increased expression of genes involved in acid-base and ion regulatory processes, specifically for vacuolar-type H^+-ATPase and the Na^+/H^+ exchanger which are proposed to be responsible for active removal of protons from the EPS (McCulloch et al., 2012; Zhao et al., in review). If this is the case, then one would expect Na/Ca_{shell} to increase as the amount of Na^+ transported into the EPS rises. Our findings lend support to this hypothesis. With decreasing seawater pH, the amount of Na^+ incorporated into the shells increased. However, a proton removal mechanism via the Na^+/H^+ exchanger is energetically expensive because the driving force for many Na^+-dependent transporters comes from the Na^+ gradient which is actively built up by the Na^+/K^+-ATPase (Pörtner et al., 2004; Melzner et al., 2009). Presumably, *R. philippinarum* may be faced with an energetic trade-off when subjected to OA, either to fulfill the energy demand of the Na^+/K^+-ATPase or allocate more energy to the synthesis of organic matrix. Therefore, a more detailed understanding of the partitioning of juvenile energy budget to shell mineralization processes may advance our understanding of the underlying mechanisms responsible for positive transgenerational effects.

As mentioned previously, moderately low pH had virtually no impact on the rate of shell growth of *R. philippinarum* that came from parents exposed to the same pH. This absence of acidification effect on shell growth is most likely a consequence of an optimal allocation of energy available for the processes of shell formation. Under moderately acidified conditions, transgenerationally acclimated clams showed a significantly lower Na/Ca_{shell} compared to those from parents grown at pH 8.1, indicating that they likely evolve less costly and more ATP-efficient ion-regulatory mechanisms to maintain pH homeostasis at the calcifying front. This shift, in turn, corresponds to an increased proportion of energy committed to the organic matrix synthesis while the amount of exogenous energy supply is kept constant. Aside from acting as

templates for crystal nucleation and growth (Marin et al., 2008), organic molecules compose a major portion of the outermost organic shell layer, i.e., the periostracum which is exceedingly important for the maintenance of shell integrity and production in more acidic and corrosive seawater (Tunnicliffe et al., 2009; Gazeau et al., 2013). Tyrosinase plays a critical role in the synthesis of proteinaceous matrix of shell periostracum (Waite and Wilbur, 1976). When exposed to elevated pCO_2 of 1120 µatm, the expression of the tyrosinase gene was significantly up-regulated in the blue mussel, *M. edulis* (Hüning et al., 2013), suggesting that this species might implement a protective mechanism against external shell corrosion. Evidently, the organic matrix formation entails a considerable amount of energetic cost which would likely account for up to 60 % of the cost for somatic growth and 150 % for gamete formation (Palmer, 1992). Therefore, an improved ability of transgenerationally acclimated clams to build and maintain their shells in acidic seawater indicates that they may be capable of fulfilling energetic demands for synthesizing organic matrix likely through an adaptive alteration in the partitioning of the energy between differential mineralization processes.

Clearly, a better understanding of the transgenerational effects of OA on bivalve shell formation requires more knowledge of the energetic basis. In this regard, valuable insights can be obtained from a more comprehensive and detailed understanding of the energetic basis linking shell formation and the sensitivity to OA during the pelagic larval stage (Waldbusser et al., 2013), despite the existence of differential mechanisms likely involved in larval and juvenile shell formation. Limited endogenous energy reserves and rapid shell growth are typical traits at the initial stage of larval shell secretion, which could increase the larval vulnerability to OA for example through the kinetic-energetic mechanism (Waldbusser et al., 2015). Therefore, it seems likely that either increasing energy reserves into eggs through maternal effects or slowing the rate of shell growth may increase the larval resistance to OA. The latter agrees well with recent findings by Waldbusser et al. (2016) according to which the rates of larval calcification and endogenous energy lipid consumption of the brooding Olympia oyster, *O. lurida*, were much lower compared to those of the broadcast spawning Pacific oyster, *Crassostrea gigas*, under OA conditions. These observations lead the authors to suggest that Olympia oysters may be able to lessen the energetic burden of calcification through slow shell building (Waldbusser et al., 2016). The metamorphosis from larva to juvenile is also an energetically expensive process during which endogenous energy reserves (e.g., glycogen and lipid stores) are rapidly depleted (Gosling, 2003). However, newly settled juveniles need to build the shells rapidly rather than slowly in order to defend themselves against predators. It is therefore very likely that increasing maternal energy investment into eggs (i.e., producing bigger eggs) following

transgenerational acclimation could provide broadcast spawned *R. philippinarum* larvae and juveniles with increased energy and resilience to cope with OA stress.

Overall, although OA is occurring at an unprecedented rate, our findings concerning shell formation demonstrate that *R. philippinarum* would likely be able to acclimate to OA projected for the end of this century through transgenerational acclimation. Similar conclusions have also been drawn from short-term acclimation and long-term evolutionary adaptation in mytilid mussels living in naturally CO_2-rich coastal habitats (Tunnicliffe et al., 2009; Thomsen et al., 2013). For example, in the inner Kiel Fjord (Western Baltic Sea) where natural upwelling of CO_2-rich deep water masses considerably lowers surface seawater pH reaching a minimum value of 7.3, *M. edulis* is one of the dominant inhabitants exhibiting local adaptation to low pH (Thomsen et al., 2013). Notably, at the Eifuku volcano (Western Pacific Ocean), *Bathymodiolus brevior* is capable of surviving in extremely acidic seawater fluctuating between 5.36 and 7.29 (Tunnicliffe et al., 2009). Nevertheless, it should be emphasized that, aside from the natural pH fluctuations, multiple niche parameters should be considered when analyzing the acclimation or adaptation of these species to OA. In particular, increased food availability could enhance bivalves' resilience against OA stress (Ramajo et al., 2016). For example, *Mytilus californianus* is a keystone species that exhibits considerable diversity in rocky intertidal ecosystems along the Californian coast where low pH conditions prevail during strong coastal upwelling events (Feely et al., 2008), i.e., this species may be adapted to strong natural pH fluctuations. Kroeker et al. (2016) examined the relationships between multiple stressors and juvenile growth of *M. californianus* spanning 1280 km of the Californian coastline and found that mussels grew fastest in dynamic conditions with frequent exposure to low pH and high food availability, and the growth was lowest in low pH and less eutrophic waters. Furthermore, differential habitats may shape differential growth responses to OA. Bivalves inhabiting the intertidal zone are used to cope with acute extracellular acidosis because of the retention of metabolically produced CO_2 and the accumulation of metabolic acids produced by anaerobic metabolism during aerial exposure (Booth et al., 1984; Burnett, 1988), so that they may be pre-adapted and more resilient to OA. Therefore in order to better understand how marine bivalves will respond to OA at the local scale, it is essential to fully consider their habitat characteristics.

5.5. Summary and conclusions

The present study suggests that *R. philippinarum* may be more resilient to ocean acidification by the end of this century than previously thought. In particular, transgenerational acclimation may greatly improve the growth performance of newly settled juvenile clams, one of the most important determinants of recruitment success and population dynamics of marine bivalves. The most probable mechanism of this acclimation ability may be the alteration of the energy budget partitioning for shell production following transgenerational exposure. At the local scale, OA may take place concomitantly with other anthropogenic environmental changes, especially coastal eutrophication which in turn, may confer environmental resilience to the offspring through an increase of food supply. Further studies should therefore make efforts to incorporate a suite of multiple stressors and carefully consider their interactive effects when analyzing the adaptive responses of marine bivalves to OA.

5.6. Acknowledgments

Not displayed for reasons of data protection

5.7. References

Bach, L.T., 2015. Reconsidering the role of carbonate ion concentration in calcification by marine organisms. Biogeosciences 12, 4939-4951.

Beniash, E., Ivanina, A., Lieb, N.S., Kurochkin, I., Sokolova, I.M., 2010. Elevated level of carbon dioxide affects metabolism and shell formation in oysters *Crassostrea virginica*. Mar. Ecol. Prog. Ser. 419, 95-108.

Booth, C.E., McDonald, D.G., Walsh, P.J., 1984. Acid-base balance in the sea mussel, *Mytilus edulis*. II: Effects of hypoxia and air-exposure on hemolymph acid-base status. Mar. Biol. Lett. 5, 359-369.

Burnett, L.E., 1988. Physiological responses to air exposure: acid-base balance and the role of branchial water stores. Am. Zool. 28, 125-135.

Caldeira, K., Wickett, M.E., 2003. Oceanography: anthropogenic carbon and ocean pH. Nature 425, 365-365.

Cole, V., Parker, L.M., O'Connor, S.J., O'Connor, W.A., Scanes, E., Byrne, M., Ross, P.M., 2016. Effects of multiple climate change stressors: ocean acidification interacts with warming, hyposalinity, and low food supply on the larvae of the brooding flat oyster *Ostrea angasi*. Mar. Biol. 163, 1-17.

Cyronak, T., Schulz, K.G., Jokiel, P.L., 2015. The omega myth: what really drives lower calcification rates in an acidifying ocean. ICES J. Mar. Sci. fsv075.

De Wit, P., Dupont, S., Thor, P., 2015. Selection on oxidative phosphorylation and ribosomal structure as a multigenerational response to ocean acidification in the common copepod *Pseudocalanus acuspes*. Evol. Appl. DOI: 10.1111/eva.12335

Djogić, R., Sipos, L., Branica, M., 1986. Characterization of uranium (VI) in seawater. Limnol. Oceanogr. 31, 1122-1131.

Doney, S.C., Fabry, V.J., Feely, R.A., Kleypas, J.A., 2009. Ocean acidification: the other CO_2 problem. Ann. Rev. Mar. Sci. 1, 169-192.

Duarte, C.M., Hendriks, I.E., Moore, T.S., Olsen, Y.S., Steckbauer, A., Ramajo, L., Carstensen, J., Trotter, J.A., McCulloch, M., 2013. Is ocean acidification an open-ocean syndrome? Understanding anthropogenic impacts on marine pH. Estuar. Coast. 36, 221-236.

FAO, The State of World Fisheries and Aquaculture, 2012. Food and Agriculture Organization of the United Nations, Rome, 2012.

Feely, R.A., Sabine, C.L., Hernandez-Ayon, J.M., Ianson, D., Hales, B., 2008. Evidence for upwelling of corrosive "acidified" water onto the continental shelf. Science 320, 1490-1492.

Fitzer, S.C., Caldwell, G.S., Close, A.J., Clare, A.S., Upstill-Goddard, R.C., Bently, M.G., 2012. Ocean acidification induces multi-generational decline in copepod naupliar production with possible conflict for reproductive resource allocation. J. Exp. Mar. Biol. Ecol. 418-419, 30-36.

Fitzer, S.C., Caldwell, G.S., Phoenix, V.R., Kamenos, N.A., 2014. Ocean acidification reduces the crystallographic control in juvenile mussel shells. J. Struct. Biol. 188, 39-45.

Frieder, C.A., Gonzalez, J.P., Levin, L.A., 2014. Uranium in larval shells as a barometer of molluscan ocean acidification exposure. Environ. Sci. Technol. 48, 6401-6408.

Gazeau, F., Parker, L.M., Comeau, S., Gattuso, J.P., O'Connor, W.A., Martin, S., Pörtner, H.O., Ross, P.M., 2013. Impacts of ocean acidification on marine shelled mollusks. Mar. Biol. 160, 2201-2245.

Gobler, C.J., Talmage, S.C., 2013. Short- and long-term consequences of larval stage exposure to constantly and ephemerally elevated carbon dioxide for marine bivalve populations. Biogeosciences 10, 2241-2253.

Goncalves, P., Anderson, K., Thompson, E.L., Melwani, A., Parker, L., Ross, P.M., Raftos, D.A., 2016. Rapid transcriptional acclimation following transgenerational exposure of oysters to ocean acidification. Mol. Ecol. DOI: 10.1111/mec.13808

Gosling, E., 2003. Bivalve growth. Bivalve molluscs: biology, ecology and culture. Fishing News Books, Blackwell, Oxford.

Heinemann, A., Fietzke, J., Melzner, F., Böhm, F., Thomsen, J., Garbe-Schönberg, D., Eisenhauer, A., 2012. Conditions of *Mytilus edulis* extracellular body fluids and shell composition in a pH-treatment experiment: acid-base status, trace elements and $\delta^{11}B$. Geochem. Geophys. Geosyst. 13. DOI: 10.1029/2011gc003790.

Hendriks, I.E., Duarte, C.M., Alvarez, M., 2010. Vulnerability of marine biodiversity to ocean acidification: a meta-analysis. Estuar. Coast. Shelf. Sci. 86, 157-164.

Hettinger, A., Sanford, E., Hill, T.M., Lenz, E.A., Russell, A.D., Gaylord, B., 2013. Larval carry-over effects from ocean acidification persist in the natural environment. Glob. Change. Biol. 19, 3317-3326.

Hettinger, A., Sanford, E., Hill, T.M., Russell, A.D., Sato, K.N.S., Hoey, J., Forsch, M., Page, H., Gaylord, B., 2012. Persistent carry-over effects of planktonic exposure to ocean acidification in the Olympia oyster. Ecology 93, 2758-2768.

Hüning, A.K., Melzner, F., Thomsen, J., Gutowska, M.A., Krämer, L., Frickenhaus, S., Rosenstiel, P., Pörtner, H.O., Philipp, E.E.R., Lucassen, M., 2013. Impacts of seawater acidification on mantle gene expression patterns of the Baltic Sea blue mussel: implications for shell formation and energy metabolism. Mar. Biol. 160, 1845-1861.

IPCC, 2013. Summary for Policymakers. In: Stocker, T.F., Qin, D., Plattner, G.-K., Tignor, M., Allen, S.K., Boschung, J., Nauels, A., Xia, Y., Bex, V., Midgley, P.M. (Eds.), Climate change 2013: The physical Science Basis. Contribution of Working Group I to the Fifth Assessment Report of the Intergovernmental Panel on Climate Change. Cambridge University Press, Cambridge, United Kingdom and New York, NY, USA, pp. 1-30.

Jochum, K.P., Nohl, U., Herwig, K., Lammel, E., Stoll, B., Hofmann, A.W., 2005. GeoReM: a new geochemical database for reference materials and isotopic standards. Geostand. Geoanal. Res. 29, 87-133.

Jochum, K.P., Weis, U., Stoll, B., Kurmin, D., Yang, Q., Raczek, I., Jacob, D.E., Stracke, A., Birbaum, K., Frick, D.A., Günther, D., Enzweiler, J., 2011. Determination of reference values for NIST SRM 610-617 glasses following ISO guidelines. Geostand. Geoanal. Res. 35, 397-429.

Jochum, K.P., Scholz, D., Stoll, B., Weis, U., Wilson, S.A., Yang, Q., Schwalb, A., Börner, N., Jacob, D.E., Andreae, M.O., 2012. Accurate trace element analysis of speleothems and biogenic calcium carbonates by LA-ICP-MS. Chem. Geol. 318-319, 31-44.

Klochko, K., Kaufman, A.J., Yao, W., Byrne, R.H., Tossell, J.A., 2006. Experimental measurement of boron isotope fractionation in seawater. Earth. Planet. Sci. Lett. 248, 276-285.

Kroeker, K.J., Kordas, R.L., Crim, R.N., Hendriks, I.E., Ramajo, L., Singh, G.S., Duarte, C.M., 2013. Impacts of ocean acidification on marine organisms: quantifying sensitivities and interactions with warming. Glob. Change. Biol. 19, 1884-1896.

Kroeker, K.J., Sanford, E., Jellison, B.M., Gaylord, B., 2014. Predicting the effects of ocean acidification on predator-prey interactions: a conceptual framework based on coastal molluscs. Biol. Bull. 226, 211-222.

Kroeker, K.J., Sanford, E., Rose, J.M., Blanchette, C.A., Chan, F., Chavez, F.P., Gaylord, B., Helmuth, B., Hill, T.M., Hofmann, G.E., McManus, M.A., Menge, B.A., Nielsen, K.J., Raimondi, P.T., Russell, A.D., Washburn, L., 2016. Interacting environmental mosaics drive geographic variation in mussel performance and predation vulnerability. Ecol. Lett. DOI: 10.1111/ele.12613.

Kurihara, H., 2008. Effects of CO_2-driven ocean acidification on the early developmental stages of invertebrates. Mar. Ecol. Prog. Ser. 373, 275-284.

Li, S., Liu, C., Huang, J., Liu, Y., Zhang, S., Zheng, G., Xie, L., Zhang, R., 2016. Transcriptome and biomineralization responses of the pearl oyster *Pinctada fucata* to elevated $_{p}CO_2$ and temperature. Sci. Rep. 6, 18493.

Lohbeck, K.T., Riebesell, U., Reusch, T.B.H., 2012. Adaptive evolution of a key phytoplankton species to ocean acidification. Nat. Geosci. 5, 917.

Marin, F., Le Roy, N., Marie, B., 2012. The formation and mineralization of mollusk shell. Front. Biosci. S4, 1099-1125.

Marin, F., Luquet, G., Marie, B, Medakovic, D., 2008. Molluscan shell proteins: primary strcuture, origin and evolution. Curr. Top. Dev. Biol. 80, 209-276.

Marshall, D.J., 2008. Transgenerational plasticity in the sea: context-dependent maternal effects across the life history. Ecology 89, 418-427.

Marshall, D.J., Morgan, 2011. Ecological and evolutionary consequences of linked life-history stages in the sea. Curr. Biol. 21, 718-725.

McCulloch, M., Trotter, J. Montagna, P., Falter, J., Dunbar, R., Freiwald, A., Försterra, G., López Correa, M., Maier, C., Rüggeberg, A., Taviani, M., 2012. Resilience of cod-water scleractinian corals to ocean acidification: Boron isotopic systematics of pH and saturation sate up-regulation. Geochim. Cosmochim. Ac. 87, 21-34.

Melzner, F., Gutowska, M.A., Langenbuch, M., Dupont, S., Lucassen, M., Thorndyke, M. C., Bleich, M., Pörtner, H.O., 2009. Physiological basis for high CO_2 tolerance in marine ectothermic animals: pre-adaptation through lifestyle and ontogeny?. Biogeosciences 6, 2313-2331.

Milano, S., Schöne, B.R., Wang, S., Müller, W.E., 2016. Impact of high pCO_2 on shell structure of the bivalve *Cerastoderma edule*. Mar. Environ. Res. 119, 144-155.

Mucci, A., 1983. The solubility of calcite and aragonite in seawater at various salinities, temperatures, and one atmosphere total pressure. Am. J. Sci. 283, 780-799.

Orr, J.C., Fabry, V.J., Aumont, O., Bopp, L., Doney, S.C., Feely, R.A., Gnanadesikan, A., Gruber, N., Ishida, A., Joos, F., 2005. Anthropogenic ocean acidification over the twenty-first century and its impact on calcifying organisms. Nature 437, 681-686.

Palmer, A.R., 1992. Calcification in marine molluscs: how costly is it?. Proc. Natl. Acad. Sci. USA. 89, 1379-1382.

Parker, L.M., O'Connor, W.A., Raftos, D.A., Pörtner, H.O., Ross, P.M., 2015. Persistence of positive carryover effects in oysters following transgenerational exposure to ocean acidification. PLoS. One. 10, e0132276.

Parker, L.M., Ross, P.M., O'Connor, W.A., 2009. The effect of ocean acidification and temperature on the fertilization and embryonic development of the Sydney rock oyster *Saccostrea glomerata* (Gould 1850). Glob. Change. Biol. 15, 2123-2136.

Parker, L.M., Ross, P.M., O'Connor, W.A., Borysko, L., Raftos, D.A., Pörtner, H.O., 2012. Adult exposure influences offspring response to ocean acidification in oysters. Glob. Change. Biol. 18, 82-92.

Pierrot, D.E., Lewis, E., Wallace, D.W.R., 2006. MS Excel program developed for CO_2 system calculations, ORNL/CDIAC-105a, carbon dioxide information analysis center. Oak Ridge National Laboratory, U.S. Department of Energy, Oak Ridge, Tennessee.

Pörtner, H.O., Langenbuch, M., Reipschläger, A., 2004. Biological impact of elevated ocean CO_2 concentrations: lessons from animal physiology and earth history. J. Oceanogr. 60, 705-718.

Ramajo, L., Pérez-León, E., Hendriks, I.E., Marbà, N., Krause-Jensen, D., Sejr, M.K., Blicher, M.E., Lagos, N.A., Olsen, Y.S., Duarte, C.M., 2016. Food supply confers calcifiers resistance to ocean acidification. Sci. Rep. 6, 19374.

Ross, P.M., Parker, L., Byrne, M., 2016. Transgenerational responses of molluscs and echinoderms to changing ocean conditions. ICES J. Mar. Sci. fsv254.

Stemmer, K., 2013. Shell formation and microstructure of the ocean quahog Arctica islandica: Does ocean acidification?. Doctoral dissertation, Staats-und Universitaetsbibliothek Bremen.

Stumpp, M., Hu, M.Y., Casties, I., Saborowski, R., Bleich, M., Melzner, F., Dupont, S., 2013. Digestion in sea urchin larvae impaired under ocean acidification. Nat. Clim. Chang. 3, 1044-1049.

Thomsen, J., Casties, I., Pansch, C., Körtzinger, A., Melzner, F., 2013. Food availability outweighs ocean acidification effects in juvenile *Mytilus edulis*: laboratory and field experiments. Glob. Change. Biol. 19, 1017-1027.

Thomsen, J., Gutowska, M. A., Saphörster, J., Heinemann, A., Trübenbach, K., Fietzke, J., Hiebenthal, C., Eisenhauer, A., Körtzinger, A., Wahl, M., Melzner, F., 2010. Calcifying invertebrates succeed in a naturally CO_2-rich coastal habitat but are threatened by high levels of future acidification. Biogeosciences 7, 3879-3891.

Thor, P., Dupont, S., 2015. Transgenerational effects alleviate severe fecundity loss during ocean acidification in a ubiquitous planktonic copepod. Glob. Change. Biol. 21, 2261-2271.

Tunnicliffe, V., Davies, K.T.A., Butterfield, D.A., Embley, R.W., Rose, J.M., Chadwick Jr, W.W., 2009. Survival of mussels in extremely acidic waters on a submarine volcano. Nat. Geosci. 2, 344-348.

Waite, J.H., 1983. Quinone-tanned scleroproteins. In: Hochachka, P.W. (Ed) The Mollusca, metabolic biochemistry and molecular biomechanics, vol 1. Academic Press, New York, p 467-504.

Waldbusser, G.G., Brunner, E.L., Haley, B.A., Hales, B., Langdon, C.J., Prahl, F.G., 2013. A developmental and energetic basis linking larval oyster shell formation to acidification sensitivity. Geophys. Res. Lett. 40, 2171-2176.

Waldbusser, G.G., Gray, M.W., Hales, B., Langdon, C.J., Haley, B.A., Gimenez, I., Smith, S.R., Brunner, E.L., Hutchinson, G., 2016. Slow shell building, a possible trait for resistance to the effects of acute ocean acidification. Limnol. Oceanogr. DOI: 10.1002/lno.10348

Waldbusser, G.G., Hales, B., Langdon, C.J., Haley, B.A., Schrader, P., Brunner, E.L., Gray, M.W., Miller, C.A., Gimenez, I., 2014. Saturation-state sensitivity of marine bivalve larvae to ocean acidification. Nat. Clim. Change. 5, 273-280.

Wheeler, A.P., 1992. Mechanisms of molluscan shell formation. In: Bonucci, E. (Ed.), Calcification in biological systems. CRC press, Boca Raton, FL, p179-216.

Xu, X., Yang, F., Zhao, L., Yan, X., 2016. Seawater acidification affects the physiological energetics and spawning capacity of the Manila clam *Ruditapes philippinarum* during gonadal maturation. Comp. Biochem. Phys. 196A, 20-29.

Youngson, N.A., Whitelaw, E., 2008. Transgenerational epigenetic effects. Annu. Rev. Genomics. Hum. Genet. 9, 233-257.

Zhao, L., Schöne, B.R., Mertz-Kraus, R., Yang, F., 2017. Insights from sodium into the impacts of elevated pCO_2 and temperature on bivalve shell formation. J. Exp. Mar. Biol. Ecol. 486, 148–154.

Zhao, L., Yan, X., Huo, Z., Yang, F., 2012. Divergent selection for shell growth in the Manila clam, *Ruditapes philippinarum*. J. World. Aquacult. Soc. 43, 878-884.

Chapter 6

*Unionid shells (*Hyriopsis cumingii*) record manganese cycling at the sediment-water interface in a shallow eutrophic lake in China (Lake Taihu)*

In review at Palaeogeography, Palaeoclimatology, Palaeoecology

Liqiang Zhao[1], Eric O. Walliser[1], Regina Mertz-Kraus[1], Bernd R. Schöne[1]

[1] Institute of Geosciences, University of Mainz, Joh.-J.-Becher-Weg 21, 55128 Mainz, Germany

Author contribution

Concept: LZ, BRS

Execution: LZ, EOW

Data collection and analysis: LZ, EOW, RMK

Writing: LZ, BRS, EOW, RMK

Abstract

Aquatic eutrophication is becoming a serious environmental problem throughout the world. The utility of bivalves as bio-filters to improve water quality and reduce algal blooms has been widely acknowledged, but the potential usefulness of bivalve shells as retrospective monitors of eutrophication-induced environmental change has received little attention. Here, we present the first multi-year, high-resolution Mn/Ca_{shell} records of the freshwater mussel, *Hyriopsis cumingii* (Lea 1852) from a shallow eutrophic lake (Lake Taihu, China). Mn/Ca_{shell} time-series of the two studied shells exhibited a remarkable degree of synchrony after being placed in a precise temporal context by means of growth pattern analysis. There is a large inter-annual variability of Mn/Ca_{shell} records during 2011–2015, with higher values occurring during the first three years. Mn/Ca_{shell} also displayed a pronounced intra-annual variability with maxima consistently occurring during the summer. The high reproducibility of Mn/Ca_{shell} time-series among contemporaneous specimens highlighted the existence of strong environmental rather than biological control on the incorporation of Mn into the shells. In particular, the striking feature of summertime Mn/Ca_{shell} maxima occurred synchronously when reducing conditions prevailed beneath the sediment-water interface (SWI). The latter resulted in substantial increases of biologically available Mn^{2+} in the sediment pore water and organic particles which were rapidly taken up by the mussels and subsequently incorporated into their shells. Therefore, Mn/Ca_{shell} can potentially serve as a high-resolution proxy of the mobility of Mn at the SWI. As demonstrated by the present study, unravelling geochemical properties of bivalve shells can help to retrospectively monitor eutrophication-induced environmental change in aquatic ecosystems.

6.1. Introduction

Manganese is a naturally abundant and widely distributed metal in aquatic sediments where it is present primarily as insoluble MnO_2 (Pedersen and Price, 1982). However, MnO_2 is highly susceptible to the redox state of the sediment and is readily reduced to soluble Mn^{2+} ion when reducing conditions prevail (Pedersen and Price, 1982). Since Mn^{2+} is less readily oxidized back to MnO_2 and has a high affinity to organic matter (Wilson, 1980), extremely high levels of Mn^{2+} are often found in the sediment pore water and organic material (e.g., Aguilar and Nealson, 1998; Gao et al., 2006; Tao et al., 2012; Giles et al., 2016). Dissolved Mn^{2+} can also easily diffuse across the sediment-water interface (SWI) into the overlying water, where it can remain in the dissolved form for periods of days (Tebo, 1991; Pakhomova et al., 2007) and/or be removed from the water column by abiogenic and microbial oxidation (Richardson et al., 1988; Aguilar and Nealson, 1998) and by bacteria and phytoplankton (Sunda and Huntsman, 1985; Schoemann et al., 1988). A substantial release of Mn^{2+} from sediment redox processes would thus exert a dominant influence on the partitioning of Mn between dissolved and particulate phases in the overlying water column. Furthermore, the reductive dissolution of MnO_2 can greatly promote the release of elemental nutrients (N and P) and trace metals (Co, Zn, Cd, Ba, Pb, etc.) from the sediment which are preferentially associated with MnO_2 (Balistrieri and Murray, 1986; Pearce et al., 2013; Giles et al., 2016). Therefore, continuous monitoring of the release of Mn^{2+} at the SWI would provide valuable information regarding the geochemical behavior of Mn and many other elements in aquatic environments as well as eutrophication caused by the surplus of nitrogen and phosphorous.

Several studies have demonstrated the feasibility of using bivalve shells to investigate temporal changes of biologically available manganese from dissolved and/or particulate sources (e.g., Nyström et al., 1996; Vander Putten et al., 2000; Markich et al., 2002; Lazareth et al., 2003; Freitas et al., 2006; Langlet et al., 2007; Barats et al., 2008; Soldati et al., 2009). Since the uptake and incorporation of Mn from the ambient environment into the shell occurs with a very short time lag (less than 24 hours; Langlet et al., 2006), Mn/Ca_{shell} holds great potential to serve as a proxy of ambient Mn^{2+} changes. Much effort has also been devoted toward a better understanding of the processes and mechanisms by which Mn^{2+} is taken up by the bivalves and subsequently incorporated into their shells. Because of similar electrochemical properties and ionic radii, Mn^{2+} may share the same transport systems with Ca^{2+} during the transport from the ambient environment to the calcifying front (Zhao et al., in review), where it primarily substitutes for Ca^{2+} in the crystal lattice during the precipitation and crystallization

of calcium carbonate (Soldati et al., 2016). More importantly, shells can potentially accommodate many orders of magnitude more Mn^{2+} ions than abiogenic carbonate through the atomic modification of the crystal lattice (Soldati et al., 2016). As such, shells can monitor occasionally striking increases of environmental Mn^{2+} concentrations. For example, it has been reported that Mn/Ca_{shell} of the freshwater bivalve, *Elliptio complanata*, can be up to 31-fold higher than that of the ambient water (Carroll and Romanek, 2008).

Eutrophication of aquatic ecosystems is becoming a serious environmental problem. There is widespread concern that eutrophication can have detrimental consequences for aquatic ecosystems such as promoting harmful algal blooms and producing secondary metabolites especially toxins, disrupting food webs and resulting in hypoxia and – in extreme cases – dead zones (Smith, 2003). The possibility of using bivalves to reduce aquatic eutrophication has been acknowledged for decades (e.g., Gifford et al., 2007; Li et al., 2010; Rose et al., 2014; Ismail et al., 2015). As of now, however, very little attention has been paid to the usefulness of geochemical properties of bivalve shells as sensitive, high-resolution recorders of physicochemical changes in eutrophic waters. As demonstrated in Fig. 6.1, freshwater unionid mussels inhabiting eutrophic rivers and lakes show much higher background levels and larger changes of Mn/Ca_{shell} than those living in oligotrophic and mesotrophic waters. Hence, Mn/Ca_{shell} records can be used to retrospectively characterize the trophic state of aquatic ecosystems.

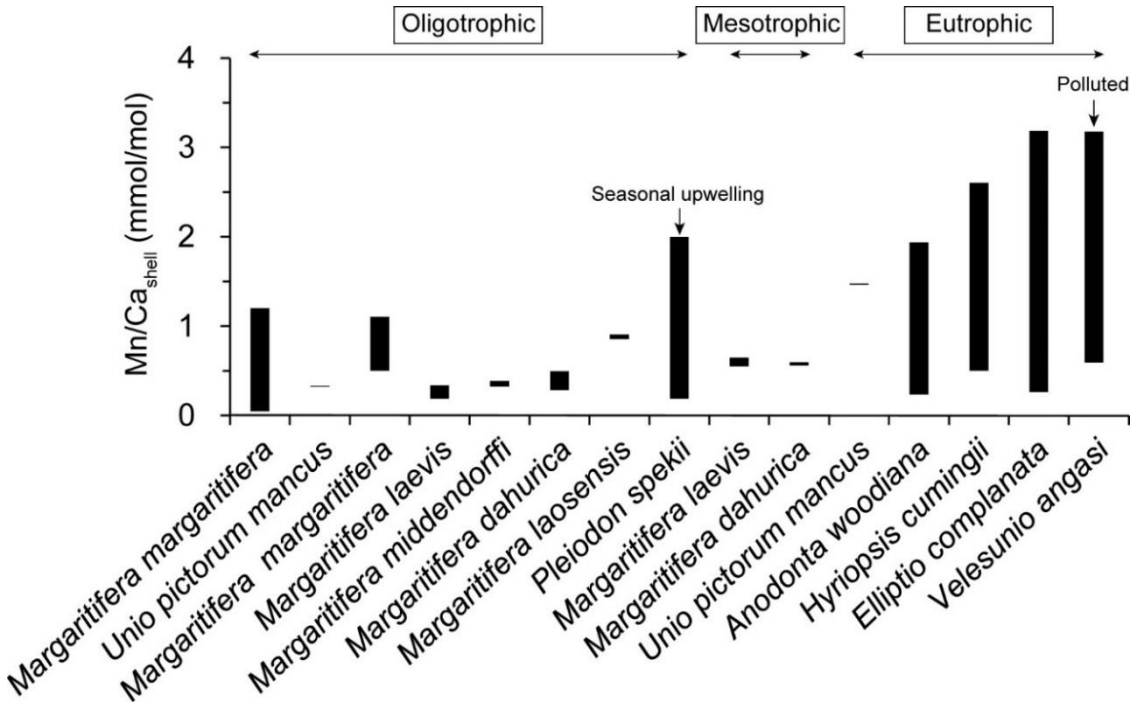

Fig. 6.1. Comparison of manganese-to-calcium ratios in shells of freshwater unionid mussels which inhabited oligotrophic, mesotrophic and eutrophic waters. Detailed information is provided in supplementary Table 6.1s.

Here, we present the first multi-year, high-resolution Mn/Ca_{shell} record in a shallow eutrophic lake based on two specimens of the freshwater unionid, *Hyriopsis cumingii*. Contrary to previous studies which almost exclusively measured the Mn contents in discrete portions by means of laser ablation–inductively coupled plasma–mass spectrometry (LA-ICP-MS), we performed line scan analysis which can provide extremely high-resolution and uninterrupted element time-series. Mn/Ca_{shell} data can be placed in a precise temporal context by means of growth pattern analysis, thereby enabling us to investigate how Mn/Ca_{shell} varied among contemporaneous specimens and fluctuated through time (on seasonal and annual time scales) and evaluate whether it provides reliable records of environmental information (especially on the mobility of biologically available Mn^{2+} at the SWI). Most importantly, we demonstrated that Mn/Ca_{shell} holds great promise for retrospective tracking of eutrophication-induced redox change, hypoxia and internal loads of nitrogen and phosphorous from the sediment to the overlying water body.

6.2. Materials and methods

6.2.1. Study site

Lake Taihu (30°55'–31°32' N, 119°52'–120°36' E; Fig. 6.2), the third largest freshwater lake in China, is a shallow eutrophic lake with a total water surface area of 2338 km^2 and an average depth of 1.9 m (Qin et al., 2007). It is an important drinking water resource for circa eight million local residents. Due to constantly increasing eutrophication, harmful cyanobacterial blooms have occurred with increasing intensity, duration and frequency since the mid-1980s, especially in the northern region of the lake (e.g., Meiliang Bay and Gonghu Bay) where frequent toxin-producing *Microcystis* blooms have been observed from late spring to early autumn (Xu et al., 2016). In late May 2007, a massive *Microcystis* bloom occurred in Gonghu Bay, leading to a serious drinking water crisis in Wuxi City and leaving circa two million inhabitants without drinking water for at least one week (Qin et al., 2010). Since then, much effort has been devoted toward monitoring the occurrence of harmful cyanobacterial blooms and elucidating the underlying mechanisms, and ample data regarding the meteorology, hydrology and hydrochemistry of the lake have been collected.

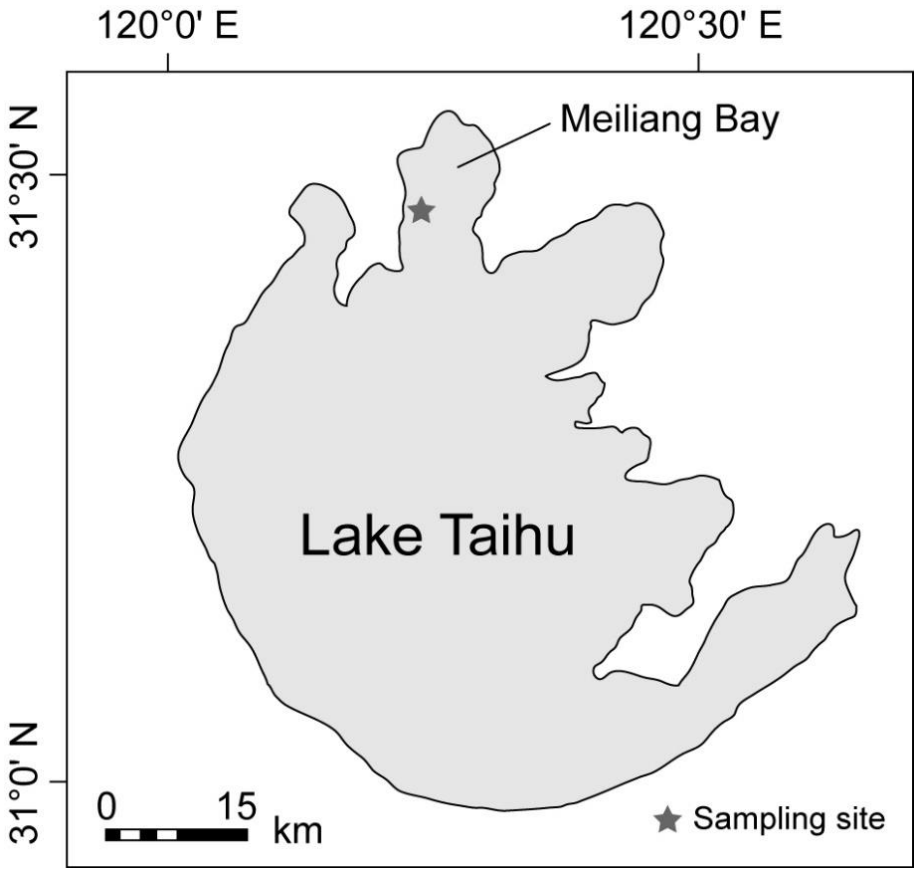

Fig. 6.2. Map of the Lake Taihu showing the sampling site in Meiling Bay

6.2.2. Study species

The freshwater pearl mussel, *Hyriopsis cumingii* (Triangle sail mussel, Bivalvia, Unionoida, Unionidae), is one of the economically most important bivalve species for the production of freshwater pearls in China (FAO, 2012). It is widely distributed in large rivers, lakes and reservoirs and considered as a dominant filter-feeder in aquatic ecosystems. Thus, aside from its commercial significance, *H. cumingii* can potentially perform an important restorative function in improving water quality and reducing aquatic eutrophication (He et al., 2014).

Shells of *H. cumingii* consist of two equally-sized and triangular shaped valves (Fig. 6.3A). The outer shell surface is covered by the periostracum which provides protection against shell dissolution. The aragonitc shell (confirmed by X-ray diffraction; Yoshimura et al., 2010) is subdivided into an outer prismatic shell layer (OSL) and an inner nacreous shell layer (ISL) (Fig. 6.3B-C). *H. cumingii* builds its shell on a periodic basis, forming distinct growth lines and increment widths in the OSL (Fig. 6.3C) and clearly visible alternating white and dark bands in the ISL (Fig. 6.3B). With these growth patterns each shell portion can be placed into a precise temporal context, thereby allowing to determine the rate of shell growth.

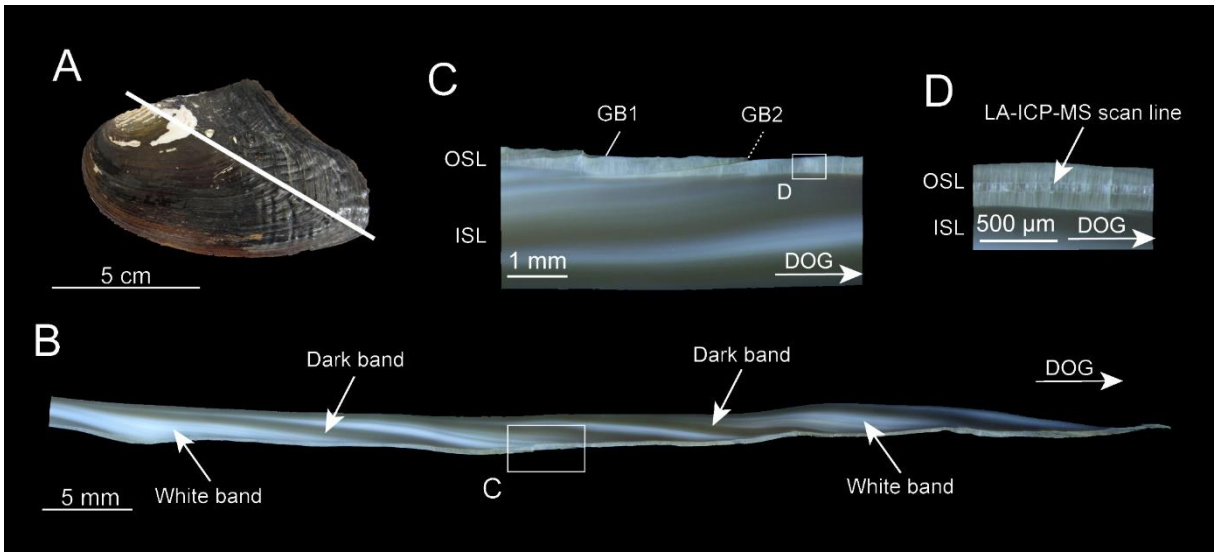

Fig. 6.3. Shell of *Hyriopsis cumingii*. (A) Outer shell surface of the left valve. Along the axis of maximum growth (white line) a three-millimeter-thick shell section was cut from the shell. (B) Cross-section of the shell showing an alternating pattern of light and dark bands. DOG = direction of growth. (C) Magnification of the cross-section of the shells revealing a thin outer shell layer (OSL) and a thick inner shell layer (ISL). One thick growth band (GB1: solid line) and one thin growth band (GB2: dash line) are distinctly developed in the OSL. (D) Magnification of the OSL indicating the LA-ICP-MS scan line.

6.2.3. Shell collection and preparation

On 18 September 2015, two specimens of *Hyriopsis cumingii*, T1 and T2, were collected by diving in the western littoral zone of Meiliang Bay, Taihu (Fig. 6.2). Soft tissues were removed immediately after collection, shells carefully cleaned with water and then air-dried in the field. Upon arrival in the laboratory, the left valve of each specimen was carefully glued to a Plexiglas cube with a quick-drying plastic welder. To protect shell material during sawing, a thin layer of JB KWIK fast-drying metal epoxy resin was applied to the shell surface along the axis of maximum growth (Fig. 6.3A). A three-millimeter-thick section along that axis was then cut from each specimen using a Buehler Isomet 1000 low-speed precision saw (Fig. 6.3B). Afterward, shell sections were mounted on glass slides, ground on glass plates with 800 and 1200 grit SiC and polished with 0.3 µm Al_2O_3 powder. Polished sections were ultrasonically rinsed within de-ionized water to remove adhering particles.

6.2.4. Growth pattern analysis

Polished shell sections were viewed under a Wild Heerbrugg M8 stereomicroscope equipped with a Schott VisiLED MC 1000 sectoral dark field illumination. Photographs were digitalized

with a Canon EOS 550D digital camera attached to the microscope. Microscopic observations clearly showed an alternating pattern of light and dark bands in the ISL (Fig. 6.3B) and one thick (GB1) and one thin (GB2) growth band in the OSL (Fig. 6.3C). To identify the ontogenetic age of each specimen, the number of alternating light and dark bands in both shell layers were counted. The distance between consecutive growth bands (e.g., GB1 to the following GB2 or GB2 to the following GB1) was measured using the free image processing software ImageJ (http://rsbweb.nih.gov/ij).

6.2.5. LA-ICP-MS analysis

Manganese (measured as ^{55}Mn) concentrations of each polished shell section were determined by means of laser ablation–inductively coupled plasma–mass spectrometry (LA-ICP-MS) in line scan mode at the Institute of Geosciences, University of Mainz. For each specimen, the LA line scan was conducted in the middle of the OSL (Fig. 6.3D) and measured ca. 63 mm in length. The OSL was analyzed because growth patterns – required to temporally contextualize chemical data – were more distinctly developed in this shell layer than in the ISL.

Analyses were performed using an ESI NWR 193 ArF excimer laser ablation system equipped with a two-volume cell (TwoVol2). The laser system was coupled to an Agilent 7500ce quadrupole ICP-MS, and manipulated at an energy density of ~3.2 J/cm^2 and a pulse repetition rate of 10 Hz. LA line scans were conducted immediately after pre-ablation on the sample surface with a rectangular beam spot of 40 × 60 µm. The scan speed was kept constant at 5 µm/s during ablating. Backgrounds were measured for 20 s prior to each scan. NIST SRM 612 (synthetic glass) was measured as calibration material, applying the preferred values reported in the GeoReM database (http://georem.mpch-mainz.gwdg.de/, Application Version 18) (Jochum et al., 2005, 2011) as the "true" concentrations to calculate the element concentrations in the samples. NIST SRM 610 (synthetic glass; n = 9), USGS BCR-2G (basaltic glass; n = 9) and MACS-3 (synthetic calcium carbonate; n = 9) were analyzed as quality control materials (QCM) to monitor accuracy and reproducibility of the measurements. ^{43}Ca was used as an internal standard for all materials. The Ca concentrations reported in the GeoReM database were applied for the reference materials, and a Ca concentration of 380,000 µg/g (measured by inductively coupled plasma–optical emission spectrometer) for the samples. For data reduction and analysis, a Microsoft Excel spreadsheet was used according to established methods (Longerich et al., 1996; Jochum et al., 2007, 2011). The average limit of the detection was 0.3 µg/g for Mn. All data points of the shells were well above the detection limit. The

measured Mn concentrations of the QCM agreed within 4 % with the preferred values of the GeoReM database (NIST SRM 610, USGS BCR-2G) and published values (USGS MACS-3, Jochum et al., 2012) and the relative standard deviations (1 RSD) were < 3.5 %.

6.2.6. CF-IRMS analysis

To constrain the duration of the main growing season of *H. cumingii*, the polished shell section from specimen T1 was used for oxygen isotope analysis ($\delta^{18}O_{shell}$). The thick ISL rather than thin OSL was analyzed in order to obtain sufficient calcium carbonate (40–120 µg). Sixty powder samples were obtained with a Rexim Minimo dental drill mounted to a stereomicroscope and equipped with a conical bit (300 µm diameter; Komet/Gebr. Brasseler GmbH & Co. KG, model no. H52 104 003). Powder samples were dissolved with concentrated phosphoric acid in helium-flushed borosilicate exetainers at 72 °C for 2 h, and afterward, the liberated CO_2 gas was measured with a Thermo Finnigan MAT 253 continuous flow-isotope ratio mass spectrometer (CF-IRMS) coupled to a GasBench II at the Institute of Geosciences, University of Mainz. Isotope data were calibrated against a NBS-19 calibrated IVA Carrara marble ($\delta^{18}O$ = – 1.91 ‰). On average, the internal precision and accuracy were better than 0.05 %. Values of $\delta^{18}O_{shell}$ were calculated against the Vienna Pee Dee Belemnite (VPDB) carbonate standard and expressed in δ-notation as the deviation from the standard in parts per thousand (‰). Note that $\delta^{18}O_{shell}$ data were not corrected for different acid fractionation factors of aragonite (shell) and calcite (NBS-19, Carrara marble). For a detailed explanation, see Füllenbach et al. (2015).

6.3. Results

6.3.1. Ontogenetic age and growing season of H. cumingii

In polished cross-sections of both *H. cumingii* specimens, an alternating pattern of light and dark bands was clearly visible in the ISL (Fig. 6.3B) which corresponded to one thick (GB1) and one thin (GB2) growth band in the OSL (Fig. 6.3C). Given that bivalves were collected alive at the beginning of fall (18 September 2015) and each specimen showed a dark band near the ventral margin (i.e., the most recently formed shell portion) as well as a summer growth band (i.e., GB2) just before that dark band, the formation of GB2 most likely resulted from a significant slowdown of shell growth during summer spawning, whereas GB1 likely represents

a winter growth cessation. Based on the number of alternating light and dark bands, specimens T1 and T2 were identified to be nine and six years-old, respectively.

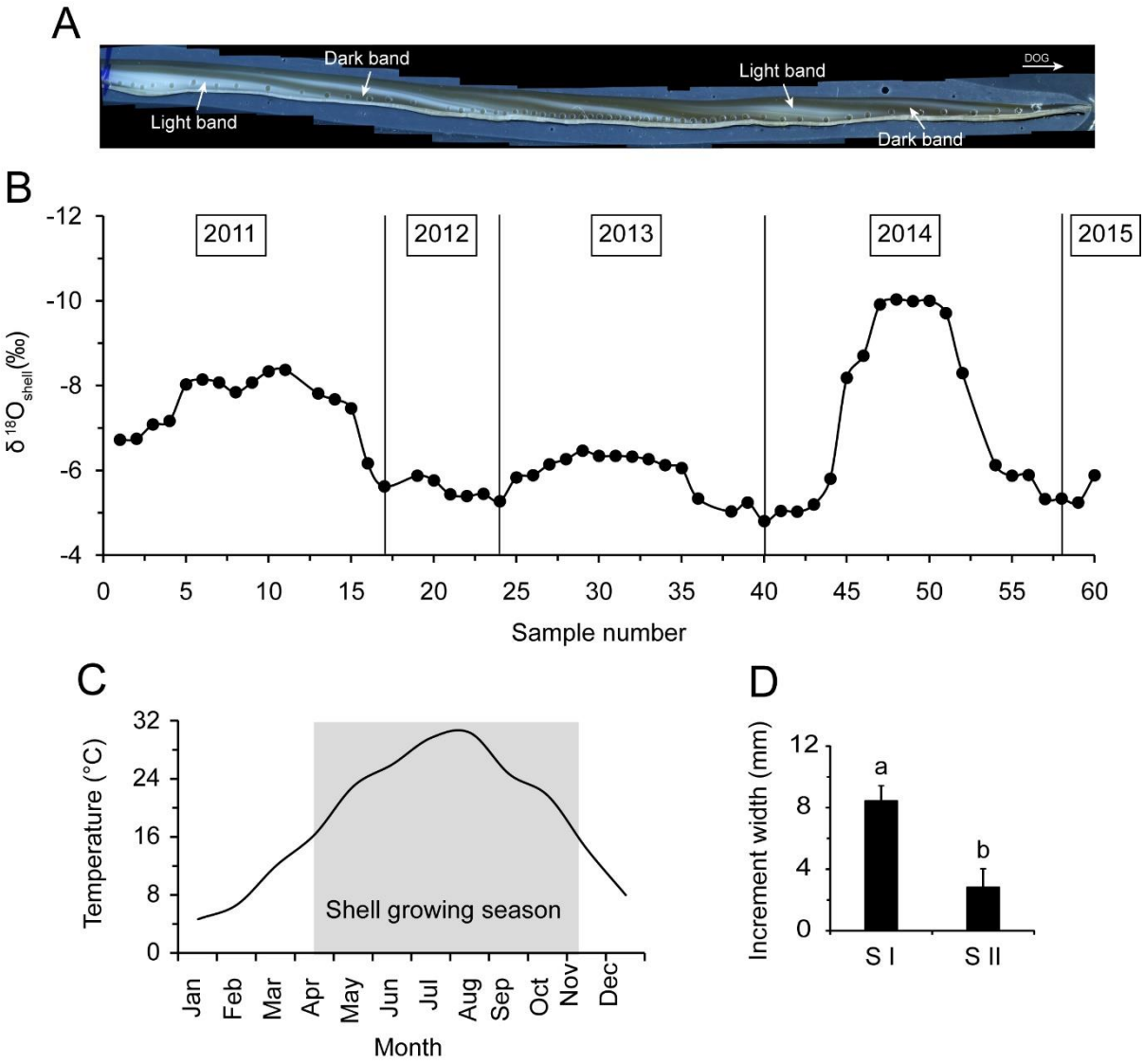

Fig. 6.4. Shell growth pattern of *Hyriopsis cumingii*. (A) Cross-section of the shell of specimen T1 with drill holes for oxygen isotope analysis ($\delta^{18}O_{shell}$). DOG = direction of growth. (B) $\delta^{18}O_{shell}$ values of specimen T1. Solid vertical lines indicate the position of annual growth lines. (C) Monthly variations of water temperature in Lake Taihu. Data were obtained from obtained from the Taihu Basin Water Resources Monitoring and Protection Bureau (www.tba.gov.cn). Grey shading indicates the duration of the main growth season of *H. cumingii*. (D) Comparison of the seasonal growth increment widths between the first growing season (from April to August) and the second growing season (from September to November). The columns denoted "a" and "b" are significantly different ($p < 0.05$). S I = first part (April to August) of the growing season; S II = second part (September to November) of the growing season.

The $\delta^{18}O_{shell}$ time-series of specimen T1 was used to verify aforementioned interpretations. During 2011–2015, annual $\delta^{18}O_{shell}$ minima occurred consistently in light bands and maxima in dark bands (Fig. 6.4A+B). Since $\delta^{18}O_{shell}$ is strongly inversely correlated to water temperature (Grossman and Ku, 1986), light and dark bands were formed in the warm and cold season, respectively. The precise timing of shell growth can be further constrained with $\delta^{18}O_{shell}$ data because they can provide reliable temperature data if $\delta^{18}O_{water}$ is known. Seasonal $\delta^{18}O_{shell}$ maxima were very similar to each other, indicating that the growing season started nearly contemporaneously in both specimens. Xu et al. (2016) investigated the daily variation of $\delta^{18}O_{water}$ in adjacent waters of the lake between 11 May 2012 and 31 December 2014 and observed that $\delta^{18}O_{water}$ varied greatly from -8.6 ‰ to -2.6 ‰ with a striking increase between late spring and fall. However, $\delta^{18}O_{water}$ exhibited only small variations during the colder months (December to April) with an average of -5.8 ‰. By employing the temperature equation of Grossman and Ku (1986) (equation 1) with a scale correction of -0.27 ‰ (Dettman et al., 1999), and taking into account the winter $\delta^{18}O_{shell}$ and $\delta^{18}O_{water}$ values of -5.1 ‰ and -5.8 ‰, respectively, the temperature at the onset of the growing season equaled 16.3 °C.

$$(1) \qquad T_{\delta^{18}O}(℃) = 20.40 - 4.34 \cdot (\delta^{18}O_{shell} - (\delta^{18}O_{shell} - (\delta^{18}O_{water} - 0.27)))$$

Accordingly, shell growth occurred largely between middle April and early November (Fig. 6.4C). It is also possible to constrain the timing of shell growth following summer spawning according to water temperature reconstructed from $\delta^{18}O_{shell}$. In 2014, for example, the average summer $\delta^{18}O_{water}$ value was -4.4 ‰ (Xu et al., 2016) and the $\delta^{18}O_{shell}$ measured at the beginning of the dark band was -6.1 ‰ (Fig. 6.4B). These values translate into a water temperature of 26.8 °C, corresponding to instrumental data that prevailed in early September 2014 (Fig. 6.4C). In summary, *H. cumingii* did not grow continuously over an eight-month growing season (April through November), but growth was reduced during summer spawning. The first growing season (S I) covers the time interval from April to August and the second growing season (S II) from September to November. Irrespective of the ontogenetic age, the average increment width during S I was significantly larger than during S II (Student's *t* test, $p < 0.05$; Fig. 6.4D).

6.3.2. Mn/Cashell time-series

Mn/Ca_{shell} time-series of the studied specimens were temporally contextualized using shell growth patterns as described further above (Fig. 6.5). Average Mn/Ca_{shell} of specimens T1 and T2 were 1.38 ± 0.43 mmol/mol and 1.13 ± 0.38 mmol/mol, respectively. However, minima and

maxima closely matched each other, i.e., 0.5 and 2.4 mmol/mol in T1 and 0.6 and 2.3 mmol/mol in T2 (Table 1), respectively. Mn/Ca_{shell} of the last three years of growth of specimens T1 and T2 compared well to each other (Fig. 6.5). Mn/Ca_{shell} time-series exhibited a high degree of similarity between the two specimens. For example, in 2013, shell showed similar, though not exactly the same, Mn/Ca_{shell} trajectories, with nearly identical Mn/Ca_{shell} maxima recorded at the beginning of SI and smaller peaks in the middle of S II. In 2014, Mn/Ca_{shell} curves of the two specimens were poorly synchronized during S I, but highly synchronized during S II (Fig. 6.5). In specimen T1, Mn/Ca_{shell} increased sharply at the beginning of S I and then decreased gradually through the remainder of the growing season (Fig. 6.5A). In specimen T2, however, Mn/Ca_{shell} time-series fluctuated strongly and displayed several intermittent peaks during S I (Fig. 6.5B). Evidently, specimens exhibited a remarkable degree of synchrony in Mn/Ca_{shell} records in 2015, with almost identical seasonal averages, minima and maxima (Table 6.1).

Mn/Ca_{shell} of specimen T1 showed very similar trajectories in 2011 and 2012 (Fig. 6.5A). Double peaks were present throughout the growing season. Mn/Ca_{shell} increased persistently and then decreased abruptly at the end of S I, whereas opposing directions occurred in S II, i.e., sharply elevated Mn/Ca_{shell} occurred at the beginning of the subsequent growing season.

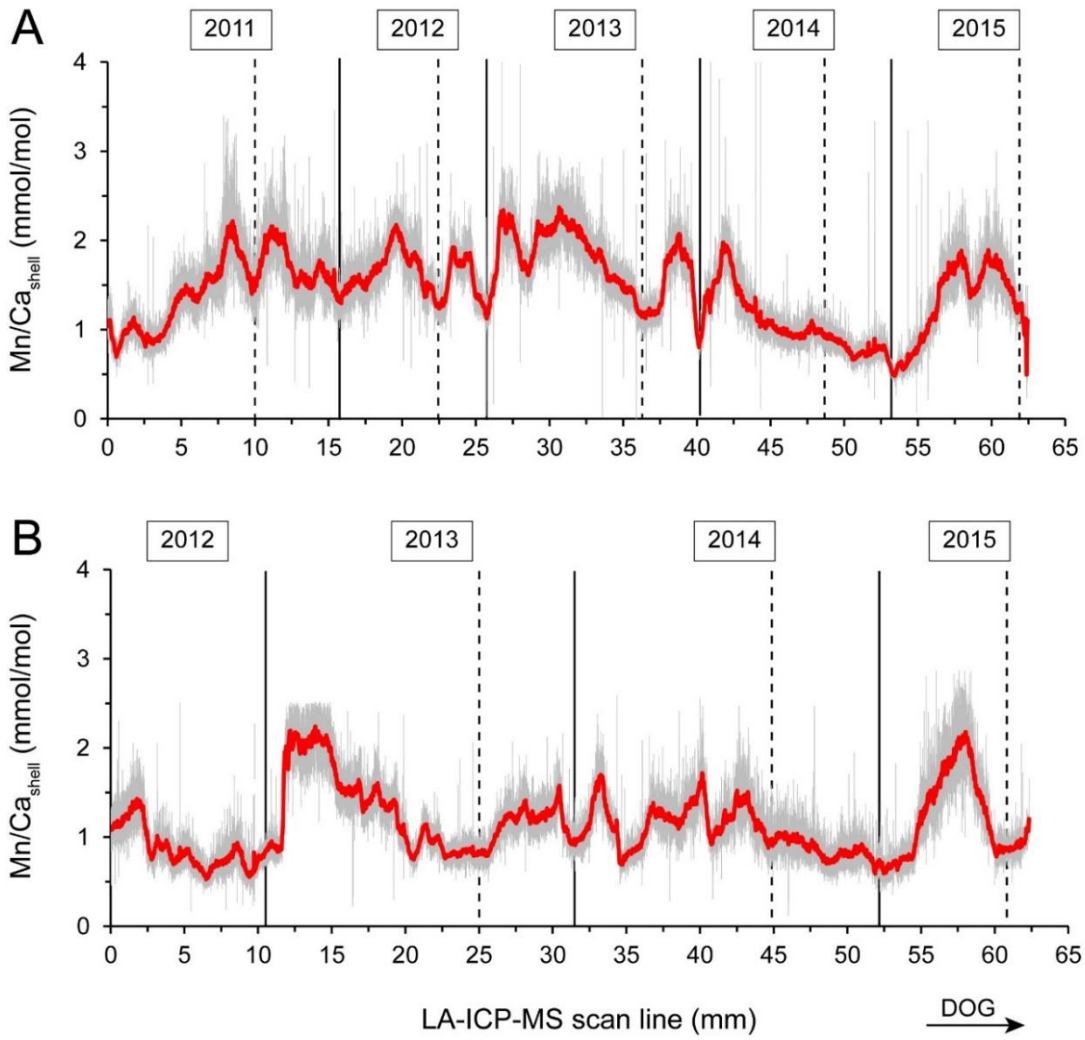

Fig. 6.5. Manganese-to-calcium ratios in the shell of *Hyriopsis cumingii*. (A) Mn/Ca$_{shell}$ time-series of specimen T1. (B) Mn/Ca$_{shell}$ time-series of specimen T2. Grey curves represent raw Mn/Ca$_{shell}$ data and thick red lines indicate smoothed data. Solid and dash vertical lines indicate the position of winter and summer growth lines, respectively. DOG = direction of growth.

Table 6.1. Summary of manganese-to-calcium ratios in the shells of *Hyriopsis cumingii*.

Shell ID	T1			T2		
Calendar year	Annual avg/min/max	Seasonal avg/min/max		Annual avg/min/max	Seasonal avg/min/max	
		S I	S II		S I	S II
2015	1.1/0.5/1.9	1.3/0.5/1.9	0.8/0.5/1.1	1.1/0.6/2.2	1.3/0.6/2.2	0.9/0.8/1.2
2014	1.0/0.6/2.0	1.2/0.8/2.0	0.8/0.6/1.0	1.1/0.6/1.7	1.2/0.7/1.7	0.9/0.6/1.1
2013	1.7/0.9/2.4	1.8/1.1/2.4	1.6/0.9/2.1	1.2/0.7/2.3	1.3/0.7/2.3	1.1/0.8/1.6
2012	1.6/1.2/2.2	1.6/1.3/2.2	1.6/1.2/1.9			
2011	1.5/0.7/2.2	1.3/0.7/2.2	1.7/1.4/2.2			

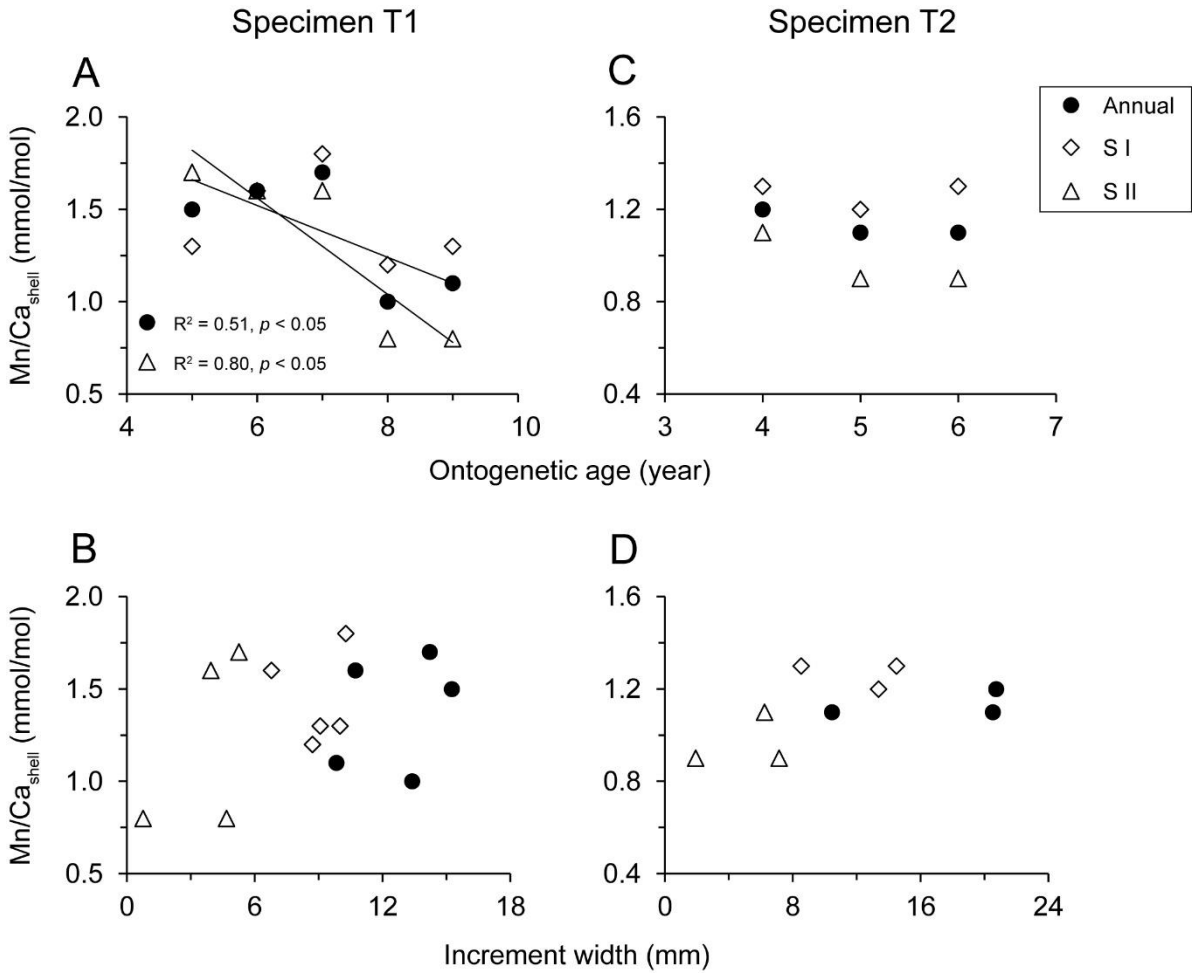

Fig. 6.6. Manganese-to-calcium ratios in the shell of *Hyriopsis cumingii* plotted against ontogenetic age and the width of shell growth increment (i.e., the rate of shell growth) in the outer shell layer. S I = first part (April to August) of the growing season; S II = second part (September to November) of the growing season.

Taking into account the ontogenetic age, however, Mn/Ca_{shell} chronologies of the studied specimens did not show consistent ontogenetic trends. For example, specimen T1 exhibited a significant ontogenetic trend toward lower annual Mn/Ca_{shell} values (Fig. 6.6A), whereas such a trend was absent in specimen T2 (Fig. 6.6C). Neither of studied specimens forming during S I exhibited a statistically significant correlation between Mn/Ca_{shell} and ontogenetic age (Fig. 6.6A and Fig. 6.6C). However, average Mn/Ca_{shell} of specimen T1 forming during S II did reveal a distinct ontogenetic trend toward lower values (Fig. 6.6A). In addition, in specimens T1 and T2, neither annual nor seasonal Mn/Ca_{shell} averages significantly correlated to increment width (Fig. 6.6B and Fig. 6.6D).

6.4. Discussion

6.4.1. Controls on manganese incorporation into the shells

It has been postulated that Mn/Ca_{shell} could potentially be influenced by vital effects such as ontogenetic age and the rate of shell growth, the latter being closely linked to the rate of crystal growth and thus kinetics. For example, Soldati et al. (2009) demonstrated the presence of a strong ontogenetic trend of Mn in the shells of *Diplodon chilensis patagonicus*. Likewise, a negative correlation between Mn/Ca_{shell} and the rate of shell growth has been reported in *Mya arenaria* (Strasser et al., 2008). However, each of these effects are likely negligibly small in the case of *H. cumingii* considering the statistically indistinguishable correlation of Mn/Ca_{shell} with either ontogenetic age or growth rate. Similar findings were also reported from a number of other bivalve species (e.g., Vander Putten et al., 2000; Lazareth et al., 2003; Freitas et al., 2006; Barats et al., 2008).

Alternatively, the existence of a common environmental control on Mn incorporation into the shell could be inferred from the high reproducibility of Mn/Ca_{shell} time-series among contemporaneous specimens from the same population. As previously demonstrated by both laboratory and field experiments, Mn/Ca_{shell} most likely reflects a variation of biologically available Mn in dissolved (e.g., Jeffree et al., 1995; Freitas et al., 2006; Carroll and Romanek, 2008; Bolotov et al., 2015) and/or particulate phases (e.g., Vander Putten et al., 2000; Lazareth et al., 2003; Langlet et al., 2007; Ravera et al., 2007). A striking increase of Mn/Ca_{shell} noted in *Mytilus edulis* (Vander Putten et al., 2000), for example, likely occurred synchronously with the spring phytoplankton bloom, during which large amounts of Mn-rich phytoplankton cells (Sunda and Huntsman, 1985) and Mn oxide particles (Richardson et al., 1988) were generated and then ingested by the mussels. Conversely, and contrary to the aforementioned observation, a pronounced increase of Mn/Ca_{shell} observed in *Pecten maximus* from the Menai Strait (North Wales, UK) preceded the onset of the spring bloom by approximately one month which probably reflected continuously enhanced levels of dissolved Mn (Freitas et al., 2006). In the same scallop species (*P. maximus*) from the Bay of Seine (France), Barats et al. (2008) noticed a distinct increase of Mn/Ca_{shell} during late summer which was interpreted to reflect the combined effect of phytoplankton sedimentation and benthic export of Mn at the SWI under intense summertime hypoxic conditions. Up to now, however, the latter contribution has rarely been quantified, presumably because long-term monitoring of manganese cycling and export at the SWI remains a very challenging task. As schematically illustrated in Fig. 6.7, the background and seasonal amplitude of Mn levels in the pore water of Lake Taihu as well as

organic particles are several orders of magnitude higher than those in the overlying water column. Given that *H. cumingii* lives completely buried in the sediment, it seems very likely that Mn/Ca_{shell} responds very sensitive to marked seasonal fluctuations of the cycling and export of bioavailable Mn at the SWI. As will be demonstrated below, two lines of evidence lend support to the significance of sedimentary contribution to the major pool of Mn incorporated into the shells.

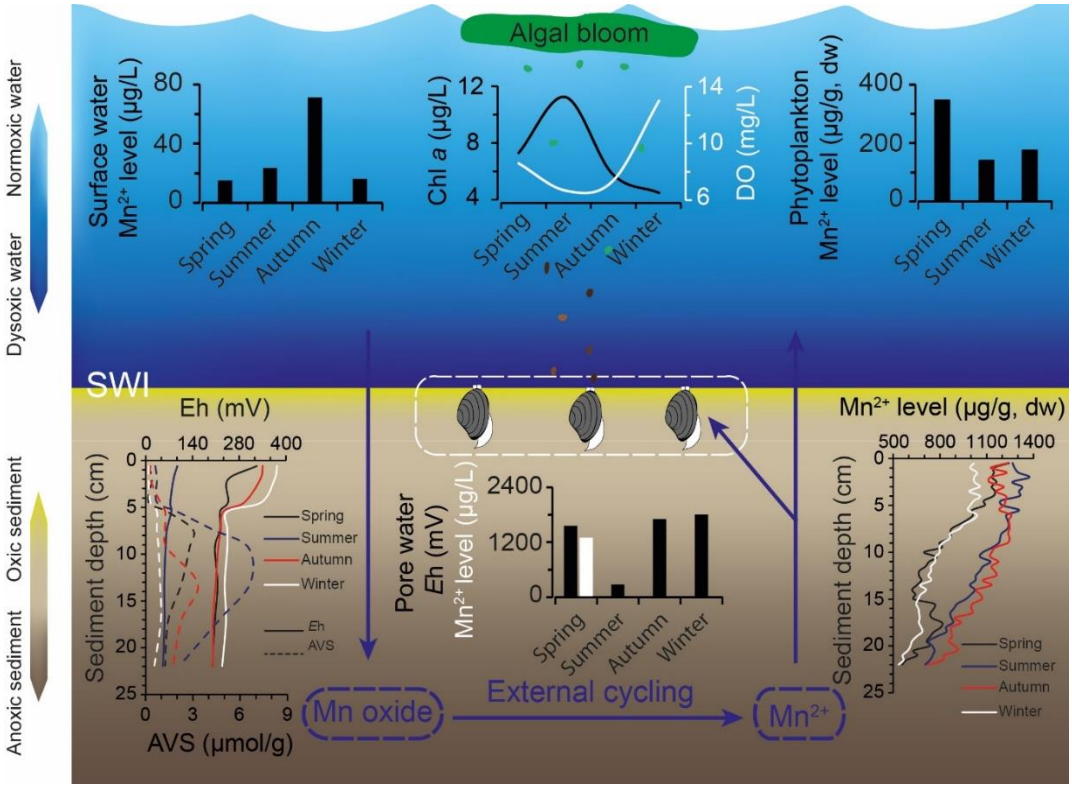

Fig. 6.7. Seasonal changes of physiochemical parameters of the sediment and overlying water in Meiliang Bay, Lake Taihu. Grey arrows indicate the external cycling of manganese (i.e., across the sediment-water interface, SWI) when reducing conditions prevail. Seasonal changes of Chlorophyll *a* (Chl *a*) and dissolved oxygen (DO) were obtained from the Taihu Basin Water Resources Monitoring and Protection Bureau (www.tba.gov.cn), and Mn^{2+} levels of the water and phytoplankton were taken from Yan et al. (2016) and Wang et al. (2015), respectively. Mn^{2+} levels in the sediment pore water and organic particles were taken from Tao et al. (2012) and Zheng et al. (2009), respectively. Seasonal changes of redox potential (*E*h) in the pore water and sediment and acid volatile sulfide (AVS) in the sediment were obtained from Yin and Fan (2011). dw = dry weight.

6.4.1.1. Uptake from Mn-rich pore water

Previous studies have shown that bivalves grown under experimental conditions preferentially incorporate the dissolved form of manganese (e.g., the reduced state of Mn^{2+}) into the shells (e.g., Carriker et al., 1980; Jeffree et al., 1995; Barbin et al., 2008). In particular, the incorporation of Mn from the ambient environment into the shell occurs rather rapidly with a

time lag of less than 24 hours (Langlet et al., 2006). These findings agree well with the free ion activity model (Campbell, 1995) according to which Mn^{2+} is the most bioavailable form of manganese and line up with the general notion that Mn^{2+} is taken up by the bivalve as an analogue of Ca^{2+} because of similar electrochemical properties and radii (Markich and Jeffree, 1994; Zhao et al., in review). Likewise, several field experiments have related larger amounts of Mn in shells to higher levels of dissolved Mn in the water column caused, for example, by exogenous inputs (Markich et al., 2002; Barats et al., 2008) and seasonal upwelling (Langlet et al., 2007). In the upper waters of Lake Taihu, dissolved Mn shows a certain degree of seasonal variation, and a threefold increase in fall (Yan et al., 2016). The latter could potentially account for relatively high secondary Mn/Ca_{shell} peaks in *H. cumingii* in the fall of 2012 and 2013, but this is clearly not the case for the summer Mn/Ca_{shell} maxima in *H. cumingii*, which in turn, underlines the existence of an important but unrecognized contributor to such peaks.

Strong release of the reductive dissolution of Mn into the pore water under changing sediment redox conditions provides a more plausible explanation for the striking feature of Mn/Ca_{shell} peaks in summer. Sediment pore water contains a much larger amount of dissolved Mn than the overlying water body, for example, being up to 80 times larger during spring (Fig. 6.7). Although few direct data exist, the seasonal variation of dissolved Mn in the pore water is actually quite predictable, because it follows an inverse pattern to that of redox potential (*E*h), i.e., reductively dissolved Mn in the pore water increases with decreasing *E*h (Gao et al., 2006; Giles et al., 2016). Hence, *E*h profiles can help to explain how dissolved Mn in the pore water fluctuates through time and depth. For example, in the pore water (0-20 cm depth) adjacent to the sampling site, *E*h varies seasonally and shows a pronounced summertime minimum (Yin and Fan, 2011). On this basis, one would expect an obvious seasonal variation of dissolved Mn in the pore water and, especially an extreme increase during summer. Clearly, the latter occurs synchronously with the Mn/Ca_{shell} maxima in *H. cumingii*.

As an infaunal species, *H. cumingii* is often completely buried within the sediment and thus exposed to the pore water which is considerably enriched in dissolved Mn. This species is considered an osmoregulator, i.e., it needs to maintain an extremely high ionic strength in the body fluids to compensate for the passive diffusion of solutes. As such, *H. cumingii* is able to efficiently absorb aqueous cations over the entire body surface, especially through the gills and mantle epithelia (Dietz, 1979; Coimbra et al., 1993). The latter is cluttered with ion channels and transporters (Deaton, 1981). Presumably due to similar electrochemical properties as Ca^{2+}, dissolved Mn coming from the pore water can diffuse freely through Ca^{2+}-channels or be actively transported by Ca^{2+}-ATPases into the hemolymph and then reach the calcifying fluids.

This interpretation compares well with the fast and sensitive valve response of *Veselunio angasi* exposed to high concentrations of aqueous Mn^{2+} (Markich et al., 2000), and the rapid and preferential uptake of free Mn^{2+} ions and incorporation into the shells of *Crassostrea gigas* (Langlet et al., 2006; Barbin et al., 2008). Therefore, it is likely that pore water represents an important source of Mn incorporated into the shells.

6.4.1.2. Uptake from Mn-rich sedimentary particles

The ingestion of Mn-rich particles has been put forward to account for the striking uptake and incorporation of Mn into bivalve shells. Most of these studies were based on epifaunal species such as *M. edulis* (Vander Putten et al., 2000), *Isognomon ephippium* (Lazareth et al., 2003) and *P. maximus* (Barats et al., 2008). Due to its role in photosynthesis, manganese can be efficiently taken up by algae and become highly concentrated within algal cells, for example, over three orders of magnitude higher than wate (Sunda and Huntsman, 1985). The rapid oxidation of soluble Mn^{2+} to an extracellular particulate form of Mn oxide is also highly dependent on the microenvironments generated by large algal aggregates or clumps (Richardson et al., 1988). Both aspects could therefore be advanced to explain the low concentration of dissolved Mn in the overlying water column during summer. Moreover, given that the decomposition and sedimentation of algae take place rapidly after a bloom, it is likely that Mn-rich algal particles are ingested and digested by epifaunal bivalves without a significant lag, thereby exhibiting a causal link between Mn/Ca_{shell} spikes and primary productivity. In the present study, summer Mn/Ca_{shell} maxima in *H. cumingii* seem to be associated with Chlorophyll *a* peaks. On the basis of such an apparent link, however, an inductive conclusion cannot be drawn. It remains largely uncertain whether infaunal bivalves are able to capture the majority of these Mn-rich particles (algae and detritus), i.e., whether their primary food source comes from suspended organic particles. The other uncertainty lies in the much larger amplitude of Mn/Ca_{shell} compared to that of Chlorophyll *a*. Therefore, it is more likely that an apparent link of the formation of Mn/Ca_{shell} peaks to algal blooms is merely a coincidence rather than causality.

Unionid mussels feed on sedimentary organic detritus by filtering the pore water or taking up particles from the sediment surface (deposit feeding) (Vaughn and Hakenkamp, 2001). In particular, the latter could contribute to a high proportion (> 50%) of their food sources (Cahoon and Owen, 1996). Based on stable nitrogen isotope data, Raikow and Hamilton (2001) investigated the dietary regime of twelve unionid species in a Michigan stream and

demonstrated that up to 80% of the total food intake derives from deposited organic particles. Taking into account the feeding behavior of unionid mussels, the high abundance of digestible organic matter in surface sediments of Lake Taihu and especially, its striking enrichment in Mn^{2+} (Fig. 6.7), it seems very likely that aside from the pore water sedimentary organic detritus represents an important source of Mn^{2+} accumulation in *H. cumingii*. In particular, the observed changes of Mn/Ca_{shell} of *H. cumingii* are temporally aligned with the seasonal and vertical profiles of Mn^{2+} in surface sediments. At the same depth as the pore water (0-20 cm depth), particulate Mn^{2+} exhibits a distinct seasonal change with the highest value occurring in summer and lowest in winter, and a striking manganese export at the SWI (0-5 cm depth) is closely related to its vertical migration when reducing conditions prevail in summertime (Zheng et al., 2009). As in the case of the pore water, the seasonal and vertical changes of particulate Mn^{2+} are also closely (and inversely) related to those of *E*h (Yin and Fan, 2011), further supporting the idea that the reduced species of manganese in the sediment is a redox product.

The role of acid volatile sulphide (AVS) in governing the bioavailability of sediment-bound divalent metals is well understood (Lee et al., 2000). Hence, monitoring the temporal and vertical variations of AVS could help to quantify the extent to which sediment-bound Mn is biologically available through time and depth. Yin and Fan (2011) demonstrated that AVS measured in Taihu's surface sediments (0-22 cm depth) showed an anomalously high value in summer and decreased almost exponentially from the SWI, agreeing well with the seasonal and vertical changes of sedimentary Mn^{2+} reported by Zheng et al. (2009) and thereby lending further support to the hypothesis that sedimentary particles should be considered as an important source of Mn incorporated into the shells.

6.4.2. Implications for reconstructing eutrophication history

As will be demonstrated below, high-resolution Mn/Ca_{shell} time-series can provide a robust basis for a better understanding of the biogeochemical processes at the SWI because the diagenetic remobilization of Mn^{2+} (from both dissolved and particulate phases) is highly sensitive to changes of the redox potential and oxygen condition in the sediment, and tightly linked to internal loads of sedimentary N and P into the overlying water body (Reddy and DeLaune, 2008).

6.4.2.1. Retrospective tracking of eutrophication-induced hypoxia

Considering that the oxygen concentration and penetration depth beneath the SWI (1) exerts a major control over the redox status of surface sediments, (2) the reductive dissolution of Mn oxyhydroxides and (3) ultimately the export of Mn^{2+} which is either released into the pore water or bound with sedimentary particles, Mn/Ca_{shell} is a promising indicator of the degree of oxygen depletion and the formation of hypoxia in bottom waters. Sustained hypoxia in shallow eutrophic lakes should seldom occur given the vertical mixing of the water column and the replenishment of atmospheric oxygen, but short hypoxic or even anoxic episodes do frequently occur following algal blooms as a consequence of the decomposition of large amounts of fresh organic detritus (Friedrich et al., 2014). In particular, hypoxia can develop rapidly during periods of calm weather and may persist over periods of hours to several days or even longer periods until strong vertical mixing replenishes oxygen in bottom waters (Zilius et al., 2014). However, it is extremely difficult to determine the critical conditions for shallow water hypoxic events due to their unpredictable and ephemeral nature. Since high-resolution Mn/Ca_{shell} profiles can accurately archive the frequency and intensity of hypoxic events, they potentially fulfil this task. Furthermore, the formation of hypoxia is intrinsically linked to the occurrence of algal blooms. The latter results in an enhanced accumulation of organic detritus in surface sediments, thereby stimulating heterotrophic bacterial metabolism and increasing sedimentary oxygen consumption (Diaz and Rosenberg, 2008). As sediments become hypoxic, the transformation and release of redox sensitive and nutritional elements across the SWI may greatly facilitate the formation and outbreak of algal blooms (Pearce et al., 2013; Shen et al., 2013). Therefore, long-term Mn/Ca_{shell} time-series would advance our understanding of the eutrophication history.

In recent years, black blooms, a phenomenon of a large aggregation of black dissolved organic matter following severe cyanobacterial blooms, have occurred more frequently and intensively in Lake Taihu (Zhang et al., 2016). This phenomenon is characterized by offensive odor and extremely low DO concentration (less than 1 mg/L), thereby severely deteriorating the water quality (Shen et al., 2014). However, monitoring and forecasting the formation and outbreak of black blooms are difficult because they occur as a consequence of synergistic effects of cyanobacterial blooms as well meteorological and hydrological conditions (Zhang et al., 2016). As a robust proxy for hypoxia and anoxia in bottom waters, Mn/Ca_{shell} could provide a faithful record of the formation and outbreak of black blooms given that the depletion of oxygen in the overlying water initially always occurs at the SWI (Diaz and Rosenberg, 2008). According to the trend and variation of Mn/Ca_{shell} time-series, there appears to be a decrease of

the frequency and intensity of black blooms over the period 2011-2015, comparing well with instrumental data. For example, three black bloom events with an area of up to 0.12, 9.2 and 2.5 km^2 were recorded on May 22, July 30 and September 7-8, 2011, respectively, whereas in 2013 a black bloom only occurred once during June 19-24 with an area of 0.17-0.65 km^2 and no outbreak (an area larger than 0.1 km^2) was observed in 2014 (Zhang et al., 2016). Therefore, the use of Mn/Ca_{shell} as a complementary tool for retrospective tracking of black blooms is clearly promising.

6.4.2.2. Retrospective tracking of internal dynamics of nitrogen and phosphorus

Considerable efforts have been made to substantially reduce the external loads of N and P in Lake Taihu for decades, but hyper-eutrophic symptoms (e.g., harmful cyanobacterial blooms and frequent hypoxic and anoxic events) have not been abated as expected (Qin et al., 2015; Zhang et al., 2016). More likely, internal loads derived from sediments represent an important and perhaps the major source of N and P in Lake Taihu (Zhu et al., 2013). However, it is extremely challenging to directly and continuously evaluate the fluxes of N and P at the SWI, hampering our understanding of their release mechanisms. Several mechanisms are probably involved in nutrient releases from the sediment, where redox-dependent and microbial-driven processes are of particular importance (Smith et al., 2011; Zhu et al., 2013). As demonstrated below, Mn/Ca_{shell} is not only a reliable indicator of SWI redox status but also reflects the potential release of N and P from the sediments, therefore shedding new light on fundamental processes controlling the retention of nutrients in the overlying water body and the formation of harmful algal blooms.

Harmful cyanobacterial blooms occurring in many shallow eutrophic lakes are mainly composed of toxic *Microcystis* spp. (Michalak et al., 2013; Qin et al., 2015). Members of this genus are unable to convert atmospheric N_2 to ammonia (NH_3), so that they require external N sources such as ammonium (NH_4^+-N) and nitrate (NO_3^--N) to maintain growth (Paerl, 2014). Zhu et al. (2013) observed that, in Lake Taihu, a large-scale decay of algal blooms resulted in a rapid decrease of DO and an increase of NH_4^+-N in the overlying water column. The latter can most likely be attributed to sediment release under hypoxic/anoxic conditions (Zhu et al., 2013), although the underlying processes are not fully understood. In another eutrophic lake (Lake Champlain, USA), Pearce et al. (2013) demonstrated that the depth of dissolved Mn^{2+} front beneath the SWI consistently represents the overall redox condition and potentially indicates the degree of NO_3^--N reduction and NH_4^+-N diffusion from the sediments, supporting

the feasibility of our idea that Mn/Ca_{shell} profiles may help to understand the internal dynamics of nitrogen.

Iron and manganese oxide minerals absorb large amounts of total P in surface sediments (Smith et al., 2011). Thus, one would expect the release of sediment P to increase as sediment redox condition becomes reduced and the rate of mineral reductive dissolution rises. Pearce et al. (2013) and Giles et al. (2016), for example, demonstrated that increased concentrations of Mn^{2+} at the SWI can potentially serve as a proxy of internal P loads to predict the occurrence of cyanobacterial blooms in Lake Champlain. It is therefore conceivable that Mn/Ca_{shell} could also be used as a retrospective indicator in this regard.

6.5. Summary and conclusions

As demonstrated by the findings of the present study, the amount of Mn incorporated into the shells of *H. cumingii* is closely coupled to changes of dissolved and/or particulate Mn^{2+} at the SWI rather than in the overlying water. Given the rapid uptake and incorporation of Mn^{2+} into the shells, Mn/Ca_{shell} holds great potential to function as a promising proxy of the cycling and export of Mn^{2+} at the SWI at an extremely high temporal resolution. More importantly, the present study demonstrates that Mn/Ca_{shell} bears great promise for retrospectively tracking of eutrophication-induced environmental change such as redox change, periodical hypoxia and the cycling of many other elements (especially N and P) from the sediment into the overlying water.

6.6. Acknowledgments

Not displayed for reasons of data protection

6.7. References

Aguilar, C., Nealson, K.H., 1998. Biogeochemical cycling of manganese in Oneida Lake, New York: whole lake studies of manganese. J. Great. Lakes. Res. 24, 93–104.

Balistrieri, L.S., Murray, J.W., 1986. The surface chemistry of sediments from the Panama Basin: the influence of Mn oxides on metal adsorption. Geochim. Cosmochim. Acta. 50, 2235–2243.

Barats, A., Amouroux, D., Pécheyran, C., Chauvaud, L., Donard, O.F.X., 2008. High-frequency archives of manganese inputs to coastal waters (Bay of Seine, France) resolved by the LA-ICP-MS analysis of calcitic growth layers along scallop shells (*Pecten maximus*). Environ. Sci. Technol. 42, 86–92.

Bolotov, J.N., Pokrovsky, O.S., Auda, Y., Bespalaya, J.V., Vikhrev, I.V., Gofarov, M.Y., Lyubas, A.A., Viers, J., Zouiten, C., 2015. Trace element composition of freshwater pearl mussels Margaritifera spp. Across Eurasia: testing the effect of species and geographic location. Chem. Geol. 402, 125–139.

Cahoon, L.B., Owen, D.A., 1996. Can suspension feeding by bivalves regulate phytoplankton biomass in Lake Waccamaw, North Carolina? Hydrobiologia 325, 193-200.

Campbell, P.G.C., 1995. A critique of the free-ion activity model. In: Tessier, A., Turner, D.R. (Eds) Metal speciation and bioavailability in aquatic systems. John Wiley & Sons, Chichester, p 45–102.

Carriker, M.R., Palmer, R.E., Sick, L.V., Johnson, C.C., 1980. Interaction of mineral elements in sea water and shell of oysters (*Crassostrea virginica* (Gmelin)) cultured in controlled and natural systems. J. Exp. Mar. Biol. Ecol. 46, 279–296.

Carroll, M., Romanek, C.S., 2008. Shell layer variation in trace element concentration for the freshwater bivalve *Elliptio complanata*. Geo-Mar. Lett. 28, 369–381.

Coimbra, J., Ferreira, K.G., Fernandes, P., Ferreira, H.G., 1993. Calcium exchanges in *Anodonta cygnea*: barriers and driving gradients. J. Comp. Physiol. B. 163, 196–202.

Deaton, L.E., 1981. Ion regulation in freshwater and brackish water bivalve mollusks. Physiol. Zool. 54, 109–121.

Diaz, R.J., Rosenberg, R., 2008. Spreading dead zones and consequences for marine ecosystems. Science 321, 926–929.

Dietz, T.H., 1979. Uptake of sodium and chloride by freshwater mussels. Can. J. Zool. 57, 156–160.

Dettman, D.L., Reische, A.K., Lohmann, K.C., 1999. Controls on the stable isotope composition of seasonal growth bands in aragonitic fresh-water bivalves (Unionidae). Geochim. Cosmochim. Acta 63, 1049–1057.

FAO, The State of World Fisheries and Aquaculture, 2012. Food and Agriculture Organization of the United Nations, Rome, 2012.

Freitas, P.S., Clarke, L.J., Kennedy, H., Richardson, C.A., Abrantes, F., 2006. Environmental and biological controls on elemental (Mg/Ca, Sr/Ca and Mn/Ca) ratios in shells of the king scallop *Pecten maximus*. Geochim. Cosmochim. Acta 70, 5119–5133.

Friedrich, J., Janssen, F., Aleynik, D., Bange, H.W., Boltacheva, N., Cagatay, M.N., et al., 2014. Investigating hypoxia in aquatic environments: diverse approaches to addressing a complex phenomenon. Biogeosciences 11, 1215–1259.

Füllenbach, C.S., Schöne, B.R., Mertz-Kraus, R., 2015. Strontium/lithium ratio in aragonitic shells of *Cerastoderma edule* (Bivalvia) – A new potential temperature proxy for brackish environments. Chem. Geol. 417, 341–355.

Gao, Y., Leemakers, M., Gabelle, C., Divis, P., Billon, G., Ouddane, B., Fischer, J.C., Wartel, M., Baeyens, W., 2006. High-resolution profiles of trace metals in the pore waters of riverine sediment assessed by DET and DGT. Sci. Total. Environ. 362, 266–277.

Gifford, S., Dunstan, R.H., O'Connor, W., Koller, C.E., MacFarlane, G.R., 2007. Aquatic zooremediations: deploying animals to remediate contaminated aquatic environments. Trends Biotechnol. 25, 60–65.

Giles, C.D., Isles, P.D.F., Manley, T., Xu, Y., Druschel, G.K., Schroth, A.W., 2016. The mobility of phosphorus, iron, and manganese through the sediment-water continuum of a shallow eutrophic freshwater lake under stratified and mixed water-column conditions. Biogeochemistry 127, 15–34.

Grossman, E.L., Ku, T.-L., 1986. Oxygen and carbon isotope fractionation in biogenic aragonite: temperature effects. Chem. Geol. Isot. Geosci. Sect. 59, 59–74.

Qin, B., Li, W., Zhu, G., Zhang, Y., Wu, T., Gao, G., 2015. Cyanobacterial bloom management through integrated monitoring and forecasting in large shallow eutrophic Lake Taihu (China). J. Hazard. Mater. 287, 356–363.

Qin, B., Xu, P.Z., Wu, Q.L., Luo, L.C., Zhang, Y.L., 2007. Environmental issues of Lake Taihu, China. Hydrobiologia 581, 3–14.

Qin, B., Zhu, G., Gao, G., Zhang, Y., Li, W., Paerl, H.W., Carmichael, W.W., 2010. A drinking water crisis in Lake Taihu, China: linkage to climatic variability and lake management. Environ. Manage. 45, 105-112.

He, H, Liu, X., Liu, X., Yu, J., Li, K., Guan, B., Jeppesen, E., Liu, Z., 2014. Effects of cyanobacterial blooms on submerged macrophytes alleviated by the native Chinese bivalve *Hyriopsis cumingii*: a mesocosm experiment study. Ecol. Eng. 71, 363–367.

Ismail, N.S., Müller, C.E., Morgan, R.R., Luthy, R.G., 2014. Uptake of contaminants of emerging concern by the bivalves *Anodonta californiensis* and *Corbicula fluminea*. Environ. Sci. Technol. 48, 9211–9219.

Jeffree, R., Markich, S., Lefebvre, F., Thellier, M., Ripoll, C., 1995. Shell microlaminations of the fresh-water *Hyridella depress* as an archival monitor of manganese concentration: experimental investigation by depth profiling using secondary-ion mass-spectrometry (SIMS). Experientia 51, 838–848.

Jochum, K.P., Nohl, U., Herwig, K., Lammel, E., Stoll, B., Hofmann, A.W., 2005. GeoReM: a new geochemical database for reference materials and isotopic standards. Geostand. Geoanal. Res. 29, 87–133.

Jochum, K.P., Weis, U., Stoll, B., Kurmin, D., Yang, Q., Raczek, I., Jacob, D.E., Stracke, A., Birbaum, K., Frick, D.A., Günther, D., Enzweiler, J., 2011. Determination of reference values for NIST SRM 610-617 glasses following ISO guidelines. Geostand. Geoanal. Res. 35, 397–429.

Jochum, K.P., Scholz, D., Stoll, B., Weis, U., Wilson, S.A., Yang, Q., Schwalb, A., Börner, N., Jacob, D.E., Andreae, M.O., 2012. Accurate trace element analysis of speleothems and biogenic calcium carbonates by LA-ICP-MS. Chem. Geol. 318-319, 31–44.

Langlet, D., Alleman, L.Y., Plisnier, P.D., Hughes, H., André, L., 2007. Manganese content records seasonal upwelling in Lake Tanganyika mussels. Biogeosciences 4, 195–203.

Langlet, D., Alunno-Bruscia, M., Rafélis, M., Renard, M., Roux, M., Schein, E., Buestel, D., 2006. Experimental and natural manganese-induced cathodoluminescence in the shell of the Japanese oyster *Crassostrea gigas* (Thunberg, 1793) from Thau Lagoon (Hérault, France): ecological and environmental implications. Mar. Ecol. Prog. Ser. 317, 143–156.

Lazareth, C.E., Vander Putten, E., André, L., Dehairs, F., 2003. High-resolution trace element profiles in shells of the mangrove bivalve *Isognomon ephippium*: a record of environmental spatiotemporal variations? Estuar. Coast. Shelf Sci. 57, 1103–1114.

Lee, B.G., Griscom, S.B., Lee, J.S., Choi, H.J., Koh, C.H., Luoma, S.N., Fisher, N.S., 2000. Influences of dietary uptake and reactive sulfides on metal bioavailability from aquatic sediments. Science 287, 282–284.

Li, X., Song, H., Li, W., Lu, X., Nishimura, O., 2010. An integrated ecological floating-bed employing plant, freshwater clam and biofilm carrier for purification of eutrophic water. Ecol. Eng. 36, 38–390.

Longerich, H.P., Jackson, S.E., Günther, D., 1996. Laser ablation inductively coupled plasma mass spectrometric transient signal data acquisition and analyte concentration calculation. J. Anal. At. Spectrom. 11, 899–904.

Markich, S.J., Brown, P.L., Jeffree, R.A., Lim, R.P., 2000. Valve movement responses of *Velesunio angasi* (Bivalvia: Hyriidae) to manganese and uranium: an exception to the free ion activity model. Aquat. Toxicol. 51, 155–175.

Markich, S.J., Jeffree, R.A., Burke, P.T., 2002. Freshwater bivalve shells as archival indicators of metal pollution from a copper-uranium mine in tropical northern Australia. Environ. Sci. Technol. 36, 821–832.

Markich, S.J., Jeffree, R.A., 1994. Adsorption of divalent trace metals as analogues of calcium by Australian freshwater bivalves: an explanation of how water hardness reduces metal toxicity. Aquat. Toxicol. 29, 257–290.

Michalak, A.M., Anderson, E.J., Beletsky, D., Boland, S., Bosch, N.S., Bridgeman, T.B., et al., 2013. Record-setting algal bloom in Lake Erie caused by agricultural and meteorological trends consistent with expected future conditions. Proc. Natl. Acad. Sci. 110, 6448–6452.

Nyström, J., Dunca, E., Mutvei, H., Lindh, U., 1996. Environmental history as reflected by freshwater pearl mussels in the river Vramsån, Southern Sweden. Ambio 25, 350–355.

Paerl, H.W., 2014. Mitigating harmful cyanobacterial blooms in a human and climatically-impacted world. Life 4, 988–1012.

Pakhomova, S.V., Hall, P.O.J., Kononets, M.Y., Rozanov, A.G., Tengberg, A., Vershinin, A.V., 2007. Fluxes of iron and manganese across the sediment–water interface under various redox conditions. Mar. Chem. 107, 319–331.

Pearce, A.R., Rizzo, D.M., Watzin, M.C., Druschel, G.K., 2013. Unraveling associations between cyanobacteria blooms and in-lake environmental conditions in Missisquoi Bay, Lake Champlain, USA, using a modified self-organizing map. Environ. Sci. Technol. 47, 14267–14274.

Pedersen, T.F., Price, N.B., 1982. The geochemistry of manganese carbonate in Panama Basin sediments. Geochim. Cosmochim. Acta. 46, 59–68.

Raikow, D.F., Hamilton, S.K., 2002. Bivalve diets in a Midwestern US stream: a stable isotope enrichment study. Limnol. Oceanogr. 46, 514–522.

Ravera, O., Beone, G.M., Trincherini, P.R., Riccardi, N., 2007. Seasonal variations in metal content of two Unio pictorum mancus (Mollusca, Unionidae) populations from two lakes of different trophic state. J. Limnol. 66, 28–39.

Reddy, K.R., DeLaune, R.D., 2008. Biogeochemistry of Wetlands: Science and Applications. CRC Press, Boca Raton.

Richardson, L., Aguilar, C., Nealson, K., 1988. Manganese oxidation in pH and O_2 microenvironments produced by phytoplankton. Limnol. Oceanogr. 33, 352–363.

Rose, J.M., Bricker, S.B., Tedesco, M.A., Wikfors, G.H., 2014. A role for shellfish aquaculture in coastal nitrogen management. Environ. Sci. Technol. 48, 2519–2525.

Schoemann, V., de Baar, H., de Jong, J., Lancelot, C., 1998. Effects of phytoplankton blooms on the cycling of manganese and iron in coastal waters. Limnol. Oceanogr. 43, 1427–1441.

Shen, Q., Liu, C., Zhou, Q., Shang, J., Zhang, L., Fan, C., 2013. Effects of physical and chemical characteristics of surface sediments in the formation of shallow lake algae-induced black bloom. J. Environ. Sci. 25, 2353–2360.

Shen, Q., Zhou, Q., Shang, J., Shao, S., Zhang, L., Fan, C., 2014. Beyond hypoxia: occurrence and characteristics of black blooms due to the decomposition of the submerged plant *Potamogeton crispus* in a shallow lake. J. Environ. Sci. 26, 281–288.

Smith, V.H., 2003. Eutrophication of freshwater and coastal marine ecosystems a global problem. Environ. Sci. Pollut. R. 10, 126–139.

Smith, L., Watzin, M.C., Druschel, G., 2011. Relating sediment phosphorus mobility to seasonal and diel redox fluctuations at the sediment-water interface in a eutrophic freshwater lake. Limnol. Oceanogr. 56, 2251–2264.

Soldati, A.L., Jacob, D.E., Glatzel, P., Swarbrick, J.C., Geck, J., 2016. Element substitution by living organisms: the case of manganese in mollusc shell aragonite. Sci. Rep. 6, 22514.

Soldati, A.L., Jacob, D.E., Schöne, B.R., Bianchi, M.M., Hajduk, A., 2008. Seasonal periodicity of growth and composition in valves of *Diplodon chilensis patagonicus* (D'Orbigny, 1835). J. Molluscan Stud. 75, 75–85.

Strasser, C.A., Mullineaux, L.S., Walther, B.D., 2008. Growth rate and age effects on *Mya arenaria* shell chemistry: implications for biogeochemical studies. J. Exp. Mar. Biol. Ecol. 355, 153-163.

Sunda, W., Huntsman, S., 1985. Regulation of cellular manganese and manganese transport rates in unicellular alga *Chlamydomonas*. Limnol. Oceanogr. 30, 71–80.

Tao, Y., Yuan, Z., Wei, M., Xiaoyu, H., 2012. Characterization of heavy metals in water and sediments in Taihu Lake, China. Environ. Monit. Assess. 184, 4367–4382.

Tebo, B.M., 1991. Manganese (II) oxidation in the suboxic zone of the Black Sea. Deep-Sea. Res. Part A: Oceanogr. Res. Rap. 38, S883–S905.

Vander Putten, E., Dehairs, F., Keppens, E., Baeyens,W., 2000. High resolution distribution of trace elements in the calcite shell layer of modern *Mytilus edulis*: environmental and biological controls. Geochim. Cosmochim. Acta 64, 997–1011.

Vaughn, C.C., Hakenkamp, C.C., 2001. The functional role of burrowing bivalves in freshwater ecosystems. Freshwater Biol. 46, 1431–1446.

Wilson, D.E., 1980. Surface and complexation effects on the rate of Mn (II) oxidation in natural waters. Geochim. Cosmochim. Acta. 44, 1311–1317.

Xu, H., Paerl, H.W., Zhu, G., Qin, B., Hall, N.S., Zhu, M., 2016. Long-term nutrient trends and harmful cyanobacterial bloom potential in hypertrophic Lake Taihu, China. Hydrobiologia DOI: 10.1007/s10750-016-2967-4

Xu, J., Xiao, W., Xiao, Q., Wang, W., Wen, X., Hu, C., Liu, C., Liu, S., Li, X., 2016. Temporal dynamics of stable isotope composition in Lake Taihu and controlling factors. Environ. Sci. 37, 2470–2477.

Yan, C., Che, F., Zeng, L., Wang, Z., Du, M., Wei, Q., Wang, Z., Wang, D., Zhen, Z., 2016. Spatial and seasonal changes of arsenic species in Lake Taihu in relation to eutrophication. Sci. Total. Environ. 563-564, 496–505.

Yin, H., Fan, C., 2011. Dynamics of reactive sulfide and its control on metal bioavailability and toxicity in metal-polluted sediments from Lake Taihu, China. Arch. Environ. Contam. Toxicol. 60, 565–575.

Yoshimura, T., Nakashima, R., Suzuki, A., Tomioka, N., Kawahata, H., 2010. Oxygen and carbon isotope records of cultured freshwater pearl mussel *Hyriopsis* sp. shell from Lake Kasumigaura, Japan. J. Paleolimnol. 43, 437–448.

Zilius, M., Bartoli, M., Bresciani, M., Katarzyte, M., Ruginis, T., Petkuviene, J., Lubiene, I., Giardino, C., Bukaveckas, P.A., de Wit, R., Razinkovas-Baziukas, A., 2014. Feedback mechanisms between cyanobacterial blooms, transient hypoxia, and benthic phosphorus regeneration in shallow coastal environments. Estuaries. Coasts. 37, 680–694.

Zhang, Y., Shi, K., Liu, J., Deng, J., Qin, B., Zhu, G., Zhou, Y., 2016. Meteorological and hydrological conditions driving the formation and disappearance of black blooms, an ecological disaster phenomena of eutrophication and algal blooms. Sci. Total. Environ. 569-570, 1517–1529.

Zhao, L.Q., Schöne, B.R., Mertz-Kraus, R., in review. Delineating the role of calcium in shell formation and elemental composition of *Corbicula fluminea* (Bivalvia). Hydrobiologia

Zheng, L., Liu, Y., Qian, X., Shi, X., 2009. The characteristics and regional differences of heavy metal contents in the sediments of Taihu Lake and Chaohu Lake. Environ. Chem. 28, 883–888.

Zhu, M., Zhu, G., Zhao, L., Yao, X., Zhang, Y., Gao, G., Qin, B., 2013. Influence of algal bloom degradation on nutrient release at the sediment-water interface in Lake Taihu, China. Environ. Sci. Pollut. Res. 20, 1803–1811.

Supplementary data

Table 6.1S. Comparison of manganese-to-calcium ratios in shells of freshwater mussels which inhabited oligotrophic, mesotrophic and eutrophic environments.

Region	Locality	Trophic status	Bivalve species	Mn/Ca_{shell} (mmol/mol)	Reference
Southern Sweden	River Vramsån	Oligotrophic	*Margaritifera margaritifera*	0.02–1.09	Nyström et al. (1996)
Northern Italy	Lake Maggiore	Oligotrophic	*Unio pictorum mancus*	0.34	Ravera et al. (2007)
Northwestern Russia	River Yud'ma	Oligotrophic	*M. margaritifera*	0.49–1.00	Bolotov et al. (2015)
Kunashir Island	River Serebryanka	Oligotrophic	*Margaritifera laevis*	0.21–0.31	Bolotov et al. (2015)
Sakhalin Island	River Adamka	Oligotrophic	*M. middendorffi*	0.32–0.35	Bolotov et al. (2015)
Far Eastern Russia	River Ilistaya	Oligotrophic	*Margaritifera dahurica*	0.34–0.45	Bolotov et al. (2015)
Northern Laos	River Nam Pe	Oligotrophic	*M. laosensis*	0.81–0.82	Bolotov et al. (2015)
East Africa	Lake Tanganyika	Oligotrophic (seasonal upwelling)	*Pleiodon spekii*	0.18–1.82	Langlet et al. (2007)
Sakhalin Island	River Tym	Mesotrophic	*M. laevis*	0.55–0.59	Bolotov et al. (2015)
Far Eastern Russia	River Komarovka	Mesotrophic	*M. dahurica*	0.53–0.54	Bolotov et al. (2015)
Northern Italy	Lake Candia	Eutrophic	*U. pictorum mancus*	1.34	Ravera et al. (2007)
Southeastern U.S.	River Savannah	Eutrophic	*Elliptio complanata*	0.14–3.09	Carroll and Romanek (2008)
Northern Australia	River Finniss	Eutrophic + polluted	*Velesunio angasi*	0.54–3.09	Markich et al. (2002)
Southern China	Lake Taihu	Eutrophic	*Anodonta woodiana*	0.18–1.76	Unpublished data
Southern China	Lake Taihu	Eutrophic	*Hyriopsis cumingii*	0.48–2.37	This study

Chapter 7

Conclusions

Without doubt, the number of studies attempting to explore element impurities of bivalve shells as environmental proxies continues to rise, despite the fact that extrinsic and intrinsic variables governing the element incorporation are still not fully understood. With the aim of deciphering the complexity of element incorporation into bivalve shells, this thesis aimed at two main aspects, namely

1. to disentangle how trace and minor elements are transferred from external sources to bivalve shells, and
2. to elucidate how their incorporation into the shell is influenced by environmental and physiological variables.

Given considerable discussion of results within each chapter, only main conclusions are drawn here, along with a brief synopsis of the study limitations and future research perspectives.

7.1 Pathways of element incorporation into bivalve shells

As demonstrated by the findings of chapter 2, calcium ions exhibited substantial effects on the amounts of Mn, Cu and Pb incorporated into the shells of *C. fluminea*, thereby highlighting the possibility that they may compete with Ca^{2+} ions in the same transport mechanisms. More specifically, blocking Ca^{2+} channels by lanthanum and Verapamil and inhibiting the activity of Ca^{2+}-ATPase by ruthenium red significantly affected the incorporation of Mn, Cu, Zn and Pb. These results lend support to the general assumption that Ca^{2+} and other divalent ions may share the same transport mechanisms because of similar ionic radii and electrochemical properties. However, this is clearly not the case for Mg, Sr and Ba, i.e., the intracellular Ca^{2+} pathways are probably not responsible for their transport. In particular, results obtained for Sr and Ba are at odds with the assumption commonly admitted for the incorporation of these two trace elements. These findings, if proven to be widespread among other bivalve species, would radically change our current understanding of the pathways of Sr and Ba incorporation into the shells (Klein et al., 1996; Carré et al., 2006; Sano et al., 2012). Therefore, it is imperative to test whether species-specific differences in element incorporation exist.

7.2 Controls on element incorporation into bivalve shells

Chapters 3–6 demonstrated complexly intertwined set of extrinsic and intrinsic factors affecting the incorporation of trace and minor elements into bivalve shells. In agreement with the results of abiogenic precipitation experiments (Gaetani and Cohen, 2006), strontium- and barium-to-

calcium ratios in *C. fluminea* shells were found to be linearly correlated to those of the water, and the amounts of Sr and Ba incorporated into the shells decreased with increasing temperature. However, despite this encouraging outcome, discrepancies were evident between abiogenic and biogenic carbonates. Findings of the thesis substantiated that growth rate (which is closely linked to the rate of crystal growth and hence, kinetics) did not influence the incorporation of Sr and Ba into *C. fluminea* shells (Chapter 3), Na into shells of *M. edulis*, *P. yessoensis* (Chapter 4) and *R. philippinarum* (Chapter 5), and Mn into *H. cumingii* shells (Chapter 6). On the contrary, fast growing synthetic carbonates contain larger amounts of Sr and Ba compared to those that were precipitated slowly (Gaetani and Cohen, 2006).

Furthermore, distribution coefficients of Sr ($K_D^{Sr/Ca} \approx 0.2$) and Ba ($K_D^{Ba/Ca} \approx 0.1$) in *C. fluminea* were circa five and ten times lower than those of abiogenic carbonates, respectively, confirming the existence of strong discriminations of Sr and Ba between the ambient water and the shells. These discriminating effects, however, were interpreted as primary sources of physiological influences in the vast majority of previous studies (Klein et al., 1996; Gillikin et al., 2005; Carré et al., 2006; Schöne et al., 2011; Sano et al., 2012). Throughout the thesis it has been emphasized repeatedly that shell formation takes place in an enclosed microenvironment rather than in the ambient environment , whereas due to the technical challenge to measure the element composition of the calcifying fluid, $K_D^{Sr/Ca}$ and $K_D^{Ba/Ca}$ in many previous studies (Bailey and Lear, 2006; Gillikin et al., 2006, 2008; Carroll and Romanek, 2008; Schöne et al., 2011) including the current research were calculated by dividing element-to-calcium ratios of the shells by those of the ambient water. Hence, great caution should be taken while employing such an approach, i.e., comparing the distribution coefficient of an element in the shell to that of abiogenic carbonate, to quantify the degree of physiological influences.

Chapters 4–5 facilitate a comprehensive understanding of how physiological influences affect the element incorporation into bivalve shells. Findings demonstrated that *M. edulis*, *P. yessoensis* and *R. philippinarum* exhibited a much stronger ability to regulate the acid-base and ionic composition of the calcifying fluid than previously thought. Presumably, bivalves respond to various environmental scenarios (e.g., global warming, eutrophication, hypoxia and metal pollution) through tight control of the acid-base and ionic regulation at the calcifying front (Li et al., 2016; Wang et al., 2016), thereby being able to encode environmental signals in the form of the element composition of the shells. Thus, environmental and physiological controls on the element incorporation do not have to be mutually exclusive, i.e., if environmental changes outweigh physiological influences on geochemical properties of the shells, one could still

expect that bivalve shells act as high-potential environmental archives. Perhaps, the most fundamental challenge to extract valuable environmental information from bivalve shells lies in the fact that the relative importance of extrinsic and intrinsic variables controlling the element incorporation remains largely unknown and can vary among differential life stages, populations and species.

In summary, laboratory experiments and field studies conducted in the current research suggest that the element concentrations of the ambient water in which bivalves lived are the most important parameter governing the element incorporation into the shells. Strong, positive relationships between the Sr, Ba and Mn contents of the shells and their corresponding levels of the ambient water compare well with previous observations (chapters 3 and 6). In particular, changes of the elvels of aforementioned elements in the water can be reflected in the shells (as least in species hitherto studied) (Langlet et al., 2006; Poulain et al., 2015). Despite physiological influences that can potentially obscure environmental signals encoded in element impurities of bivalve shells, they still hold great promise to serve as environmental proxies.

7.3 Limitations of the current research

1. Experiments present herein, with the exception of the chapter 6, were carried out under controlled laboratory conditions and did not incorporate the full complexity of natural environments that bivalves experienced. Therefore, the potential offset of empirically calibrated relationships obtained under realistic scenarios should be taken into account.
2. Accumulating evidence highlights the existence of species- and habitat-specific effects on the element composition of bivalve shells (Schöne, 2008; Gillikin et al., 2008). Hence, findings of the current research may not be applicable to other species or other populations of the same species.

7.4 Future research perspectives

1. Future studies should determine the relative contribution of water and food to trace and minor elements incorporated into bivalve shells. Evidently, such knowledge is of particular importance because many elements can be taken up by the bivalves from dissolved and particulate phases. As yet, however, the proportion of elements deriving from the food remains largely unknown, hampering the potential use of element signatures as proxies for primary production.

2. Future studies also need to delineate the pathways of trace and minor elements into marine bivalve shells. Marine bivalves are osmoconformers with identical element composition of the hemolymph and the ambient water (Wada and Fujinuki, 1976). Hence, particular attention should be drawn on the role of the outer mantle epithelium in the element transport.
3. Furthermore, trace and minor elements of bivalve shells should be analyzed in different shell layers to avoid any potentially confounding microstructural influences.

7.5 References

Bailey, T.R., Lear, C.H., 2006. Testing the effect of carbonate saturation on the Sr/Ca of biogenic aragonite: a case study from the River Ehen, Cumbria, UK. Geochem. Geophys. Geosyst. 7, Q03019.

Carré, M., Bentaleb, I., Bruguier, O., Ordinola, E., Barrett, N.T., Fontugne, M., 2006. Calcification rate influence on trace element concentrations in aragonitic bivalve shells: evidences and mechanisms. Geochim. Cosmochim. Acta. 70, 4906–4920.

Carroll, M., Romanek, C.S., 2008. Shell layer variation in trace element concentration for the freshwater bivalve *Elliptio complanata*. Geo-Mar. Lett. 28, 369–381.

Gaetani, G.A., Cohen, A.L., 2006. Element partitioning during precipitation of aragonite from seawater: a framework for understanding paleoproxies. Geochim. Cosmochim. Acta. 70, 4617–4634.

Gillikin, D.P., Dehairs, F., Lorrain, A., Steenmans, D., Baeyens, W., André, L., 2006. Barium uptake into the shells of the common mussel (*Mytilus edulis*) and the potential for estuarine paleo-chemistry reconstruction. Geochim. Cosmochim. Acta. 70, 395–407.

Gillikin, D.P., Lorrain, A., Navez, J., Taylor, J.W., André, L., Keppens, E., Baeyens, W., Dehairs, F., 2005. Strong biological controls on Sr/Ca ratios in aragonitic marine bivalve shells. Geochem. Geophys. Geosyst. 6, Q05009. DOI: 10.1029/2004GC000874.

Gillikin, D.P., Lorrain, A., Paulet, Y.M., André, L., Dehairs, F., 2008. Synchronous barium peaks in high-resolution profiles of calcite and aragonite marine bivalve shells. Geo-Mar. Lett. 28, 351–358.

Klein, R.T., Lohmann, K.C., Thayer, C.W., 1996. Sr/Ca and $^{13}C/^{12}C$ ratios in skeletal calcite of *Mytilus trossulus*: covariation with metabolic rate, salinity, and carbon isotopic composition of seawater. Geochim. Cosmochim. Acta. 60, 4207–4221.

Langlet, D., Alunno-Bruscia, M., Rafélis, M., Renard, M., Roux, M., Schein, E., Buestel, D., 2006. Experimental and natural manganese-induced cathodoluminescence in the shell of the Japanese oyster *Crassostrea gigas* (Thunberg, 1793) from Thau Lagoon (Hérault, France): ecological and environmental implications. Mar. Ecol. Prog. Ser. 317, 143–156.

Poulain, C., Gillikin, D.P., Thebault, J., Munaron, J.M., Bohn, M., Robert, R., Paulet, Y.-M., Lorrain, A., 2015. An evaluation of Mg/Ca, Sr/Ca, and Ba/Ca ratios as environmental proxies in aragonite bivalve shells. Chem. Geol. 396, 42–50.

Sano, Y., Kobayashi, S., Shirai, K., Takahata, N., Matsumoto, K., Watanabe, T., Sowa, K., Iwai. K., 2012. Past daily light cycle recorded in the strontium/calcium ratios of giant clam shells. Nat. Comm. 3, 761.

Schöne, B.R., 2008. The curse of physiology – Challenges and opportunities in the interpretation of geochemical data from mollusk shells. Geo-Mar. Lett. 28, 269–285.

Schöne, B.R., Zhang, Z., Radermacher, P., Thébault, J., Jacob, D.E., Nunn, E.V., Maurer, A.F., 2011. Sr/Ca and Mg/Ca ratios of ontogenetically old, long-lived bivalve shells (*Arctica islandica*) and their function as paleotemperature proxies. Palaeogeogr. Palaeoclimatol. Palaeoecol. 302, 52–64.

Wada, K., Fujinuki, T., 1976. Biomineralization in bivalve molluscs with emphasis on the chemical composition of the extrapallial fluid. In Bryan, N.M., Wilbur, K.M. (eds), Mechanisms of Mineralization in the Invertebrates and Plants. University of South Carolina Press, Georgetown, 175–190.

Wang, X., Wang, M., Jia, Z., Wang, H., Jiang, S., Chen, H., Wang, L., Song, L., 2016. Ocean acidification stimulates alkali signal pathway: a bicarbonate sensing soluble adenylyl cyclase from oyster *Crassostrea gigas* mediates physiological changes induced by CO_2 exposure. Aqua. Toxic. 181, 124–135.

Curriculum Vitae

Not displayed for reasons of data protection